Volume IV, 1960

TRANSACTIONS of the SOCIETY OF RHEOLOGY

Editor: E. H. LEE
Brown University

Preface 1
C. Richard Soderberg: Presentation of the Bingham Medal to Egon Orowan 3

SYMPOSIUM ON MECHANICS OF CONTINUA

Herschel Markovitz: Introduction to the Symposium on Mechanics of Continua 7
C. Truesdell: Modern Theories of Materials 9
Barry Bernstein: Relations between Hypo-elasticity and Elasticity 23
J. L. Ericksen: Theory of Anisotropic Fluids 29
Abstracts of Additional Papers Presented at the Symposium on Mechanics of Continua 41

SYMPOSIUM ON ADHESION AND RHEOLOGY

Raymond R. Myers: Introduction to the Symposium on Adhesion and Rheology 43
D. H. Kaelble: Theory and Analysis of Peel Adhesion: Bond Stresses and Distributions 45
Franklin S. C. Chang: The Peeling Force of Adhesive Joints 75
Robert A. Erb and Robert S. Hanson: The Tensile Strength and Tacky Behavior of Polymeric Liquids 91
Abstracts of Additional Papers Presented at the Symposium on Adhesion and Rheology 117

Ray D. Hoffman and Raymond R. Myers: Flow Down an Inclined Plane. 119
Richard H. Roydhouse: Rheology and Dental Materials 131
S. R. Bodner: On Anomalies in the Measurement of the Complex Modulus. 141
Wladimir Philippoff: Concentration Dependence of the Stress-Optical Coefficient 159
Wladimir Philippoff: Stress-Optical Properties of Silicones 169
H. W. Greensmith, L. Mullins, and A. G. Thomas: Rupture of Rubber 179
Seihun Chang, Francis H. Ree, Taikyue Ree, and Henry Eyring: Rheological Properties of Molecules in Fibers 191
Alfred H. Nissan, H. G. Higgins, and A. Lagani, Jr.: The Significance of Rheology in the Making and Using of Paper 207

(*continued*)

INTERSCIENCE PUBLISHERS NEW YORK • LONDON

L. W. Morland and E. H. Lee: Stress Analysis for Linear Viscoelastic Materials with Temperature Variation 233
Frederick H. Gaskins, John G. Brodnyan, Wladimir Philippoff, and Edmund Thelen: The Rheology of Asphalt. II. Flow Characteristics of Asphalt 265
John G. Brodnyan, Frederick H. Gaskins, Wladimir Philippoff, and Edmund Thelen: The Rheology of Asphalt. III. Dynamic Mechanical Properties of Asphalt 279
Malcolm L. Williams: Thermodynamics of Stretching of Nylon Fibers. 297
Walter H. Bauer, Duane O. Shuster, and Stephen E. Wiberley: Flow Properties of Lithium Stearate-Oil Dispersions 315
C. C. McCabe: Rheological Measurements with the Brabender Plastograph 335
J. E. McKinney, H. V. Belcher, and R. S. Marvin: The Dynamic Compressibility of a Rubber-Sulfur Vulcanizate and Its Relation to Free Volume 347
Abstracts of Additional Papers Presented at the Society of Rheology Meeting, November 4–6, 1959 363

Copyright © 1960 by
Interscience Publishers, Inc.

Library of Congress Catalog
Card Number 57-11926

INTERSCIENCE PUBLISHERS, INC.
250 Fifth Avenue, New York 1, N. Y.

For Great Britain and Northern Ireland:
INTERSCIENCE PUBLISHERS LTD.
88/90 Chancery Lane, London, W. C. 2

PRINTED IN THE UNITED STATES OF AMERICA BY MACK PRINTING CO., EASTON, PA.

TRANSACTIONS of the SOCIETY OF RHEOLOGY

VOLUME IV · 1960

FHW

INTERSCIENCE PUBLISHERS · NEW YORK · LONDON

WHT

Preface

Volume IV of the *Transactions of the Society of Rheology* (1960) comprises the majority of the papers presented at the Thirtieth Anniversary Meeting of the Society held at Lehigh University, November 4–6, 1959. Abstracts are included of those papers not printed in full, with the reference to the complete paper where this is available at this time. Two Symposia were arranged for this Meeting, and the papers so invited are printed together ahead of the contributed papers, with an introductory statement by the member arranging them. The first symposium on Mechanics of Continua was organized by Dr. Herschel Markovitz, and the second on Adhesion by Professor R. R. Myers. Mr. J. T. Bergen as Program Chairman for the Meeting was, with his Committee, responsible for arranging the full, varied, and interesting program.

At the banquet during the meeting, the Bingham Medal was presented to Dr. Egon Orowan, George Westinghouse Professor of Mechanical Engineering at the Massachusetts Institute of Technology. Professor C. Richard Soderberg's introduction of Professor Orowan and a photograph immediately follows this Preface.

In addition to the technical program mentioned above, general interest talks to commemorate the Thirtieth Anniversary of the Society were presented by founding members of the Society after luncheon on each of the three days. The speakers were: Professor Markus Reiner, Dr. Melvin Mooney, and Miss R. M. Karapetoff Cobb. During the course of the meeting, Professor J. D. Ferry presented his impressions of rheological research in Europe following a recent extensive visit there. Professor Raymond R. Myers, Chairman of the Local Arrangements Committee, was, with his Committee, responsible for a full program of supporting activities which ensured the success of the Meeting.

The Officers of the Society for 1960 are:

President
J. H. Elliott
Research Center
Hercules Powder Co.
Wilmington 99, Del.

Vice-President
J. D. Ferry
Department of Chemistry
University of Wisconsin
Madison, Wis.

Secretary-Treasurer
W. R. Willets
Titanium Pigment Corp.
99 Hudson Street
New York 13, N. Y.

Editor
E. H. Lee
Division of Applied Mathematics
Brown University
Providence 12, R. I.

The Executive Committee includes the new officers, last year's President, J. H. Dillon, and also R. S. Marvin and J. P. Tordella as elected members.

I would like to take this opportunity to thank the referees and authors, and especially Mrs. Ezoura Fonseca, for the diligent and expert assistance which made it possible to get the majority of the papers to the printer within just over three months of the Meeting.

E. H. Lee

Providence, Rhode Island
April, 1960

TRANSACTIONS OF THE SOCIETY OF RHEOLOGY IV, 3–5 (1960)

Presentation of the Bingham Medal to Egon Orowan

C. RICHARD SODERBERG, *Massachusetts Institute of Technology, Cambridge, Massachusetts*

I consider it a great honor to have the opportunity of paying tribute to the work of Dr. Egon Orowan on this occasion. I also recall with pleasure my acquaintance with Professor Bingham during the years preceding the formation of this society.

As I look back upon my own career as an engineer, I find that there have been great changes in points of view with regard to the problem of mechanical strength. It is more than an accident that the period also spans a decade more than the life of this society. In the early years there was an almost exclusive attention to the framework of the theory of elasticity. I remember being deeply impressed, as a young man, over a statement made by an engineer whom I admired very much, that the question of determining the effects of stresses, particularly those leading to failure, was far more important and far more involved than the one that usually occupied us in those days: the determination of the stresses themselves.

This now sounds self-evident, but it serves as a reminder of the narrow point of view of the engineer of that day. It also serves to remind us of the great body of knowledge which has been brought together since that time by the group of creative scientists to which Dr. Orowan belongs. Even in those days we had competent metal-

lurgists, chemists, and physicists in addition to the people preoccupied with the field of strength of materials. But the real significance to this problem of the structure of matter was vaguely realized by only a few.

This reminder of the situation in the years following World War I is more than a quaint recollection of a primitive past; the observation unfortunately has much truth even today. Engineering education has not yet fully faced up to the needs for knowledge in fields like solid state physics. We still train specialists whose backgrounds are too narrow to enable them to deal with the real problems—we fill the minds of young engineering graduates with facts of obsolete engineering practices, when we should train them in the basic sciences.

My own principal field has been that of power. By the end of the nineteen twenties it was clear that the future of steam power lay in the possibility of utilizing high temperatures and high pressures. This gave impetus to the already existing field of high temperature metallurgy, and gradually we became accustomed to deal with substances whose behavior was far from the idealized elastic state. The significance of this field was soon to explode into greater magnitude when, in the early years of World War II, the gas turbine emerged as the major factor in aircraft propulsion.

I mention these developments merely because they happen to be part of my own preoccupation. There were other parallel fields of endeavor, such as the ones which have formed the major scope of activity of this society. The behavior of textile fibers, of baker's dough, of muscular fibers, of rubbers, of plastics, of earth and rocks are no less important objects of study than that of the metals.

In our search for knowledge in these new fields, we came to appreciate the contributions of names of distinguished scientists who were revealing the facts of this complicated subject. The list is a long one—Ludwik, Nadai, Becker, G. I. Taylor, Jeffries, Bingham, Prandtl, v. Karman, and Griffith are only a few of the names. Perhaps the most important lesson to the engineer was the realization that great minds considered it worth while to give their full attention to this class of problems.

It was in this period that I discovered the name Orowan, so that in terms of literature and communication of ideas he is an old acquaintance. It was not until 1948 that I first met him, however, and in 1950 he joined the staff of M.I.T.

His influence in this position has been very great, but the real impact of his presence among us will not be fully appreciated until later. In the meantime he has continued to build edifice after edifice in his field, all serving to illuminate some deep question. The list of such structures is indeed a long one. I shall only remind you of a few, such as:

Dislocations and dislocation mechanisms of cleavage fracture in 1934
Fatigue and strain hardening in 1938
Theory of transient creep in 1947
Griffith-Orowan fracture criterion in 1949
Velocity theory of fracture of steel in 1952
Theory of deep-focus earthquakes in 1956
Theory of mountain building in 1957

Each one of these accomplishments represents the final focusing of thoughts extending over many precious years. I thus consider Egon Orowan a worthy member of the distinguished group of scientists who have received the Bingham Medal.

Introduction to the Symposium on Mechanics of Continua

HERSHEL MARKOVITZ, *Mellon Institute, Pittsburgh, Pennsylvania*

Although the Society of Rheology and even the word "rheology" have been in existence for only a few decades, the study of continuum mechanics has been going on for several centuries. Recent theoretical work in the mechanics of continua is especially pertinent to the study of the more complicated deformation properties with which rheologists usually deal. One of the purposes in arranging this symposium was to acquaint the members of the Society with this recent theoretical work.

Since the decimal system is commonly used in our culture today it has become customary that anniversaries numbered in multiples of ten be considered occasions for making historical reviews. We therefore asked Professor Truesdell to point out some of th landmarks in the history of our subject. Dr. Bernstein and Professor Ericksen present some of their recent results on two model systems—the hypoelastic material and anisotropic fluids, respectively. Dr. Coleman and Professor Noll in two joint communications describe their attempts to find out what light is shed on deformation problems by thermodynamics.

TRANSACTIONS OF THE SOCIETY OF RHEOLOGY IV, 9–22 (1960)

Modern Theories of Materials

C. TRUESDELL, *Consultant, Heat Division, National Bureau of Standards, Washington, D.C.**

A main point of departure for rheology is the second paper of Maxwell[1] on the kinetic theory, published in 1867, where a simple concept of one-dimensional linear viscoelasticity is introduced. While Maxwell left it for later generations to obscure his straightforward notions of continuum mechanics by the intermediary of springs and dashpots, his approach to the subject may fairly be said to have dominated it until 1945; while he claimed to describe viscosity "independently of hypothesis," in fact his treatment is entirely hypothetical and drastically over-simplified in three regards:

(1) It embodies only one out of infinitely many equally simple and natural types of viscoelastic response.

(2) It is linear.

(3) It is one dimensional.

The first failing became apparent soon, and much of the older literature of rheology seems to concern itself with trying to reach in a finite number of steps the infinitely many possible generalizations. In the end, infinitely many relaxation times were mastered with the aid of Fourier integrals; though variously expressed in terms of different models, in effect an arbitrary function is introduced. While an empirical fit to any data can be obtained in this way, and some correlation of data from different circumstances is possible, the second and third failings of Maxwell's analysis are not remedied. Linearization means different things in different circumstances. In the theory of viscoelasticity, linearization limits the validity of the results to small distortions from a preferred state. While many of the materials the theory is intended to describe are liable to flow, the premises of the theory are violated if any great amount of flow oc-

* Mailing address: 801 N. College Avenue, Bloomington, Indiana.

curs; in physical terms, while linearized viscoelasticity may be approximately valid for the internal friction incident to slight deformation, it is plainly of no relevance for the elastic recovery of fluids. Worse than this, many solutions obtained within the theory indicate that a deformation which is initially small will tend to grow large, violating the assumptions under which it was derived. Whether or not the whole approach is consistent with the principles of mechanics is a question never raised. While the one-dimensional treatments presume uniformity of various quantities, it is not at all clear that such uniformity is possible under the geometrical conditions holding in the apparatus used to get data to be compared with the theoretical results. A first test which any theory must pass is that, in all circumstances to which it may be applied, it be self-consistent and at least not obviously absurd. If rheology is concerned with large deformations, most of the theoretical work in its literature fails to meet this simplest of criteria.

As the beginning of the second period in rheology I might take Merrington's celebrated photograph, published in 1943, of a fluid swelling as it emerges from steady flow in a tube.[2] Whether or not this is a nonlinear phenomenon may not be obvious, but certainly it is not a one-dimensional phenomenon. One thing is sure: To constrain the fluid within the cylinder just before it leaves, the walls of the tube must be supplying a pressure greater than atmospheric pressure; in other words, the normal pressure on a plane parallel to the direction of flow is greater than the ambient pressure. For incompressible substances, at least, such a phenomenon is not included in the classical concept of a fluid in any of the three-dimensional linearized viscoelastic theories that grew up around Maxwell's one-dimensional proposal and are still studied in some circles today.

While in order to conform to accepted doctrines in the philosophy of science I ought to present Figure 1 as showing the crucial experiment that started all the theorists trying to explain this exciting new phenomenon, it would be a little unfair to do so, since some, at least, of the theorists did not learn about the photograph until years after they had published their theories. Motives of theorists are sometimes inscrutable, and I will not try to explain them. Rather, as the starting point of the second period, I shall take a paper published by Reiner[3] in 1945, in which he went back to the definition of fluid given by Stokes[4] 100 years earlier and put it into mathe-

Fig. 1. Merrington's efflux phenomenon.

matical form without adopting the customary linearization. Stokes conceived a fluid as a material in which all differences of pressure from that given by the thermal equation of state are assignable functions of the rate at which the shape of the material is changing:

$$\mathbf{s} = -p\mathbf{1} + \mathbf{f}(\mathbf{d}), \qquad \mathbf{f}(0) = 0 \tag{1}$$

where $\mathbf{s}$ is Cauchy's stress tensor and $\mathbf{d}$ is Euler's stretching tensor. This theory includes a very simple concept of pure viscosity. Whether this idea is physically correct may now be seen to be less important, in the history of rheology, than the determination of its mathematical consequences. For Reiner was able to show, rediscovering an older result from the theory of invariants, that for all polynomial functions $\mathbf{f}$ in eq. (1), it is possible to replace eq. (1) by the apparently simpler relation

$$\mathbf{s} = (-p + A)\mathbf{1} + B\mathbf{d} + C\mathbf{d}^2 \tag{2}$$

where A, B, C are scalar polynomial functions of the principal scalar invariants of $\mathbf{d}$. Various proofs of this *representation theorem for isotropic tensors* have been given, under clearer and weaker hy-

potheses, by various authors. Its importance lies in the survey it furnishes of all the infinitely many special theories of viscosity included in Stokes's proposal [eq. (1)]. In particular, it gives an immediate qualitative explanation of the swelling observed by Merrington. For in a simple shearing flow we have

$$\mathbf{d} \propto \begin{Vmatrix} 0 & 1 & 0 \\ 1 & 0 & 0 \\ 0 & 0 & 0 \end{Vmatrix} \tag{3}$$

hence

$$\mathbf{d}^2 \propto \begin{Vmatrix} 1 & 0 & 0 \\ 0 & 1 & 0 \\ 0 & 0 & 0 \end{Vmatrix} \tag{4}$$

Substitution into eq. (2) shows that the normal stresses *cannot* be equal, if $\mathbf{d} \neq 0$, except in the very special theories for which $C = 0$. Far from being in any way extraordinary, Merrington's effect is *typical* of nonlinearity. Its presence indicates nonlinearity but does not confirm any particular nonlinear theory. When we realize that the representation theorem applies to any continuous relation between two symmetric tensors of second order, we see that inferences from it apply not only to the theory of simple viscosity but also to various theories of elastic and plastic response.

While what was just said is somewhat vague, it may be rendered more precise by appeal to a number of exact solutions of the full set of equations of the theory of nonlinear viscosity and of the classical theory of finite hyperelasticity in the incompressible case, obtained by Rivlin[5–8] in 1947–1949. On the one hand, these solutions, especially those for elasticity, yield precise mathematical predictions, within the respective theories, for several situations of great practical and experimental interest: in elasticity, simple extension, simple shear, simple torsion, and inflation of a hollow circular tube; in nonlinear viscosity, simple shearing, flow down a cylindrical tube, flow within concentrically rotating cylinders, and spiral flow. On the other hand, and more important, these solutions enable whole classes of theories to be compared and contrasted, for the functions such as A, B, C which enter the equations are left arbitrary. The material constants of the classical theories have been replaced by *material functions* specifying the stress arising in response to a particular deforma-

tion. Unlike the dozens of purely arbitrary constants scattered within the older rheological theories, however, these are delimited: they may depend upon the deformation only in a particular way, shown to follow mathematically from the original defining equations.

By 1949 it could be said fairly that all work on the foundations rheology done before 1945 had been rendered obsolete. The phenomenon of normal stresses had been shown to be of second order, while departures from the classically assumed linear relation between shearing tractions and rates of shearing are of third order in the rates. The old viscometers, designed without a thought of normal stresses, had fixed opaque walls to help the experimenter overlook the most interesting effect in the apparatus or to prevent his measuring the forces supplied so as to negate it. By theory, the phenomenon of normal stresses was straightaway seen to be a universal one, to be expected according to all but very special kinds of nonlinear theories. Of course a result so universally to be expected must have been occurring for a long time in nature, and it was quickly seen that many familiar effects, such as the tendency of paints to agglomerate upon stirring mechanisms, as well as some carefully concealed mysteries of the artificial fiber industry, are examples of it, though a century of linear thinking in physics had blinded theorists to the possibility that simple mechanics, rather than chemistry, is all that is needed in explanation.

Successful prediction of certain striking effects might be thought to produce a comfortable triumph of the theorists, but it did not. From the position of being unable to explain the phenomena of nature we were converted, almost overnight, to being able to explain them too easily: Almost any sort of proper nonlinear theory would do. Thus began a two-fold search, in theory and in experiment, for features of the effects which could serve to distinguish one theory from another. It is much easier for a philosopher of science to tell us that science is experimental than it is for an experimenter to measure something important correctly. Moreover, since theory allows such latitude, any measurement of values of a single quantity, such as a shearing stress, is useless unless correlated to measurements in a different experiment on the same substance. Theory reveals, however, certain relations of a universal kind which do not require numerical determination of any modulus. In the theory based upon Stokes's ideas, for example, the pressure on a plane normal to a shearing flow equals

that on a shearing plane and is unequal to that on the plane of shearing; this is true *whatever* are the values of the material functions A, B, C. From certain semi-theoretical arguments Weissenberg[9] in 1947 asserted that, on the contrary, the pressures on all planes parallel to the flow should be equal. Here is a case of open conflict on a matter which is closer to experimental measurement than are most results obtained by theorists. Considerable argument has arisen over the ramifications of this difference, but it seems that current opinion regards the Reiner-Rivlin theory, while typical of nonlinear continuum mechanics and attractively simple, as inadequate to represent any physical material yet tested. A very recent unpublished study by Coleman and Noll shows that this is only to be expected from the theoretical standpoint as well.

In this second period of theoretical rheology, we have said, *some particular idea of material response was laid down, put into precise mathematical from, and explored by exact mathematical analysis.* Another idea of this kind, which I proposed [10–11] in 1953 and later named "hypoelasticity," replaces the classical concept of elastic response by a relation among time rates:

$$d\mathbf{s}/dt = \mathbf{f}(\mathbf{s},\mathbf{d}) \tag{5}$$

The motivation is to eliminate the perfect memory of the initial state, which characterizes the classical theory, and instead to consider a material responding only to changes from the immediately preceding state. As soon as time rates occur in a theory, however, a new problem arises, for if a relation of the type of eq. (5) holds in one reference frame, it cannot hold in another rotating with respect to it. Now this is not right, for the response of a material is independent of the observer. Therefore the ordinary time derivative on the left-hand side of eq. (5) should be replaced by a derivative which is the same for all observers. In a special case, an equivalent problem had been recognized and solved long ago by Cauchy[12]; that it is precisely this problem which makes generalization of Maxwell's viscoelasticity to three dimensions not a trivial matter was recognized in 1903 by Zaremba,[13–14] who gave an adequate solution for another special case; and a general solution was given in 1950 by Oldroyd,[15] who, however, did not state the problem he had solved clearly enough for other students to see what it was until they found it out for themselves. In 1955 the whole matter was set straight by Noll,[16] who

stated the above requirement clearly as a postulate for all theories of materials and indicated the variety of methods by which it may be solved; the principle is now known as *material objectivity* or *material indifference*, but this brings us past the second period of the subject.

While the second period, which may be regarded as closed by *The Mechanical Foundations of Elasticity and Fluid Dynamics*[17] in 1952–1953, gained a number of theoretical predictions of remarkable completeness, these are the least of what it gave us. Next is the fact that with little exaggeration, *there are no one-dimensional problems:* A situation which is one dimensional in a linear theory is automatically two dimensional or three dimensional in any reasonable nonlinear theory. More important is the *independence in theory* which resulted from the realization that any sort of admissible nonlinearity would yield the correct general kind of behavior, and that to account for the phenomena, far from being difficult, was all too easy. Of a theory, we learned that both less and more had to be expected. To calculate the creep in a buckled elliptical column with a square hole in it is too much until the response of materials shall be better understood than it is today; to be satisfied with a normal stress of the right sign and order, with an adjustable coefficient, is too little until the response of the *same* material in a *variety* of situations is determined and correlated, with no material constants or functions altered in the process. What is needed is a theory of theories.

To gain such a theory, we have to recognize that the main tool used in the second period is the concept of *invariance*. Three distinct kinds of invariance in addition to classical tensor concepts were used:

(*1*) The invariance resulting from the fact that *space is three dimensional*. For the simpler theories, this is the real content of the representation theorem. In a space of two dimensions, clearly, the normal stress effect in nonlinear viscosity would not occur, since it results only from the term $C\mathbf{d}^2$ in eq. (2). In a four-dimensional space, there would be a term $D\mathbf{d}^3$ allowing a wholly new kind of normal and shear stress complications not present in the three-dimensional case.

(*2*) *Invariance of response*, expressed by the principle of material indifference.

(*3*) *Invariance of manifestation*. According to the *principle of equipresence*, which I proposed[18,19] in 1949, all phenomena occurring contribute to all effects resulting, except as forbidden by other re-

quirements of invariance. Deformation, for example, gives rise not only to stress, as in the earlier nonlinear theories, but also to flow of energy, not included as a possibility in any classical theory. This phenomenological principle corresponds to the fact that on the molecular scale it is the same molecular actions which are giving rise to all the gross effects. The separation of effects familiar in the classical linear theories is a consequence of the different tensorial character of the variables, combined with linearization, nothing else.

While invariance was the chief servant of the theorist in the second period, in the third and current period it has become the master. The *most general response* consistent with the phenomena and the accepted requirements of invariance is sought. After this has been determined, different kinds of material possibilities are classified according to different kinds of more special invariance exhibited. While I shall not try to summarize this work, I mention that the program, as far as pure mechanics is concerned, has been brought to some measure of completion by Noll.[20,21] He begins from a *principle of determinism*, according to which the stress at a given particle in any material is determined by all the past experience of a small neighborhood of that particle:

$$\mathbf{s} = \overset{\tau = t}{\underset{\tau = -\infty}{\mathfrak{F}}}[\operatorname{grad} \mathbf{x}]$$

$\mathfrak{F}$ being a functional of the deformation gradient at all times from $-\infty$ to t. This theory, with a different emphasis, had been proposed earlier by Green and Rivlin.[22] Nearly all the theories of the second period are included as special cases. Noll then defines the *isotropy group* of a material as the group of transformations of the material particles under which all material properties are invariant. A simple fluid, for example, is defined as one having the largest possible isotropy group. This viewpoint, while it may seem somewhat abstract, has the virtues not only of conciseness but also of simplicity in concept. It is really much easier to understand and visualize physically than is the older kind of idea in which one or another quantity is supposed purely formally to be a function of one or more particular variables, so that a mass of elaborate tensorial calculation ensues. For example, Coleman and Noll[23] have succeeded in showing that Rivlin's solutions[24] for viscometers according to the viscoelastic theory of Rivlin and Ericksen,[25] involving eight material func-

tions, can be extended to all materials satisfying this very general definition of a fluid, and that in fact, as previously conjectured by Markovitz,[26] only three material functions are needed to describe and correlate all these exact solutions. On the basis of these solutions, a rational program of viscosity measurements at last becomes possible; as I understand, it is being undertaken by Markovitz. More than this, the result shows the extreme insensitivity of the classical viscometric tests to the nature of the fluid. All simple fluids behave in essentially the same way in all these tests, with three material functions, no more, disposable and determinable, in principle, by a proper sequence of measurements in *any one* of the classical tests, leaving room for check against the results of the others. This is both a gain and a loss: a gain in that as far as viscometric measurements are concerned, the experimenter may forget about most of the possible distinctions between one kind of fluid and another and thus drastically simplify his program; a loss in that now we know that two fluids which behave just alike in all the classical viscometers may, and generally will, behave entirely differently from each other in some other situation, such as, say, flow in an elliptical pipe, as is shown by some studies of Ericksen[27,28] in a more special theory.

The most interesting work now being done concerns amplification of the mechanical theories to include thermal and electromagnetic effects. This I will not describe. Instead, I shall revert to a different aspect of the mechanics of deformation, the molecular one.

Since the experiments exhibiting the most dramatic nonlinearities are done on polymers, theories of long chain molecules have been much cultivated, and it is natural that the effects themselves have become associated with a complex molecular structure. This is not right, nor is it correct to think that complex structure is necessary for such effects to be noticeable or to predominate over the classical linear response. I have mentioned Maxwell's paper[1] of 1867 on the kinetic theory as a major source of rheology; apparently, however, the rheologists did not read past the first few pages, for the latter part of the paper illustrates Maxwell's ideas of viscoelasticity by detailed elaboration of a particular molecular model, the dilute monatomic gas. No structure could be simpler: the molecules are points which move in straight lines at constant speed between their relatively rare encounters with one another, at which they rebound according to a specified law. This may not be a kind of material in which rheologists

are interested, but the kinetic theory has one great advantage over the theories of long chain molecules, namely, that it has been put into a mathematically precise, unequivocal, and universally accepted form, meaningful and properly invariant for deformations of any magnitude and excitations of any kind. In a word, it is a fully dynamical theory, though one of celebrated difficulty.

After their common start, rheology and the kinetic theory of gases pursued their separate ways until 1956, when I had the good luck to hit upon the exact solution in the kinetic theory for a kind of simple shearing flow.[29] The same solution was found also by Galkin[30] in Russia. The law of collision is assumed to be a repulsion as the inverse fifth power of the distance, not a good model for real gases but nevertheless sufficient for illustrating how an assembly of molecules in rapid motion may behave; in fact, more realistic laws of molecular interaction will lead rather to more than to less complicated gross effects. As usual, the velocity field studied is

$$u = Ky, \qquad v = 0, \qquad w = 0 \tag{6}$$

where u is the velocity in the x-direction and K is a constant, and also we assume that the density

$$\rho = \text{const. in space and time} \tag{7}$$

It is then impossible that the stresses in this steady flow can be steady, for work is continually being done upon the fluid, so that it will heat more and more, and since $p = R\rho\vartheta$, p must increase steadily. The theory is a fully thermomechanical one; not only the equations of motion but also the equation of energy is taken into account; and the linear viscosity is proportional to the temperature, $\mu = \alpha\vartheta$. It turns out that the governing parameter is the *truncation number* $\mathfrak{Z}$,

$$\mathfrak{Z} = \mu K/p = \alpha K/R\rho \tag{8}$$

which I had introduced for continuum mechanics[31] in 1948. When $\mathfrak{Z}$ is small, the rate of shearing is not too great and the density is not too low, while large values of $\mathfrak{Z}$ correspond to rapid shearing or to low densities. If we neglect a transient which is rapidly damped as time increases, the ratios of the remaining pressures $p_{ij}{}^D$ to the corresponding static pressure p^D turn out to be functions of $\mathfrak{Z}$ only. The behavior of the ratios $p_{ij}{}^D/p^D$ is most easily assessed from Figure 2.

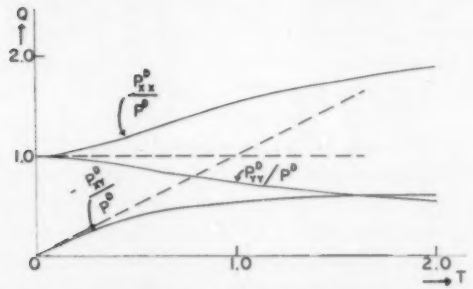

Fig. 2. Pressure ratios in shear flow of a Maxwellian gas. The dashed lines represent the linear approximations.

The straight lines show the pressures according to the linear theory of viscosity. The full lines exhibit characteristic features of the nonlinear theories of continua. As $\mathfrak{Z}$ increases, the shear stress falls rapidly from the Newtonian value; before this effect, which is of third order in $\mathfrak{Z}$, becomes noticeable, however, the second order normal stress effects manifest themselves. Since $p_{yy}{}^{D} = p_{zz}{}^{D}$, the normal stresses on all planes parallel to the flow are equal; that is, the Weissenberg relations are satisfied, though this fact should not be taken as implying any validity to the assumptions from which they were first inferred. The pressures on these planes are less than the mean pressure, while the normal pressure is greater. As soon as $\mathfrak{Z}$ is as large as 1, all the effects of nonlinearity are of the same order as would be the linear ones in a linear theory. Since the model is not an accurate one for real gases, accurate numerical values are not informative, but a rough idea can be gained by inserting for α an empirical value of μ/θ for air at 288°K. This gives

$$\mathfrak{Z} = 2.2 \times 10^{-13}(K/\rho) \tag{9}$$

if K is measured in sec.$^{-1}$ and ρ is measured in g./cc. At 1 atm., then, a rate of shearing of the order of 0.5×10^{10} sec.$^{-1}$ is required in order to get $\mathfrak{Z}$ so large as 1. This is indeed a high rate of shearing. However, large values of $\mathfrak{Z}$ may be gotten instead simply by rarefying the gas. In a vacuum of 10^{-10} atm., $\mathfrak{Z} = 1$ for the rather slow shearing of 0.5 sec.$^{-1}$. Effects of nonlinearity in gases are to be expected as the rule in high altitude flight, where, it is believed, the density falls ultimately to arbitrarily small values.

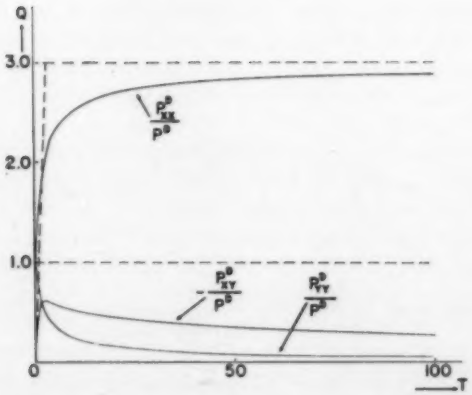

Fig. 3. The same solution as in Fig. 2, but for a greater range of truncation numbers.

Without any claim in regard to experiment, but only as a specimen of what a real molecular theory predicts, consider the behavior of the pressures when $\mathfrak{z}$ is allowed to grow 100 times as large (Fig. 3).

The linear effects are now scarcely perceptible. The ratio of shearing stress to mean pressure rises to the maximum value 0.61 when $\mathfrak{z} = 2.5$; thereafter it decreases and approaches 0 slowly as $\mathfrak{z} \to \infty$. Thus even the classical notion that the greater the shearing rate, the greater is the shearing stress, must be abandoned. This is not so startling as it might first seem, for both the shearing stress and the mean pressure increase very rapidly in time in order to maintain the shearing; that the ratio of these two quantities, which is independent of time, is less for a more rapid shearing only reflects the growth of the normal stresses, which of course contribute to the mean pressure but not to the shearing stress. While the normal stresses on planes parallel to the flow diminish to 0, that on a plane normal to the flow increases rapidly until it dominates the phenomenon. This is easy to understand in terms of the molecular model, for when the gas is very thin, so that collisions are rare, in order to maintain the distribution of mean velocity in the shearing flow it is necessary that the individual molecular velocities must be aligned in almost the same way. Thus transfer of momentum across the planes

parallel to the flow is insignificant in comparison to transfer across the planes normal to the flow. This explanation makes us realize that some of the typical effects of nonlinear continuum mechanics have long been familiar, though differently regarded, in the phenomena occurring in evacuated tubes. This is not the only class of results which have, on the basis of puerile confusion of sufficiency with necessity, been deemed outside the sphere of continuum mechanics. Let it be expressly noted that for the special flow just studied, the *exact results* predicted by the kinetic theory include formulas for the stresses which are simply and easily recognized as special cases of those given by the Zaremba-Noll theory of viscoelasticity.

The example of the Maxwellian gas suggests that the effects of nonlinear viscosity, far from being peculiar to a complex molecular structure, are to be expected from *any* molecular structure. Indeed, as should be plain from the researches in the continuum theories, those effects are not at all extraordinary. Nonlinear irreversible response is typical of mechanics.

References

1. Maxwell, J. C., *Phil. Trans. Roy. Soc. London*, **157,** 49 (1867); *Phil. Mag.*, (4) **35,** 129, 185 (1858). Papers **2**, 26–78.
2. Merrington, A. C., *Nature*, **152,** 663 (1943).
3. Reiner, M., *Am. J. Math.*, **67,** 350 (1945).
4. Stokes, G. G., *Trans. Cambridge Phil. Soc.*, **8** (1844–1849), 287 (1845). Papers **1**, 75–129.
5. Rivlin, R. S., *Phil. Trans. Roy. Soc. London*, **A241,** 379 (1948).
6. Rivlin, R. S., *Proc. Roy. Soc. London*, **A195,** 463 (1949).
7. Rivlin, R. S., *Proc. Roy Soc. London*, **A193,** 260 (1948).
8. Rivlin, R. S., *Proc. Cambridge Phil. Soc.*, **45,** 88 (1949).
9. Weissenberg, K., *Nature*, **159,** 310 (947).
10. Truesdell, C., *J. Rational Mech. Anal.*, **2,** 593 (1953).
11. Truesdell, C., *J. Rational Mech. Anal.*, **4,** 83, 1019 (1955).
12. Cauchy, A., *Ex. Math.*, **4,** 293 (1829); *Œuvres*, (2) **9,** 243.
13. Zaremba, S., *Bull. Int. Acad. Sci. Cracovie*, **1903,** 594.
14. Zaremba, S., *Bull. Int. Acad. Sci. Cracovie*, **1903,** 614.
15. Oldroyd, J. G., *Proc. Roy. Soc. London*, **A200,** 523 (1950).
16. Noll, W., *J. Rational Mech. Anal.*, **4,** 3 (1955).
17. Truesdell, C., *J. Rational Mech. Anal.*, **1,** 125 (1952). See also Ref. 10.
18. Truesdell, C., U. S. Naval Research Lab. Report No. P-3553 (1949); *J. Math. Pures Appl.*, (9) **30,** 111 (1951).
19. Truesdell, C., *Appl. Mech. Rev.*, **12,** 75 (1959).
20. Noll, W., Carnegie Inst. Tech. Rep. No. 17, Air Force Off. Sci. Res. (1957).

21. Noll, W., *Arch. Rational Mech. Anal.*, **2** (1958/9), 197 (1958).
22. Green, A. E., and R. S Rivlin, Brown Univ. Rep. No. C11-17 (1956); *Arch. Rational Mech. Anal.*, **1** (1957/8), 1 (1957).
23. Coleman, B. D., and W. Noll, *Arch. Rational Mech. Anal.*, **3**, 289 (1959).
24. Rivlin, R. S., *J. Rational Mech. Anal.*, **5**, 179 (1956).
25. Rivlin, R. S., and J. L. Ericksen, *J. Rational Mech. Anal.*, **4**, 323 (1955).
26. Markovitz, H., *Trans. Soc. Rheol.*, **1**, 37 (1957).
27. Ericksen. J. L., *Quart. Appl. Math.*, **14**, 319 (1956).
28. Criminale, W. O., Jr., J. L. Ericksen, and G. L. Filbey, Jr., *Arch. Rational Mech. Anal.*, **1** (1957/8), 410 (1958).
29. Truesdell, C., *J. Rational Mech. Anal.*, **5**, 55 (1956).
30. Galkin, V. S., *Prikl. Mat. Mekh.*, **20**, 445 (1956).
31. Truesdell, C., *Proc. Natl. Acad. Sci. U.S.*, **34**, 342 (1948).

Synopsis

Theoretical work on rheological materials shows three distinct phases. (*1*) Early work, to 1945: Simple models, mainly one dimensional and linear, are constructed by analogy to discrete systems. Various coefficients are named. (*2*) Intermediate period, 1945–1955: Ideal materials exhibiting nonlinear response are defined explicitly as exact mathematical realizations of a simple idea. Their properties are studied by means of general theorems and special exact solutions. (*3*) Current phase, from 1955: The most general constitutive equations consistent with the observed phenomena are determined. Work of the second and third kinds is summarized, with particular reference to the different roles of methods of invariance. Open problems are stated.

TRANSACTIONS OF THE SOCIETY OF RHEOLOGY IV, 23–28 (1960)

Relations between Hypo-elasticity and Elasticity

BARRY BERNSTEIN, *U. S. Naval Research Laboratory, Washington, D.C.*

Introduction

The equations of hypo-elasticity were introduced by Truesdell.[5] It was his stated intention to find a new concept of elastic behavior, mutually exclusive with the theory of finite strain, which reduces to the classical theory of elasticity under the appropriate assumptions. But Noll[4] has shown that every isotropic finitely elastic body, for which the stress-strain relations are invertible, is also a hypo-elastic body. It is natural, then, to ask if hypo-elasticity includes finite elasticity and to seek conditions under which a hypo-elastic material is elastic. Our purpose here is to state without proof the results of some researches on these questions, reserving the mathematical arguments for publication elsewhere.

Elasticity

A motion of a material[2,4] is a set of smooth mappings into space of a set of material points and time. Material points are designated by numerical values of three quantities, X^A, $A = 1, 2, 3$, called material coordinates, which may be taken, for example, to be the cartesian coordinates of the positions of the material points at some time. Time is denoted by t. Thus the functions, or mappings, which give a motion may be written

$$x^i = \mathbf{x}^i(X^A,t) \qquad i = 1,2,3 \qquad (1)$$

where lower case italic letters denote cartesian coordinates of positions in space, bold face letters indicate functions, and light face letters denote their values (when the distinction is important). The displacement gradients, $x_A{}^i$, are defined by

$$x_A{}^i \equiv \partial \mathbf{x}^i(X^B,t)/\partial X^A \tag{2}$$

and their inverses $X_i{}^A$ are obtained by solving eq. (1) for X^A,

$$X^A = \mathbf{X}^A(x^i,t) \tag{3}$$

and writing

$$X_i{}^A \equiv \partial \mathbf{X}^A(X^J,t)/\partial x^i \tag{4}$$

A material is called elastic in the sense of Cauchy, or Cauchy elastic, if its constitutive relations have the form

$$t^{ij} = \mathbf{t}^{ij}(x_A{}^i,X^B) \tag{5}$$

where t^{ij} denotes stress. Henceforth, all tensors with lower case italic indices will be cartesian tensors, so these indices may be written up or down interchangeably. Summation from 1 to 3 will be understood on all indices repeated in a term.

If there exists a scalar function

$$\Sigma(x_A{}^i,X^B)$$

so that eq. (5) takes the form

$$t_j{}^i = \frac{\rho}{\rho_0}\, x_A{}^i \frac{\partial \Sigma(x_B{}^k,X^D)}{\partial x_A{}^j} \tag{6}$$

where ρ is the mass density and ρ_0 is the mass density at X^B for some fixed value of $x_B{}^k$, the material (5) will be said to be elastic in the sense of Green, or Green elastic. Green elastic materials are Cauchy elastic materials for which there exists a strain energy function.

Hypo-elasticity

The equations of hypo-elasticity may be written in the form[4]

$$\overset{\circ}{t}_{ij} \equiv \dot{t}_{ij} - t_{ik}\omega_{jk} - t_{jk}\omega_{ik} = \mathbf{A}_{ijkl}(\mathbf{t}_{pq})d_{kl} \tag{7}$$

where the dot denotes material differentiation, and

$$\omega_{ij} = {}^1/_2[(\partial v_i/\partial x^j) - (\partial v_j/\partial x^i)],$$
$$d_{ij} = {}^1/_2[(\partial v_i/\partial x^j) + (\partial v_j/\partial x^i)],\ v_i = \dot{x}^i$$

and $\mathbf{A}_{ijkl}$ is an isotropic tensor function of stress. Alternatively, eq. (7) may be written in the form

$$\dot{t}_{ij} = \mathbf{B}_{ijkl}(t_{pq})X_l{}^A\dot{x}_A{}^k \tag{8}$$

In general, eqs. (7) or (8) are not in themselves sufficient to define a hypo-elastic material. We now define a representation of a hypo-elastic material.

Consider a smooth manifold of material points $\mathfrak{M}$. An assignment of values of t_{ij} and $x_A{}^k$, subject to the compatibility conditions

$$\partial x_A{}^k/\partial X_B{}^k = \partial x^s/\partial X^A$$

over $\mathfrak{M}$ will be called a stress-configuration pair and denoted by

$$\{t_{ij}, x_A{}^k\}$$

Given two stress-configuration pairs,

$$\{\overset{1}{t}_{ij}, \overset{1}{x}_A{}^k\} \text{ and } \{\overset{2}{t}_{ij}, \overset{2}{x}_A{}^k\}$$

it may or may not be possible to find a solution of eq. (8), subject to the compatibility conditions, for which $\{\overset{1}{t}_{ij}, \overset{1}{x}_A{}^k\}$ gives the initial values and $\{\overset{2}{t}_{ij}, \overset{2}{x}_A{}^k\}$ the final values. But it is to be noted that if we group the stress-configuration pairs into classes, two such pairs being in the same class if it is possible to get from one to the other by a solution of eq. (8), subject to the compatibility conditions, then these classes are equivalence classes and are mutually exclusive. *A representation of a hypo-elastic material is given by eq.* (7) *or* (8) *and one such equivalence class of stress configuration pairs.* We would say that two representations define the same material if they differ by a transformation of material coordinates.

To illustrate the motivation for this definition, consider the following set of hypo-elastic equations:

$$\mathring{t}^{ij} = -(t^{kk}/3)\delta^{ij}d^{ll} \tag{9}$$

It can be shown that if the stress is ever a hydrostatic pressure at a material point, it is always such, and conversely, if it is once not a hydrostatic pressure it is never such. If it is once a hydrostatic pressure at all material points, the material is a perfect gas, which is elastic in the sense of Green. Otherwise, the material is not elastic even in the sense of Cauchy. Thus in general to define a representation of a hypo-elastic material, we must specify at least one stress-configuration pair.

This matter is of course related to ordinary differential equations where, in order to specify a solution, one must give some conditions, such as initial conditions, in addition to the equations themselves. Indeed, the equations of hypo-elasticity may be regarded as a set of ordinary differential equations.

Conditions for a Hypo-elastic Material to Be Elastic

The first result which we state in this section is the following:

If a hypo-elastic material has the property that in any motion, at the end of which the material points return to the same positions which they had at the beginning, the work done by the stresses is non-negative, then it must be zero and the material is elastic in the sense of Green.

Results of this type have been proven before. Caprioli[3] showed that if for a Cauchy-elastic material there is a preferred value of the strain such that in any motion in which this preferred value is the initial value, the work done by the stresses is non-negative, then the material is elastic in the sense of Green. Bernstein and Ericksen[6] proved theorems of this type for the existence of stress energy functions in hypo-elasticity.

Now we turn to the eqs. (7) and (8) themselves. Necessary and sufficient that there be a Cauchy-elastic material satisfying eq. (8) is that the overdetermined system of differential equations

$$\partial t_{ij}/\partial x_A{}^k = B_{ijkl}X_l{}^A \tag{10}$$

have a solution. The standard theory for such systems[1] may be applied to obtain integrability conditions, the first set of which reads

$$(\partial B_{ijkl}/\partial t_{rs})B_{rspq} - (\partial B_{ijpq}/\partial t_{rs})B_{rskl} - B_{ijkq}\delta_{pl} + B_{ijpl}\delta_{kq} = 0 \tag{11}$$

Further integrability conditions are derived by differentiating those already obtained with respect to $x_A{}^k$ and eliminating first derivatives by the use of eq. (10). If by this process more than six independent integrability conditions occur, then there is no elastic material satisfying eq. (8). If, however, the total number is $k \leq 6$, then there exist elastic materials satisfying eq. (8) with $6\text{-}k$ of the components of stress assigned arbitarily for one value of $x_A{}^i$.

Necessary and sufficient that all hypo-elastic materials satisfying eq. (8) *be elastic in the sense of Cauchy is that* eq. (11) *hold identically in* t_{ij}. Furthermore, we may show: *Given that a hypo-elastic material*

satisfying eqs. (7) *and* (8) *is elastic in the sense of Cauchy, necessary and sufficient that it be elastic in the sense of Green is that*

$$A_{ijkl} + t_{ij}\delta_{kl} = A_{klji} + t_{lk}\delta_{ji} \tag{12}$$

for all values of stress that occur.

Necessary and sufficient that all hypo-elastic materials satisfying eqs. (7) *and* (8) *be elastic in the sense of Green is that* eqs. (11) *and* (12) *hold identically in* t_{ij}.

Conclusion

It can be seen, from the above discussion, that among hypoelastic materials, those which are also elastic form a special class. Whether all elastic materials are hypo-elastic must be answered in the negative. An elastic material is isotropic with respect to a given reference configuration (i.e., set values of $x_A{}^i$ over $\mathfrak{M}$) if its constitutive equations are invariant with respect to arbitrary orthogonal transformations (including rotations, reflections, and translations) of the reference configuration. An elastic hypo-elastic material is isotropic with respect to a given reference configuration if and only if the stress is a uniform hydrostatic pressure for the reference configuration. Since there are anisotropic elastic materials for which the stress may be made a uniform hydrostatic pressure, we have examples of anisotropic elastic materials which cannot be hypo-elastic. Moreover, examples of elastic isotropic materials which are not hypo-elastic may be obtained if the restriction that the stress-strain relations are invertible is relaxed.

The foregoing is an attack on the relations between hypo-elasticity and elasticity in which criteria are sought for both theories to define the same material. The author believes, however, that the relations between these theories would be better seen in terms of some more general theory which is just general enough to include both hypo-elasticity and elasticity. This we set as a problem for future study.

References

1. Eisenhart, L. P., *Differential Geometry*, Princeton Univ. Press, Princeton, 1947.
2. Truesdell, C., *J. Rational Mech. Anal.*, **1**, 125 (1952).
3. Caprioli, L., *Boll. Un. Mat. Ital.*, (3) **10**, 481 (1955).
4. Noll, W., *J. Rational Mech. Anal.*, **4** (1955).

5. Truesdell, C., *J. Rational Mech. Anal.*, **4**, 83 (1955).
6. Bernstein, B., and J. L. Ericksen, *Arch. Rational Mech. Anal.*, **1**, 396 (1958).

Synopsis

The equations of hypo-elasticity are not in general sufficient to define a material. It is necessary in addition to indicate one stress-strain configuration. Conditions may be written which test whether any or all materials satisfying a given set of hypo-elastic equations are elastic in the sense of Cauchy or in the sense of Green. If the hypo-elastic material is a work hardening material, it must be elastic in the sense of Green.

TRANSACTIONS OF THE SOCIETY OF RHEOLOGY IV, 29–39 (1960)

Theory of Anisotropic Fluids

J. L. ERICKSEN,* *The Johns Hopkins University, Baltimore, Maryland*

I. Introduction

We present results of recent researches on properly invariant theories of anisotropic fluids. These suggest that such theories are better able to describe the observed behavior of some fluids commonly regarded as isotropic than are comparably simple theories of isotropic fluids. They also provide a basis for exploring this possibility.

We restrict our attention to fluids having a single preferred direction at each point. One might visualize these as fluids consisting of particles which are figures of revolution, the preferred direction being the axis of revolution. This general type of symmetry is assumed in theories of liquid crystals, as is discussed by Oseen.[1] However, the theories to be discussed exclude a type of long range interaction which seems to be important in these liquids.

II. Equations of Motion

Equations of conservation or balance of mass, linear momentum, moment of momentum, and energy provide a starting point for formulating theories of continua. Let v denote any material volume with boundary s and let ρ, $\mathbf{p}$, $\mathbf{m}$, and e denote the densities of these quantities. The usual forms of these laws are then

$$\frac{d}{dt}\int_v \rho dv = 0$$

$$\frac{d}{dt}\int_v \mathbf{p} dv = \oint \mathbf{t} ds + \int_v \mathbf{f} dv \tag{1}$$

* Consultant, National Bureau of Standards.

$$\frac{d}{dt}\int_v \mathbf{m}dv = \oint_s \mathbf{r}\times\mathbf{t}ds + \int_v \mathbf{r}\times\mathbf{f}dv$$

$$\frac{d}{dt}\int_v edv = \oint_s (\mathbf{v}\cdot\mathbf{t} - q)ds + \int_v \mathbf{v}\cdot\mathbf{f}\,dv$$

where $\mathbf{t}$ is the stress vector, $\mathbf{f}$ the body force per unit volume, $\mathbf{r}$ the position vector from any origin, $\mathbf{v}$ the velocity, and q the heat flow. These will suffice for our purposes. It is our opinion that, for liquid crystals, generalizations of these of the type discussed by Grad[2] should be used. As usual, we assume the existence of a stress tensor t_{ij} and heat flux vector q_i such that

$$t_i = t_{ij}\nu_j, \qquad q = q_i\nu_i \tag{2}$$

where ν_i is the unit normal to s, directed outward relative to v. Under relatively weak smoothness assumptions, the existence of these can be derived by reasoning entirely similar to that used by Noll.[3]

A single preferred direction can be described by a vector $\mathbf{n}$. We assume that

$$\mathbf{p} = \rho\mathbf{v},\ \mathbf{m} = \rho(\mathbf{r}\times\mathbf{v} + \mathbf{n}\times\dot{\mathbf{n}}),\ e = \rho(\epsilon + {}^1\!/_2\,\mathbf{v}\cdot\mathbf{v} + {}^1\!/_2\,\dot{\mathbf{n}}\cdot\dot{\mathbf{n}}) \tag{3}$$

where the dot denotes the material derivative and ϵ is internal energy per unit mass. As is discussed by Ericksen,[4] eq. (3) is suggested by calculations of linear momentum, moment of momentum, and kinetic energy of a dumbbell molecule. In this model, $\mathbf{v}$ is identified with the velocity of the center of mass and $\mathbf{n}$ is proportional to the vector joining the two masses. If we set $\mathbf{n} = 0$ in eq. (3), we obtain relations commonly used in continuum mechanics.

Oseen's[1] work as well as further consideration of the above model suggests that we should also introduce equations of the form

$$\rho\ddot{n}_i = g_i \tag{4}$$

Ericksen[4] shows that eqs. (1)–(4) imply that

$$\dot{\rho} + \rho\dot{x}_{j,j} = 0 \tag{5}$$

$$\rho\ddot{x}_i = t_{ij,j} + f_i \tag{6}$$

$$\rho\dot{\epsilon} = t_{ij}d_{ij} - g_i\dot{n}_i - q_{j,j} \tag{7}$$

$$n_ig_j - n_jg_i + t_{ij} - t_{ji} = 0 \tag{8}$$

where

$$2d_{ij} \equiv \dot{x}_{i,j} + \dot{x}_{j,i}$$
$$\hat{n}_i \equiv \dot{n}_i - w_{ij}n_j$$
$$2w_{ij} \equiv \dot{x}_{i,j} - \dot{x}_{j,i}$$

A determinate system of equations is obtained by assuming:

(*a*) There is a local caloric equation of the form $\epsilon = \epsilon(\rho, n_i, s)$, where s is entropy per unit mass.

(*b*) t_{ij}, g_i, and q_i are all functions of ρ, n_i, $\hat{n}_i$, $v_{i,j}$, T, and $T_{,j}$, linear in the variables $\hat{n}_i$, $v_{i,j}$, and $T_{,j}$. Here T denotes absolute temperature, given by $T = \partial\epsilon/\partial s$.

(*c*) The form of these relations is preserved under all time dependent proper orthogonal coordinate transformations.

(*d*) The structure represented by $\mathbf{n}$ is symmetric with respect to reflections in planes parallel and perpendicular to $\mathbf{n}$.

It then follows that

$$\epsilon = \epsilon(\rho, n^2, s), \qquad n^2 = n_i n_i \tag{9}$$

$$\begin{aligned} t_{ij} = {} & (\alpha_0 + \alpha_1 d_{kk} + \alpha_2 d_{km}n_k n_m + \alpha_3 \hat{n}_k n_k)\delta_{ij} \\ & + (\alpha_4 + \alpha_5 d_{kk} + \alpha_6 d_{km}n_k n_m + \alpha_7 \hat{n}_k n_k)n_i n_j \\ & + \alpha_8 d_{ij} + \alpha_9 d_{ik}n_k n_j + \alpha_{10} d_{jk}n_k n_i + \alpha_{11} n_i \hat{n}_j + \alpha_{12} n_j \hat{n}_i \end{aligned} \tag{10}$$

$$q_i = \beta_0 T_{,i} + \beta_1 n_k T_{,k} n_i \tag{11}$$

$$\begin{aligned} g_i = {} & (\gamma_0 + \gamma_1 d_{kk} + \gamma_2 d_{km}n_k n_m + \gamma_3 n_k \hat{n}_k)n_i \\ & + (\alpha_9 - \alpha_{10})d_{ij}n_j + (\alpha_{12} - \alpha_{11})\hat{n}_i \end{aligned} \tag{12}$$

where the α's, β's, and γ's are functions of ρ, n^2, and T. An alternative to eq. (9) results from introducing the free energy

$$\varphi \equiv \epsilon - Ts = \varphi(\rho, n^2, T) \tag{13}$$

Using eqs. (7) and (13), one can compute the rate of production of entropy and show that the Clausius-Duhem inequality becomes

$$\begin{aligned} T[\rho\dot{s} + (q_i/T)_{,i}] = {} & \left(t_{ij} + \rho^2 \frac{\partial\varphi}{\partial\rho}\delta_{ij}\right)d_{ij} - \left(g_i + 2\frac{\partial\varphi}{\partial n^2}n_i\right)\hat{n}_i \\ & - q_i T_{,i}/T \geqq 0 \end{aligned} \tag{14}$$

For details, we refer to Ericksen.[4] Among other things, eq. (14) implies that

$$\alpha_0 = -\rho^2(\partial\varphi/\partial\rho), \qquad \gamma_0 = -2(\partial\varphi/\partial n^2) \tag{15}$$

It also opens the possibility of introducing Onsager relations in eqs. (10)–(12). The equality in eq. (14) provides a basis for describing heating caused by flow. For the remainder of the discussion, we assume isothermal flow and ignore eq. (14), which is generally inconsistent with this assumption.

In the above treatment, we have proceeded as if any value of n^2 could be attained in equilibrium. We feel that the basic equations are applicable to fluids for which this may not be true. We have less faith in the Clausius-Duhem inequality and Onsager relations. As will be made clear in Section IV, the linearity assumption in (*b*) does not rule out nonlinear behavior.

As is discussed by Ericksen,[4] two further assumptions simplify the equations considerably. One is the common assumption of incompressibility. The other is that the "molecular inertia" $\rho\ddot{\mathbf{n}}$ is negligible. In the steady state solutions discussed below, $\ddot{\mathbf{n}} = 0$, so the later assumption is rigorously satisfied. Otherwise, it is similar to the approximation generally made in mechanistic theories of suspensions wherein the inertia of suspended particles is neglected. With these simplifications, the governing equations reduce to

$$t_{ij} = t_{ji} = -p\delta_{ij} + (\lambda_1 + \lambda_2 d_{km}n_k n_m)n_i n_j + 2\lambda_3 d_{ij} + 2\lambda_4(d_{ik}n_k n_j + d_{jk}n_k n_i) \quad (16)$$

$$\hat{n}_i = (\mu_1 + \mu_2 d_{km}n_k n_m)n_i + \mu_3 d_{ij}n_j \quad (17)$$

$$\dot{x}_{j,j} = d_{jj} = 0 \quad (18)$$

$$\rho\dot{\bar{x}}_i = t_{ij,j} + f_i \quad (19)$$

where p is an arbitrary pressure and the λ's and μ's are functions of n^2.

A still simpler theory has been studied by Ericksen.[5] It can be obtained from eqs. (16) and (17) by requiring that the magnitude of $\mathbf{n}$ be invariable, as it would be if $\mathbf{n}$ represented a rigid rod or dumbbell. The λ's and μ's then becomes constants. For consistency, we must then set

$$\mu_1 = 0, \qquad \mu_3 = -n^2\mu_2 \quad (20)$$

III. Viscoinelastic Fluids in Shear

Fluids permitting variations in density or in n^2 will exhibit some springiness or elasticity. The simplest theory mentioned above

might be called a theory of viscoinelastic fluids since it excludes these variations. Response of such a fluid to the simple shearing motion

$$v_1 = Kx_2, \qquad v_2 = v_3 = 0, \qquad K = \text{const.} \tag{21}$$

is analyzed by Ericksen.[5] For $-1 \leqq \mu_3 \leqq 1$, $\mathbf{n}$ varies periodically with time. Equations describing this motion are identical in form with those deduced by Jeffery[6] for the motion of an ellipsoid of revolution in a Newtonian fluid. According to Jeffery's calculation,

$$\mu_3 = (a^2 - b^2)/(a^2 + b^2) \tag{22}$$

where a is the length of the unequal axis, and b is the common length of the other two. According to Mason and Bartok,[7] these equations are well confirmed experimentally for macroscopic particles if μ_3 is treated as an empirical constant. For rodlike particles, use of eq. (22) leads to error. As follows from eq. (16), the stresses will also vary periodically with time. Mean stresses, obtained by averaging these over a period, are similar to stresses predicted by the Navier-Stokes equations.

For $|\mu_3| > 1$, the behavior is quite different. Instead of varying periodically with time, $\mathbf{n}$ approaches a fixed position lying in the plane of shear and making an angle ψ with the streamlines, where

$$\tan \psi = [(\mu_3 - 1)/(\mu_3 + 1)]^{1/2}$$

It is easily seen that, for $\mu_3 > 1$, ψ lies between 0° and 45° while for $\mu_3 < -1$ it lies between 45° and 90°. As $\mathbf{n}$ moves toward this position, the stresses vary with time. This gives rise to a type of stress relaxation effect. A plot of the steady state value of the shear stress $\tau = t_{12}$ vs. the rate of shear K is given in Figure 1. The plot coincides

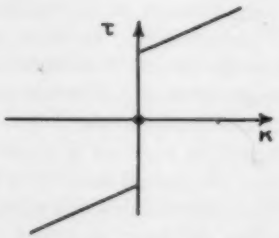

Figure 1.

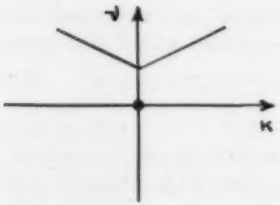

Figure 2.

with that for a Bingham material, the apparent yield stress being proportional to λ_1.

As is clear from equations given by Oldroyd,[8] three-dimensional theories of isotropic fluids which predict this type of behavior involve rather unpleasant singularities. Here this behavior is predicted by very smooth equations.

If we plot a steady state normal stress difference, say $\nu = t_{11} - t_{22}$ vs. K, we obtain Figure 2. When $\lambda_1 = 0$, ν is proportional to $|K|$.

Simpler theories of isotropic fluids invariably predict that ν is a simple function of K^2, which yields quite a different plot. Experimental data on polyisobutylene solutions, particularly that recorded by Greensmith and Rivlin,[9] suggest that, as a good first approximation ν is proportional to $|K|$. In other respects, the theory is unsuitable for these fluids. A modified theory more appropriate for these is discussed below.

IV. Viscoelastic Fluids

In dilute solutions of polyisobutylene at rest, the polyisobutylene molecules are generally thought to be randomly coiled, therefore they define no preferred directions. In shear, it is thought that they stretch out and align themselves at some definite angle relative to the streamlines. This angle probably depends on the rate of shear. We thus have a preferred direction, the direction of greatest stretch, which can be represented by a vector $\mathbf{n}$ whose magnitude measures the amount of stretch. We should then have $\mathbf{n} = 0$ at rest. If we assume that distance between neighboring atoms in a molecule is not sensibly affected by flow, we have an upper bound that n^2 cannot exceed, determined by the average length of a fully extended mole-

cule. These thoughts suggest that a theory of the general type considered here might be used to describe these fluids, but that the theory of viscoinelastic fluids is unsuitable. The following analyses are motivated by these considerations.

In general, the assumption that $\mathbf{n} = 0$ is consistent with the governing equations. The equations then reduce to the Navier-Stokes equations. For any given flow problem, we may expect to have a solution with $\mathbf{n} \equiv 0$, others with $\mathbf{n} \neq 0$. For certain ideal fluids, the equations will require that $\mathbf{n} = 0$ in equilibrium. In flow, the configuration described by $\mathbf{n} = 0$ may be stable or unstable. To, illustrate this, we consider the shear flow given by eq. (21). For it, we must have $\dot{\rho} = 0$ by eq. (5). To investigate stability of $\mathbf{n} = 0$, we linearize $\mathbf{g}$, given by eq. (12), with respect to $\mathbf{n}$ and insert the resulting expression in eq. (4). This gives

$$\begin{aligned} \dot{n}_1 &= An_1 + (B - C)Kn_2 + 2C\dot{n}_1 \\ n_2 &= An_2 + (B + C)Kn_1 + 2C\dot{n}_2 \\ \dot{n}_3 &= An_3 + 2C\dot{n}_3 \end{aligned} \tag{23}$$

where

$$\rho A = \gamma_0, \qquad 2\rho B = \alpha_9 - \alpha_{10}, \qquad 2\rho C = \alpha_{12} - \alpha_{11} \tag{24}$$

Here the quantities on the right are evaluated at $\mathbf{n} = 0$, which means that $\dot{A} = \dot{B} = \dot{C} = 0$. It is a straight forward matter to obtain a general solution of the system (23). Omitting detail, we find that all solutions approach $\mathbf{n} = 0$ in time if and only if one of the following sets of conditions hold:

(*a*) $B^2 \geqq C^2, \quad C < 0, \quad A < 0, \quad A^2 > (B^2 - C^2)K^2$

(*b*) $B^2 < C^2, \quad C < 0, \quad A < 0, \quad -4C^2A > (C^2 - B^2)K^2$

When neither of these conditions hold, $\mathbf{n} = 0$ will of course represent an unstable configuration. If (*a*) and (*b*) holds for K sufficiently small, it will not hold for K exceeding the critical value K_0 given by

$$\begin{aligned} K_0^2 &= A^2/(B^2 - C^2) \qquad \text{if } B^2 > C^2 \\ &= 4C^2A/(B^2 - C^2) \qquad \text{if } B^2 < C^2 \end{aligned}$$

excluding the exceptional case where $B^2 = C^2$.

For a subclass of materials such that (a) holds at low rates of shear, there is a steady state solution with $\mathbf{n} \neq 0$ for $K^2 > K_0^2$ such that the steady state value of $\mathbf{n} \to 0$ as $K \to K_0$. This is not true of materials for which (b) holds. To obtain the steady state value of $\mathbf{n}$, we set $\mathbf{g} = 0$, which yields the equations

$$(\gamma_0 + \gamma_2 K n_1 n_2) n_1 + (\alpha - \beta) K n_2 = 0 \tag{25}$$

$$(\gamma_0 + \gamma_2 K n_1 n_2) n_2 + (\alpha + \beta) K n_1 = 0 \tag{26}$$

$$n_3 = 0 \tag{27}$$

where

$$2\alpha = \alpha_9 - \alpha_{10}, \qquad 2\beta = \alpha_{12} - \alpha_{11} \tag{28}$$

Hence $\mathbf{n}$ lies in the plane of shear and we may write

$$n_1 = n \cos \psi, \qquad n_2 = n \sin \psi \tag{29}$$

where ψ is the angle determined by $\mathbf{n}$ and the streamlines. Multiplying eq. (25) by n_2, eq. (24) by n_1, and subtracting, then using eq. (29), we find that

$$\tan^2 \psi = (\alpha + \beta)/(\alpha - \beta) \tag{30}$$

Since α and β may depend on n^2, this determines the direction of $\mathbf{n}$ in terms of its magnitude. We can determine how n^2 is related to K by eliminating n_1, n_2, and ψ from eqs. (25), (29), and (30), which yields

$$n_1 = n[(\alpha - \beta)/2\alpha]^{1/2}, \quad n_2 = xn[(\alpha + \beta)/2\alpha]^{1/2}, \quad x = \pm 1 \tag{31}$$

$$\{\gamma_0 + xK\gamma_2 n^2[(\alpha^2 - \beta^2)/4\alpha^2]^{1/2}\}[(\alpha - \beta)/2\alpha]^{1/2} + xK(\alpha - \beta)[(\alpha + \beta)/2\alpha]^{1/2} = 0 \tag{32}$$

This will be satisfied for $K = K_0$, $n^2 = 0$ if we choose x so that

$$\gamma_0(\alpha - \beta)x < 0 \quad \text{when } K > 0 \tag{33}$$

$$> 0 \quad \text{when } K < 0$$

Under quite general conditions, for $K^2 > K_0^2$, there will exist a unique solution $n^2 = f(K)$ of eq. (32), with x selected as in eq. (33), such that $f(K) \to 0$ as $K \to K_0$. This will sometimes be true only for K sufficiently close to K_0. There may also be solutions of eq. (32) such that n^2 does not approach zero as $K \to K_0$. These questions

would bear investigation. We have made no general investigation of them. In particular cases, there is a solution of the type described for all $K^2 > K_0^2$ which is stable in the same sense that $\mathbf{n} = 0$ is stable when (a) holds. We restrict our attention to these cases and assume that the $\mathbf{n}$ thus determined is what the fluid prefers.

If γ_0 remains bounded, we can effectively set it equal to zero in eq. (31) for K sufficiently large, obtaining after some simplification

$$\gamma_2 n^2 + 2\alpha = 0 \tag{34}$$

The procedure described thus gives the steady state value of $\mathbf{n}$ as a continuous function of K, $\mathbf{n} = \mathbf{F}(K)$ with

$$\mathbf{F}(K) = 0 \qquad \text{for } K^2 < K_0^2$$

$$\mathbf{F}(K) \to \mathbf{n}_\infty = \text{const.} \qquad \text{for } K \to \infty$$

where $\mathbf{n}_\infty$ is obtained from eqs. (31) and (34). A similar conclusion can be drawn in cases where γ_0 increases without bound but γ_0/K approaches a limit as $K \to \infty$. For the $\mathbf{n}$ thus defined, we may calculate steady state stresses using eq. (16), which reduces to

$$\begin{aligned}
t_{11} - t_{22} &= (\lambda_1 + \lambda_2 K n_1 n_2)(n_1^2 - n_2^2) \\
t_{22} - t_{33} &= (\lambda_1 + \lambda_2 K n_1 n_2) n_2^2 + 2\lambda_4 K n_1 n_2 \\
t_{12} &= (\lambda_1 + \lambda_2 K n_1 n_2) n_2 n_1 + (\lambda_3 + \lambda_4 n^2) K \\
t_{13} &= t_{23} = 0
\end{aligned}$$

For $K^2 < K_0^2$, $\mathbf{n} = 0$ and the stresses reduce to those of a Newtonian fluid with viscosity

$$\lambda_3\big|_{n=0} \tag{35}$$

For high rates of shear, we have as a first approximation

$$\begin{aligned}
t_{11} - t_{22} &= \lambda_2 n_1 n_2 (n_1^2 - n_2^2)\big|_{n=n_\infty} K \\
t_{22} - t_{33} &= (\lambda_2 n_1 n_2^4 + 2\lambda_4 n_1 n_2)\big|_{n=n_\infty} K \\
t_{12} &= (\lambda_2 n_1^2 n_2^2 + \lambda_4 n^2)\big|_{n=n_\infty} K
\end{aligned} \tag{36}$$

At a given rate of shear, this approximation may of course be better for one stress component than it is for another. As might be expected, this is essentially the same as would be obtained for a vis-

coinelastic fluid. At intermediate rates of shear $\mathbf{n}$, hence the stresses, will vary in a rather complicated way with the rate of shear.

In experiments on polyisobutylene solutions such as are summarized by Markovitz,[10] the normal stresses seem to be nearly proportional to K for relatively large rates of shear, as predicted by eq. (36). This is discussed by Criminale et al.[11] At still higher rates of shear, departures from proportionality are seen. These may be due to factors not included in the analysis such as heating or secondary flows. At lower rates of shear, proportionality fails, the observed behavior being more complicated, as the theory implies. From eqs. (35) and (36), the apparent viscosity varies from one constant value at low rates of shear to another at high rates. The existence of two such limiting viscosities in polyisobutylene solutions seems to be confirmed by experiment. Recent data pertinent here are that of Brodnyan et al.[12] The existence of an interval of rate of shear values in which the behavior is strictly Newtonian, as predicted by theory, is not confirmed nor denied by data which we have seen. In general, there is an interval in which any departures from Newtonian behavior are within experimental error.

These rather qualitative considerations suggest that a theory of the type discussed here may described a fluid like a polyisobutylene solution rather well. More detailed calculations and better experimental data will be required to determine how well. As Markovitz[10] points out, there are unresolved discrepancies in experimental results obtained from different types of instruments. The rather sketchy analyses given here do little more than help delimit the class of theories which seem promising for this purpose.

References

1. Oseen, C. W., *Trans. Faraday Soc.*, **29,** 883 (1933).
2. Grad, H., *Comm. Pure Appl. Math.*, **5,** 455 (1952).
3. Noll, W., *Proc. Berkeley Symp. on Axiomatic Method*, 1959.
4. Ericksen, J. L., *Arch. Rational Mech. Anal.*, **4,** 231 (1960).
5. Ericksen, J. L., *Rheol. Acta*, forthcoming.
6. Jeffery, G. B., *Proc. Roy. Soc. London*, **A245,** 161 (1922).
7. Mason, S. G., and W. Bartok, *Rheology of Disperse Systems*, Pergamon, London, 1959, pp. 16–48.
8. Oldroyd, J. G., *Proc. Cambridge Phil. Soc.*, **43,** 100 (1947).
9. Greensmith, H. W., and R. S. Rivlin, *Phil. Trans. Roy. Soc. London*, **A245,** 399 (1953).

10. Markovitz, H., *Trans. Soc. Rheol.*, **1**, 37 (1957).
11. Criminale, W. O., Jr., J. L. Ericksen, and G. L. Filbey, Jr., *Arch. Rational. Mech. Anal.*, **1**, 410 (1958).
12. Brodnyan, J. G., F. H. Gaskins, and W. Philippoff, *Trans. Soc. Rheol.*, **1**, 109 (1957).

Synopsis

We have summarized recent work on theories of anisotropic fluids, drawing attention to a class of theories whose predictions resemble observed behavior of polyisobutylene solutions in steady shear flow. Further research will be required to determine how well these theories can describe the behavior of such fluids. It seems rather likely that they will do well in describing many steady flow situations. From what is known of the linear behavior of such fluids, it would seem that a theory adequate for vibration problems should include linear viscoelasticity theory as a special case. Since the theories discussed seem not to, they may well be found wanting when applied to situations commonly thought of as dynamic.

Abstracts

On the Concepts of Equilibrium in Continua. Part I

BERNARD D. COLEMAN, *Mellon Institute*, and WALTER NOLL
Carnegie Institute of Technology, Pittsburgh, Pennsylvania

We have attempted to develop a rigorous theory of thermostatics for continuous bodies in arbitrary states of finite strain. In this theory the concepts of mechanical and thermal equilibrium are given precise definitions. Two physical postulates are assumed. From these postulates we prove the existence of elastic potentials for stress-strain relations and we derive a tensor inequality which restricts the constitutive equations of thermostatics. When the inequality is specialized for fluids and solids it yields not only the known inequalities of hydrostatics and infinitesimal elasticity, but also some new inequalities for hydrostatics and elastostatics (including finite elasticity).

On the Concepts of Equilibrium in Continua. Part II

BERNARD D. COLEMAN, *Mellon Institute*, and WALTER NOLL, *Carnegie Institute of Technology, Pittsburgh, Pennsylvania*

A discussion is given of the various precise mathematical meanings which can be given in a theory of thermostatics to the physical notion of the stability of a global state of a body.

The results presented in Parts I and II of this paper are published in the *Archive for Rational Mechanics and Analysis*, **4**, No. 2 (December 1959).

END OF SYMPOSIUM

TRANSACTIONS OF THE SOCIETY OF RHEOLOGY IV, 43–44 (1960)

Introduction to the Symposium on Adhesion and Rheology

RAYMOND R. MYERS, *Lehigh University, Bethlehem, Pennsylvania*

An individual who encounters a problem in adhesion has to do a certain amount of soul-searching in order to be sure his approach to the problem is not subject to bias. Most rheologists who have considered the problem assert that adhesion is more closely allied to mechanical properties than interfacial forces; a colloid chemist or surface chemist will incline toward the opposite view and seek relations involving surface free energies, contact angles, and other parameters of thermodynamic significance.

At present the two schools are at opposite poles, despite the fact that some of our best adhesives rheologists are also thoroughly imbued with surface chemical concepts. One of the objectives of this symposium is to focus the attention of rheologists on the rheological problems in order that they can be carried to an early stage of fruitful development. Perhaps then the interfacial aspects will be clearer.

An additional degree of schizophrenia exists in the division among rheologists, themselves, of adhesion problems into liquid and solid. In the first case, rupture of a liquid adhesive has been adequately represented by a well-known equation of Stefan for the extension of a single filament of radius R and thickness h_0:

$$T = \frac{3\eta R^4}{t}\left(\frac{1}{h_0^2} - \frac{1}{h^2}\right)$$

where the tension T depends directly on the viscosity of the medium and inversely on the time of separation; recent work, however, has shown that rapid separation of the adhering members induces cavitation and requires certain modifications of the Stefan equation which are still in various stages of confirmation. In the second case, the strength of a solid adhesive is so highly dependent on accidental in-

clusions that it is almost impossible to derive information of molecular significance regarding the adhesive.

It is in the area of solid adhesives that most problems involving the strength of structural adhesives are encountered. The brittle fracture of solids covers interesting problems which border on those encountered in developing a super adhesive, and the amount of overlap in these two fields of endeavor could be used as a measure of how successful the adhesion technologist has been. The paucity of papers on solid fracture suggests that we are far from the ideal adhesive.

The problems associated with liquid or tacky adhesives are practically all encountered in the *application* of the adhesive, in contrast with the situation involving the solid state in which problems are encountered in the performance or testing of the adhesive. This fact seems to have escaped the attention of earlier authors, but it is brought out vividly in this symposium: three papers are concerned with performance of a sandwich during peeling, and two are devoted to the deformation and flow characteristics of liquids during their application to various substrates.

The papers by Drs. Kaelble, Bickerman (abstract only), and Chang are complementary in their treatment of the forces required to separate a thin film of material capable of withstanding prolonged stress. The offerings of Erb and Hanson, and of Miss Cobb (title only) cover the behavior of coatings while they are still in the liquid state. Erb and Hanson point out that under the conditions of rapid separation which accompany the decomposition of an adhesive, the liquid can also exert a pronounced tensile pull on the substrate; Miss Cobb is more concerned with the penetration of an adhesive coating into a porous substrate in the moments immediately following its deposition.

One firm conclusion can be drawn from a consideration of the papers appearing in this symposium: the rheological aspects of adhesion *are* important. In the hopes of resolving or avoiding any conflict with the proponents of the interfacial approach, it seems appropriate to point out that the rheologist is chiefly concerned with the general aspects of adhesion without regard to the atomistic picture, while the interfacial chemist is more likely to be concerned with specific problems involving the adherence of a particular adhesive-substrate combination. Both disciplines are bound to achieve certain goals independently, but in the final analysis the two must complement each other in order to provide a working knowledge of adhesion.

TRANSACTIONS OF THE SOCIETY OF RHEOLOGY IV, 45–73 (1960)

Theory and Analysis of Peel Adhesion: Bond Stresses and Distributions

D. H. KAELBLE, *Central Research Department, Minnesota Mining and Manufacturing Company, St. Paul, Minnesota*

Introduction

Previous analysis of the mechanics and mechanisms of peel, a treatment general with respect to angle of peel, has identified two potential modes of failure interface propagation.[1] These failure mechanisms are identified as boundary cleavage and boundary shear. Cleavage stresses, normal to the bond plane, are highly localized at the bond boundary where the flexible member undergoes a sudden transition from maximum to zero curvature. The shear stresses, parallel to the bond plane, are distributed throughout the bond.

The cleavage stress distribution has been analyzed by Spies[2] and Bikerman[3] for peel at a ninety degree angle of removal. This discussion undertakes an extension of the bond stress analysis in peel by applying the more general definition of the mechanisms and mechanics now available. This treatment remains general with respect to angle of peel, thus defining bond stresses from the limiting condition of zero angle peel (simple shear) to high peel angles. By combinations of the relations resulting from this analysis and the previous treatment of process mechanics, new insight into the peel process is developed.

Theory

A. Basic Assumptions

The previous assumptions concerning an idealized form of tensile peel termed "simple stripback" are adopted for this discussion.[1]

In addition certain assumptions concerning properties of the interlayer are necessary. For completeness, all assumptions concerning the process are included below:

I. Properties of the Flexible Member
   A. Of slender rectangular cross section
   B. Elastically (Hookian) deformed
   C. Bonded and unbonded portions of semi-infinite length
   D. Flexible and extensible

II. Properties of the Adhesive Interlayer
   A. Display elastic deformation
   B. A sharply defined bond boundary exists at $x = 0$

III. Properties of the Forces
   A. All forces uniformly distributed across the bond width
   B. Applied force—acts in tension along the central plane of the flexible member
   C. Bond shear forces—distributed over the bonded interface of the flexible member
   D. Bond stripping forces—a highly localized parallel array, perpendicular to the bond plane

IV. A steady-state unbonding process (applied force and rate constant with time)

These assumptions are individually amplified upon in subsequent sections.

A schematic view of the adhesive joint in the zone of peel is represented in Figure 1. During steady-state peel the $x - y$ coordinate system translates to the left at a uniform velocity relative to the

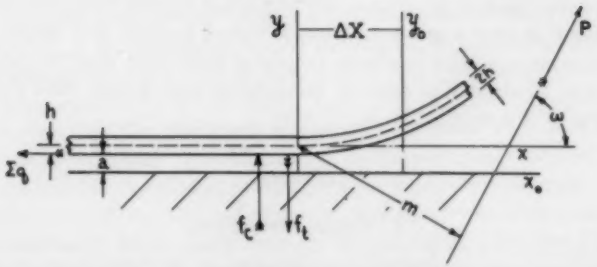

Fig. 1. External forces acting on the flexible member.

TABLE I
Nomenclature of Principal Terms

Symbol	Definition
P	peel force
W	work of peel
m	moment arm of peel force P about 0
M	bond moment of force
ω	angle of peel
$2h$	flexible member thickness
a	adhesive interlayer thickness
b	bond width
f	reactive bond force in cleavage
q	reactive adhesive shear force
σ	bond stress due to force f
λ	bond stress due to force q
E	Young's modulus of flexible member
I	moment of inertia of flexible member cross section about the neutral axis
Y	Young's modulus of the adhesive interlayer
G	shear modulus of the adhesive interlayer
$d\omega/ds$	exact curvature of the flexible member at $x = 0$
R	exact radius of curvature at $x = 0$
α	$(G/2Eah)^{1/2}$
β	$(Yb/4EIa)^{1/4}$

TABLE II
Statement of Peel Mechanics

Mechanism	Cleavage	Shear	Combined
Forces	$p_c = p \sin\omega$ $= \Sigma f_t - \Sigma f_c$ $= \Sigma f$	$p_S = p \cos\omega$ $= \Sigma q$	$p = (p_c^2 + p_S^2)^{1/2}$
Moments of force	$M_c = p \cdot m_c$ $= \Sigma f \cdot x$	$M_S = p \cdot m_s$ $= h \cos\omega \Sigma q$	$M = p \cdot m$ $= M_c + M_S$
Moment arm	$m_c = m - h\cos\omega$	$m_s = h\cos\omega$	$m = \left[\frac{2EI(1-\cos\omega)}{p}\right]^{1/2}$ $= 2R(1-\cos\omega)$

stationary $x_0 - y_0$ reference coordinates. Since the properties of the applied and induced forces relative to the $x - y$ coordinates are invarient with time, conditions of instantaneous static equilibrium

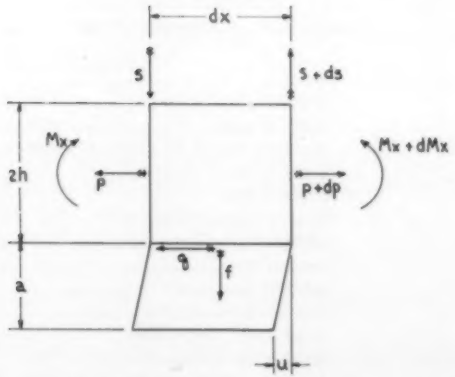

Fig. 2. Forces and moments acting on an increment of the flexible member.

apply. The principle terms of nomenclature associated with Figure 1 and subsequent discussion are defined in Table I. A statement of the peel mechanics[1] as they apply to this discussion is presented in Table II.

The nature of the forces acting on a section of the flexible member of length (dx) located a distance ($-x$) from the origin of the translating $x - y$ coordinates is illustrated in Figure 2. Bending forces in the flexible member produce bending moments (M_x) and ($M_x + dM_x$). Shear forces in the flexible member are represented by (s) and ($s + ds$). The reactive forces of the adhesive interlayer are represented by a tensional force (f) and a shear force (q). Applying the condition of equilibrium of external moments and forces to this flexible member section we find for the forces:

$$ds + f = 0 \tag{1}$$

$$dp + q = 0 \tag{2}$$

and for the moments:

$$dM_x + s dx - qh = 0 \tag{3}$$

where:

$$dM_{xc} + dM_{xs} = dM_x \tag{4}$$

$$dM_{xc} = -sdx \tag{5}$$

$$dM_{xs} = +qh \tag{6}$$

The moment dM_{xc} is the incremental bending moment due to bond cleavage and the moment dM_{xs} is the incremental bending moment due to bond shear.

B. Bond Cleavage Stress

The derivation of the cleavage stress function involves application of eqs. (1) and (5) and the exact relation for bending deformation:[3]

$$EI(d\omega/ds)_c = M_c$$

A detailed derivation of the cleavage stress function is provided in Appendix IA. The resulting equation for cleavage stress at point $(-x)$ in the bond may be written as:

$$\sigma = 2\beta e^{\beta x} [(\beta M_c + P \sin \omega) \cos \beta x + \beta M_c \sin \beta x]/b \tag{7}$$

or

$$\sigma = \sigma_0 e^{\beta x} (\cos \beta x + K \sin \beta x) \tag{8}$$

where

$$K = \beta M_c/(\beta M_c + P \sin \omega) = \beta m_c/(\beta m_c + \sin \omega) \tag{9}$$

and

$$\beta = (Yb/(4EIa)^{1/4} \tag{10}$$

The cleavage stress function defined by eqs. (7) or (8) is graphically described in Figure 3 where the ratio of interior stress (σ) to boundary stress (σ_0) is plotted versus βx, a relative measure of displacement from the bond boundary. The two curves illustrate the general form of the cleavage stress function as a highly damped harmonic function involving alternating regions of tension and compression. The influence of K, the dimensionless parameter defined by eq. (9), is shown in Figure 3 where the curves represent the values of $K = 0$ and $K = 1.0$. The factor β defined by eq. (10) has the dimension of reciprocal length and defines the full cyclic wavelength by factor $2\pi/\beta$. The β parameter may be defined as a cleavage stress concentration factor in the sense that increasing values of β concentrate the stress in a smaller active area near the bond boundary.

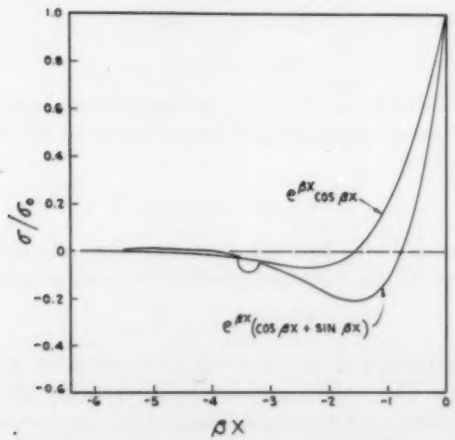

Fig. 3. The cleavage stress function for $K = 0$ and $K = 1.0$.

Evaluation of the cleavage stress function provides new relations for the summed cleavage forces Σf and moments of force Σfx. With regard to the forces, by introducing the relation $f = -\sigma b dx$ into eq. (8) and rearranging into integral form we may write:

$$\Sigma f = -b\sigma_0 \int_0^{-\infty} e^{\beta x} \cos \beta x \, dx + K \int_0^{-\infty} e^{\beta x} \sin \beta x \, dx$$

evaluating the above integral we obtain:

$$\Sigma f = b\sigma_0(1 - K)/2\beta = P_c \tag{11}$$

Since $f = p \sin \omega$, eq. (11) may be written as:

$$P = \sigma_0 b(1 - K)/2\beta \sin \omega \tag{12}$$

By substitution of the factor β as given by eq. (10) into the above expression we may rewrite eq. (12) in a form similar to the Bikerman[3] equation for peel through a Hookian solid:

$$P = 0.380 b\sigma_0 (E/Y)^{1/4} a^{1/4} (2h)^{3/4} (1 - K)/\sin \omega \tag{13}$$

Equation (13), at a peel angle of 90°, is identical to the Bikerman equation except for the appearance of the additional term $(1 - K)$. The Bikerman theory implicitly assumes $K = 0$ when, in fact, K, as the forthcoming discussion will demonstrate, may be very close

to unity at 90° peel and slight changes in K exert a powerful influence on the factor $(1 - K)$.

The summation of cleavage moments of force Σfx may also be evaluated in terms of eq. (8) by introducing the relation $fx = -\sigma bxdx$ into this expression with rearrangement into the following integral form:

$$\Sigma fx = -b\sigma_0 \int_0^{-\infty} xe^{\beta x} \cos \beta x \, dx + K \int_0^{-\infty} xe^{\beta x} \sin \beta x \, dx$$

evaluating this integral we obtain:

$$\Sigma fx = Kb\sigma_0/2\beta^2 = M_c \tag{14}$$

From consideration of the conditions of force and moment equilibrium the expression for bond cleavage stress and distribution have been developed in eqs. (7) through (9). Application of these expressions to the summation of cleavage forces and moment produces the expressions for the cleavage force P_c as given by eq. (11) and cleavage moment M_c as given by eq. (14).

C. Bond Shear Stress

Derivation of the shear stress function involves application of eq. (2) and is developed in Appendix IB. The resulting equation for the shear stress function may be written as:

$$\lambda = (P \cos \omega \, \alpha e^{\alpha x})/b \tag{15}$$

or:

$$\lambda = \lambda_0 e^{\alpha x} \tag{16}$$

where:

$$\alpha = (G/2Eah)^{1/2} \tag{17}$$

Equations (15) and (16) express the shear stress function as a simple exponential decay form with maximum shear stress at the bond boundary ($x = 0$) and monotonically diminishing stress magnitude with increased values of $(-x)$. The factor α defined by eq. (17) is also in dimensions of reciprocal length and represents a shear stress concentration factor in a manner similar to the cleavage factor β. In other words, increased values of α decrease the active bond area under high shear stress.

Substituting the relation $\lambda = -q/bdx$ into eq. (16) with rearrangement into integral form we obtain:

$$\Sigma q = -\lambda_0 b \int_0^{-\infty} e^{\alpha x}\, dx$$

Evaluating the above integral we obtain:

$$\Sigma q = \lambda_0 b/\alpha = P_s \tag{18}$$

where eq. (18) expresses the summation of bond shear forces. Since the shear moment of force is simply $M_s = h\Sigma q$, eq. (18) becomes:

$$h\Sigma q = \lambda_0 hb/\alpha = M_s \tag{19}$$

Equations (15) through (17) then provide the expressions for shear stress and distribution. The summation of shear forces produce the relations for the shear force P_s and shear moment M_s as given by eqs. (18) and (19), respectively.

D. Combined Stresses

Discussion of the two previous sections has concerned the cleavage and boundary shear functions as more or less independent stress mechanisms. The mechanics of peel[1] provide relations for steady state peel in terms of the combined stresses in cleavage and boundary shear. In terms of the equilibrium of bond forces we obtain:

$$P = [P_c^2 + P_s^2]^{1/2}$$

which upon substitution of eqs. (11) and (18) becomes:

$$P = \left(\left[\frac{b\sigma_0(1 - K)}{2\beta}\right]^2 + \left[\frac{\lambda_0 b}{\alpha}\right]^2\right)^{1/2} \tag{20}$$

The equation for equilibrium of bond moments may be written:

$$P = \frac{M^2}{2EI(1 - \cos\omega)} = \frac{(M_c + M_s)^2}{2EI(1 - \cos\omega)}$$

Substituting eqs. (14) and (19) into the above expression we obtain upon simplification and rearrangement:

$$P = ba\left[\frac{K\sigma_0}{(2Y)^{1/2}} + \frac{3^{1/2}\cos\omega\,\lambda_0}{(2G)^{1/2}}\right]^2 (1 - \cos\omega)^{-1} \tag{21}$$

In eq. (21), which is simplified by substitution of eqs. (10) and (17) for (β) and (α), respectively, it may be noted that no parameters defining the geometry or rheology of the flexible member appear directly.

In addition to the equations of peel in terms of combined forces, eq. (20) and combined moments of force, eq. (21), we may develop a very general expression for peel in terms of the total work of peel. The work of peel is defined as the product of peel force and its displacement along its line of action. The total work of peel (W) may be expressed as the sum of two work components as follows:

$$W = W_T + W_D \tag{22}$$

where W_T is the nonrecoverable work of translation of the bond boundary as previously defined by the peel mechanics and the following equation:[1]

$$W_T = p(1 - \cos \omega)\Delta X$$

The above equation for W_T is meaningful in terms of the bond stresses when we substitute for the term P(1 − cos ω) available from the expression for combined moments available in eq. (21) and rewrite as follows:

$$W_T = ba\left[\frac{K\sigma_0}{(2Y)^{1/2}} + \frac{3^{1/2}\cos\omega\,\lambda_0}{(2G)^{1/2}}\right]^2 \Delta X \tag{23}$$

Since in our primary assumptions for this discussion we consider finite elastic deformation of the flexible member, we must include a term W_D which defines the recoverable work of flexible member deformation in tension. This recoverable work of deformation W_D is expressed by the following equation:

$$W_D = p^2\Delta X/4bhE$$

The above expression for W_D can also be given physical significance in terms of the bond stresses in terms of the relation for combined peel force expressed in eq. (20) by substitution in terms of (P^2) as follows:

$$W_D = \frac{b}{4}\left[\frac{\sigma_0^2(1 - K)^2(ha)^{1/2}}{3(YE)^{1/2}} + \frac{2\lambda_0^2 a}{G}\right]\Delta X \tag{24}$$

in which the expressions for β and α as given by eqs. (10) and (17) have been applied to reduce the equation to prime variables.

From eqs. (22), (23), and (24) we may now provide a general expression for the effective work of peel per unit area unbonded as expressed by the ratio $W/b\Delta X$ in the following equation:

$$W/b\Delta X = a\left[\frac{K\sigma_0}{(2Y)^{1/2}} + \frac{3^{1/2}\cos\omega\,\lambda_0}{(2G)^{1/2}}\right]^2 + \frac{1}{4}\left[\frac{\sigma_0^2(1-K)^2(ha)^{1/2}}{3(YE)^{1/2}} + \frac{2\lambda_0^2 a}{G}\right] \quad (25)$$

E. Supplemental Relations

In the relations for combined stress expressed in eqs. (20) and (21) three factors—K, σ_0, and λ_0—and their dependence upon peel angle bear further development and understanding. Let us first consider the cleavage stress factor (K). By substitution of the exact relation for flexible member bending $M_c = EI/R_c$ into eq. (14) for the condition $\omega = 180°$ and any other angle, assuming $b/2\beta^2$ independent of angle we may write:

$$R_c = (\sigma_{0\pi}/K\sigma_0)R_{c\pi} \quad (26)$$

where $\sigma_{0\pi}$ and $R_{c\pi}$ are respectively the boundary cleavage stress and radius of cleavage curvature at $\omega = \pi$. Since from the mechanics we may write $m_c = 2R_c(1 - \cos\omega)$, upon substitution of eq. (26) into this expression we obtain:

$$m_c = \frac{2\sigma_{0\pi}R_{c\pi}}{K\sigma_0}(1 - \cos\omega) \quad (27)$$

Substitution of the above expression into eq. (9) and rearrangement produces the following quadratic equation for K:

$$\frac{K^2\sigma_0\sin\omega}{2\beta\sigma_{0\pi}R_{c\pi}(1-\cos\omega)} + K - 1 = 0 \quad (28)$$

where, when cleavage is the controlling stress mechanism of failure $\sigma_0 = \sigma_{0\pi}$, the function of K versus ω may be calculated by solution of the quadratic. However, when shear is the predominating mechanism the cleavage boundary stress becomes variable with peel

angle and further knowledge of the relation between σ_0 and λ_0 with angle ω is required.

Solving eqs. (7) and (16) for $x = 0$ and recognizing that $M_c = p \cdot m_c$ we may write:

$$\sigma_0/\lambda_0 = \frac{2\beta}{\alpha}\left(\frac{\beta m_c}{\cos\omega} + \tan\omega\right) \tag{29}$$

Introducing, from the mechanics, the relation $m_c = 2R(1 - \cos\omega) - h\cos\omega$ into the above relation and rearranging we obtain:

$$\frac{\sigma_0}{\lambda_0} = \frac{(3Y)^{1/2}}{(G)}\left[\frac{2R(1 - \cos\omega)}{h\cos\omega} - 1\right] + \frac{2\beta}{\alpha}\tan\omega \tag{30}$$

An alternate method of expressing eq. (29) is provided by solving eq. (9) in the following terms:

$$\beta m_c = \frac{K\sin\omega}{1 - K}$$

Substituting this relation into eq. (29) provides the following expression:

$$\frac{\sigma_0}{\lambda_0} = \frac{2\beta}{\alpha}\left(\frac{1}{1 - K}\right)\tan\omega \tag{31}$$

for the cleavage to stress ratio. These several relations involve the use of both the cleavage boundary radius of curvature (R_c) and the combined radius of curvature in peel (R) which are interrelated by the following expression:

$$R = R_c + \frac{h\cos\omega}{2(1 - \cos\omega)} \tag{32}$$

We will consider steady state peel failure to proceed by a single predominating stress mechanism. The predominating stress mechanism is characterized by a critical boundary stress which is independent of angle. Thus for peel by cleavage (when $\sigma_0/\lambda_0 > \sigma_{0\infty}/\lambda_{0\infty}$):

$$\sigma_0 = \sigma_{0\infty}$$

$$\lambda_0 = \sigma_{0\infty}\left[\frac{2\beta}{\alpha}\left(\frac{1}{1 - K}\right)\tan\omega\right]^{-1} \tag{33}$$

and for peel by boundary shear (when $\sigma_0/\lambda_0 < \sigma_{0\pi}/\lambda_{00}$):

$$\sigma_0 = \lambda_{00}\left[\frac{2\beta}{\alpha}\frac{1}{1-K}\tan\omega\right] \tag{34}$$

$$\lambda_0 = \lambda_{00}$$

where $\sigma_{0\pi}$ is the boundary cleavage stress at $\omega = 180°$ and λ_{00} the boundary shear stress at zero angle of peel.

Solution for the function of K with peel angle proceeds in a straight forward manner where cleavage predominates since the ratio $\sigma_0/\sigma_{0\pi}$ in the first term of eq. (28) is unity. However, when the angle of peel is in a range where boundary shear predominates a technique of successive approximation solution applies. One may solve eq. (28) by first assuming $\sigma_0/\sigma_{0\pi} = 1.0$. We take the approximate K value for this solution and apply it to the solution of σ_0 from eq. (34). The new value of $\sigma_0/\sigma_{0\pi}$ in eq. (28) produces a different approximate K value and this routine of circuitous resubstitution is repeated until both K and σ_0 converge to constant values.

Experimental

The use of self adhering or "pressure sensitive" bond interlayers in the peel adhesion experiments reported in this study provides a very close approximation to the steady state peel condition required by theory. This type interlayer also provides a convenient means of altering the effective rheological properties as measured by moduli (Y) and (G), and the apparent adhesion parameters as measured by boundary stresses (λ_0) and (σ_0) by merely changing the time scale of the experiment as controlled by peel rate.

Two basic types of peel experiments are utilized in this study of peel adhesion phenomena. The measurement of peel force as a function of peel angle is the first of these methods. As later discussion will indicate, the nature of this P versus ω function provides very basic information concerning the bond. The second method provides for direct experimental measurement of the internal and boundary cleavage stress associated with steady state peel by means of the "split-beam transducer." Results of the second type of measurement provide data of a new and fundamental nature since any assumptions of an arbitrary stress distribution and flexible member deformation are not a requirement for analysis.

A rather explicit additional criteria for the range of experimental conditions is provided by eq. (22) of the theory which defines the total work of peel (W) in terms of a work of boundary translation (W_T) and work of flexible member deformation (W_D). All peel measurements reported here are conducted under conditions where W_D is negligible compared to W_T. Consideration of any peel experiment in terms of these work contributions points up several interesting facts concerning steady state peel where $W_D = W$. First, the applied peel rate corresponds directly to the rate of bond boundary propagation, a circumstance not available in most tests for bond strength where a rate of strain may be applied but failure propagation is uncontrolled. Second, measurement and analysis of the process of failure interface propagation are much simplified by the fact we are dealing with a geometric one-dimensional event or a line propagation as opposed to much more complicated geometries of failure in most other bond types.

All-Angle Peel Measurement

A previously described, peel tester and technique are applied to provide steady-state measurements over a wide range of peel angles and peel rates.[1] Peel force measurements were conducted from angles of less than 10° to 180° and rates of 0.02, 0.2, 2.0, and 20.0 in./min. The bonds in these experiments involve a rigidly clamped cellophane substrate, self adhering adhesive interlayer, and flexible members of (*a*) cellophane, (*b*) glass cloth, and (*c*) aluminum foil. Tests were conducted at 25 ± 1°C. and 50 ± 5% R.H. The combined reproducibility of the bonding and peel test was about ±4%.

Split-Beam Transducer Measurement

The prototype apparatus and technique of cleavage stress measurement have been previously reported.[5] The basic element of the apparatus is a split substrate, one side of which is rigid and the other side in the form of a slightly deflectable beam which senses normal forces by means of a deflection transducer. As the peel bond boundary proceeds perpendicularly across the line split from the inactive to active substrate, the accumulation of normal bond forces (Σf) acting through the adhesive is measured. This first derivative of this measured Σf response with respect to displacement is a measure of bond stress in an area increment (bdx).

Results and Discussion

Low Angle Peel

As previously mentioned, the primary stress mechanism of failure interface propagation may be assessed from a knowledge of the relative magnitudes of the boundary cleavage stress σ_0 and boundary shear stress λ_0. Equation (30) provides the relation for (σ_0/λ_0) for all peel angles. This function is evaluated for four hypothetical bond constructions where R is considered as a constant and $Y = 3G$. Table III presents the characteristics of the bonds evaluated. Bonds

TABLE III
Bond Properties for Evaluation of σ_0/λ_0 Function[a]

Bond	*A*	*B*	*C*	*D*
$2h$ (in.)	a	a	$4a$	$4a$
E, psi	$1{,}000Y$	Y	$1{,}000Y$	Y
$6R/h$	240	240	60	60
$2\beta/\alpha$	25.7	4.05	18.4	3.24

[a] $a = 0.001$ (in.); $b = 0.50$ (in.); $R = 0.02$ (in.); $Y = 1.0 \times 10^3$ (lb./in.^{2}); $G = Y/3$.

A and *C* represent bonds where the flexible member Young's modulus (E) is high compared to the adhesive modulus (Y). Bonds *B* and *D* have flexible member and adhesive modulus of comparable magnitude. Similar backing thicknesses provide equivalent R/h ratios for bonds *A* to *B* and *C* to *D*.

Examination of eq. (30) indicates that the factor $2\beta/\alpha$ exerts the controlling influence at very low angles and the $6R/h$ factor predominates at higher angles. At zero angle peel the limiting value of $\sigma_0/\lambda_0 = -3.0$. Figure 4 illustrates the nature of these functions, where the factor $(\sigma_0/\lambda_0) + 3$ is plotted on a logarithmic scale versus peel angle over a range of low angles, for bonds *A* through *D* described in Table III. If we assume the cleavage failure predominates when $\sigma_0/\lambda_0 > 3.0$ and boundary shear when $\sigma_0/\lambda_0 < 3.0$, then on Figure 4 the value $(\sigma_0/\lambda_0 + 3) = 6.0$ is the line of demarkation between cleavage and shear as controlling mechanisms. In Figure 4, when $(\sigma_0/\lambda_0 + 3) = 3.0$ the cleavage stress σ_0 makes the transition from tensile (+) to compressive (−) stress in comformance with the criteria of peel mechanics. At decreasingly smaller peel angles in

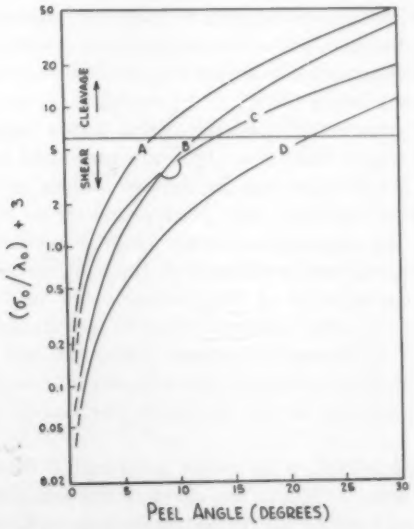

Fig. 4. The boundary stress ratio function at low peel angles.

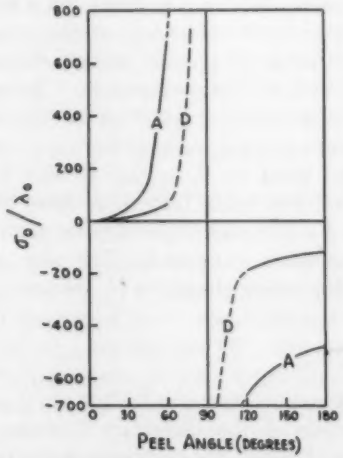

Fig. 5. The boundary stress ratio function at high peel angles.

Figure 4 we note the convergence of boundary stress ratios of A to C and B to D is controlled by the factor $2\beta/\alpha$. With increasing peel angle a similar convergence appears between A to B and C to D as controlled by the factor $6R/h$.

Plots of the calculated boundary stress ratios σ_0/λ_0 over the full range of peel angles from 0 to 180° are presented in Figure 5 for bonds A and D which present the extreme values both factors $2\beta/\alpha$ and $6R/h$. This cartesian plot presents no detail at the low peel angles where the cleavage-boundary shear transition takes place. Figure 5 illustrates the discontinuity in the σ_0/λ_0 function at $\omega = 90°$ due to the disappearance of shear stress. For peel angles greater than 90° the σ_0/λ_0 ratio is negative due to the change in sign of the shear stress as it reverses direction. Over the full range of high angles the absolute magnitude of the boundary stress ratio $|\sigma_0/\lambda_0| \gg 3.0$ indicating cleavage as the dominant mechanism for both bonds A and D.

For a particular bond of the group A through D described in Table III we may further evaluate the effect of the boundary stress ratio (σ_0/λ_0) upon peel force (P) in the transition from cleavage to boundary shear. As defined in eqs. (29) through (31), we consider a principal boundary stress associated with the dominate stress mechanism of failure which is independent of peel angle and a secondary boundary stress determined from the boundary stress ratio function for the bond. Bond C of Table III presents the characteristics most analogous to the bonds evaluated experimentally. By selecting a principal cleavage boundary stress $\sigma_{0\pi} = 1{,}000$ psi and several principal cleavage to shear boundary stress ratios; $\sigma_{0\pi}/\lambda_{00} = 3.0$ for bond C—1, $\sigma_{0\pi}/\lambda_{00} = 10.0$ for bond C—2, $\sigma_{0\pi}/\lambda_{00} = 40.0$ for bond C—3, we calculate the several functions, force (P) versus peel angle (ω), presented in Figure 6. For peel angles greater than zero, eq. (21) for the combined moments is applied. The zero angle condition is defined by eq. (20) which simplifies to become:

$$P = \lambda_{00} b/\alpha$$

The stress ratio function for bond C illustrated in Figure 4 defines both the magnitude of the secondary boundary stress and the critical peel angle at which the dominate stress mechanism changes from cleavage to shear.

The upper curve of Figure 6 represents the peel force calculated for predominating cleavage failure. Bond *C*-3 changes from cleavage to shear as the predominating failure mechanism at approximately 45° peel angle, and with decreased angle the peel force decreases until very low angles where it increases to the zero angle limit. Bond

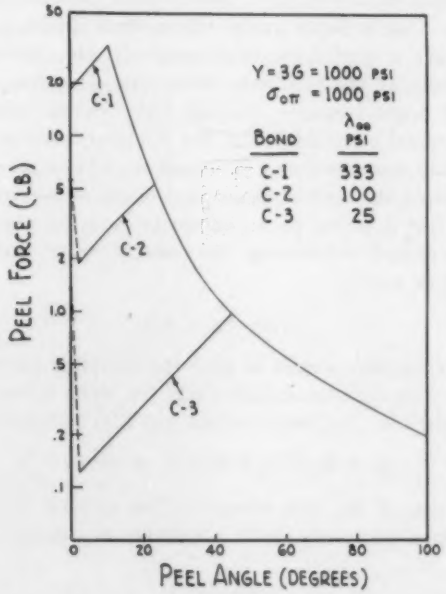

Fig. 6. The calculated peel force (P) versus angle (ω) function at low angles.

C-2 displays a similar response with transition in the dominate stress mechanism of failure but at a lower angle, about 23°, for the transition. Bond *C*-1 displays a peel force maximum at the peel angle of stress mechanism transition, about 10°, but no minimum at lower peel angles. The difference between bond *C*-1 and the other bonds of Figure 6 is that for this bond the terms of eq. (21) are:

$$\frac{\sigma_{0\pi}}{(2Y)^{1/2}} = \frac{3^{1/2}\lambda_{00}}{(2G)^{1/2}}$$

but for bonds C-2 and C-3 they are

$$\frac{\sigma_{0x}}{(2Y)^{1/2}} > \frac{3^{1/2}\lambda_{00}}{(2G)^{1/2}}$$

For the hypothetical bonds considered here, we are led to the conclusion that where a transition is made from cleavage to shear a force maxima will occur on a steady-state peel force versus angle curve. Also, that at lower angles where shear predominates we may also experience a peel force minimum. In this discussion of the theoretical form of the boundary stress ratio functions and the peel force versus angle response through the cleavage-shear transition we have assumed artificially that the boundary radius of curvature R is a constant and the factor K is unity. This is an obvious oversimplification of the more complicated exact response predicted by the theory, but it serves as an adequate basis for the general conclusions developed concerning the steady state force-angle peel function at low angles.

High Angle Peel

At sufficiently high angles of peel the cleavage stress mechanism is the dominating process of failure and the shear stress contribution becomes negligible. In this instance eq. (21) becomes:

$$p = ba(K^2\sigma_{0x}^2/2Y)\,(1 - \cos\omega)^{-1} \qquad (35)$$

A consideration of the dependence of the variable K in the above expression upon peel angle sheds interesting new insight into the peel

TABLE IV
Approximate Cleavage Stress Distribution Multiplier Factor (K)

Case	—	—	*C*	*A*	*D*	*B*	—	—
$2\beta R_c$	0.1	1.0	3.30	9.36	18.56	52.4	100	500
ωdegrees	K	K	K	K	K	K	K	K
1	0.029	0.089	0.156	0.247	0.330	0.485	0.594	0.838
10	0.089	0.255	0.412	0.583	0.699	0.844	0.906	0.978
30	0.151	0.400	0.597	0.766	0.853	0.937	0.965	—
60	—	0.530	—	0.870	—	—	—	—
90	—	0.620	—	0.915	—	—	—	—
120	—	0.710	—	0.965	—	—	—	—
150	—	0.820	—	0.980	—	—	—	—
180	1.00	1.00	1.00	1.00	1.00	1.00	1.00	1.00

adhesion process in this range of high peel angles. As previously mentioned, the value of K at any angle of peel may be calculated by eq. (28) which becomes:

$$\frac{K^2 \sin \omega}{2\beta R_{c\pi}(1 - \cos \omega)} + K - 1 = 0 \tag{36}$$

where for this discussion $\sigma_0 = \sigma_{0\pi}$. Table IV presents tabulated values of K calculated from the above expression. The selected values of $2\beta R_c$ include the four bonds discussed in Table III and Figure 4. Examination of eq. (35) produces the following equation:

$$P = 2K^2 P_\pi (1 - \cos \omega)^{-1} \tag{37}$$

where P_π refers to the peel force at 180° peel angle. Figure 7 presents curves of peel force versus angle for two values of $2\beta R_{c\pi}$. A peel

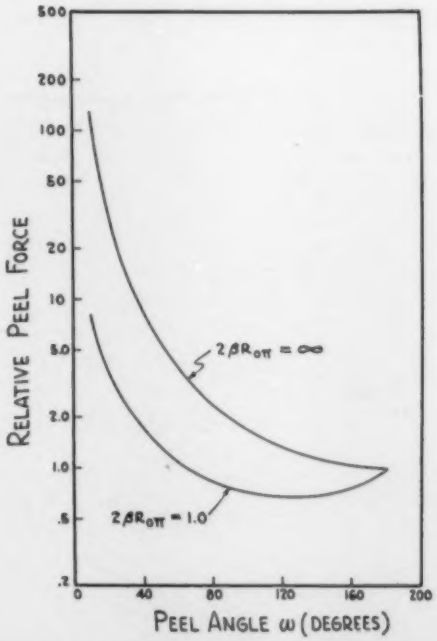

Fig. 7. The calculated peel force (P) versus angle (ω) function at high angles.

force $P_s = 1.0$ is assumed for both bonds. The value of $2\beta R_{cs} = 1.0$, a magnitude characteristic of self adhering adhesive bonds, produces a minimum in the peel force versus peel angle function, as shown in Figure 7, between 90 and 180°. The second curve for $2\beta R_{cs} = \infty$ produces the simple inverse relation of peel force and $(1 - \cos \omega)$. An earlier discussion of peel phenomena discussed this minimum peel force occurring at high angles in terms of inelastic buckling of the flexible member.[1] While this earlier explanation is valid, it now is apparent that the dependence of K upon peel angle provides the more direct and theoretically compatible explanation of this feature of the steady state force-angle function at high angles. In this brief discussion of high angle peel we have ignored the contribution of the shear stress mechanism to the peel force P as indicated by eq. (35).

All-Angle Peel

Individual discussions of low and high angle peel obviously oversimplify a rather complicated response which involves a good deal

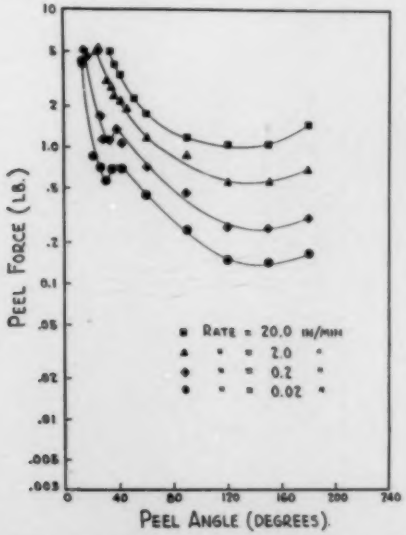

Fig. 8. Peel force (P) versus angle (ω) for cellophane tape (adhesive thickness $a = 0.0002$ in.).

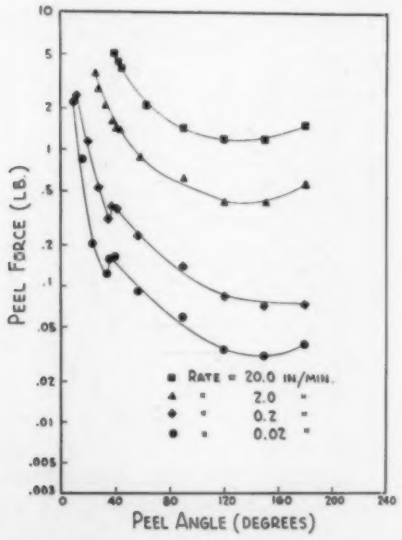

Fig. 9. Peel force (P) versus angle (ω) for cellophane tape (adhesive thickness $a = 0.0018$ in.).

of overlapping of the prime stress mechanisms as they occur at very low (at or near zero) and high (at or near 180) angles of peel. Experimental all-angle peel measurements at constant rate of peel for selected self-adhering bonds provide a penetrating insight into this more complicated real response.

Figure 8 presents peel force versus angle data for a bond comprising a cellophane flexible member of thickness $2h = 1.5 \times 10^{-3}$ in. and transparent adhesive interlayer of thickness $a = 2.0 \times 10^{-4}$ in. As indicated in Figure 8, increasing peel rate increases peel force at all angles. At the lower peel rates, 0.02 and 0.2 in./min., a maxima-minima in peel force occurs at angles between 30 and 40°. At the higher rates of peel, and correspondingly higher peel forces, this phenomena does not occur at equivalent angles of peel. It is this maxima-minima in the P versus W function we associate with the cleavage to boundary shear transition in predominating boundary failure mechanism.

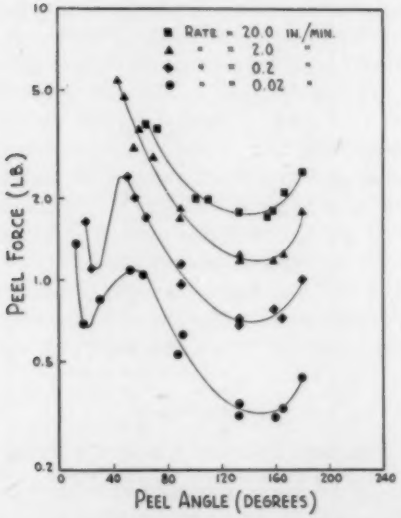

Fig. 10. Peel force (P) versus angle (ω) for glass cloth tape.

Figure 9 presents similar data for a pressure-sensitive bond identical in character to that discussed in Figure 6 except the adhesive interlayer thickness $a = 1.80 \times 10^{-3}$ in. for this bond. The ninefold increase in adhesive interlayer thickness, aside from reducing peel forces at the peel rates of 0.02 and 0.2 in./min., displays properties in Figure 9 very similar to those of the thinner adhesive layer discussed previously.

The peel response of a pressure-sensitive bond utilizing a glass cloth flexible member is illustrated in Figure 10. A very pronounced maxima-minima may be noted in the peel force versus angle curves at the lower rates of 0.02 and 2.0 in./min. The data for the lowest rate, 0.02 in./min., indicate a smooth transition of peel force in this region rather than a sharp discontinuity in peel force.

The effect of a metal flexible member, aluminum foil, in combination with a pressure-sensitive adhesive bond is displayed in the peel force curves of Figure 11. Here a sharp decrease in peel force is realized at the low peel rates of 0.02 and 0.2 in./min. as the peel angle decreases below a critical value of 36 to 40°. No appearance of a

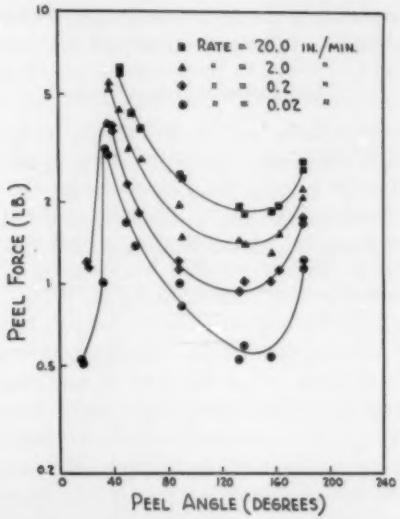

Fig. 11. Peel force (P) versus angle (ω) for aluminum foil tape.

force minima was recognized in measurements carried to less than 20° in peel angles for these two lower rates of peel. The common characteristic of the four bonds evaluated in Figures 8 through 11 is that peel force increases with peel rate for all angles of measurement. At high angles of peel the data in Figures 8 through 11 all display the force minimum at angles between 120 and 160° as predicted by the variance in the K factor with peel angle and illustrated in Figure 7. At low angles of peel and low rates the experimental data display the maxima-minima in peel force associated with the cleavage to shear transition in predominating mechanism of boundary translation as illustrated in Figure 6. The confirmation of the experimental peel force versus angle functions to the calculated functions substantially confirm the assumptions of theory. The condition of the steady-state as controlled by the rate and temperature of peel determine the rheological response as defined by interlayer moduli Y and G and the effective adhesion characteristics as determined by the boundary stresses $\sigma_{0\sigma}$ and λ_{00}. In other words, the experiments tend to confirm the hypothesis that these rheological

and adhesion properties in peel are independent of the angle of peel for a constant condition of steady state peel.

The Propagating Boundary

An additional and direct test of this theory as it applies to the self-adhering bonds discussed here is provided in the direct experimental evaluation of internal boundary stresses in bonds of this type during steady-state peel and comparison to the theoretical form of the stress distribution. Measurements of this type are available

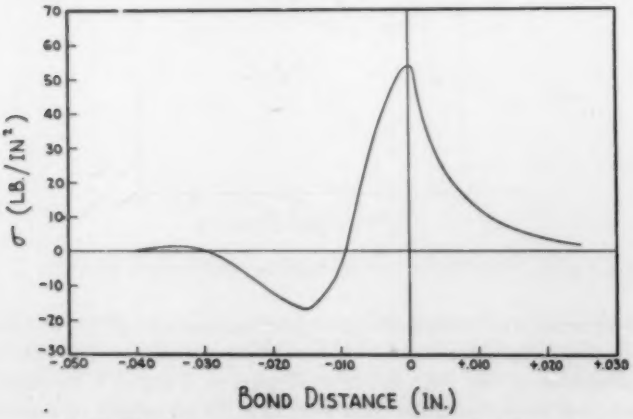

Fig. 12. The cleavage stress as measured in steady state peel.

for the cleavage stress distribution by use of a special instrument termed the "split beam transducer"[5] which measures the cleavage stresses acting through the adhesive interlayer upon the adherend. A typical directly measured cleavage stress function is presented in Figure 12 for a bond involving a self-adhering adhesive and cellulose acetate flexible member where:

Adhesive thickness (a)	= 0.001 in.
Flexible member thickness ($2h$)	= 0.0015 in.
Peel angle (ω)	= 90°
Peel rate	= 2.0 in./min.
Temperature	= 25 ± 1°C.
Relative humidity	= 50 ± 5%

The general features of the theoretical cleavage stress functions, as previously illustrated in Figure 3, are evident. The cleavage stresses display a narrow region of maximum tensile stress at $x = 0$. Proceeding toward the bond interior, $-x$ direction, we recognize the region of compressive stress and interior tensile stress.

The chief deviation of experiment from predictions from theory occurs at the boundary. Rather than stress approaching a maximum at $x = 0$ and dropping discontinuously to zero, we experience a broad region positive average stress in the region of $+x$ values. This phenomenon is associated with the well-recognized stranding or tooth formation which is a mechanism of failure beyond the scope of the assumptions of theory. Gent and Lindley[6] have recently recognized and theoretically treated a similar phenomena, which operates through the nucleation of internal flaws, as they occur in tensile stressing of bonded rubber cylinders of high width to thickness ratio. In the well-vulcanized examples of Gent and Lindley these internal flaws did not control the strength of the bond presumably due to the crosslinked network which inhibited their propagation through flaw mechanisms. An analogous phenomena of void nucleation has been recently reported by Myers, Miller, and Zettlemeyer,[7] in the splitting of liquid films where flow regions allow void propagation and cavitation. In bonds involving self-adhering adhesives, comprising non-crosslinked polymeric adhesives, a phenomena of teething as shown by the split beam experiment, Figure 12, could reasonably represent a condition intermediate between that of viscous liquids and crosslinked elastomers.

Graphical analysis of Figure 12 indicates the summed bond cleavage forces $\Sigma f = 0.486$ lb. and the summation of cleavage moments of force $\Sigma fx = M_c = 4.73 \times 10^{-3}$ lb. in. These factors may be applied to the calculation of the flexible member modulus from an equation of the peel mechanics[1] (see Table II) which does not depend on the particular form of the stress function. For 90° peel the equation becomes:

$$E = (\Sigma fx)^2/2I\Sigma f = 1.59 \times 10^5 \text{ psi}$$

where $I = 1.45 \times 10^{-10}$ (in.^{4}). This calculated modulus is in reasonable agreement with the expected values for cellulose acetate. Ignoring the already discussed deviation of the stress function of

Figure 12 from theoretical predictions, let us calculate the adhesive Young's modulus from eq. (14) which may be rewritten for 90° peel:

$$Y = K^2\sigma 2EIab/M_c = 15.0 \text{ psi}$$

where by assumption $K = 1.0$, and from Figure 12, $\sigma_0 = 54$ psi. The calculated value for adhesive Young's modulus is in a range of magnitude in agreement with expectations and typical of self-adhering adhesives.

Appendix I

IA. The Cleavage Boundary Stress Function

Applying the condition of equilibrium of external moments and forces we obtain the following relations:

$$ds + f = 0 \tag{1}$$

$$dM_x + sdx = 0 \tag{2}$$

Introducing the exact relation for bending deformation[2]

$$EI(d\omega/ds)_C = M_c$$

and recognizing the valid approximation $(d\omega/ds)_C = (d^2y/dx^2)$ applicable to small bending defections we obtain:

$$EI(d^2y/dx^2) = M_c \tag{3}$$

which relates the flexible member Young's modulus (E), moment of inertia about the neutral axis (I), and curvature (d^2y/dx^2) to the bending moment M.

Differentiating eq. (3) twice we obtain:

$$EI(d^4y/dx^4) = d^2M_c/dx^2 \tag{4}$$

Rearranging eq. (2) and differentiating we obtain:

$$-ds/dx = d^2M_x/dx^2 \tag{5}$$

Combining eqs. (4) and (5) we obtain:

$$EI(d^4y/dx^4) = -ds/dx \tag{6}$$

From eq. (1):

$$ds = -f = Ybydx/a \tag{7}$$

where Y is the adhesive interlayer Young's modulus, a the interlayer thickness, and b the bond width. Rearranging eq. (7) and combining with eq. (6) we obtain:

$$(d^4y/dx^4) + (Yb/EIa)y = 0 \tag{8}$$

Applying the standard method for solving linear differential equations of this type, we write:

$$(D^4 + Yb/EIa)y = 0 \tag{9}$$

where D is the operator (d/dx). If we assume the convention:

$$\beta = (Yb/4EIa)^{1/4} \tag{10}$$

then eq. (9) becomes:

$$(D^4 + \beta^4)y = 0 \tag{11}$$

which may be solved by standard procedures, recognizing $y = 0$ for high negative values of x, to obtain:

$$y = e^{\beta x}(A \cos \beta x + B \cos \beta x) \tag{12}$$

where:

$$A = (\beta M_c + P \sin \omega)/2\beta^2 EI$$

$$B = M_c/2\beta^2 EI$$

Solving in terms of the adhesive interlayer stress $\sigma = yY/a$, eq. (12) becomes upon substitution for A and B and rearrangements

$$\sigma = \frac{Ye^{\beta x}}{2\beta^3 EIa}\beta M_c(\cos \beta x + \sin \beta x) + P \sin \omega \cos \beta x \tag{13}$$

The tensional-compressional stresses associated with cleavage are completely defined, within the scope of the original assumptions, by eq. (13).

1B. The Shear Stress Function

Applying the condition of equilibrium of external forces we obtain:

$$dp + q = 0 \tag{14}$$

The flexible member tensile stress (ϕ) is:

$$\phi = P/2hb$$

which upon differentiation and rearrangement becomes:

$$dp = 2hbd\phi \tag{15}$$

The shear modulus of the adhesive interlayer may be expressed as follows:

$$G = (-q/bdx)/(u/a) = -qa/ubdx$$

or:

$$q = -Gubdx/a \tag{16}$$

where $-q$ is the applied shear force to the interlayer, and u is the shear displacement of the interlayer. Substituting eqs. (15) and (16) into eq. (14) we obtain:

$$2hbd\phi - (Gubdx/a) = 0$$

or:

$$d\phi = Gudx/2ah \tag{17}$$

The total flexible member tensional deformation at x equals the adhesive shear deformation u. Therefore the tensional strain in increment dx is:

$$du/dx = \phi/E \tag{18}$$

Differentiating eq. (17)

$$d^2\phi/dx^2 = (G/2ah)(du/dx)$$

and substituting we obtain:

$$d^2\phi/dx^2 = (G/2Eah)\phi$$

or:

$$(d^2\phi/dx^2) - (G/2Eah)\phi = 0 \tag{19}$$

if we let:

$$\alpha^2 = G/2Eah \tag{20}$$

then by operator notation eq. (19) becomes

$$(D^2 - \alpha^2)\phi = 0 \tag{21}$$

Solving eq. (21) by standard methods we obtain:

$$\phi = C_1e^{-\alpha x} + C_2e^{\alpha x} \tag{22}$$

Since $\phi = 0$ for high negative values of x we obtain:

$$C_1 = 0$$

$$C_2 = (P \cos \omega)/2bh$$

differentiating eq. (22) we obtain:

$$d\phi/dx = C_2 \alpha e^{\alpha x} \tag{23}$$

The expression for the adhesive shear stress, $\lambda = Gu/a$, may be substituted into eq. (17) to provide the relation:

$$d\phi/dx = \lambda/2h \tag{24}$$

combining eqs. (23) and (24) we may write the shear stress function:

$$\lambda = (P \cos \omega \, \alpha e^{\alpha x})/b \tag{25}$$

References

1. Kaelble, D. H., *Trans. Soc. Rheol.*, **3**, 161 (1959).
2. Spies, G. J., *Aircraft Eng.*, **25**, No. 289, 64 (1953).
3. Bikerman, J. J., *J. Appl. Phys.*, **28**, 1484 (1957).
4. Timosbenko, S., *Theory of Elastic Stability*, McGraw-Hill, New York, 1936.
5. Johnson, E. G., and D. H. Kaelble, "Apparatus for the Measurement of Normal Stress Distribution in Adhesive Bonds During Peel," presented at the April, 1959, Meeting of the American Physical Society, Cambridge, Mass. (to be published).
6. Gent, A. N., and P. P. Lindley, *Proc. Roy. Soc. London*, **A249**, 195 (1959).
7. Myers, R. R., J. C. Miller, and A. C. Zettlemeyer, *J. Colloid Sci.*, **14**, 287 (1959).

Synopsis

A previous theory is extended to provide expressions, general with respect to stripping angle, for the boundary stresses and bond stress distributions. The treatment is developed in terms of two stress mechanisms. Boundary cleavage involves tension-compression stress and predominates at high angles of peel. At some low range of peel angles, predicted from theory, boundary shear provides the controlling mechanism. Measurement of peel force as a function of angle of peel and rate identify the transition in failure mechanism from cleavage to boundary shear and provide comparison data for theoretical force-angle functions. The results of direct measurement of the internal cleavage stresses, by means of a new experimental device termed the "split-beam transducer," further characterize this bond failure mechanism.

TRANSACTIONS OF THE SOCIETY OF RHEOLOGY IV, 75–89 (1960)

The Peeling Force of Adhesive Joints

FRANKLIN S. C. CHANG, *Mystik Adhesive Products, Inc., Northfield, Illinois*

The peeling force of adhesive joints has been an interesting subject for scientific investigations as well as industrial applications, since adhesive finds ever-increasing usage. A great deal has been published about the phenomenon. For examples, De Bruyne and Houwink[1] reviewed this subject extensively; Busse and co-workers[2] designed a special instrument for the measurement of peeling force; Taylor and co-worker[3] attempted an explanation by use of interaction between dipoles of adhesive and ions of adherend surface; McLaren and co-workers[4] measured the peeling resistance of various polymers between two layers of cellophane; Bright[5] calculated activating energy of adhesive. As the variables involved are not readily isolated from one another, the peeling force is generally used to represent the adhesive or cohesive property of the joint, or even the polymer in the cases of single-component adhesives. The conclusions thus obtained are difficult to generalize, although the peeling force of adhesive joints is related to the adhesion or cohesion of the adhesive. Spies[6] and Bikerman[7] made attempts to understand the mechanics of peeling by calculating the peeling force of adhesive joints made of a Hookian solid under the conditions that the deflection angle is small and the length of adherend in the strained region is infinitely long. These conditions are unlikely to be encountered in practical peeling, and the requirement of a Hookian solid can only be approximated at very high peeling speed. This paper is a preliminary report of the efforts in this laboratory to treat the peeling force of adhesive joints in general terms, including the effect produced by the combination of peeling speed and viscoelastic nature of adhesive.

General Equations

Strings are breaking and forming in the strained region during the peeling of adhesive joints. The peeling can be considered as a special tensile testing with multiple specimens. The stress in each string is given by the theory of plastics as a function of elongation and time rate of elongation.

$$S = S\left(\epsilon, \frac{d\epsilon}{dt}\right)$$

The form of this function is dictated by the mechanical model chosen to represent the adhesive mass. For the three-element model, shown in Figure 1, chosen in this discussion in order not to make the treatment too elaborate, the stress S in the string is

$$S = E_1\epsilon_1 = E_2\epsilon_2 + \eta d\epsilon_2/dt$$

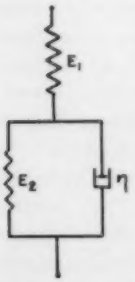

Fig. 1. A 3-element mechanical model.

where E_1 and E_2 are the Young's moduli of the elastic elements, respectively, η the viscosity of the dashpot, and ϵ_1 and ϵ_2 the elongations in the series and parallel parts of the model, respectively. Then

$$\frac{dS}{dt} + \frac{E_1 + E_2}{\eta} S = E_1\left(\frac{E_2}{\eta}\epsilon + \frac{d\epsilon}{dt}\right) \qquad (1)$$

where ϵ is the total elongation ($= \epsilon_1 + \epsilon_2$). By the use of the relation $dL = vdt$, where dL is an infinitesimal length of adherend and v the instantaneous velocity of adherend, equal to the instantaneous peeling speed, eq. (1) can be changed into

$$\frac{dS}{dL} + bS = E_1\left(\frac{E_2}{\eta v}\,\epsilon + \frac{d\epsilon}{dL}\right) \tag{2}$$

where $b = (E_1 + E_2)/\eta v$.

The elongation ϵ is defined as

$$\epsilon = -1 + (y + y_0)/y_0 \cos\omega \tag{3}$$

where y_0 designates the thickness of the adhesive film, and ω the angle between the string and the ordinate y of adherend. Let y take the form of an infinite series

$$y = \Sigma a_i L^i$$

where a_i are constants The end condition that there is neither elongation nor bending at the origin requires that $y = 0$ and $\theta = 0$ when $L = 0$. Since $dy/dL = \sin\theta$, dy/dL must be null at $L = 0$. Therefore $a_0 = a_1 = 0$. For convenience all higher terms than L^4 are omitted. This omission is justified *post facto* for the reason that the L^4 term is already small, for all practical application, as compared to the previous terms. Thus

$$y = a_2L^2 + a_3L^3 + a_4L^4 \tag{4}$$

$$\sin\theta = dy/dL = 2a_2L + 3a_3L^2 + 4a_4L^3 \tag{5}$$

$$\cos\theta = 1 - 2aL^2 - 6a_2a_3L^3 - (8a_2a_4 + 9a_3^2/2 + 2a_2^4)L^4 - (12a_3a_4 + 12a_2^3a_3)L^5 - (8a_4^2 + 16a_2^3a_4 + 27a_2^2a_3^2 + 4a_2^6)L^6 - \ldots \tag{6}$$

The value of ω depends on the geometrical arrangement of the peeling concerned, which can be expressed in terms of L as shown later in the discussion of individual cases. Then ϵ may be written as a polynomial of L, so that eq. (2) can be integrated. Let

$$y_0\left(\frac{E_2}{\eta v}\,\epsilon + \frac{d\epsilon}{dL}\right) = \Sigma\alpha_n L^n \tag{7}$$

where α_n are constants. Then eq. (2) becomes

$$\frac{dS}{dL} + bS = \frac{E_1}{y_0}\,\Sigma\alpha_n L^n$$

and

$$\frac{y_0 S}{E_1} = \sum_{r=0}^{\infty} \sum_{n=1}^{r} (-1)^{n+r} \frac{n!\alpha_n L^r}{r!b^{n-r+1}} - \exp\{-bL\} \sum_{n=1}^{r} (-1)^n \frac{n!\alpha_n}{b^{n+1}} \qquad r \leqslant n$$

$$= \sum_{r=2}^{\infty} \sum_{n=1}^{r} (-1)^{n+r+1} \frac{n!\alpha_n L^r}{r!b^{n-r+1}} \qquad r > n \tag{8}$$

The calculation of a_i can be readily made by means of the theory of beams on elastic foundation.[8] The bending angle θ is related to the load in the following manner:

$$\frac{d^3\theta}{dL^3} = \frac{1}{EI} \frac{dV}{dL} \tag{9}$$

where E and I are the Young's modulus and moment of inertia of the bent adherend, respectively, and dV the load on dL. Since $dy/dL = \sin\theta$, the left side of eq. (9) can be expressed in the derivatives of y.

$$\frac{d^3\theta}{dL^3} = (1 - y_1^2)^{-5/2} [y_4(1 - y_1^2)^2 + 3y_1y_2y_3(1 - y_1^2) + y_2^3(1 + 2y_1^2)] \tag{10}$$

where y_i are the ith derivative of y. The projection of an infinitesimal area WdL on the reference plane which is taken at the root of the string perpendicular to the center line of the string (cf. Fig. 3), is $WGdL$, W being the width of the joint. The force on this area along the string is $-WGSdL$, of which the component normal to the adherend is $-WG^2SdL$. Therefore

$$\frac{1}{EI} \frac{dV}{dL} = -\frac{WSG^2}{EI} \tag{11}$$

Substituting eqs. (10) and (11) into eq. (9),

$$y_4(1 - y_1^2)^2 + 3y_1y_2y_3(1 - y_1^2) + y_2^3(1 + 2y_1^2) = -\frac{WSG^2}{EI}(1 - y_1^2)^{5/2} \tag{12}$$

Expressing y_i in terms of L by use of eq. (5) and collecting terms, eq. (12) can be readily transformed into

$$8a_2^3 + 24a_4 + 144a_2^2a_3L + (240a_2^2a_4 + 540a_2a_3^2 + 64a_2^5)L^2 + \ldots$$

$$= -\frac{WSG^2}{EI}(1 - 10a_2^2L^2 - 30a_2a_3L^3 + \ldots) \quad (13)$$

When S and G are written as polynomials of L, SG^2 will be also a polynomial of L, say, $\Sigma\beta_jL^j$. Then after transposing, eq. (13) becomes

$$8a_2^3 + 24a_4 + \frac{\beta_0W}{EI} + \left(144a_2^2a_3 + \frac{\beta_1W}{EI}\right)L +$$

$$\left(240a_2^2a_4 + 540a_2a_3^2 + 64a_2^5 + \frac{\beta_2W}{EI}\right)L^2 + \ldots = 0$$

This equation is true for all values of L, so that all individual terms must vanish. Thus

$$8a_2^3 + 24a_4 + \frac{\beta_0W}{EI} = 0$$

$$144a_2^2a_3 + \beta_1W/EI = 0$$

$$240a_2^2a_4 + 540a_2a_3^2 + 64a_2^5 + \beta_2W/EI = 0 \quad (14)$$

The force F required to peel the adhesive joint is equal to the resistance in the direction of the peeling force offered by strings in the strained region.

$$dF = -WGHSdL \quad (15)$$

where $WSGdL$ is the force in the string as discussed previously and H represents the geometrical relation between this force and the peeling force. H is also readily expressed in the form of a polynomial of L, so as

$$GH = \Sigma\zeta_mL^m \quad (16)$$

Combining eqs. (8), (15), and (16) and integrating, with the negative sign ignored,

$$F = \frac{WE_1}{y_0}\sum_{r=2}\sum_{m=0}\sum_{n=1}(-1)^{n+r+1}\frac{n!\alpha_n\zeta_mL^{r+m+1}}{r!(r+m+1)b^{n-r+1}} \quad r > n \quad (17)$$

Individual Cases

Several arrangements of adherends generally used in peeling adhesive joints are sketched in Figure 2. The so-called 90° peeling shown in Figure 2a, hereafter referred to as L-peeling, is carried out with the joint and one of the adherends remaining flat and the free end of the other adherend perpendicular to the joint. This type of peeling was used by Busse and co-worker[2] and recommended in ASTM

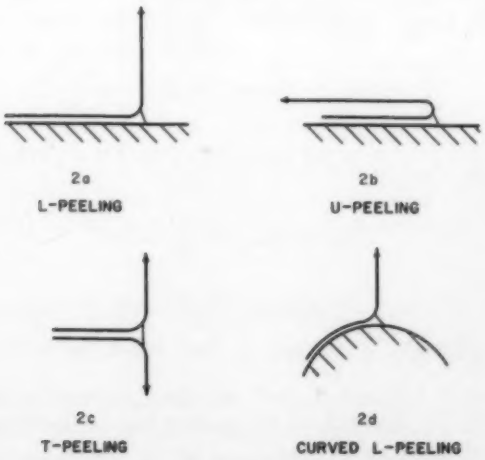

Fig. 2. Types of peeling of adhesive joints.

Standard D429 for testing rubber-to-metal joint and suggested by this author[9] for testing tack of pressure-sensitive tape. The widely applied 180° peeling, designated as U-peeling in this work, is depicted in Figure 2b, in which one adherend remains flat as in the previous case, but the other adherend is bent back into the direction parallel to the unpeeled part of the joint. Two examples of U-peeling can be found in ASTM Standard D1000 and the work of Bright.[5] Figure 2c shows the third type of peeling, in which both free ends of adherends are bent away through a 90° angle from the joint. The cohesion strength of joint can be measured with this arrangement. The ARL test[10] for metal-to-metal joint and unwinding test for adhesive tape are examples of the case shown in Figure 2d, in which

the joint is shaped into an arc of a circle and then one adherend is peeled away from the joint to a vertical position. As far as the elongation of the adhesive film and the relative coordinates of the strained region are concerned, this arrangement is very similar to that of L-peeling. Therefore, no special treatment is needed for this type of peeling.

Case I. L-*Peeling*

The relative position of string to adherends for this case is detailed in Figure 3. The two ends of string are at the same abscissa before the string is stretched. If the flexible adherend is not stretchable

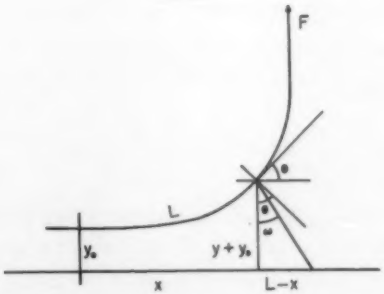

Fig. 3. L-peeling.

as is assumed in this treatment, the length of adherend from the origin to the upper end of string is equal to the distance from the lower end of string to the y-axis, at any stage of stretching. Then it is apparent from the figure that

$$1/\cos\omega = (1 + \tan^2\omega)^{1/2} = \left[1 + \left(\frac{L - x}{y + y_0}\right)^2\right]^{1/2}$$

$$\doteq \left[1 + \left(\frac{L - x}{y}\right)^2\right]^{1/2} \qquad (18)$$

The approximation is permissible because y_0 is much smaller than y in a large part of the strained region and in the region where y_0 is not negligible $(L - x)$ is almost nil. Since $dx/dL = \cos\theta$, inserting eq. (6) and integrating,

$$x = L\left[1 - \frac{2}{3}a_2^2L^2 - \frac{3}{2}a_2a_3L^3 + \ldots\right] \tag{19}$$

As will be shown later, $\tan\omega$ is always less than 1, and eq. (18) is expandable. Substituting eqs. (19) and (4) for x and y in eq. (18) yields, after expansion,

$$\begin{aligned}1/\cos\omega = {} & 1 + 2a_2^2L^2/9 + 5a_2a_3L^3/9 \\ & + (47a_3^2/120 + 28a_2a_4/45 + 98a_2^4/405)L^4 + (a_2^3/90a_2 \\ & + 14a_3a_4/15 + 544a_2^3a_3/405)L^5 + \ldots \end{aligned} \tag{20}$$

By definition

$$\epsilon = y/y_0\cos\omega + (1 - \cos\omega)/\cos\omega$$

The second term in the last expression can be ignored and

$$\epsilon \doteq y/y_0\cos\omega$$

Inserting eq. (20),

$$\begin{aligned}\epsilon y_0 = {} & a_2L^2 + a_3L^3 + \left(\frac{2}{9}a_2^3 + a_4\right)L^4 + \frac{7}{9}a_2^2a_3L^5 \\ & + \left(\frac{57}{60}a_2a_3^2 + \frac{38}{45}a_2^2a_4 + \frac{98}{405}a_2^5\right)L^6 \\ & + \left(\frac{1}{2}a_3^3 + \frac{19}{15}a_2a_3a_4 + \frac{71}{45}a_2^4a_3\right)L^7 + \ldots \end{aligned} \tag{21}$$

Then eq. (8) becomes

$$\begin{aligned}\frac{y_0S_L}{E_1} = {} & a_2L^2 + \left(-2a_2b + 6a_3 + \frac{2a_2E_2}{\eta v}\right)\frac{L^3}{3!} + \left[2a_2b^2 - 6a_3b\right. \\ & \left. - \frac{2a_2bE_2}{\eta v} + 6\left(\frac{8}{9}a_2^3 + 4a_4 + \frac{a_3E_2}{\eta v}\right)\right]\frac{L^4}{4!} + \ldots \end{aligned} \tag{22}$$

It is apparent that the geometrical function G in this case is

$$\begin{aligned}G = {} & \cos(\theta - \omega) \\ = {} & \cos\theta\cos\omega + \sin\theta\sin\omega \\ = {} & \cos\omega(\cos\theta + \sin\theta\tan\omega) \\ = {} & 1 - \frac{8}{9}a_2^2L^2 - \frac{26}{9}a_2a_3L^3 \\ & - \left(\frac{232}{45}a_2a_4 + \frac{271}{15}a_3^2 + \frac{136}{135}a_2^4\right)L^4 - \ldots \end{aligned} \tag{23}$$

It follows that in the polynomial SG^2 of eq. (13)

$$\beta_0 = 0$$

$$\beta_1 = 0$$

$$\beta_2 = \frac{a_2 E_1}{y_0}$$

Putting these values into eq. (14) yields

$$a_2 = (WE_1/16EIy_0)^{1/4} = (3E_1/4Ey_0\delta^3)^{1/4}$$

$$a_3 = 0$$

$$a_4 = -a_2^3/3 \tag{24}$$

since $I = W\delta^3/12$, where δ is the thickness of the adherend. Now a_2 and a_4 are related, so we may drop the subscript of a_2 and express y as

$$y = aL^2(1 - a^2L^2/3)$$

$$a^4 = 3E_1/4Ey_0\delta^3 \tag{25}$$

It may be observed that the constant a is comparable to the quantity defined as the characteristic of the system in the theory of beams on elastic foundation for small bending angle. Therefore, a may be called the characteristic of the joint. It can be shown that by differentiating eq. (25) twice, $\sin\theta$ has a maximum at $aL = 1/\sqrt{2}$. This shows that the treatment will not cover the region beyond $L = 1/\sqrt{2}a$. However, in this region near $\theta = \pi/2$, coalition of string may happen. This phenomenon is certainly not included in this discussion, which needs special consideration, if it is involved.

In the derivation it was assumed that $\tan\omega < 1$, so eq. (18) can be expanded. As the maximum value for aL is $\leq 1/\sqrt{2}$, it is readily verified that $1/\cos\omega$ [eq. (20)] $< \sqrt{2}$. Therefore, ω is $< \pi/4$ and the expression (18) is expandable. Combining eqs. (22) and (24),

$$S_L = \frac{E_1 a}{y_0} L^2 \left[f_0 + \frac{2E_1}{E_1 + E_2}(-f_1 bL/3! + f_2 b^2L^2/4! - f_3 b^3L^3/5! + \ldots) \right]$$

$$f_0 = 1 - a^2L^2/9 - 16a^4L^4/3^4 \cdot 5 - \ldots$$

$$f_1 = 1 - \frac{3! \cdot 4!}{2 \cdot 5!} \cdot \frac{1}{9} a^2L^2 - \frac{3! \cdot 6!}{2 \cdot 7!} \cdot \frac{16}{3^4 \cdot 5} a^4L^4 - \ldots$$

$$f_2 = 1 - \frac{4!\cdot 4!}{2\cdot 6!}\cdot\frac{1}{9}a^2L^2 - \frac{4!\cdot 6!}{2\cdot 8!}\cdot\frac{16}{3^4\cdot 5}a^4L^4 - \ldots$$

$$f_3 = 1 - \frac{5!\cdot 4!}{2\cdot 7!}\cdot\frac{1}{9}a^2L^2 - \frac{5!\cdot 6!}{2\cdot 9!}\cdot\frac{16}{3^4\cdot 5}a^4L^4 - \ldots \qquad (26)$$

The y-component of the stretching force in string is the force resisting peeling. It is obvious that the function $H = \cos\omega$. Dividing eq. (23) by eq. (20), we obtain the constants ζ_m for GH.

$$\zeta_1 = \zeta_3 = \zeta_5 = \zeta_7 = \zeta_9 = 0$$

$$\zeta_0 = 1 \qquad \zeta_2 = -10a^2/3^2$$

$$\zeta_4 = 14a^4/3^4 \qquad \zeta_6 = 4a^6/3^2$$

$$\zeta_8 = 13a^8/3^3 \qquad \zeta_{10} = -44a^{10}/3^3 \qquad (27)$$

Thus the peeling force for this case is

$$F_L = \frac{WE_1aL^3}{3y_0}\left[g_0 + \frac{6E_1}{E_1+E_2}\left(-\frac{g_1bL}{4!} + \frac{g_2b^2L^2}{5!} - \frac{g_3b^3L^3}{6!} + \ldots\right)\right]$$

$$g_0 = 1 - \frac{89}{135}a^2L^2 + \frac{34}{945}a^4L^4 + \ldots$$

$$g_1 = 1 - \frac{106}{135}a^2L^2 + \frac{65}{567}a^4L^4 + \ldots$$

$$g_2 = 1 - \frac{52}{63}a^2L^2 + \frac{67}{567}a^4L^4 + \ldots$$

$$g_3 = 1 - \frac{6}{7}a^2L^2 + \frac{10}{81}a^4L^4 + \ldots \qquad (28)$$

Case II. U-*Peeling*

The geometry of strained region in U-peeling is very much the same as that of L-peeling, so that the stress and elongation functions are identical to eqs. (21) and (27). The peeling force required, however, is the sum of the x-components of the force in string.

$$dF_V = WS \sin \omega \cos (\theta - \omega) dL$$

$$GH = \sin \omega \cos (\theta - \omega)$$

$$= \tan \omega \cos \omega \cos (\theta - \omega)$$

$$= \Sigma \zeta_m L^m$$

$$\zeta_0 = \zeta_2 = \zeta_4 = \zeta_6 = \zeta_8 = 0$$

$$\zeta_1 = 2a/3 \qquad \zeta_3 = -88a^3/3^3 \cdot 5$$

$$\zeta_5 = -148a^5/3^5 \cdot 5 \cdot 7 \qquad \zeta_7 = 64a^7/3^5$$

$$\zeta_9 = 14a^9/3^3$$

The peeling force F_V is

$$F_V = \frac{2WE_1}{3y_0} a^2L^4 \left[g_0 + \frac{2E_1}{E_1 + E_2} \left(-\frac{g_1 bL}{3!} + \frac{g_2 b^2 L^2}{4!} - \frac{g_3 b^3 L^3}{5!} + \ldots \right) \right]$$

$$g_0 = \frac{1}{4} - \frac{49}{2 \cdot 3^3 \cdot 5} a^2L^2 + \frac{61}{2^2 \cdot 3^4 \cdot 5 \cdot 7} a^4L^4 + \ldots$$

$$g_1 = \frac{1}{5} - \frac{47}{3^2 \cdot 5 \cdot 7} a^2L^2 + \frac{62}{3^6 \cdot 5 \cdot 7} a^4L^4 + \ldots$$

$$g_2 = \frac{1}{6} - \frac{23}{2^2 \cdot 3^2 \cdot 5} a^2L^2 + \frac{7}{2 \cdot 3^4 \cdot 5} a^4L^4 + \ldots$$

$$g_3 = \frac{1}{7} - \frac{1}{9} a^2L^2 + \ldots$$

Case III. T-*Peeling*

In the case of T-peeling the strained region is symmetrical to a plane passing through the center of the joint, as shown in Figure 2c, only one half of the joint needs consideration. Therefore, y_0 in the general equations designates one half of the thickness of adhesive film. The only other consideration which has to be applied is that the angle ω has the only value of zero. The case has been discussed by this author in another paper.[11] Any discussion would be repetitious, but the results are included for the purpose of comparison as follows:

$$S_T = \frac{E_1 a L^2}{y_0}\left[1 - \frac{a^2L^2}{3} + \frac{2E_1}{E_1+E_2}\left\{-\frac{bL}{3!} + \frac{b^2L^2}{4!} + \left(1 - \frac{4a^2}{b^2}\right)\left(-\frac{b^3L^3}{5!} + \frac{b^4L^4}{6!} + \dots\right)\right\}\right]$$

$$F_T = \frac{WE_1aL^2}{3y_0}\left[g_0 + \frac{6E_1}{E_1+E_2}\left(-\frac{g_1bL}{4!} + \frac{g_2b^2L^2}{5!} - \frac{g_3b^3L^3}{6!} + \dots\right)\right]$$

$$g_0 = 1 - \frac{7}{5}a^2L^2 + \frac{4}{7}a^4L^4 + \dots$$

$$g_1 = 1 - \frac{22}{15}a^2L^2 + \frac{8}{5}a^4L^4 + \dots$$

$$g_2 = 1 - \frac{46}{21}a^2L^2 + \frac{14}{27}a^4L^4 + \dots$$

$$g_3 = 1 - \frac{11}{7}a^2L^2 + \frac{18}{35}a^4L^4 + \dots$$

Discussion

In the stress equation, eq. (8), when the speed of peeling is high enough so that $b(= (E_1 + E_2)/\eta v)$ is small enough to make all terms containing bL negligible, the stress and peeling force are then no longer influenced by change in peeling speed, since the equations contain no v. Equations (26) and (28) for L-peeling, for instance, become

$$S_L = f_0 E_1 a L^2 / y_0 \tag{30}$$

$$F_L = g_0 W E_1 a L^2 / 3y_0 \tag{31}$$

On the other hand, when the peeling speed v is small enough to make $\exp\{-bL\}$ vanish, all the other terms in eqs. (8) and (17) will vanish except those with $r = n$ and n is even.

$$S_L = \frac{f_0 E_1 E_2 a L^2}{y_0(E_1 + E_2)} \tag{32}$$

$$F_L = \frac{g_0 W E_1 E_2 a L^2}{3y_0(E_1 + E_2)} \tag{33}$$

Since there is no viscosity term in these equations the adhesive acts like a Hookian solid at both high and low peeling speeds. Further-

more, if L^*, the value of L at the breaking point of string, is put into eqs. (30) and (32), the stress will be the ultimate stress. As the ultimate stress will not become infinity or zero under these extreme conditions, aL will have values other than infinity and zero. Therefore, the peeling force will go neither to infinity at infinitely high peeling speed nor to zero at infinitely low peeling speed. These predictions about the limits of the peeling force agree with the experimental data obtained by Busse and co-workers with pressure-sensitive tape and glass adherend.[2]

When eq. (32) is substituted into eq. (13), the resulting value for the characteristic of the joint is

$$a^4 = \frac{3E_1E_2}{4Ey_0\delta^3(E_1 + E_2)} \tag{34}$$

The value of a differs to that given by eq. (24) when bL is less than unity. It is likely that a varies with v, and eqs. (24) and (34) give the limiting values of a. Experiments carried out in this laboratory with joints made of pressure-sensitive tapes showed that a changes but slowly with v, perhaps in an exponential manner. Thus, in a narrow range of peeling speeds one could consider a as constant to v, especially in the high speed region where $bL < 1$ and in the low speed region where $\exp\{-bL\}$ is nil.

It should be emphasized that the application of eqs. (26) and (28) for L-peeling and similar equations for other types of peeling is limited to the cases of high peeling speed where $bL < 1$, while eqs. (32) and (33) can be applied to cases of low peeling speed where $\exp\{-bL\}$ is nil. For intermediate peeling speeds, one should use the general expression for peeling force, which can be calculated by substituting the exponential form of S in eq. (8) into eq. (15) and integrating. The result is

$$\begin{aligned}\frac{Fy_0}{WE_1} = &\sum_{i=0}\sum_{r=0}\sum_{n=1}(-1)^{n+r}\frac{n!}{r!}\frac{\alpha_n\zeta_i}{r+i+1}\frac{L^{i+r+1}}{b^{n-r+1}} \\ &- \sum_{i=0}\sum_{n=1}(-1)^n\, n!i!\,\frac{\alpha_n\zeta_i}{b^{n+i+2}} \\ &+ \exp\{-bL\}\sum_{j=0}\sum_{i=0}\sum_{n=1}(-1)^n\,\frac{n!i!}{j!}\,\frac{\alpha_n\zeta_iL^j}{b^{n+i-j+2}} \qquad (35) \\ &\qquad r \leqslant n \qquad j \leqslant i\end{aligned}$$

When the interfacial force between adhesive and adherend is overcome by the stress in the string, the string detaches from the adherend. The failure is then said to be adhesionwise and the peeling force is called adhesion strength, according to the practice in the adhesive trade. The maximum stress permissible in the string in L-peeling with adhesion failure, for instance, is $A/\cos \omega^*$, where A designates the apparent adhesion between adhesive and adherend and ω^* is the angle of the detaching string. In the case where the interfacial force is larger than the ultimate stress in the string, the break occurs in the adhesive phase, and the failure is cohesive. When the joint is made of two lengths of pressure-sensitive tape and the break occurs between the layers of adhesive, the limiting factor may be called cohesion of the adhesive. In all events, the maximum allowable stress in the string before failure is limited by adhesion or ultimate stress or cohesion, while the maximum allowable stress in turn determines the value of the length of flexible adherend in the strained region, namely L^*. In other words, these properties of the adhesive do not effect the form of the force equation which is dictated by the construction of the joint and the condition of peeling, but furnish the upper limit to the peeling force integral. This is the reason why no mention is made about the nature of failure in the derivation of peeling force equations.

Besides offering theoretical analysis of peeling force of adhesive joints, the theory will (*1*) yield a system for characterizing the adhesive with four or more mechanical constants, such as E_1, E_2, η, and A; and (*2*) open up, through the study of apparent adhesion and cohesion, a way for investigating a group of interesting factors which are frequently talked about, such as surface condition of adherend, wetting property of adhesive, and dwelling time.

The author wishes to express his thanks to Mystik Adhesive Products, Inc. for permission to publish this work.

References

1. De Bruyne, N. A., and R. Houwink, *Adhesion and Adhesives*, Elsevier, New York, 1951.

2. Busse, W. F., J. M. Lambert, and R. B. Verdery, *High-Polymer Physics*, Chemical Publ. Co., New York, 1948, p. 300.

3. Taylor, D., Jr., and J. E. Rutzler, Division of Paint, Plastics, and Printing Ink Chemistry, Am. Chem. Soc., New York, Sept. 1957, Preprints p. 408.

4. McLaren, A. D. et al., *Ind. Eng. Chem.*, **40,** 329 (1948); *J. Polymer Sci.*, **3,** 652 (1948); *ibid.*, **5,** 463 (1951).
5. Bright, W. M., *Adhesion and Adhesives*, Wiley, New York, 1954, p. 130.
6. Spies, G. J., *Aircraft Eng.*, **25,** No. 289, 64 (1953).
7. Bikerman, J. J., *J. Appl. Phys.*, **28,** 1484 (1957).
8. Hetényi, M., *Beams on Elastic Foundation*, University Michigan Press, Ann Arbor, 1946.
9. Chang, F. S. C., *Rubber Chem. and Tech.*, **30,** 847 (1957).
10. De Bruyne, N. A., and R. Houwink, *Adhesion and Adhesives*, Elsevier, New York, 1951, p. 479.
11. Chang, F. S. C., *J. Appl. Phys.*, **30,** 1839 (1959).

Synopsis

Peeling of adhesive joint is mechanically a process of stretching the adhesive strings in the region of deformed adherend, and can be treated as multiple-specimen stretching. By using a three-element mechanical model to represent the adhesive, practical expressions of peeling force and stress in the string are derived for various geometrical arrangements conventionally used in different peeling tests. Application of these expressions will yield (*1*) analysis of peeling force in terms of nature of the adherend, viscoelastic characteristics of adhesive, peeling speed, and apparent interfacial force; (*2*) a group of parameters for characterizing adhesive; and (*3*) open up a way to study a number of interesting factors, e.g., surface condition of adherend, wetting property of adhesive, and dwelling time.

TRANSACTIONS OF THE SOCIETY OF RHEOLOGY IV, 91–116 (1960)

The Tensile Strength and Tacky Behavior of Polymeric Liquids*

ROBERT A. ERB, *The Franklin Institute Laboratories for Research and Development, Philadelphia, Pennsylvania,* and ROBERT S. HANSON, *Drexel Institute of Technology, Philadelphia, Pennsylvania*

Tacky behavior in general is related to the tensile strength of liquids as well as to the rheological and geometrical considerations in the systems under study. The technique used in this investigation of tacky behavior involves the rapid separation of parallel plates between which a liquid is contained, and permits quantitative measurement of the phenomena occurring during liquid film-splitting processes.

Tensile strength is a property which can be observed when a liquid is subjected to a tensile stress (or a negative pressure) under such circumstances that it cannot relieve the stress by viscous flow. These circumstances include complete confinement, or partial confinement with rapid stress application. The tensile strength is the maximum stress or negative pressure sustainable before the liquid breaks.

A number of techniques have been used to experimentally measure the tensile strength of liquids. These include stressing the liquid in a metal bellows or piston-cylinder apparatus, using centrifugal force with bent open-ended tubes containing the liquid, and rapidly separating parallel plates between which the liquid is contained. Values often vary widely with the method and investigator. For example, for water there are reported tensile strengths from -0.2 to -227 atm.[1] The lower values do not represent the limiting tensile strength of the liquid, but rather premature cavitational failure. The studies of Briggs[2–4] appear to have high reliability. His values for organic liquids in general are in the order of hundreds of negative atmospheres;

* This paper is based on a thesis presented by R. A. Erb to Drexel Institute of Technology in partial fulfillment of the requirements for the M.S. degree, June, 1959.

the same order of magnitude might also be expected for polymeric liquids.

Theoretical considerations also predict high limiting tensile strengths for various liquids. Considerations based on the relationship between the internal and external pressure for a bubble in a liquid, and the bubble radius and surface tension of the liquid give the following expression for the maximum negative pressure sustainable by the liquid.

$$P_L = 2\gamma/r_{max} \tag{1}$$

where γ is the surface tension of the liquid (dynes/cm.), and r_{max} is the radius of the largest bubble present in the system.[5] Thus, water containing a maximum size bubble of radius 150 A. would sustain approximately 100 negative atmospheres, or, with a radius of 15 A., 1000 negative atmospheres. In practice, spontaneously formed elementary cavities will determine the maximum tensile stress sustainable by a liquid. Fisher[6] and Bernath,[7] applying the nucleation theory of Volmer,[8] have derived expressions for quantitatively estimating the limiting tensile strengths of liquids. Table I, related to a compilation by Bernath, compares the calculated limiting tensile strengths by the methods of Bernath and Fisher; included are measured values for the four liquids by Briggs.

TABLE I
Limiting Tensile Strengths for Four Liquids at Approximately 25°C.

Liquid	Calculated		Measured,
	By Bernath (bars)	By Fisher (bars)	Briggs (bars)
Mercury	20,200	22,600	425
Water	1,140	1,340	263
Acetic acid	266	326	287
Benzene	287	343	130

We include these calculated and measured values to show the magnitude of tensile strengths which can properly be expected for unfilled liquid systems. This is important because of the tendency for a number of investigators in the field of tacky behavior to consider cavitation in liquids to occur more or less automatically at approxi-

mately zero pressure, with occasional allowances to minus one or two atmospheres.

Tacky behavior, itself, is a subject that has been rather widely investigated. For the purposes of this paper we will define tack as a measure of resistance to pulling apart of two surfaces which have a liquid (or, to be more general, a viscously deformable material) between them.

The magnitude of tack is related to the rate of separation, the geometry of the system, and the rheological characteristics of the liquid. The basic expression for the separation of flat plates with a liquid interlayer which deforms viscously was first given by Stefan[9] in 1874. One form which gives the force necessary to separate circular flat plates from an initial to a final interplate distance in a given time is:

$$F = \frac{3\pi\eta R^4(1/h_1^2 - 1/h_2^2)}{4t} \tag{2}$$

where F is the force (dynes), η is the viscosity of the liquid (poises), R is the radius of the plates (cm.), h_1 and h_2 are the initial and final separations (cm.), respectively, and t is the time (sec).

Banks and Mill[10] derived the following modification of Stefan's equation:

$$A - P_0 = 3\eta U/h^3R^2 \tag{3}$$

where A is the pressure on the liquid at the outside of the plates (usually equals 1 atm. or about 10^6 dynes/cm.^{2}), P_0 is the pressure at the center of the liquid (dynes/cm.^{2}), and U is the instantaneous velocity of separation of the plates (cm./sec.). This form of the equation is of particular interest because it relates P_0, the pressure at the center of the sample, to the separation velocity U. Thus we can see that the maximum stress which the liquid can sustain gives a maximum limit to the velocity of cavitation-free plate separation. After cavitation, Stefan's equation is no longer valid to relate force and separation rate.

The areas of greatest interest in the study of tacky behavior are those ultra-Stefan or non-Stefan situations which involve (*a*) cavitation, and/or (*b*) elastic behavior of the interlayer material. This applies especially, for example, to studies in the fields of printing and pressure-sensitive adhesives.

Two classes of instruments which have been of value in studying tack of liquids are (*a*) roller systems and (*b*) separating flat plate systems.

Roller systems have as advantages that they can easily produce high-speed film splitting and thus permit detection of elastic effects and cavitation, with observation facilitated by the essentially steady-state conditions present. A disadvantage is that stress-strain functions cannot be experimentally measured for a single element of material. Examples of roller system studies include those of Reed[11] (the Inkometer); Banks and Mill;[12] Myers, Miller, and Zettlemoyer[13,14] (the "discone"); and Voet and Geffken.[15] One interesting conclusion in this last study, where it was shown that elastic effects (in printing inks) overshadow viscous effects at printing press speeds, was in their statement concerning filament elongation: "For most commercial inks the maximum stress appears to have an order of magnitude of 10^7 to 10^9 dynes/sq. cm." These high figures of about 10 to 1000 bars are in line with the experimental results obtained in our study.

Separating flat plate systems have the advantage that the liquid deformation and break for a given geometrical element can be quantitively followed through its various stages. A disadvantage, at least historically, has been the difficulty of applying proper instrumentation, particularly for high-speed film splitting. A number of examples of studies with separating flat plate systems are found in the literature. Green[16] used a slow-speed, constant load apparatus (the Tackmeter), which apparently operated entirely in the Stefan range; no correlation of "tack" as measured and "picking" of a printing ink (a non-Stefan phenomenon) was found, for example. Wetzel[17] has used an Instron Tensile Testing Machine with pressure-sensitive adhesive materials. Banks and Mill[10] employed weights and springs in a slow-speed, flat plate apparatus.

Strasburger[18] used a piezo-electric transducer and an oscilloscopic recording of the forces with a flat plate system. Separation velocities up to 4 cm./sec. were used. He obtained traces of different shapes corresponding to Stefan and ultra-Stefan type behavior. His curves of force versus time are similar in shape to some seen in our work, but we differ in interpretation. Two of his points on which we differ for unfilled systems are (*a*) that initial cavitation occurs at close to zero pressure, perhaps to minus one or two atmospheres (here he

follows Banks and Mill), and (*b*) that increase in the separation of the plates subsequent to cavitation is defined by a viscous bubble-enlargement mechanism. Concerning the cavitation at zero or very small negative pressures, we showed earlier that this is not a theoretical requirement, and we shall see, in the experimental results following that it is not a practical requirement. It is possible that Strasburger's instrumentation may not measure accurately the peak force in the extremely short period before cavitation occurs (which in some of our work was less than $^1/_{4000}$ sec.). Concerning the second point, a viscous bubble-enlargement analysis does not adequately define the situation because of the rapid conversion of the initial cavitation bubbles to filaments in most cases. Furthermore, in many high speed operations (with printing inks, for example) *elastic* behavior of the filaments becomes the mechanism of importance. The conclusions by Strasburger may have been altered significantly if a continuous observation of the physical events occurring during film splitting had been coupled directly with the force measurements.

Experimental Method

The experimental technique used in our study consists basically of enclosing a layer of the liquid to be tested between parallel flat surfaces of two blocks of metal of known mass, with the top block subsequently removed rapidly and the behavior of the liquid and the motion of the blocks being followed by high-speed motion picture photography. From the motion (if any) of the bottom block the force transmitted by the liquid can be determined, using Newton's Second Law of Motion. The position of the bottom block was measured to ±0.01 cm. in this study (with corrections being made for wobble, when present).

The technique described is highly suitable for the quantitative study of the behavior of liquids between separating plates. It provides a complete record during the separation process of the following: (*a*) Time (in approximately $^1/_{4000}$ sec. increments with the present equipment); (*b*) Liquid elongation (and rate of elongation); (*c*) Force across the liquid; (*d*) Minimum cross-sectional area of the liquid, and thus; (*e*) Maximum stress (force per unit area) across the liquid; (*f*) Energy required for the cavitation and the filament elongation processes.

All of these measured quantities are correlated with each other and with direct observation of physical events simultaneously occurring, such as filamentation, liquid break, and elastic recovery. None of the experimental techniques described in the literature for studying the behavior of liquids between rapidly separating parallel plates appear to offer this much information, particularly with reference to correlating the physical events to the quantitative measurements. Further, this separating plate system has an advantage over the steady state systems (roller type) in that each phase of the splitting is studied and analyzed separately, as well as compositely, for the above-mentioned quantities.

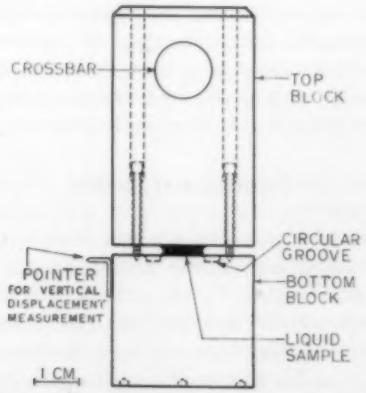

Fig. 1. Diagram of top and bottom blocks with liquid in place.

Instrumentation and technique similar to this has been used by Stone, Schiefer, Fox, Smith, and McCrackin[19] for studying the high-speed tensile properties of yarns. The technique was also used later to test Mylar film in long strips.[20]

In our test apparatus, stainless steel blocks are set on a vertical pillar which can be rotated so that the top block crossbar can be lifted by the projections on a 2 m. circumference flywheel. A mechanical switching arrangement synchronizes rotation of the blocks into firing position with the start of a 4000 frames/sec. 16 mm. Fastax camera. The flywheel is free-turning with the velocity at impact determined by a Strobotac stroboscopic device and timing

marks. Lighting is accomplished by a single 750 w. reflector lamp placed behind a diffusing screen so as to silhouette the sample, blocks, and transparent stationary reference scale. By using opaque vertical bordering areas on the diffusing screen, sharp delineation of the clear liquid during extension is obtained through a lens effect; internal discontinuities (e.g., cavitation) show up as opacities.

All measurements from the films were made directly from projected images (on ground-glass viewer screen) or from photographic enlargements. The number of frames per second was determined from timing marks on the film.

Figure 1 is a diagram of the top and bottom blocks with the liquid to be tested in place. The distance between the polished plane faces of the top and bottom block is adjustable by four pointed screws that sit in depressions in the surface of the bottom block. Two bottom blocks, each of 200 g. mass, were made for this experimental program. Circular grooves of two different diameters, 0.93 and 1.21 cm., were used to define the boundaries of the liquid under test. The plane surfaces were cleaned with chromic acid cleaning solution, followed by a distilled water rinse and air dry, before each use to maximum adhesion. Great care was taken to insure freedom from air bubble entrapment during assembly, though the sample liquids were not degassed or otherwise specially treated.

Results and Discussion

Ten sequences of liquid deformation and break were filmed (100 ft. of movie film in each case). Five polymeric or high molecular weight liquids having viscosities in their Newtonian region of flow of from 60 poises to 1.2×10^6 poises were studied. Table II gives the test conditions and observed behavior for each filmed run. Seven distinguishable types of tacky behavior were seen, based on mono- and multifilamentation, viscous and elastic deformation, and cohesive and adhesive breaks; five types are illustrated in this paper.

In Figure 2 is illustrated (from Film 2) a simple monofilament-type of viscous deformation, in this case with a 200 poise polybutene. No cavitation or discontinuity-formation is evident with this film or the similar Films 1 and 3. This type of liquid deformation is of the type treated with Stefan's equation or, more correctly, Healey's equation, which applies to the situation in which total immersion of the plates is not maintained throughout separation. The 200 g.

TABLE II
Materials, Conditions, and Observed Behavior for Photographically Instrumented Test Runs

Film no.	Liquid tested	Species	Approx. aver. mol. wt.	Viscosity at 25°C. of liquid in Newtonian flow region, poises,	Clearance between planes in sample holder, cm.	Initial minimum diameter of liquid sample, cm.	Camera speed at moment of impact, frames/sec.	Impact velocity of wheel projections, cm./sec.	Observed behavior
1	Paraplex G-53 (Rohm & Haas)	Polyester	3380	60	0.20	0.8	3240	200	Single filament viscous failure.
2	OB-15 (Natl. Bureau of Standards)	Polybutene	700	200	0.20	0.80	3900	490	Single filament viscous failure.
3	"	"	"	"	0.10	0.8	3860	500	Single filament viscous failure.
4	Vistanex, LM, MH Grade (Esso)	Polyisobutylene	10,800	1.2×10^6	0.30	0.77	4080	550	Single filament elastic deformation, cohesive break, and recovery.
5	"	"	"	"	0.20	1.29	3830	550	Multiple filament elastic deformation, adhesive break (from top block face), and recovery.

6	"	"	"	"	0.30	0.92	3870	600	Single filament elastic deformation, cohesive break, and recovery.
7	"	"	"	"	0.30	1.29	3900	550	Multiple filament elastic deformation and recovery without break.
8	SIAB (Tennessee Eastman)	Sucrose acetate isobutyrate	847	2.5×10^3	0.10	1.50	3900	660	Multiple filament viscous deformation and partly cohesive break; partial adhesive stripping from top and bottom block faces.
9	"	"	"	"	0.20	1.54	3900	600	Adhesive break (from bottom block face) and subsequent multiple filament viscous deformation of fringe.
10	Dimethyl Silicone A (General Electric)	Dimethyl polysiloxane		1.75×10^4	0.30	0.95	3900	670	Single filament elastic deformation, adhesive break (from bottom block face), and recovery.

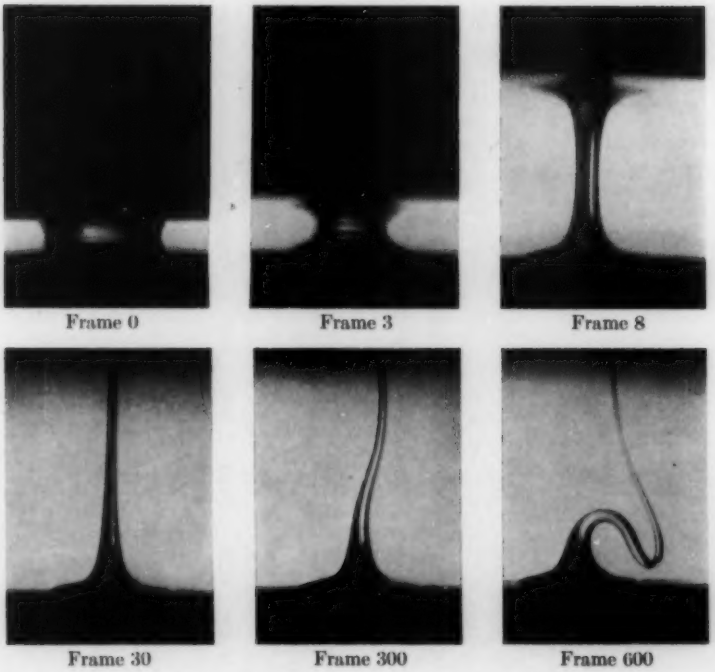

Fig. 2. Monofilamental viscous deformation, cohesive break (Film 2).

bottom block is not lifted in any of the three films; thus no measure of the force across the liquid can be obtained from this source, except that, because no motion occurred, the force would be expected to be less than 200 g. times the gravitational constant (980 cm./sec.^{2}) or 2×10^5 dynes. A rewriting of the Healey equation variation given by Hoekstra and Fritzius[21] is:

$$F = 3\eta V^2/8\pi t h_1^4 \qquad (4)$$

where t is the time (sec.) to "separate" the plates and V is the volume of the liquid sample. F here is $^1/_2 F$ in Stefan's equation (2). Using this equation for the experiment in Film 2, assuming a time of five frames for when the resistance to separation afforded by the liquid sample would be nil, F is in the order of 1.2×10^5 dynes, which is not

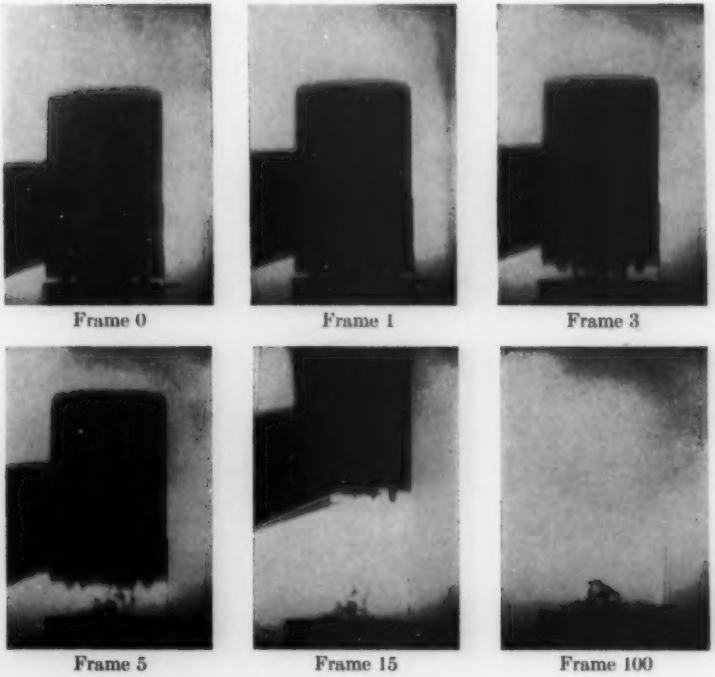

Fig. 3. Multifilamental viscous deformation, co-adhesive break (Film 8).

sufficient, as seen above, to lift the bottom block. One thing of interest in Films 1, 2, and 3 is that the filament remains unbroken, though sagging, throughout the thousands of frames after impact.

In Figure 3 is illustrated (from Film 8) a multiple filament viscous deformation with a partly cohesive break, with sucrose acetate isobutyrate, a 2500 poise liquid. For *viscous* (that is, non-elastic) deformation of a liquid in a constant-velocity separating flat plate system it would be expected from considerations of Stefan's or Healey's equation that the highest stress would be in the first moments of displacement because of the extremely rapid decrease of the resisting force as the interplate distance increases. Thus we would expect that if cavitation would occur at all it would occur in the first moments of displacement. (By cavitation here is meant the forma-

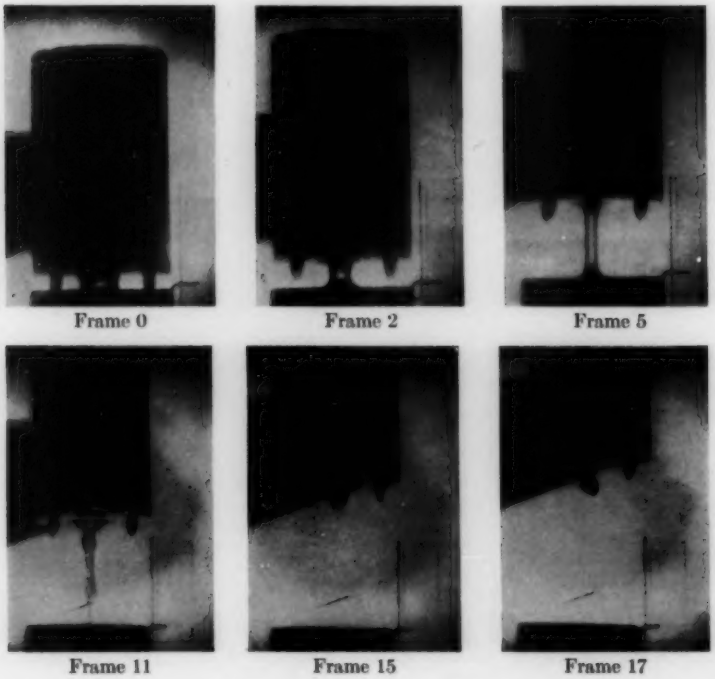

Fig. 4. Monofilamental elastic deformation, adhesive break (Film 10).

tion of discontinuities either in the bulk material or between the material and the plate surface.) And indeed in both of the films (8 and 9) in which viscous behavior and cavitation occur discontinuities are seen by the first frame ($^1/_{4000}$ sec.) after impact. Note in Figure 3, the opacity of the liquid at Frame 1; in Frames 2 and 3 (illustrated) light can be seen through the break. The extended filments do not recoil elastically; no substantial recoverable extensibility would be expected to occur with SAIB which has compact, ball-shaped molecules.

A quantitative determination of the force sustained by the liquid, possible because of the slight lifting of the bottom block in Film 8, indicates that the SAIB has a tensile strength of at least 13 bars. How much greater than 13 bars is not known because the failure that

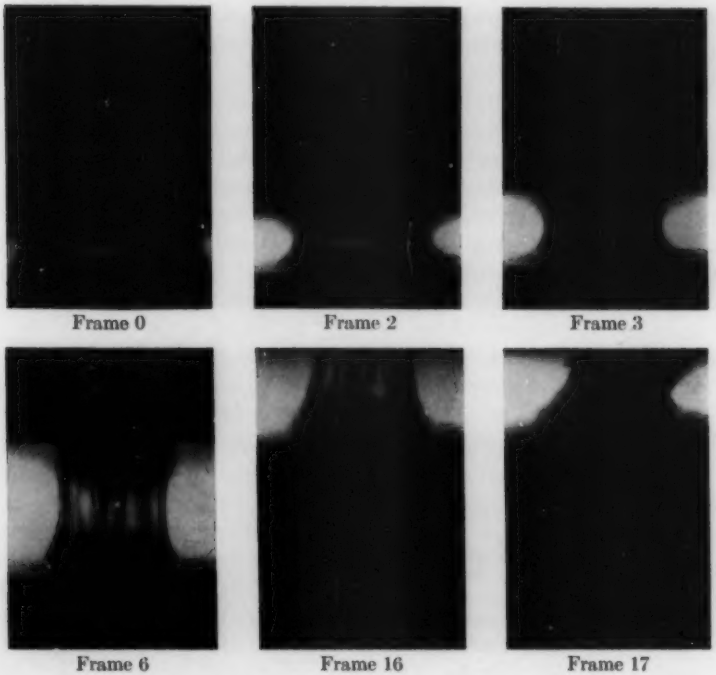

Fig. 5. Multifilamental elastic deformation, adhesive break (Film 5).

occurred was not primarily cohesive (as seen from examination of the block surfaces after the test). That this is more an adhesive strength than bulk cohesive strength is verified by an analysis of Film 9 with the same material in which, with a complete failure at the bottom block interface, a limiting stress of 11.4 bars was measured.

In Figure 4 is illustrated (from Film 10) a single filament elastic deformation, adhesive break, and recovery, with a 1.75×10^4 poise silicone. The adhesive failure is seen to start in Frame 5 on the lower left-hand edge of the liquid filament, at about 430% elongation. This separation continues until a small area remaining in Frame 11 breaks free. Elastic recovery occurs to the limit in Frame 15, with the mass subsequently continuing to bounce around to other configurations such as in Frame 17. The degree with which the silicone

deforms with low force (note that the bottom block is not lifted) indicates that the material has a very low dynamic modulus of elasticity.

In Figure 5 is illustrated (from Film 5) a multiple filament elastic deformation, adhesive break, and recovery with a 10^6 poise polyisobutylene. The inception of cavitation is clearly visible in Frame 3, with multiple filaments well defined by Frame 6. At Frame 16 an adhesive break occurred at the top block (confirmed by examination of the blocks after test). Elastic recovery is well along by Frame 17 with the collapse of the extended filaments seen.

A measurement of the forces involved throughout the plate separation is possible because of the extended period of acceleration of the bottom block. Table III lists the measured results by alternate frames through the adhesive break.

Certain conclusions of interest are seen from examination of Figure 5 and the corresponding data in Table III:

TABLE III
Measured Results from Film 5

Frame No.	Elongation, (h/h_0), $(h_0-0.2$ cm.)	Increase in interplate distance, $h-h_0$, cm.	Vertical position of bottom block (cm.)	Force transmitted across liquid, 10^6 dynes	Mean stress across top block interface, 10^6 dynes cm.$^{-2}$	Maximum tensile stress on liquid, 10^6 dynes cm.$^{-2}$
0	1.00	0.00	0.00	0.00	0.0	0.0
2	1.40	0.08	0.01	47.2	31.5	65.3
4	2.80	0.36	0.09	36.2	24.1	>74.0
6	3.90	0.58	0.21	29.8	19.9	>84.9
8	5.00	0.80	0.36	22.8	15.2	>83.2
10	5.85	0.97	0.55	20.8	13.8	>88.7
12	7.0[a]	1.22[a]	0.78	18.9	12.6	>92[a]
14	8.1[a]	1.42[a]	1.03	17.5	11.6	>94[a]
16	9.1[a]	1.63[a]	1.25	15.6	10.4	>96[a]
18	Collapsed		1.60	0.0	Failure	—

[a] Extrapolated.

(*a*) Cavitation does not by necessity occur as rapidly where elastic deformation is involved as with solely viscous deformations. Theoretically, and practically as seen in Films 8 and 9, if cavitation

will occur at all where viscous deformation is involved in a separating flat plate system, it will occur in the very first instants. In both Films 8 and 9 the cavitation was well along by Frame 1, $^1/_{3900}$ sec. after impact. In Film 5 (Fig. 5) with an elastic deformation, on the other hand, the cavitation that occurs is not visible until Frame 3. This delay with subsequent cavitation indicates that the stress on the liquid does not decrease, as the plates separate, with the rapidity found in a viscously deforming system behaving according to the Stefan-Healey type expression. Indeed, from Table III we see that the stress on the test material actually increases during the plate separation process (even after cavitation).

(*b*) A plot of force vs. time from the data in Table III is shaped very much like the oscillogram traces which Strasburger[18] presents and designates as peak-and-hump type behavior. It is interesting to note that his analysis assumes cavitation and subsequent *viscous* bubble growth, whereas we see here that an elastic behavior can produce this shape trace. Additionally, examination of the non-elastic type failures of Films 8 and 9 does not suggest the presence of a hump of sustained force even though cavitation did occur in both cases. It is suggested here that Strasburger was detecting some elastic effects in those cases in which a hump was formed.

(*c*) The experimentally measured tensile strength of the polyisobutylene appears to be somewhat higher when elongated than when not. The initial cavitation, first visible in Frame 3 at a mean elongation of 1.9, occurred at about 70 bars negative pressure (see Table III). Immediately after cavitation the configuration of the liquid shifted to a multifilamental structure as the elongation continued to increase. By frame 10 there was a mean elongation of about 6 and a maximum tensile stress on the liquid of greater than 88 bars. An exact value could not be determined from the single view available of the multiple filaments as the minimum cross-sectional area of the liquid could not be directly calculated. Thus a higher-than-actual value was indirectly calculated by dividing the volume of the liquid by the distance between plates (i.e., by assuming a uniform cross-sectional area throughout). This calculated value may be too high by a factor of 1.5 or 2, as suggested by the concentration of material near the top and bottom plates (see Fig. 5, Frame 6). By Frame 16, the instant of adhesive break, the mean elongation was about 9 with a corresponding tensile stress on the liquid of greater than 96 bars,

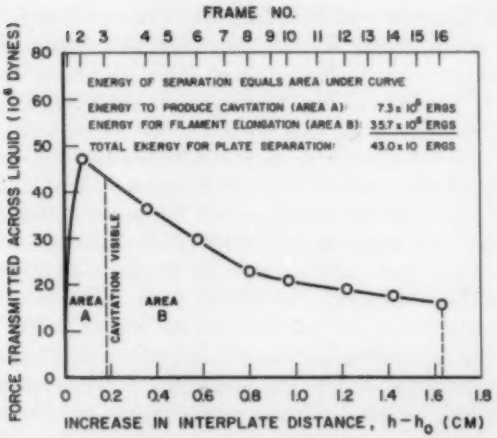
FRAME NO.
1 2 3 4 5 6 7 8 9 10 11 12 13 14 15 16
ENERGY OF SEPARATION EQUALS AREA UNDER CURVE
ENERGY TO PRODUCE CAVITATION (AREA A): 7.3 x 10⁶ ERGS
ENERGY FOR FILAMENT ELONGATION (AREA B): 35.7 x 10⁶ ERGS
TOTAL ENERGY FOR PLATE SEPARATION: 43.0 x 10 ERGS
FORCE TRANSMITTED ACROSS LIQUID (10⁶ DYNES)
80
60
50
40
30
20
10
0
AREA A
CAVITATION VISIBLE
AREA B
0 0.2 0.4 0.6 0.8 1.0 1.2 1.4 1.6 1.8
INCREASE IN INTERPLATE DISTANCE, h−h₀ (CM)

Fig. 6. Force plotted against interplate distance (Film 5).

with no failure occurring. Indeed the maximum stress on the polyisobutylene at this point was, no doubt, more than 100 bars and possibly as high as 200 bars. That the tensile strength of this polyisobutylene is that high is confirmed by the results of the subsequent analysis of Film 6 which is with the same material. Thus we see that the tensile strength of the liquid polymer is greater in the highly elongated state than when only slightly extended. During the extension process the long polymer chains "straighten" and line up in a semi-crystalline manner, which, according to general polymer experience, leads to a higher tensile strength than for the equivalent unoriented polymeric material.

(*d*) The energy expended in the film splitting can be readily calculated along with the answer as to whether the main energy requirements lie in the cavitation process and initial filament formation or in the subsequent elongation of the filaments. The energy total at any given point is given by

$$E = \int_0^{h-h_0} F dh \tag{5}$$

where E is the energy (ergs) to separate the plates from h_0 to h, F is the instantaneous force (dynes) across the sample, and h is the interplate distance (cm). This value of E is equal to the area under the

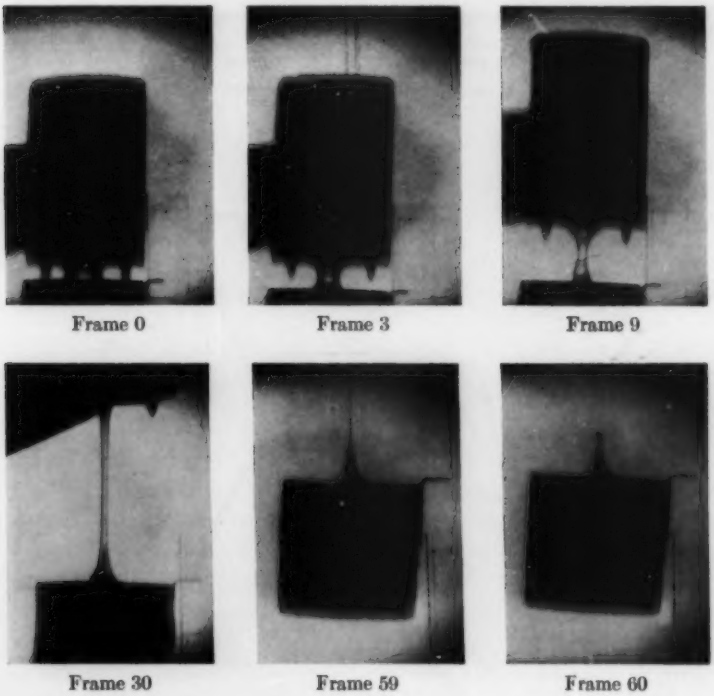

Fig. 7. Monofilamental elastic deformation, cohesive break (Film 6).

curve in a plot of F vs. $h - h_0$. Figure 6 is such a plot from the data obtained from Film 5. From measurement of the area under the curve we see that a total energy of 43.0×10^6 ergs was required for the separation of the plates through to the adhesive failure which occurred at approximately 900% overall elongation. Of this energy, 7.3×10^6 ergs was required up to the point of visible cavitation (Frame 3) and the remaining 35.7×10^6 ergs was required to elongate the multiple filaments. Thus, in this, the energy required to elongate the filaments was about five times that required to initiate cavitation and begin multiple filament formation. This is expected to be in sharp contrast to a viscously deforming system where the prime energy expenditure should be needed to initiate cavitation

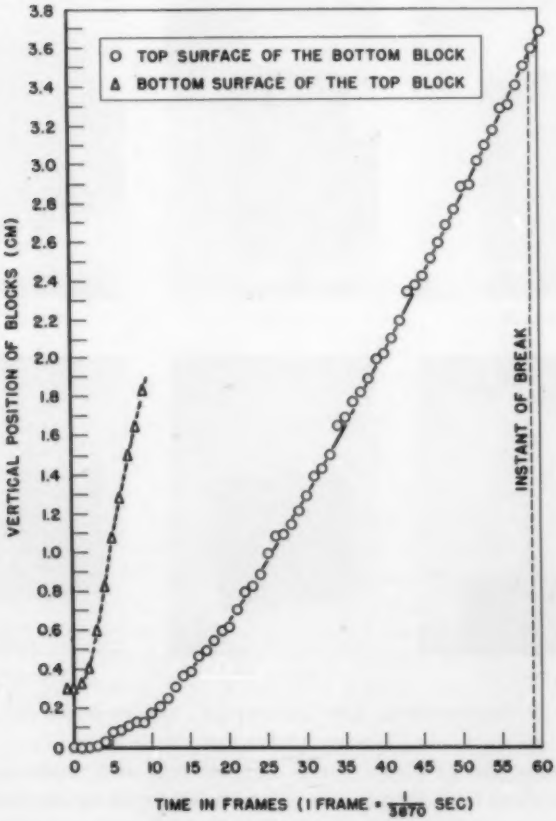

Fig. 8. Vertical position of bottom block plotted against time (Film 6).

because of the extremely rapid subsequent drop-off of resistance by the liquid to further plate separation.

In Figure 7 is illustrated (from Film 6) a single filament elastic deformation, cohesive break, and recovery, with the 10^8 poise polyisobutylene, with sufficiently high forces transmitted across the liquid during deformation to accelerate the bottom block rapidly. Ideal conditions are present for analysis of stresses on the liquid as the

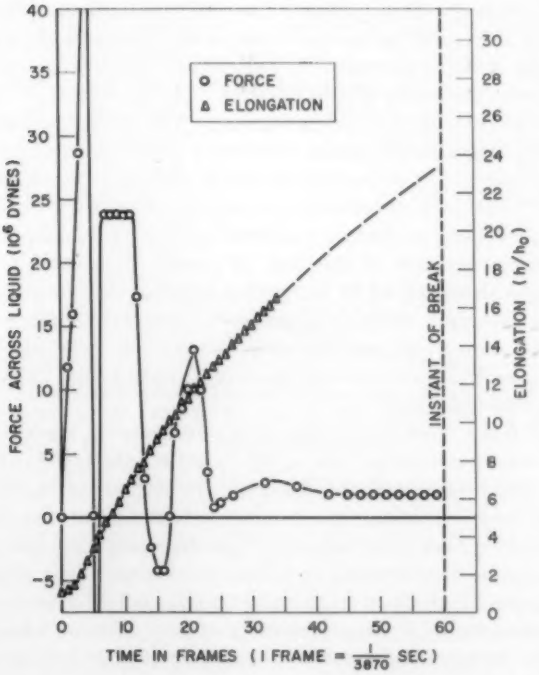

Fig. 9. Force and elongation plotted against time (Film 6).

forces can be measured through an extended acceleration period (59 frames) before break and the minimum cross-sectional area can be determined directly from the diameter of the filament.

One phenomenon of note is the extreme rapidity of the elastic recovery as seen in Frames 59 and 60. Assuming, for example, that the point of rupture is at the upper boundary of Frames 59 or 60 as shown, the material at the point of rupture would have traveled at a velocity of 6800 cm./sec. to reach its outermost position in Frame 60.

The following is a graphical analysis of some of the data from Film 6. (A similar analysis was made on Film 4, also representing a monofilamental deformation of the 10^6 poise polyisobutylene.)

The first graph shown, Figure 8, is a plot of position of the bottom block vs. time, and is the initial one made in a comprehensive force and stress analysis procedure. The vertical position is measured to the nearest hundredth of a centimeter. (In the graph the top block position is also plotted for a few frames.) The quantity of importance from this graph is the slope (measured at frame intervals) of the position-time curve of the bottom block; this quantity is the instantaneous velocity in centimeters per frame. The fitted curve is very smooth and slightly concave upwards (indicating a positive acceleration) except for part of the first 20 frames after impact. In this first region there appear to be rapid changes in the force transmitted through the liquid, causing equivalent changes of the slope in Figure 8. From the slope of an instantaneous velocity vs. time curve, instantaneous accelerations were obtained and, from these, instantaneous forces across the liquid.

Figure 9 is a dual plot of force and elongation vs. time. Here the force is seen constant at 1.79×10^6 dynes for the last 5 milliseconds before tensile failure of the filament; this value at the instant of break is used to calculate the tensile strength of the material. The elongation vs. time data plot very well on a smooth curve which is slightly concave underneath from Frame 5 to 59. The extrapolation from Frame 34, the last measureable point, indicates that at failure the elongation (h/h_0) was in the order of 23. This corresponds very well to an extrapolated value of elongation from 20 to 22 at break for the same polyisobutylene in Film 4.

The first portion of the force vs. time curve shows a very strong oscillatory nature which appears to rapidly damp out and disappear by about Frame 40. At two minimum points negative force vectors are plotted, which indicate that a downward "push" rather than the usual upward "pull" is being applied to the bottom block at these instants. It is theorized that these effects may be due to the passage of pulsation waves (originating from the initial impact movement of the top block) longitudinally through the liquid sample for several cycles. It is noted that such waves are predicted by Voet and Geffken[15] in their viscoelastic theory of film splitting.

To get the maximum stress on the liquid sample at any point we need to know the instantaneous value of the minimum cross-sectional area. To get this, the minimum diameters of the liquid filament are measured from the individual frames. A plot of minimum diameter

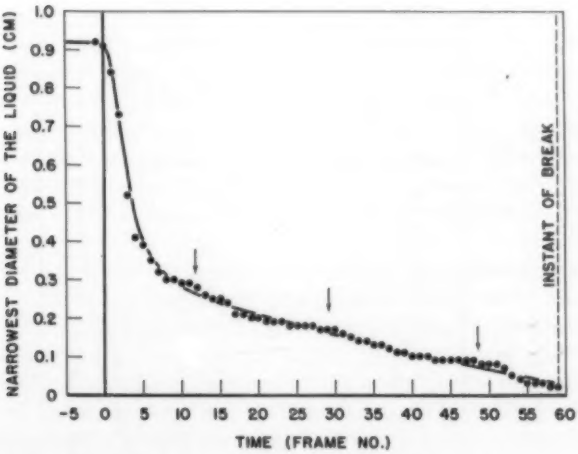

Fig. 10. Minimum diameter of liquid plotted against time (Film 6).

vs. time is shown in Figure 10. A smooth curve was fitted to the points, with the latter part of this curve being almost a straight line, but with a very slight upward concavity. It is seen, however, that the measured points impose a vibrational pattern, possibly sinusoidal (see the arrows for maximum deviations) on the base curve. Whether the base curve or the individual measured points are used in calculating the cross-sectional area is of some importance, particularly in the last few frames up to and including the instant of break where a more than twofold area difference exists. While it appears that the sinusoidal-type pattern is due to vibrations in the polyisobutylene filament itself rather than equivalent variations in gross elongation which do not occur (see Fig. 9), either value may be more nearly correct for calculating the true area. To wit: (*a*) with a longitudinal cross section, the directly measured points or a plotted sinusoidal-type curve would be properly used as the effective diameter would indeed be varying as observed; (*b*) an elliptical cross section with vibratory interchange of the major and minor axes might be present, in which case the mean value might be represented by the solid curve shown in Figure 10. No decision has been made at this point as to the proper effective diameter; this could be determined experimentally

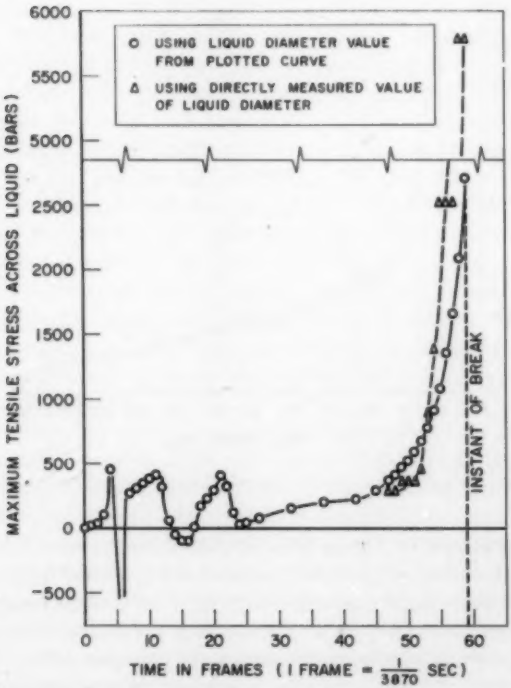

Fig. 11. Maximum tensile stress on liquid plotted against time (Film 6).

in the future by the use of a mirror arrangement to provide a simultaneous right-angle view of the filament.

Figure 11 is a plot of tensile stress vs. time for the single filament extension and break. The tensile stress for each instant is obtained by dividing the value of the force (plotted in Fig. 9) by the cross-sectional area (from the diameters plotted in Fig. 10). The oscillatory character is retained in the first part of the curve, but the amplitude is fairly small compared to the stress magnitude recorded in the last five frames before break. It is notable that three cycle peaks before Frame 25 produced apparent tensile stresses of 400 bars without failure. The tensile stress values of particular interest, however, are those at the instant of break (Frame 59). These values

are: 2.7×10^9 dynes cm.$^{-2}$ (2700 bars), using liquid diameter value from solid curve in Figure 11; 5.8×10^9 dynes cm.$^{-2}$ (5800 bars), using directly measured value of liquid diameter as seen in Figure 11.

These tensile strengths are high, and are indeed higher than expected at the beginning of this study. It is noted, however, that these values obtained ($2.7–6 \times 10^9$ dynes cm.$^{-2}$) are very close to those which Voet and Geffken[15] expected to occur in the filaments of printing inks in high-speed film splitting, namely $10^7–10^9$ dynes cm.$^{-2}$.

The values for the tensile strength of elongated Vistanex LM polyisobutylene obtained in the present study are expected to represent essentially the ultimate tensile strength of this material. Two conditions for maximum values in this type of system (long chain linear polymer) were present: (*a*) extremely high elongation (2300%), and (*b*) very brief loading period. The extreme elongation permitted an anisotropic arrangement of the polymer molecules in a pattern oriented parallel to the direction of stress; this linear-type arrangement is well known to have a high tensile strength in the direction of alignment, thus leading to high values. The very brief loading times increase the sustainable stress in the viscoelastic material by minimizing viscous relaxation during the stressing period, among other effects. It is repeated that these values into the thousands of bars are believed to represent essentially the ultimate tensile strength of the elongated polyisobutylene. Note for comparison that cavitation in the same polyisobutylene in Film 5 when essentially unelongated ($h/h_0 = 1.9$) occurred at about 70 bars a much lower, but nevertheless substantial, tensile stress.

Summary

In this study of the tensile strength of polymeric liquids and tacky behavior, the application of this technique to liquid film splitting and the discovery of the wealth of information obtainable from it appears to be the most valuable result of the entire program. It is felt that many problems in this field can use this technique with particular fruitfulness. A good part of its utility lies in the fact that results (energies, stresses, etc.) are given in absolute units (ergs, bars, etc.); this is in contrast to many of the instruments and techniques described in the first section which use arbitrary or relative units. The further value of this technique is that it correlates the quantities of

force, stress, energy, elongation, and cross-sectional area with themselves and with time, and correlates all of these with physical events (e.g., cavitation, mono- or multifilamentation, cohesive or adhesive failure, and viscous or elastic deformation). The technique appears to be unique in this respect.

A second valuable result of the program is the discovery that initial cavitation in the liquids occurs at substantially higher negative pressures (e.g., about minus 13 bars, or more, for sucrose acetate isobutyrate and minus 70 bars for polyisobutylene) than a number of previous investigators would have considered to happen in practice.

A third valuable result of this program was the determination of the ultimate tensile strength of the viscoelastic polyisobutylene liquid, which was found to be in the thousands of bars (about 2.7 to 6×10^9 dynes cm.$^{-2}$), considerably higher than for the same material unstrained.

A fourth valuable result of this program was from the measurements with the multiply filamenting polyisobutylene system whereby it was seen that considerably less energy was required in the initial cavitation and filament formation process than in the filament elongation process.

In general the Voet and Geffken[15] viscoelastic theory of film splitting appears to be verified by these results, as opposed to proposed cavitation mechanisms which do not consider filament behavior to be of importance.

The technique used in this investigative program can be extended to a wide variety of viscoelastic materials to provide fundamental knowledge about their properties. The technique is capable of further refinements and improvements by, for example, using a variety of bottom block masses (other than just the 200-g. size used in this program), using a bottom and top block designed to insure cohesive breaks, incorporating mirror or stereo techniques to study configurations in depth, and employing higher speed motion picture cameras to study cavitation and other rapid phenomena in even more detail.

Thanks are due to Mr. Edmund Thelen for his helpful discussions during the course of this work, and to Mr. Alan Dietrich for his help on a number of the mechanical details of the impact apparatus. Appreciation is expressed to The Franklin Institute for use of laboratory space and facilities, including the Fastax camera.

References

1. Scott, A. F., F. D. Ayres, and W. L. Nyborg, "Tensile Strength and Surface Tension of Liquids," in *American Institute of Physics Handbook*, McGraw-Hill, 1957, New York.

2. Briggs, L. J., *J. Appl. Phys.* **21,** 721 (1950).

3. Briggs, L. J., *J. Chem. Phys.* **19,** 970 (1951).

4. Briggs, L. J., *J. Appl. Phys.*, **24,** 488 (1953).

5. Birkhoff, G., and E. Zarantonello, *Jets, Wakes, and Cavities*, Academic Press, New York, 1957, p. 315.

6. Fisher, J., *J. Appl. Phys.*, **19,** 1062 (1948).

7. Bernath, L., *Ind. Eng. Chem.*, **44,** 1310 (1952).

8. Volmer, M., *Kinetik der Phasenbildung*, Theodor Steinkopff, Dresden and Leipzig, 1939.

9. Stefan, J., *Sitzber. Akad. Wiss. Wien. Math.-Natur. Kl. Abt. II*, **69,** 713 (1874).

10. Banks, W., and C. Mill, *J. Colloid Sci.*, **8,** 137 (1953).

11. Reed, R., *Am. Ink Maker*, **17,** 27 (1939).

12. Banks, W., and C. Mill, *Proc. Roy. Soc. London*, **A223,** 414 (1954).

13. Miller, J., and R. Myers, *Trans. Soc. Rheol.*, **2,** 77 (1958).

14. Myers, R., J. Miller, and A. Zettlemoyer, *J. Colloid Sci.*, **14,** 287 (1959).

15. Voet, A., and C. Geffken, *Ind. Eng. Chem.*, **43,** 1614 (1951).

16. Green, H., *Ind. Eng. Chem.*, **13,** 632 (1941).

17. Wetzel, F., *Preprint Div. PPPI, Am. Chem. Soc.*, **17,** No. 1, 225 (1957).

18. Strasburger, H., *J. Colloid Sci.*, **13,** 218 (1958).

19 Stone, W., H. Schiefer, G. Fox, J. Smith, and F. McCrackin, *Textile Research J.*, **25,** 520, 529, 701 (1955).

20. Bersch, C., F. McCrackin, and K. Plitt, *Modern Plastics*, **35,** No. 2, 171 (1957).

21. Hoekstra, J., and C. Fritzius, "The Rheology of Adhesives," in *Adhesion and Adhesives*, N. DeBruyne and R. Houwink, eds., Elsevier, New York, 1951, Chap. 3.

Synopsis

The tensile strength of liquids appears to have considerable importance in describing tacky behavior in unfilled systems. An apparatus is described whose operation involves the rapid separation of flat plates between which the liquid is contained, the bottom plate being a block of known mass whose vertical motion is followed by a high-speed motion picture camera (4000 frames/sec.), permitting measurement of the instantaneous forces operating across the liquid couple.l with a simultaneous recording of the events occurring during the plate separation. Five high molecular weight liquids, with viscosities in the Newtonian flow range of from 60 to 1.2×10^6 poises, were studied. Photographic sequences showing five different types of tacky behavior are shown; viscous and elastic deformations, cohesive and adhesive breaks, and single and multiple filament formation (the latter with cavitation) are distinguishable in the various modes of failure. Stress analy-

ses of film failures showed a high viscosity polyisobutylene to have a tensile strength of about 70 bars when essentially unelongated and several thousand bars when elongated 2300%. Filament elongation was seen to require more energy than cavitation and initial filament formation in a system behaving elastically.

Abstracts

Experiments on Peeling

J. J. BIKERMAN
Department of Civil and Sanitary Engineering, Massachusetts Institute of Technology, Cambridge, Massachusetts

The force W_0 required to peel an aluminum or nickel ribbon glued to a rigid glass plate with a polyethylene or a poly(vinyl acetate) was determined and compared with the theory (partly new). The experimental force was smaller than the calculated (often in a ratio between 2 and 5), and the difference was due to two distinct stress concentrations. For highly extensible adhesives, their elongation in the pull direction was associated with Poisson's contraction in a direction normal to the pull; the stress distribution caused by this lateral contraction made W_0 a linear function of ribbon width w instead of being proportional to w. For near-Hookean adhesives at small total elongation, W_0 was found proportional to w; the stress concentration dangerous for these materials occurred at the sharp bend in the ribbon. The postulated damage to brittle adhesives caused by the ribbon deformation could be reproduced without bending, namely by stretching the ribbon beyond its yield stress.

[Published in *J. Appl. Polymer Sci.*, **2**, 216 (1959).]

Effect of Viscosity on the Penetration of Adhesives into Paper

(By Title)

R. M. KARAPETOFF COBB
Lowe Paper Co., Ridgefield, New Jersey

END OF SYMPOSIUM

TRANSACTIONS OF THE SOCIETY OF RHEOLOGY IV, 119–129 (1960)

Flow Down an Inclined Plane

RAY D. HOFFMAN* and RAYMOND R. MYERS, *Department of Chemistry, Lehigh University, Bethlehem, Pennsylvania*

Previous theoretical studies[1–6] on the flow of a liquid layer with one free boundary generally have assumed steady state conditions in which the amount of material per unit volume on the plate was constant. The changing conditions at the liquid front in transient flow down an inclined plane distinguish the present study from earlier work and provide the basis for a new relationship governing the flow properties of Newtonian liquids and shear-sensitive materials. An outcome of this work is that a "shear-thinning index" is derived for certain types of dispersions.

APPARATUS AND METHODS

An enameled steel plate (22 × 28 cm.) produced by the Shepherd Company of Cincinnati, Ohio, was used as the flowplate. It contained four small wells at the top to hold the sample. One or more wells were filled with liquid, the plate tilted, and the material allowed to flow over the graduated surface. Additional flowplates without wells were constructed of glass and metals. Unless otherwise specified, the enameled plate was employed in obtaining the data reported here.

The plate was mounted in a rigid adjustable holder which permitted control of the tilt angle θ (see Fig. 1). Runs were made at room temperature, which was recorded. Except during those runs when the amount of material was deliberately varied, the material was put into the well and leveled with a spatula.

The material was allowed to flow down the plate after it was tilted until it reached a "zero line." On the enameled plate, this line was

* Francis MacD. Sinclair Fellow in Chemistry.

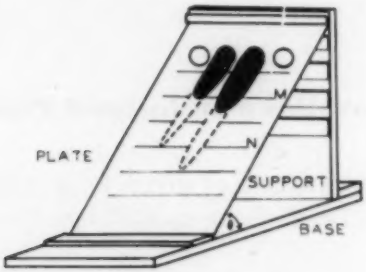

Fig. 1. Flowplate and holder.

4.3 cm. from the center of the well. At this point timing of the flow was begun; and, as the liquid crossed successive marks, the aggregate flow time at that point was recorded. Typical data are shown in Table I.

TABLE I
Experimental Flow Times for Polybutene[a]

D, cm.	t, sec.	D, cm.	t, sec.
1.25	7.0	7.50	76.5
2.50	16.5	8.76	99.5
3.75	27.5	10.00	124.5
5.00	41.5	11.25	154.5
6.25	56.5		

[a] A hydrocarbon (designation H-100) of $\eta = 207$ poises at the temperature employed (25.5°C.), $\theta = 57°$.

The Newtonian liquids, whose viscosities ranged from 80 to 500 poises, consisted of polybutenes (molecular weight range: 500 to 1200), linseed oil 130–150*, and other viscous polymers. Non-Newtonian dispersions studied included a series of tack-graded black inks prepared by the Interchemical Corporation, two series of commercial process inks, and other dispersions which varied widely in shortness and consistency. Two additional series of dispersions contained calcium carbonate (surface area = 13.8 m.²/g.) dispersed in polybutene H-100, and calcium carbonate dispersed in linseed oil

* A bodied linseed oil of about 130–150 poises viscosity at room temperature.

130–150. Volume concentrations of each series ranged from 5 to 10%. Each was hand-mixed and run twice through a three-roll mill.

RESULTS AND DISCUSSION

A. Newtonian Liquids

1. Development of the Empirical Equation

The flow of the liquid is retarded by the friction of the plate. In Figure 2, the time to flow a certain distance D is plotted against D,

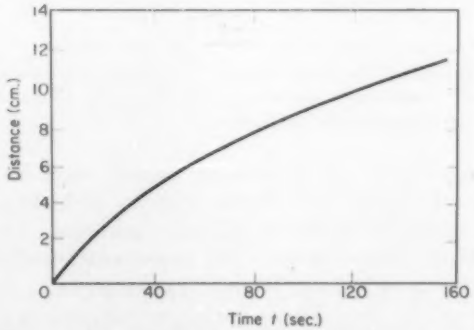

Fig. 2. Distance of flow as a function of time. Polybutene (#24), 165 poises, 57° inclination. Slope = $dD/dt \equiv v$.

the slope of this curve being the instantaneous velocity v. A plot of v against D gives a typical first-order decay curve whose intercept on the velocity axis corresponds to the initial velocity v_0. The empirical velocity-distance curve is then expressed as

$$\log v/v_0 = -kD \tag{1}$$

The velocity v is dD/dt, but as a first approximation let v be equated to D/t, the average velocity of the liquid front from zero distance to distance D, which is in terms of directly measurable quantities. The resulting equation is expressed in the inverted form as

$$\log t/D = kD + C \tag{2}$$

where C is a constant to be evaluated later.

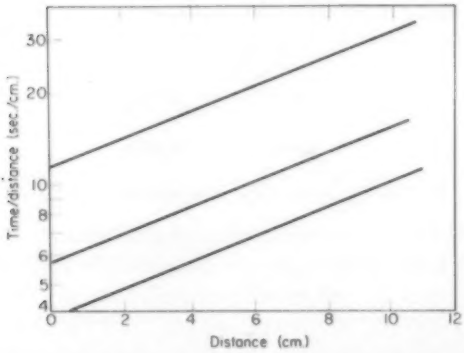

Fig. 3. Experimental flow decay curves. Top line: Polybutene, 212 poises, 38° inclination. Middle line: Polybutene, 212 poises, 57° inclination. Bottom line: Linseed oil, 142 poises, 57° inclination.

Experimental data on Newtonian liquids were analyzed by plotting log t/D against D. Figure 3 shows such data chosen to illustrate a variety of angles of tilt and viscosities. The lines are denoted as Flow Decay Curves. The approximation of the average velocity D/t for the differential velocity is adequate.

The slope of the Flow Decay curves is independent of η and θ, while the intercept is a function of both variables. The slope is 0.034 ± 0.003 cm.$^{-1}$ for Newtonian liquids on the enameled plate. The data were analyzed in order to obtain the relation of η and θ to the intercept of the Flow Decay Curve. The empirical equation which is obtained is

$$\log t/D = 0.034D + \log \eta - \theta - 0.60 \qquad (3)$$

A single determination of t/D, which is customary with flowplate test procedures, does not yield η with much accuracy because of the several variables involved in a one-point determination.

A variety of materials was examined in order to determine if composition influences the slope. Table II shows that from the polar poly(vinyl acetate) solution to the inert polybutene, the slope remained constant within experimental error.

The final step in the development of the empirical equation consists in identifying the last term of eq. (3). Varying amounts of a 205

TABLE II
Effect of the Chemical Nature of Liquids

Material	Polymer type	η, poises	Slope
Alkaline solution of Elvadex vinyl polymer	Vinyl acetate	26	0.031
Acryloid	Vinyl ether	700	0.036
Sorbitan monolaurate	Fatty acid monoester	105	0.032
Linseed oil 130–150	Glyceride	180	0.032
Polybutene H-300	Hydrocarbon	650	0.036
Varnish V-415-H	Bodied linseed oil	2500	0.031

TABLE III
Effect of Volume of Material on Flow Decay

Volume, V, cc.	C
1.5	1.04
2.0	0.93
2.5	0.84
3.0	0.77
3.5	0.76

poise polybutene (ρ = 0.88 g./cc.) were run on the flowplate, and gave the expected constant slope. The intercept, on the other hand, contained a contribution due to the volume of material flowing as well as one due to gravity (ρg). The volume contribution is shown in Table III, where the inverse relation between C (of eq. (2)) and volume is observed. The result, when added to eq. (3), is

$$\log t/D = aD + \log \eta - \theta - \log \rho g - \log V + 2.80 \qquad (4)$$

Now

$$-(\log \rho g + \log V) = -\log V\rho g = -\log mg = -\log F \qquad (5)$$

Hence, the force due to gravity upon the liquid is empirically obtained.

2. Development of the Theoretical Equation

An analysis of steady flow in a liquid column by Hunter, Fallah, and Nash[1] provided the basis for a similar equation for the inclined plane,

$$\bar{v} = (\rho g h^2/3\eta) \sin \theta \tag{6}$$

where $\bar{v}$ is the average velocity and is defined as D/t, g is the acceleration due to gravity, ρ is the liquid density, and h is the average film thickness. This equation describes the rate of flow of the liquid down an inclined surface, *assuming steady state flow*. The objective is to cast eq. (6) into the form of eq. (3). If D/t is substituted for $\bar{v}$, and logarithms are taken of both sides, then

$$\log t/D = \log \eta - 2 \log h - \log \sin \theta - \log \rho g + \log 3 \tag{7}$$

Equation (7) is now compared with eq. (4), and the same dependence of t/D on viscosity is noted. The linear term in D is matched by a log term in h; θ is approximated so closely by log sin θ over the range of angles used that the empirical data fit the log sin θ term almost as well as they fit θ; and the constant terms of the empirical equation are matched in theory by a log ρg (density times gravitational constant) term.

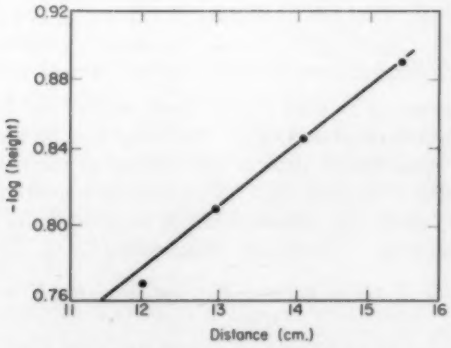

Fig. 4. Relationship of stream height to distance of flow.

The key to understanding why the inclined plane offers possibilities for measuring structure buildup (and at the same time does an unpredictable job with viscosity) can be found in eq. (7). For a Newtonian liquid on an inclined plane, where η is constant, every term on the right side of eq. (7) is constant except h. In the present instance, flow occurs from a limited reservior of material so that h decreases as the flow proceeds; consequently, log t/D increases

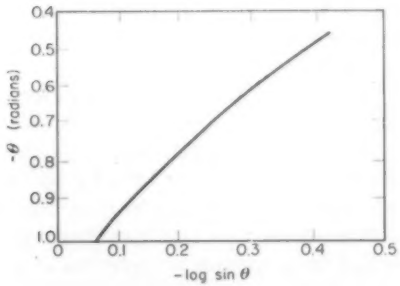

Fig. 5. Relationship between θ and log sin θ.

monotonically. Thus, even a Newtonian liquid slows down as the length of the film increase. This behavior is normal, and does not depend on internal structure, wetting, surface tension, or any other factor that depends upon the nature of the liquid.

Proper analysis of flowplate data requires the relationship between h and D to be known. Figure 4 shows, from data taken in the course of this study, that $-\log h$ is linearly related to D. This dependence turns out to be twice that which is predicted by comparison of eqs. (4) and (7).

Next, the near linear dependence of log sin θ on the angle θ was demonstrated (Fig. 5), thereby confirming that in every major detail, the steady state theoretical equation and the nonsteady state empirical equation are identical for Newtonian liquids.

3. Interfacial Considerations

In the original derivation of the flow equation it was assumed that the width of the flowing liquid was infinite. Hopf[2] considered this factor in developing an equation for steady flow down an inclined plane with finite flow stream widths:

$$v = (g\rho \sin \theta h^2/3\eta)(1 - 0.63\, h/b) \tag{8}$$

The last term in parentheses is a correction factor describing the condition of finite width of the flow stream. In practice, this equation has not been used to correct data for such effects but it is of interest to examine the reasons for which such a correction might have to be used.

The liquid stream will change its effective width because of two variables. They are wetting of the surface by the liquid, and the shape of the flow stream as it emerges from the reservoir. The more readily that the surface wets, the more quickly can the liquid spread in a direction transverse to the direction of the flow; the result is a lowering of h by a process not accounted for in the general theory, and a slight change in the slope of the Flow Decay Curve.

Table IV shows data taken to analyze these factors. Each slope is an average of three to six runs. It is evident from Table IV that changing the surface from wetting to nonwetting affected the slope

TABLE IV
Effect of Wetting upon the Flow Decay Curves

Surface	Slope,[a] cm.$^{-1}$	
	Spherical well	Flat surface
Enameled steel	0.033	0.026
Silicone-treated enameled steel	0.027	0.021
Stainless steel		0.022[b]
Plate glass		0.022

[a] Polybutene H-300, $\eta = 750$ poises, $\theta = 57°$.
[b] Polybutene H-100, $\eta = 220$ poises.

about 20 to 25%, while changing from a spherical reservior to no reservoir at all altered the flow pattern such that the slope was changed nearly 50%. Considerable effort must be taken to obtain the same surface from run to run and to use the same type of reservoir.

B. Shear-Sensitive Liquids

Equation (3) provides a basis for describing non-Newtonian flow upon the inclined plane. If a liquid is shear-sensitive, the only term in eq. (3) which changes during flow is log η. If the structure builds up or breaks down due to a gravitationally-influenced shear rate, then viscosity changes, with the result that the slope of the equation appears to change. Thus *changes in viscosity affect the slope although the slope, itself, is independent of viscosity.* In most experiments with

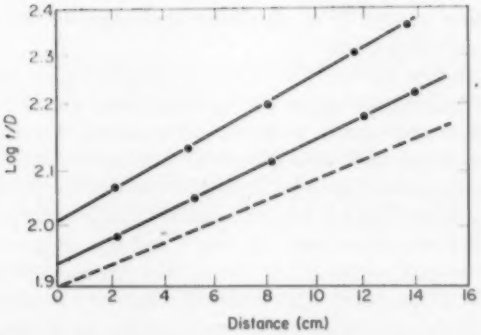

Fig. 6. Flow decay of shear-sensitive materials. Top line: Process yellow ink (m = 0.054). Middle line: Process red ink (m = 0.039). Bottom line: Newtonian liquid (m = 0.034).

shear-sensitive materials, the experimental curve remained linear (as, e.g., in Fig. 6), although in several significant cases it curved upward.

The slope of log t/D vs. D for Newtonians averaged 0.034. For every dispersion investigated, the slope either remained 0.034 cm.$^{-1}$ or increased in magnitude. This finding indicates that dispersions either build up structure or remain at constant viscosity during flow. A slope of 0.034 cm.$^{-1}$ indicates that no structural change occurs as stress decreases, and therefore the system is "long." Slopes above

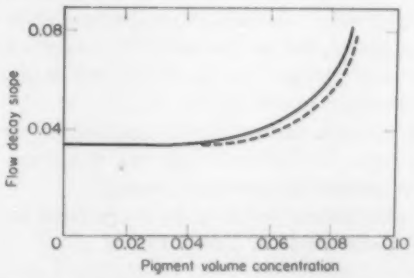

Fig. 7. Dependence of flow decay slope on pigmentation. Solid line represents calcium carbonate dispersed in linseed oil; dashed line represents the same pigment dispersed in 150 poises polybutene.

0.034 denote a sensitivity of structure to change of stress characteristic of "short" dispersions.

In order to test the usefulness of the flowplate as a means of detecting and quantitatively characterizing shear-sensitive flow, two series of dispersions were prepared in a range of concentrations. Calcium carbonate of known surface area was used as the dispersed phase, with one series dispersed in polybutene and the other in linseed oil. These dispersions are known to pass from Newtonian to shear-thinning behavior somewhere between 3 and 9% volume concentration.[7] The slopes of the Flow Decay Curves for various concentrations (Fig. 7) increased most drastically between 6 and 8%. Thus a value is obtained which corresponds quite adequately to other properties, such as viscosity and yield value, in representing the rheological behavior of material as a function of concentration.

CONCLUSIONS

1. The use of an inclined plane as a viscometer requires greater attention to the variables affecting its operation than has been paid heretofore. Flow, even of Newtonian liquids, decays steadily because the applied stress decreases as the liquid flows down the plate.

2. Flow Decay Curves (log time per unit distance of flow versus distance) are suggested as the means of analyzing flow down an inclined plane.

3. The slopes of the Flow Decay Curves are identical for all Newtonian systems studied, providing the same reservoir of material is used in all comparisons. A slight dependence of slope on wettability of the surface is noted, but no dependence is observed on the angle of tilt, the temperature (within reasonable control limits), the viscosity, or the chemical nature of the liquid.

4. When flow down any incline is analyzed as prescribed above, shear sensitivity can be detected from the raw data, in contrast to the difficulty in measuring absolute viscosity.

5. A new quantitative index of recovery from shear thinning is based on the slope of the Flow Decay Curve.

The authors are pleased to acknowledge the constructive comments of L. Stoloff, J. Daen, and various members of the National Printing Ink Research Institute, particularly A. C. Zettlemoyer, D. J. Bernardi, C. F. Geffken, C. B. Blake, A. Voet, R. S. Shepherd, and J. G. Curado.

References

1. Fallah, R., T. Hunter, and A. Nash, *J. Soc. Chem. Ind.*, **53,** 369T (1934).
2. Hopf, L., *Ann. Physik*, **33,** 777 (1910).
3. Severs, E. T., and J. M. Austin, *Trans. Soc. Rheol.*, **1,** 191 (1957).
4. Paslay, P. R., and A. Slibar, *Trans. Soc. Rheol.*, **2,** 255 (1958).
5. Jeffreys, H., *Proc. Cambridge Phil. Soc.*, **26,** 204 (1930).
6. Jackson, M. L., *A.I.Ch.E. Journal*, **1,** 231 (1955).
7. Zettlemoyer, A. C., and G. Lower, *J. Colloid, Sci.*, **10,** 29, (1955).
8. Myers, R. R., D. R. Brookfield, F. R. Eirich J. D. Ferry, and R. N. Traxler, *Trans. Soc. Rheol.*, **3,** 000 (1959).

Synopsis

The flow of Newtonian and shear-thinning liquids down an inclined plane was studied with the objective of estimating the degree of shear sensitivity from a simple test. An empirical relation called the Flow Decay Curve was obtained, by means of which a wide variety of materials was characterized by the decrease in velocity of the advancing front with distance of flow. In general the decrease was an exponential function of distance, and the magnitude of the exponent provided an index of shear thinning, independent of viscosity. The Flow Decay Curve was compatible with a theoretical equation based on hydrodynamic flow principles.

TRANSACTIONS OF THE SOCIETY OF RHEOLOGY IV, 131–140 (1960)

Rheology and Dental Materials

RICHARD H. ROYDHOUSE, *Northwestern University Dental School, Chicago, Illinois*

In dental treatment many materials and techniques are used; two forms of repairs are undertaken. First, there are those replacements placed within the teeth and these are called *restorations*. Those placed between the teeth or on the soft gums when the teeth are lost are called *prosthetic appliances*. Both of these may be made in two ways. The direct method describes the technique where the appliance, or more often the restoration, is made in the mouth. The other technique, the indirect, depends upon the making of an accurate replica of the oral structures, and the fabrication is done in the laboratory.

For aesthetic and hygienic reasons it is desirable that the restorations fit accurately, and accuracy here is in terms of bacterial size, five to ten μ. Retention within the mouth of both types depends upon this close fit or, alternatively, the creation of mechanical locks.

Materials

The main materials used for restorations are:

(*1*) *Amalgam.* Fine filings of a silver-tin alloy are mixed with mercury to form a plastic amalgam which is then placed in pieces in the cavity that has been cut by the dentist. While suitably confined, the plastic material is packed with small pluggers to condense the mass, adapt it to the walls, and squeeze out some of the mercury. Crystallization occurs, and after 5 to 10 minutes the restoration is hard enough to prevent fracture.

(*2*) *Silicate cement.* An alumino-silicate glass ground to fine particles is spatulated with a solution of orthophosphoric acid. A sand-and-water mix is obtained; this is placed in the cavity, packed if possible and held to the correct external contour with a cellophane

strip. A matrix of silicic acid gel forms, holding undissolved particles together. The set material has a high hardness number and is rigid but slightly soluble.

(*3*) *Zinc phosphate cement.* Zinc oxide is mixed with varying proportions of a solution of orthophosphoric acid. Any consistency from a doughy mass to a creamy liquid is obtained and this sets by crystallization.

(*4*) *Cast gold and fused porcelain.* These restorations are made by the indirect method and are cemented into place with zinc phosphate cement. Wax patterns, for cast gold inlays as they are called, may be obtained in the mouth. The wax is warmed, pressed into place and carved to shape, and removed when chilled. A refractory of silica and gypsum is used to make the mold, into which molten gold may be forced.

Prosthetic appliances are made by the indirect technique and are cast in gold alloys, chrome-cobalt alloys, or molded from methyl methacrylate in gypsum molds. The replicas for these are made of some gypsum product poured into negatives obtained in what are called impression materials.

Techniques

In general, the less plastic the restorative materials before insertion, the greater the strength and the durability of the restoration. The operator determines the time he requires for handling by adjusting the setting rate. But that which alters the setting rate also alters the consistency. The consistency should be such that adaption to the walls of the cavity is possible and yet also such that packing with small instruments causes condensation rather than skewering; the elimination of voids is essential for strength and the attainment of smooth polished surfaces.

The following are closely related: (*1*) handling time or setting rate, (*2*) liquid and powder proportions, (*3*) final physical and chemical properties, (*4*) plasticity low enough to allow adaption, and (*5*) plasticity high enough to permit packing.

Silicate cement can be taken for an example of the above. The setting rate is affected by temperature and humidity, and the operator controls this by the temperature of the mixing instruments and by the liquid/powder ratio. The latter markedly alters the con-

sistency, the final strength, and solubility in the mouth (due to the proportion of slightly soluble matrix formed). A large percentage of these are failures as permanent restorations. A thick consistency in hot weather sets before packing, and good adaption is not possible; if too "thin," packing is not possible, except for a brief period, and a poor strength and increased solubility result.

Little, if any, rheological investigations of restorative materials have been reported. The specifications for these materials issued by the American Dental Association originating from the National Bureau of Standards avoid complexity by using totally empirical measures. The specified test, a "one-point" test (where slump is assisted by pressure) was established[1] by averaging the consistencies used by a number of dentists.

The need for investigation is undoubted. At the moment of insertion of restorative materials the consistency and the rate of change of consistency are the most urgent considerations of the dentist. The very best restorative materials are no use if they cannot be inserted readily. The dentist, it must be remembered, is working rapidly upon a small hole in a warm, moist, dark restricted region that is likely to move, resist, and complain.

In *impression techniques* the consistency of the impression materials when a replica of teeth and gums is required is of paramount importance. The displacement of the soft tissues of the palate and about the teeth and jaws is determined by the plasticity of the impression material. Thus the accuracy of any replica is affected.

The technique for taking impressions is as follows: An impression tray roughly shaped to the region to be recorded is filled with impression material and is pressed against the patient's oral structures. The consistency of the material increases, some to comparatively unyielding materials, others to a more flexible state. Into this negative plaster of Paris is poured. For impression materials many strange mixtures are used. "Impression compound" is a mixture of fats, oils, and resins that is soft at about 45°C. and hard at body temperature. "Reversible hydrocolloid" is an agar-agar gel which is softened in warm water. "Irreversible hydrocolloid" is a mixture of sodium-calcium alginate systems, pectins, and carboxy-celluloses. Silicone and polysulfide rubbers used are compounded so that they polymerize at mouth temperature. Plaster of Paris has been used for over a century for these purposes.

The difficulties arise because the tissues of the mouth vary in reaction to forces. For example, if a thick putty-like consistency is used, the replica will show the soft regions of the mouth depressed and the hard regions relatively elevated. Thus any appliance made thereupon will press heavily upon the soft regions in the mouth. Many involved techniques using different materials in turn and other complicated procedures have been advocated, but dentists are not yet agreed whether differential recording is good or bad, or even whether it can be done. It would seem logical to have some knowledge of consistency of these materials before their effects are considered.

Measures of Consistency

Dental Rheology is notable for the paucity of the literature. Spence[2] in 1902 worked with ropes of impression compound and measured their flow under gravity. Penetration tests were also tried on this material. In 1925 the classical dental investigation was done by Crowell and Saunders[3] under the direction of Bingham; they measured the flow of impression compound with an extrusion method. Modified slump tests have been used on many of the dental materials; the substance is pressed out by a weighted plate rather than allowed to flow from a certain shape under the effects of gravity. Worner of Melbourne[4,5] investigated the dubious validity of such tests. Other attempts to measure flow have failed for reasons similar to Worner's findings, that is, a measure based on the time taken for one shape to turn into another under some arbitrary load when the substance is not homogeneous and is also setting, cannot be very accurate, and must vary with the rate of setting.

Utility rather than considerations of molecular structure makes testing for dental purposes depend on models rather than classical viscometers; a paper by Kennedy[6] clearly justifies technical rheologists in choosing such systems. However, an outline of the phenomena to be measured is attempted first.

The previous brief review of technical dentistry shows what qualifications are required to describe dental consistency.

1. The yield value. This is defined as the load above which flow commences, or is observable under the conditions of the test. Such a measure indicates the adaption of plastic materials when pressed into a cavity under a given load, the size of the instrument best

employed to pack it, the force best used on a particular instrument with a particular material, the thickness of the final layer formed when a material is pressed out between two surfaces and so on, to mention but a few possible implications. In impression procedures the yield values shows the amount of force that will deform soft tissues beneath the impression.

2. The apparent viscosity. Bingham's modification of Newton's Law or similar variant of a power law with provision for the yield value is suggested as a basis for determining this flow-load relationship, for stiff materials will be tested. This measure of shearing rate will not be of primary concern to the dentist; will it flow or not is more important than the shearing rate.

3. The flow-load changes. The D-τ relationship will show whether an increase in force used in a particular task will benefit the technique or speed up the operation. These materials are setting, and time is important for the comfort of the patient.

4. Thixotropy. This measure will be defined to indicate the effects of disturbance during the mixing and preparation of the material, rather than the effects of flow. Techniques for mixing may thus be guided in terms of changes produced in yield value and apparent viscosity when the mixture is being used in the mouth.

5. The rate of change of consistency. The change in yield value and apparent viscosity due to the setting action defines the working time and consistency at any particular time. Changes in dimension after set has finished in those materials used to produce replicas is partly due to relaxation. The distortion from this source is related to the set of the material during the formation of the replica. The ideal would be to complete the impression before any setting has occurred, and therefore the setting rate and initial point is defined.

Some qualifications for equipment to measure these properties are as follows: (*1*) The machine must be readily broken down for cleaning purposes, for these materials set during test, and some of them are quite tough. (*2*) The testing conditions shall resemble service conditions. (*3*) The results must give some values for the above measures.

The parallel plate plastometer is chosen for it may be easily cleaned, is simple to make, and appeals as a model similar in size and geometry. The squashing of materials between two surfaces is common to many dental techniques. The five criteria can be given values, although

interpretation of results has proved most difficult. The yield value is given by the terminal separation of the plates or some function of this related with time. The apparent viscosity is obtained from the rate of approach of the plates, when the effects of the changing yield value have been removed. Variation in the load upon the plates shows the D-τ relationship. Thixotropy shows as a change in yield value and apparent viscosity due to some variation in mixing technique or with changes in shearing rate. If consistency is measurable, then changes therein can be detected.

Experimental Work

An interest in the fit of dentures and the techniques used for the fabrication of dentures lead to an investigation into alginate impression materials; these are universally used, low in price, and easy to handle. A sodium-calcium alginate system or similar gelling system is made up as a powder, heavily loaded with fillers, which is spatu-

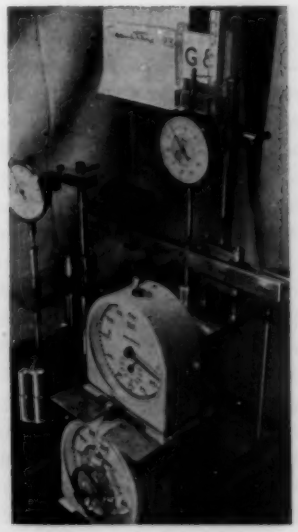

Fig. 1. A view of the apparatus used to establish tests for dental materials; two viscometers are used to test each mixture simultaneously, and the clocks record the elapse of time from start of mixing and from start of recording.

lated in a rubber bowl with a certain measure of water. The thick creamy paste produced is reputed to maintain a constant consistency while calcium ions, produced from calcium sulfate in the mix, are removed by a soluble phosphate, then the balance towards insoluble calcium phosphate is favored. A friable, slightly flexible solid is formed in the mouth and this may be withdrawn from around undercuts.

Some of the difficulties in testing are due to the nature of the material. As used, it is a mixture of gelling medium, filler, and air. The size and amount of air bubbles cannot be controlled without departing from the conditions of use. A given consistency cannot be produced although standardization of techniques may be rigorously adhered to; a statistical approach to the results is necessary. A homogeneous mix is not available; this was demonstrated by the erratic behavior of a falling sphere in the mix. Its path, traced by x-rays, was altered by the varying size of air bubbles encountered. Metal must be kept out of contact with the alginate system for it enters into the reaction. The fabrication of accurate parts in acrylic resin is difficult, particularly if the parts are alternately wet and dry. The machine used was designed after that of Dienes and Klemm.[7] Recordings of the time and separation of the plates were made by photographing the assembly at regular intervals with a 35-mm. camera.

Interpretation of Results

The time, t, and the separation of the plates, h, with the constants from the area of the plates and the force thereon must be related to given the measures already mentioned. Four main groups of equations for such analysis can be distinguished.

1. Stefan's Equation[8] relates t and h parabolically and is derived from Newton's Law. The yield value does not figure in this, and claim[9] has been made that at the low shear rates between the plates only Newtonian behavior need be expected. This is not so for thick materials such as those used in this investigation.

2. Derivations from power laws, such as that of Williams,[10] have been fitted to experimental data.

3. Bingham modifications of Newton's Law have served as a basis for some derivations, and the yield value figures in the final equation.

4. Mathematical descriptions of plots of t vs. h have been found and various arbitrary consistency variables postulated. This method

depends perhaps too much upon accuracy in the experiment and graphical work.

Because stiff materials are tested, the existence of a yield value is assumed, and its appearance in the equations is necessary. The system, first described by Peek,[11] where the yield value operates upon the distribution of flow between the plates (see Nadai[12]) seems acceptable. It is possible to derive an alternative to Peek's equation using another approximation. Peek derived

$$-\frac{dh}{dt} = K\frac{h(h-\alpha)^2}{\eta}$$

and the alternative is

$$-\frac{dh}{dt} = K\frac{\alpha(h-\alpha)^2}{\eta}$$

where h is the distance between the plates, t is the time, K is related to the plate area and force upon the upper plate, η is the apparent viscosity, and α is a value in terms of separation, related to the yield value.

Experimental Values

Experimental values of t and h are found to be related in logarithmic form[13] as these materials set. The equation,

$$h = a + be^{-ct} \tag{1}$$

gives highly significant coefficient of correlation between t and h of the order 0.99, when a regression analysis is done on transformed data. Alterations in machine and mixture constants were detectable in the constants a, b, and c in this empirical equation.

The association of derived and experimental equations has proved to be difficult, for simple relationships are assumed to occur in the changing yield value and apparent viscosity, if suitable approximations are made; the previous equation can be rewritten with $f(\eta,t)$ $f(\alpha,t)$ representing these changing values.

$$-\frac{dh}{dt} = K\frac{f(\alpha,t)[h-f(\alpha,t)]^2}{f(\eta,t)}$$

The existence of these two, and the fact that no run can be duplicated, means that two plastometers must be used for each mixture, so that two sets of a, b, and c are obtained for the solution of the equations. The use of the eq. (1) simplifies analysis because the range over which the plates move is no longer of great concern; this has been the subject of many papers by Scott.[14]

The yield value plays a large part in the interpretation of the results, and the effects of its change must be extracted before the determination of $f(\alpha,t)$ is possible. In these experiments the relation between yield value and experimental values seems to have a logarithmic form as,

$$f(\alpha,t) = a/(1 + bc^{-t})$$

The apparent viscosity seems to increase exponentially. These findings are in accord with those of Richardson[15] who shows similar curves graphically when the setting of gelling solutions was examined by a method employing the damping of oscillations.

Conclusion

This is a descriptive paper, rather than one providing detailed technical results. Some analysis of techniques used dentally should precede testing of the materials to be used in those techniques. Rheological considerations are shown to be important and yet have been much neglected. The criteria suggested are minimum considerations for any dental material. Some experiments show the typical difficulties faced by technical Rheologists, but it can be claimed that the basis for the analysis is more sound than some form of random sampling.

The work described in this paper was supported by the University of Otago Dental School, Dunedin, New Zealand.

References

1. Paffenbarger, G. C., *J. Am. Dental Assn.*, **27,** 1611 (1940).
2. Spence, S. J., *Items of Interest*, **24,** 336 (1902).
3. Crowell, W. S., and A. Saunders, *J. Phys. Chem.*, **29,** 1267 (1925).
4. Worner, H. K., *Australia Dental J.*, **44,** 277 (1940).
5. Worner, H. K., and M. N. Anderson, *Australian Dental J.*, **47,** 217 (1943).
6. Kennedy, A. J., *Nature*, **170,** 875 (1952).
7. Dienes, G. J., and H. F. Klemm, *J. Appl. Phys.*, **17,** 458 (1952).
8. Stefan, M. J., *Akad. Wiss. Wien. Math-Natur. Classe Abt.* **2, 69,** 713 (1874).

9. Dillon, J. H., and N. Johnston, *Physics*, **4,** 225 (1933).
10. Williams, I., *Ind. Eng. Chem.*, **16,** 362 (1924).
11. Peek, R. L., *J. Rheol.*, **3,** 345 (1932).
12. Nadai, A., *Plasticity*, McGraw-Hill, New York, 1931.
13. Pearl, R., and L. J. Reed, *Proc. Natl. Acad. Sci. U.S.*, **6,** 275 (1920).
14. Scott, J. R., *J. Sci. Instr.*, **30,** 145 (1953).
15. Richardson, E. G., *Trans. Farad. Soc.*, **29,** 494 (1933).

Synopsis

A brief review of dental techniques and materials suggests the usefulness of rheology in testing and understanding the behavior of these materials. Little has been investigated or reported upon in this application, and a set of criteria for dental materials is given; these are the yield value, the apparent viscosity, flow-load changes, thixotropy, and the rate of change of consistency; the first is most important. Parallel plate plastometry is chosen as a system for testing because of its simplicity of operation and aptness as a model of the dental techniques. Some general conclusions related to this machine and its application are given, but the paper is of a descriptive nature.

TRANSACTIONS OF THE SOCIETY OF RHEOLOGY IV, 141–157 (1960)

On Anomalies in the Measurement of the Complex Modulus

S. R. BODNER, *Brown University, Providence, Rhode Island*

Introduction

One aspect of the investigation of the inelastic behavior of metals at elevated temperatures has been the measurement of viscoelastic properties under conditions for which the material behavior is essentially linear. The measurements have included determining the complex modulus, or alternatively, the dynamic elastic modulus and damping, as a function of frequency at various temperatures. They were carried out using the resonance apparatus previously described.[1] In this technique the properties are obtained from the natural frequencies and amplitude decay curves of vibrating specimens. The specimens were long rods, generally 3 ft. long and $^1/_2$ in. in diameter, and were set into either transverse or longitudinal vibration. The equipment was modified to permit the specimens to be subjected to high temperatures and to constant axial tensile loads. The latter facility was initially introduced to measure changes of the dynamic modulus during high temperature creep.

Under certain conditions in the application of the resonance technique, various resonances were observed in addition to the natural frequency spectrum. A separate program was undertaken to investigate the characteristics of these resonances, and the present paper constitutes an initial report on this study. The most important result is the correlation of the additional resonances with the resonance dispersions observed by Fitzgerald in his measurements of the frequency variation of the complex compliance of a number of materials.[2–6] Since the experimental technique employed in the present tests is completely different from Fitzgerald's, the results serve as an independent verification of his general findings, namely, the occurrence of the resonance dispersions in the materials.

The present experiments also show that the additional resonances are a direct consequence of the existence of an initial stress state in the specimens. The resonances have been observed in specimens containing residual stresses and in specimens subjected to static tensile or compressive loads. The resonances vanished upon annealing or upon removal of the external loads. Cylindrical anisotropy, such as results from an axial load on a long cylinder, was shown not to be a factor. Tests on an unstressed rod that had pronounced cylindrical anisotropy did not reveal any additional resonances.

Both Fitzgerald's specimens and those discussed here that exhibited the additional resonances were characterized by an initial stress state. In addition, both methods of testing result in small magnitude oscillatory variations of the initial stresses. In Fitzgerald's tests the variations rise from nonlinear coupling of the applied oscillatory shearing stress and the axial stress. In the present tests they arise from coupling and, more directly, from the method of applying the oscillatory forces. The basic mechanism that results in the resonances appears to be the existence of modes for which the effective spring constant is a function of the initial stresses on which are superposed small oscillatory variations. Such systems have been the subject of extensive mathematical treatment,[7,8] and it is well known that various combinations of parameters can lead to unstable motions which would be observed as apparent resonances. This mechanism serves as a possible explanation of Fitzgerald's results in which the frequency of the applied shearing stress was appreciably lower than the lowest natural frequency of the samples.

A particularly unusual effect observed by Fitzgerald for some materials, e.g., lead and sodium chloride, was the occurrence of negative damping values in narrow frequency regions. The magnitude of the negative damping decayed with time but could be reinforced by increasing the static compression. A unique method of energy conversion appears to be operating in this case in which the energy of initial compression is transformed by the stress relaxation process into energy of oscillation. In terms of the mechanism previously discussed, the stress reduction results in a reduction of the effective spring constant for the mode of oscillation which, in turn, can lead to negative work being done by the spring force.

Although the experiments indicate that the resonant modes are

functions of the initial stress state, they are not conclusive as to the origin of the modes. It was shown[7,8] that if the rigidity of an elastic system depends upon a stress, then harmonic variations of that stress can result in instability. A number of the additional resonances observed in the resonance tests as well as in Fitzgerald's tests would appear to be in this category and therefore explainable by continuum mechanical analysis. This does not rule out the possibility, however, that some high frequency resonant modes of microscopic origin that depend on the stress state may be brought into resonance by the stress variation. Indeed, the characteristics of certain resonances in specimens that contain residual stresses tend to support this possibility. A considerable amount of further theoretical and experimental work appears to be necessary before the sources of the resonances can be determined.

Description of Apparatus

The experimental arrangement for the vibration tests to obtain the frequency dependence of the dynamic elastic modulus and damping is shown in Figure 1. The specimen was a circular rod that was generally 3 ft. long and $^1/_2$ in. in diameter which was suspended by fine wires at the nodal points corresponding to a free-free beam. Constant axial tension could be applied to the specimen by a wire and pulley system. The wires were long and thin (10 ft. by $^1/_8$ in. diameter) and were attached to the rod ends by swivel connections to minimize the restraint of the wires to the end motion of the specimen. Various checks were made to ensure that the wires themselves did not introduce additional resonances into the system. Static axial compression was obtained by using a hollow cylindrical specimen with a thin central wire that was loaded in tension by plates at the ends of the specimen.

The specimens were set into oscillation by passing an alternating current of chosen frequency through a coil wound around one end of the rod. Lateral oscillations would result from positioning the magnetic field about the coil as shown in Figure 1. Longitudinal oscillations would be obtained by locating the magnets along the longitudinal axis. The lateral loading method resulted in a small axial component. Although this effect was insignificant in the tests with unloaded specmens, it was probably related to the occurrence of the additional resonances observed with the preloaded specimens,

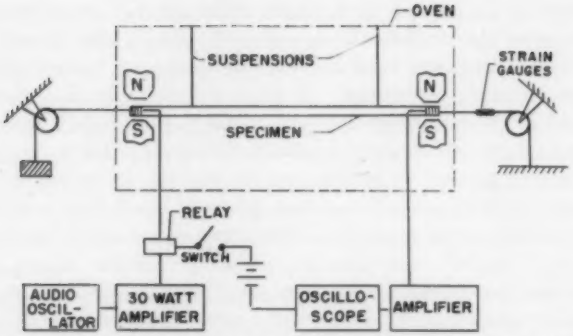

Fig. 1. Experimental arrangement for forced and free vibrations of specimens subjected to axial tension.

The response of the system to the forced oscillation was obtained by a similar coil and magnet arrangement at the other end of the rod. The voltage induced in the coil by the motion was amplified and observed on an oscilloscope. The natural frequencies and therefore the elastic modulus at those frequencies could then be determined. Damping values were obtained either from the width of the response curves or from the decay of the oscillation upon closing the driving circuit. Since the properties are measured only at the natural frequencies of the specimen by this method, it is necessary to change the specimen length to obtain details of the frequency variation. The frequency range of the equipment was from 10 to 4000 cycles/sec.

For testing at high temperatures the specimens were placed in a well-insulated oven capable of temperatures to 1200°F. The interior of the oven could be maintained at almost constant temperature and the control system accuracy was about ±3°F.

Preliminary Experiments—Comparison with Results of Fitzgerald

One of the experiments in the high temperature inelasticity program was the determination of the frequency dependence of the elastic modulus of a soft aluminum alloy (2S). Room temperature lateral vibration tests on an unloaded specimen that had been cold worked revealed two closely spaced resonance peaks at about 2800 cycles/sec. where a single natural frequency was expected. Rotation of the axis of lateral oscillation did not alter the effect as would be expected

for a specimen of elliptic cross section. The double resonance peaks remained until the specimen temperature was raised to the annealing temperature of the aluminum alloy (about 700°F). Further tests on the specimen at room and elevated temperatures gave only the natural frequency spectrum, indicating that the double resonance effect was due to residual stresses in the specimen. In all the tests on unloaded rods, spurious resonances were never observed with annealed aluminum specimens or with lead specimens (which anneal slowly at room temperature).

Subsequent tests on rods subjected to constant axial tension showed similar additional resonances. The checks that tend to eliminate the tensile load wires as a source of the additional resonances were as follows.

(*a*) Clamping the wires to fixed supports at various locations along their lengths did not influence the location or intensity of the spurious resonances. If the wires were a factor due to coupling of vibrations of the specimen and the wires, then the length and flexibility of the wires would tend to affect the results.

(*b*) High vibration damping material, a sponge rubber, was fastened to the wires along most of their lengths with no effect on the resonances.

(*c*) The additional resonances did not occur at the same frequencies for specimens of different materials, indicating that they were not due to simple resonances of the tensile wires.

The observation of the spurious resonances in the vibration tests dictated a comparison with the recent findings of Fitzgerald.[2–6] Fitzgerald's apparatus is not of the resonance type and has the important advantage that the components of the complex compliance can be obtained at arbitrarily close frequency intervals. The specimen in his tests is a short cylinder, about the size of an aspirin tablet, which is clamped and held between relatively rigid plates. A small oscillatory shearing stress is applied to the specimen and measurements are taken which determine the ratios of the strain components (in and out of phase with the stress) to the stress. The components of the complex modulus or its reciprocal, the complex compliance, can then be readily evaluated for the frequency of the test.

For a large number of materials, including metals, polymers, single salt crystals, and glasslike substances, Fitzgerald obtained dispersions at particular frequencies that correspond to sharp resonances. A

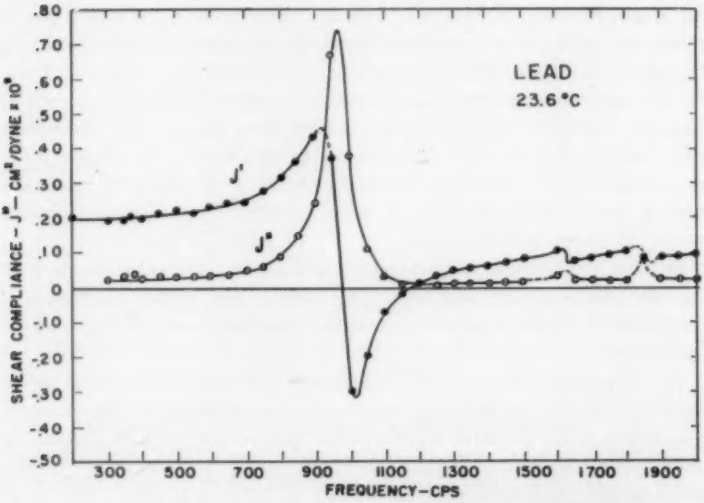

Fig. 2. Typical resonance dispersion obtained by Fitzgerald.[2]

typical result is shown in Figure 2 which was obtained with a lead specimen. The parameters J' and J'' are the real and imaginary components, respectively, of the complex compliance.

The resonances observed by Fitzgerald were in the audio range, 50–5000 cycles/sec., which was appreciably below the lowest natural frequency of the samples. Extensive checks tended to eliminate the equipment as a possible source of the resonances. The experimental resonance dispersions bore a close resemblance to that of the mechanical model shown in Figure 3, and the experimental results could be expressed in terms of the model parameters. The significant aspect of this comparison was the high values of the "induced mass per unit length," m/l, for the materials. An alternative representation of the results was by means of a stress-strain-strain rate law of the form:

$$\sigma = k_0\epsilon + k_1\dot{\epsilon} + k_2\bar{\epsilon}$$

Some of the general observations of Fitzgerald on the location and characteristics of the resonances were that they depend upon the initial clamping stress, elapsed time between clamping and testing, temperature, material state, and orientation in the case of aniso-

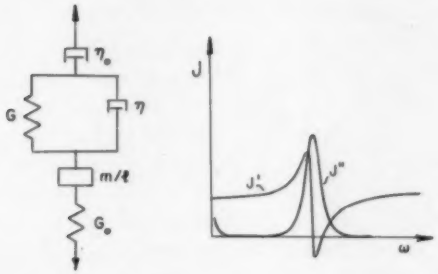

$$J' = \frac{1}{G_o} + \frac{1}{G}\left[\frac{(1-\omega^2/\omega_r^2)}{(1-\omega^2/\omega_r^2)^2 + \omega^2\tau^2}\right]$$

$$J'' = \frac{1}{\omega\eta_o} + \frac{1}{G}\left[\frac{\omega\tau}{(1-\omega^2/\omega_r^2) + \omega^2\tau^2}\right]$$

$$\omega_r^2 = \left[G/(m/\ell)\right]$$

Fig. 3. Mechanical model and associated frequency dependence of compliance to represent resonance dispersion.

tropic samples. The time effect was especially apparent in relatively soft materials that experience stress relaxation. In the lead tests annealing the samples removed all but one of the resonances over the range of testing. A very prominent resonance at about 2850 cycles/sec. was common to the metals tested (lead, aluminum, and indium), and in samples of some other materials.

Negative damping at particular frequencies was observed for the metals and sodium chloride and quartz crystals. The negative absorption decreased slowly with time but could be re-established by increasing the compressive strain, indicating that a relationship probably exists between the negative damping, the static compressive stress, and the stress relaxation process. Materials that either had very large natural damping or did not experience significant stress relaxation did not show any negative damping.

The spurious resonances observed in the present vibration tests on the loaded specimens were extremely sharp and had appreciably lower amplitudes than those corresponding to the natural frequencies of the rod. They could be readily overlooked in experiments de-

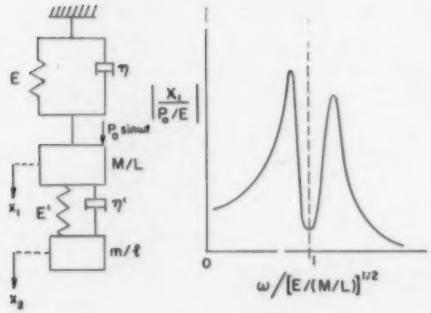

$$(M/L)\ddot{X}_1 + EX_1 + E'(X_1 - X_2) + \eta\dot{X}_1 + \eta'(\dot{X}_1 - \dot{X}_2) = P_0 \sin\omega t$$

$$(m/\ell)\ddot{X}_2 + E'(X_2 - X_1) + \eta'(\dot{X}_2 - \dot{X}_1) = 0$$

Fig. 4. Two degree of freedom model and associated response to a periodic force.

signed to obtain only the natural frequencies unless an additional resonance happened to occur close to one of those frequencies. In this event the response in the neighborhood of the natural frequency would consist of two prominent peaks (such as appeared in the rod with residual stresses). Such a response characteristic is typical of a two degree of freedom system, Figure 4, for which the natural frequencies of the individual components are either equal or very close. In representing results of the vibration tests by the mechanical model of Figure 4, M/L represents the mass term in the expression for the frequency of a laterally vibrating circular rod with free ends. The frequency is given by

$$f = (E\alpha^4 r^2/16\pi^2 L^4 \rho)^{1/2} \tag{1}$$

where r, L, and ρ are the radius, length, and mass density of the rod, respectively, E is Young's modulus for the material, and α is one of the solutions of the frequency equation

$$\cos\alpha \cosh\alpha = 1 \tag{2}$$

depending upon the mode of oscillation. The mass term in the representation of the lateral oscillation of a beam by a simple spring mass system with spring constant E is therefore

$$M/L = 16\pi^2 L^4 \rho/\alpha^4 r^2 \tag{3}$$

The mass m/l in Figure 4 can be considered to correspond to Fitzgerald's "induced mass" since its existence depends upon a mode other than those predicted by classical elastic vibration theory. In the model shown in Figure 4, the coupling spring between the masses G_1 is taken to supply the total spring force to the mass element m/l. This is understood to be only a possible, and the simplest, method of representation of the results and not an idealization of the actual physical situation. If the natural frequencies of the individual spring-mass systems are assumed to be equal, then the value of m/l can be readily determined from the frequencies of the resonance peaks [see, e.g., p. 115 of Ref. 9]. The present tests were not sufficiently sensitive to calculate damping values for the double resonance condition.

Although the representation of the results of the different experiments by similar models is interesting, the analogy between the models should not be carried too far. Both models are simply the mechanical implications of the occurrence of resonances in both methods of testing that are not predicted by classical theory. They may, however, be due to entirely different causes in either case.

Experimental Program and Results

As a result of the previous observations, an experimental program was undertaken in the attempt to obtain better insight into the nature of the additional resonances. The preliminary experiments fairly firmly established that the resonances are directly attributable to the presence of either residual or applied stresses in the specimen. The following tests were directed toward obtaining quantitative data and toward attempting to determine the source of the resonances. All of the tests were based upon obtaining the response of the specimens to forced lateral oscillations. Unfortunately, meaningful longitudinal vibration tests were not possible with the present apparatus due to the driving forces and the response pickup being extremely small for this mode of forced oscillation.

(*a*) Further tests were performed on unloaded 2S aluminum alloy specimens that were subjected to some cold working during their manufacture. For the specimen size, a natural frequency was expected at 2800 cycles/sec. Double resonance peaks that were re-

movable by annealing were found at 2800 and 2850 cycles/sec. in two of the twelve specimens tested. In terms of the model parameters of Figure 4, for a beam length of 35 inches, diameter $^1/_2$ inch, and vibrating in the ninth mode ($\alpha = 29.8$), the calculation of M/L from eq. (3) gives $M/L = 85{,}000$ g/cm. The ratio of natural frequencies for the two modes is $2850/2800 = 1.02$. From eq (50) of Ref. 9, the corresponding value of m/l is 140 g/cm. From Fitzgerald's work on pure aluminum, Ref. 2, the value of m/l calculated by fitting the resonance at 2890 cycles/sec. to the model response, Figure 3, was 790 g/cm. (This value was communicated to the author by Professor Fitzgerald.) Although any comparison of the representative models may have little or no meaning, it is interesting to note that the "induced mass" values are at least of the same order of magnitude. (Anything closer would have been fortuitous.) A test on a shorter length beam also showed a double resonance at about 2800 cycles/sec. which was close to one of the natural frequency values. The fact that the additional resonances at about 2850 cycles/sec. were so common for many materials and both methods of testing does sug-

TABLE I

Resonant Frequencies of Aluminum Alloy (28) Rod under Tension (Lateral Vibration)[a]

No load	$\sigma = 454$ psi	$\sigma = 870$ psi	$\sigma = 1280$ psi	$\sigma = 1710$ psi
57	33, 41, 61, 76, 105	31, 42, 51, 73, 85	35, 48, 61, 86, 98, 107	41, 55, 67, 87, 95, 110, 120
164	149, 177, 218, 257	128, 167, 201	172, 184	185, 189, 200
333	324, 380, 412	339, 430	343, 472	344, 500
562	531, 681	555	545, 575	560, 571, 600
852	840	725, 850	745, 860	875, 1108
1192	1212	1238	1238, 1258	1270
1588	1550, 1620 1740, 1770	1505, 1628	1515, 1670, 1820	1535, 1720
2038	1960, 2000, 2080, 2160	2000	2020	2010
2545	2410, 2660	2490	2470, 2620	2505
3100	3030	3030, 3070	3050	3090
3695	3450, 3680	3530, 3680	3710	3800

[a] Rod dimensions: 35 in. long, $^1/_2$ in. diameter. Tension wire attachments at rod ends.

TABLE II
Resonant Frequencies of Lead Rod under Tension (Lateral Vibration)[a]

No load	σ = 586 psi	σ = 963 psi	σ = 1138 psi
15.9	9.3, 23.3	19.7	14.0
45.5	43.5, 67.9	39.0, 69.0	40.2, 60.0
89.1	106	94, 108	114
146	155	153	145, 157, 164
221	221	211	213, 227, 257
311	302	292, 340, 380	289, 302
412	423	426	390, 433
532	520	508, 610	490, 518, 588
661	612, 655, 722	700	618, 707
808	805	750, 780	760, 778
972	935	881	866
1133	1129	1112, 1140	1128
1313	1260	1230	1231
1512	1438, 1488, 1530	1520	1530
1722	1680	1650, 1740	1615, 1645, 1780
1925	1915	1810	1855, 1955
2170	2075, 2195	2015, 2080	2085
2405	2460	2530	2570
2685	2590, 2710	2690	2710
2920	2900	—	2890
3230	3250, 3480	3250, 3500	3540

[a] Rod dimensions: 36 in. long, 1/2 in. diameter. Tensile wire attachments at rod ends.

gest that they may be due to a basic physical property on the microscopic level.

(*b*) Tests on unloaded lead specimens did not reveal any additional resonances.

(*c*) Tests on an unloaded fiberglass rod that was strongly orthogonally anisotropic did not show additional resonances. The anisotrophy that results from the application of axial load on a cylindrical rod therefore does not, by itself, appear to be an important factor in these tests.

(*d*) A number of lateral vibration tests were made on lead, aluminum, and polyethylene rods subjected to constant axial load. All these tests showed additional resonances which varied in a complicated manner with the axial load. The results of some of these tests are listed in Tables I, II, and III. As in Fitzgerald's tests, the effect

of the axial stress was completely reversible as long as it did not exceed the elastic limit.

(*e*) A hollow tube of aluminum alloy (3S) was placed in compression by stressing a central wire against the tube ends. The axial stress in the tube was measured by strain gages. This specimen also exhibited additional resonances when laterally vibrated. The resonant

TABLE III

Resonant Frequencies of Polyethylene Rod under Tension (Lateral Vibration)[a]

No load	σ = 110 psi	σ = 266 psi	σ = 575 psi	σ = 865 psi
24.3	24.0, 37.5	15.2, 25.3, 35.8, 44.0	14.9, 31.6, 46.0, 55.5	16.7, 39.4, 57.5, 67.8
52.0	51.9, 58.8	69.0	86.0	102
89.0	84.8, 114, 119	90.5, 94.8, 106	132	154
134	164	142, 188	166, 184	209
194	213, 227	244, 269	233, 270	265
262	265, 289	298, 331	293, 345	325, 380
337	350	382	388, 433	420, 465
426	412	455	506	532

[a] Rod dimensions: 36 in. long, $^1/_2$ in. diameter. Tension wire attachments at rod ends.

frequencies for a series of tests with increasing axial compression are listed in Table IV.

TABLE IV

Resonant Frequencies of Aluminum Alloy (3S) Tube under Compression (Lateral Vibration)[a]

No load	σ = 760 psi	σ = 1820 psi	σ = 2170 psi
170	162, 240	161, 220, 339	163, 239, 365
503	495, 590	450, 500, 600, 750	470, 515, 640, 800
1005	1000, 1090	998, 1090, 1290	960, 1000, 1145, 1345
1650	1650, 1770	1645, 1980	1550, 1650, 2050
2480	2480, 2630, 3390	2470, 3390	2470, 2800, 3390

[a] Tube dimensions: 30$^1/_4$ in. long, $^7/_8$ in. outer diameter, $^1/_{16}$ in. wall thickness. Steel end plates ($^1/_8$ in. thick) and central tension wire added. Lowest longitudinal natural frequency = 2800 cycles/sec.

Discussion of Results

The character of the additional resonance obtained in the present tests and of those observed by Fitzgerald point to the dependence of the resonances on the initial stress state of the specimens. The general problem of the resonances appears to result from the specimens exhibiting modes of oscillation in which the effective spring constant is a function of initial stresses which are caused to vary harmonically during the tests. The resonance would then be due to the phenomenon known as "parametric excitation." All the experimental evidence appears to support this conjecture. The most common governing for systems of this class is the Mathieu equation. For a simple spring mass system with harmonically varying spring constant, the equation takes the form

$$M\ddot{x} + (K + \Delta K \sin \omega_k t)x = 0 \tag{4}$$

where ω_k is the frequency of the variation. In the application under discussion, the spring constant K would be a function of the initial stress in the specimen and ΔK would be a consequence of the applied oscillatory forces.

For certain ranges of parameters the solution of eq. (4) becomes unstable, that is, the amplitude increases indefinitely with time. The mathematical treatment of eq (4) has been very extensive,[7] and the stability regions have been established. Figure 5, which is based upon Figure 24 of Ref. 7, gives a portion of the regions of stability for combinations of the parameters (ω_n/ω_k) and $(\Delta K/K)(\omega_n/\omega_k)$, where ω_n is the basic frequency of the system,

$$\omega_n^2 = K/M$$

The sloping lines in Figure 5 are lines of constant $\Delta K/K$. For low $\Delta K/K$ the lines lie mostly in stable regions although they intersect narrow regimes of instability. An important characteristic of eq. (4) is that unstable motions can occur even though the frequency of parametric variation ω_k may be appreciably less than the basic natural frequency ω_n.

The effect of the addition of a viscous damping term in eq. (4) is discussed in Ref. 8. The damping term, among other effects, eliminates the narrow instability regions at low $\Delta K/K$. However, if the combination of parameters of a system would have fallen in

one of these unstable regions in the absence of damping, the motion of the damped system would be similar to the resonance of a simple damped spring-mass system.

The experimental techniques for both the vibrating rod tests and Fitzgerald's tests contain features that could be represented by equations similar to eq. (4). In addition, both sets of experimental results have characteristics which are similar to those of the solutions of eq. (4).

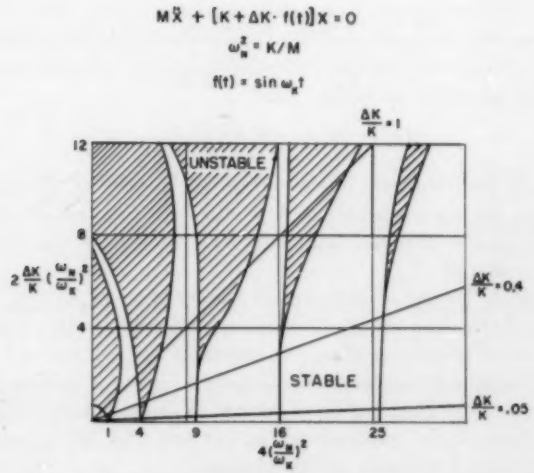

Fig. 5. Stability chart for system with variable spring constant.

The case of laterally vibrating rods subjected to oscillatory axial loads is discussed in Ref. 8. The bending rigidity of a rod is a function of the axial stress. Harmonic fluctuations of that stress leads to eq. (2.14) of Ref. 8 which, upon elimination of the space variable, is a Mathieu equation. A preliminary examination of the additional resonances obtained with the axially loaded rods indicates that they have the general characteristics of those predicted by the analysis of Ref. 8. Details of the comparison will be presented in a subsequent report. It would appear then that the additional resonances observed in the preloaded bar tests may be completely explainable in terms of

a continuum mechanical analysis based on the general results of Ref. 8.

The additional resonance observed in the neighborhood of 2800 cycles/sec. on the unloaded bars containing residual stress poses a more perplexing problem. This was the only additional resonance in the range 50 to 3500 cycles/sec. and occurred for bars of various lengths. As previously discussed, it may result from high frequency modes on the microscopic level that arise from the presence of residual stresses. Under imposed vibrations the system would again be governed by an equation of the Mathieu form for which instabilities can arise even though the applied frequency is small compared to the natural frequency of the mode. A considerable amount of further work is necessary on this aspect of the problem.

Fitzgerald's method of testing also appears to lead to parametric excitation conditions. In his tests the specimen was compressed axially and was subjected to oscillatory shearing stress. On the basis of second-order elasticity theory, the shear stress would result in a longitudinal stress at twice the shear frequency. The elastic constants are functions of the axial stress and would therefore experience sinusoidal fluctuations. The equations for the coupled shear and longitudinal oscillations would then be of the Mathieu type with forcing terms added. In Fitzgerald's tests the amplitude variation of the effective spring constant would be small, that is, $\Delta K/K$ would be small. The unstable regions of the Mathieu equation for this condition occur over very narrow frequency bands which is a characteristic of his tests.

The formulation and solution of the governing second-order elasticity equations is needed before anything more definite can be said about the resonances in Fitzgerald's tests. It is possible that the resonances may be due to both continuum mechanical effects and effects on the microscopic level. The elasticity solution is required before the resonances can be sorted out. The reason that the resonances are not noticed in other measurements of the complex modulus is that their existence and observation depends upon the specimen being initially stressed and the measurements being sensitive and taken over closely spaced frequency intervals.

Negative damping values were obtained by Fitzgerald in the neighborhood of some large resonances for materials that showed stress relaxation. The apparent dependence of the spring constant

in the resonance mode on the initial stress was previously discussed. If this stress decreases exponentially with time then, omitting the periodic fluctuation, the governing equation can be expressed as

$$\ddot{x} + (K/M)e^{-nt}\, x = 0 \tag{5}$$

Upon making the substitution

$$u = (K/M)^{1/2}\,(2/n)e^{-nt/2} \tag{6}$$

eq. (5) becomes

$$u^2\, x'' + ux' + u^2 x = 0 \tag{7}$$

where $(\ )'$ indicates differentiation with respect to u. Equation (7) is the Bessel equation of order zero whose solution is

$$x = AJ_0(u) + BY_0(u) \tag{8}$$

Since Y_0 becomes infinitely large (negatively) as $u \to 0$, or as $t \to \infty$, the motion is unstable and is analogous to the motion of a simple spring-mass system with negative damping. If the stress relaxation effect of eq. (5) exceeds that of natural material damping, then apparent negative damping values result. In effect, the sample transforms the energy of initial compression into oscillatory energy through the stress relaxation process. A more complete analysis of this case would involve the inclusion of the time decay of the spring constant and material damping in the governing Mathieu type equations.

Conclusions

Lateral vibration tests on long rods subjected to residual or applied stresses have revealed resonances in addition to the natural frequency spectrum of classical theory. The resonances seem to be related in a number of respects to those observed by Fitzgerald. The governing equations for the resonant systems appear to be of the Mathieu form in which the fluctuating spring constant terms are functions of the stress state of the specimen. For some tests the governing equations may be derivable from continuum mechanical considerations whereas others indicate that the excited modes may be of microscopic origin. A qualitative explanation is presented for the occurrence of negative damping values in Fitzgerald's tests.

References

1. Bodner, S. R., and H. Kolsky, "Stress Wave Propagation in Lead," in *Proc. Third U. S. Nat. Congr. Appl. Mech.*, June 1958.
2. Fitzgerald, E. R., *Phys. Rev.*, **108,** 690 (1957).
3. Fitzgerald, E. R., *J. Chem. Phys.*, **27,** 1180 (1957).
4. Fitzgerald, E. R., *J. Appl. Phys.*, **29,** 1442 (1958).
5. Fitzgerald, E. R., *Phys. Rev.*, **112,** 765 (1958).
6. Fitzgerald, E. R., *Phys. Rev.*, **112,** 1063 (1958).
7. McLachlan, N. W., *Theory and Application of Mathieu Functions*, Clarendon Press, Oxford, 1947.
8. Lubkin, S., and J. J. Stoker, *Quart. Appl. Math.*, **1,** 215 (1943).
9. Den Hartog, J. P., *Mechanical Vibrations*, 3rd ed., McGraw-Hill, New York, 1947.

Synopsis

Resonance tests on aluminum and lead specimens reveal multiple resonance peaks, i.e., resonances in addition to the natural frequencies of the system, when the specimens are subjected to uniform static stress or contain residual stresses. The multiple resonance peaks can be interpreted in the same manner as the resonance dispersions observed by Fitzgerald. Experiments have been carried out which show that the phenomenon is directly related to the presence of either residual or applied static stresses. A tentative explanation of the phenomenon is presented which is based upon the mathematical representation of the experiments by Mathieu-type equations. The additional resonances are interpreted as instabilities of the solution of the Mathieu equation.

TRANSACTIONS OF THE SOCIETY OF RHEOLOGY IV, 159–168 (1960)

Concentration Dependence of the Stress-Optical Coefficient

WLADIMIR PHILIPPOFF,* *The Franklin Institute, Philadelphia, Pennsylvania*

In a series of papers,[1] measurements of viscosities and flow birefringence of a number of systems at higher concentration have been reported. In the preceding paper, measurements in a birefringent solvent have been described. These measurements were made at a series of temperatures and have been extended to cover a range of concentrations at a constant temperature. The problem we are going to deal with here is the calculation of parameters characteristic for the solute from measurements on solutions in which the solvent has an appreciable flow birefringence. For the analysis of these conditions two theories are applicable. The first one, developed for rigid suspensions essentially by Peterlin,[2] considers the rate of shear, D, and the rotary diffusion constant, D_r, as the factors that determine the conditions. The second theory originated from Lodge's[3] statement that the extinction angle χ_0 in flow birefringence is identical with the angle χ_m between the principal tensile stress and the direction of flow. This angle χ_m is the quantity measured with the so-called "normal stresses," for instance, with the Weissenberg Rheogoniometer. This basic idea has now been accepted by several researchers; in one recent paper Janeschitz-Kriegl[4] proved its generality. However, this relationship is obviously not valid when we consider very dilute solutions: the birefringence of the solvent always occurs in the direction $\chi = 45°$ to the direction of flow, and its magnitude is strictly proportional to the shearing stress τ (a constant stress-optical coefficient C). The solute gives values that are not always proportional to the shearing stress and are oriented to the direction of flow at an angle χ_0 far dif-

* Present address: Esso Research & Engineering Co., Linden, N. J.

ferent from 45°. The problem is now how to derive parameters from measurements under conditions where the birefringence of a solvent is comparable to that of the solution. The first publication in this direction was by Peterlin and Signer[5] who analyzed the measurements of Schmidli.[6] Peterlin considered that the interaction of the separate molecules causes a local increase in viscosity over that of the solvent and deduced that measurements at higher concentrations could be correlated by arithmetically subtracting from the shearing stress of the solution the value given by the solvent. Practically, the degree of birefringence Δn is a function of the specific viscosity: $\eta_{sp} \times D \times \eta_0$, where η_0 is the viscosity of the solvent. However, he did not discuss the birefringence of the solvent. Janeschitz-Kriegl[7] in a recent publication simply subtracts the birefringence of the solvent from the one of the solution at the same D and plots it over the Peterlin expression; this amounts to plotting Δn vs. $D\eta_0\eta_{sp} = \Delta\tau$. In both these methods one arithmetically subtracts the values of both Δn and η_0 of the solvent from that of the solution. It is improbable that this can be done accurately, the reason being that the directions of the birefringence components and the stress components of solvent and solution are not identical. We have to find a method that takes this into account and therefore must expand the Peterlin-Signer treatment to conditions where the components are at substantially different angles towards the direction of flow. To achieve this, we make two assumptions: (*1*) that the birefringence is oriented at an angle of 45° referred to the shear stress of the partial system (solvent or solute) or parallel to the principal tensile stress and (*2*) that we can use the superposition principle developed by Sadron[8]—namely, that the birefringence of a mixture is given by a vectorial addition of the degrees of birefringence Δn oriented under an angle of $2\chi_0$ toward the direction of flow. This construction has not been elaborated by Sadron but is a geometrical conclusion from his well-known formula for an i-component system:

$$\Delta n^2 = (\sum_i \Delta n_i \sin 2\chi_i)^2 + (\sum_i \Delta n_i \cos 2\chi_i)^2$$

and

$$\tan 2\chi = \frac{\sum_i \Delta n_i \sin 2\chi_i}{\sum_i \Delta n_i \cos 2\chi_i}$$

We obviously need a separate calculation of the optical conditions and the mechanical conditions because the relation of the stress-optical coefficients of solvent and solute can be different from the relation of the shearing stresses determined by the solvent and by the solute.

Experimental

The solutions investigated were the same described in preceding papers—namely, a polyisobutylene in a "white oil" which is a mixture of saturated branched paraffins and naphthenes. A check of the literature showed that the values for the stress-optical behavior of our sample of white oil was nearly identical to the one previously investigated by Signer (510 Br). The initial solution of 3% concentration was diluted to 2, 1, and 0.5% and investigated at 25°C. in

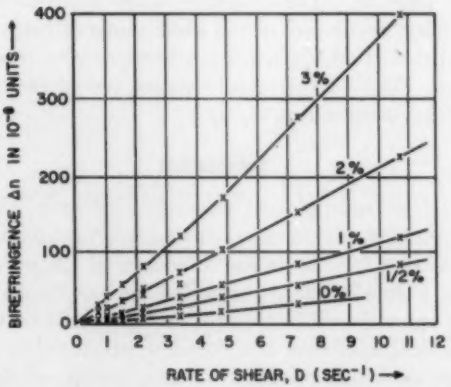

Fig. 1. Dependence of the degree of birefringence Δn on the rate of shear D for solutions of polyisobutylene in "white oil."

the described instrument together with the solvent. The stress-optical coefficient of the solvent was determined in the previous paper as independent of the temperature and equal to 550 Br (10^{-13} cgs) whereas the polyisobutylene has a $C = \sim 1500$ Br. These values are quite comparable to each other. The value of 550 Br for the solvent is not particularly high, as a study of the literature showed that solvents like cetane or methylnaphthalene have respective values

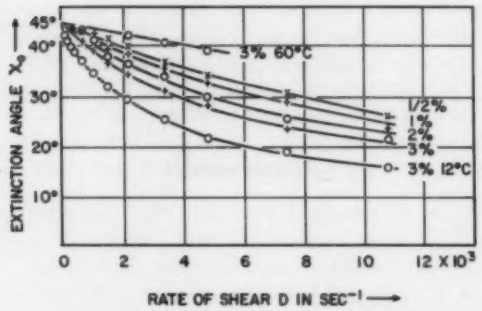

Fig. 2. Dependence of the extinction angle χ on the rate of shear D for solutions of polyisobutylene in "white oil."

of 1100 and 1900 Br. The viscosities of the solutions were measured with a capillary viscometer in the same range of rates of shear, and it was found that the 0.5% solution was essentially Newtonian in the whole range. The experimental results are shown in Figure 1, Δn vs. D, and in Figure 2, χ_0 vs. D.

Evaluation

In Figure 3, we have plotted the results shown in Figures 1 and 2 in the way we have previously done—namely, as Δn vs. $\tau_{max.} = \tau / \sin 2\chi = 1/2\ \Delta p$ where Δp is the difference of the principal stresses. We see from Figure 3 that the expected lines at the 45° slope do not coincide for the different concentrations as should be the case when the stress-optical coefficient is a characteristical value for the solute. They change, as is shown in Figure 3, from a value similar to the more concentrated solutions of polyisobutylene (1500 Br) down to the value of 550 Br for the solvent. On Figure 4, C is shown along with the relative viscosity, η_{rel}, at low shear rates. Obviously the concept of a constant stress-optical coefficient is not valid when the solvent gives a measurable contribution both to the birefringence and to the viscosity. We therefore tried to modify the evaluation in the general fashion outlined above. In Figure 5, we have replotted the results of Figures 1 and 2 in the way suggested by Peterlin and Signer—namely, the amount of change in birefringence $\Delta\Delta n$ vs. the increase in shear stress $\Delta\tau = D\eta_0\eta_{sp}$. We see that this treatment

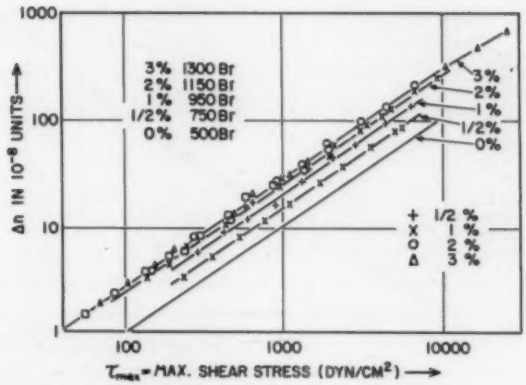

Fig. 3. Degree of birefringence Δn vs. max. shear stress or $^1/_2\Delta\ p$ for all the solutions.

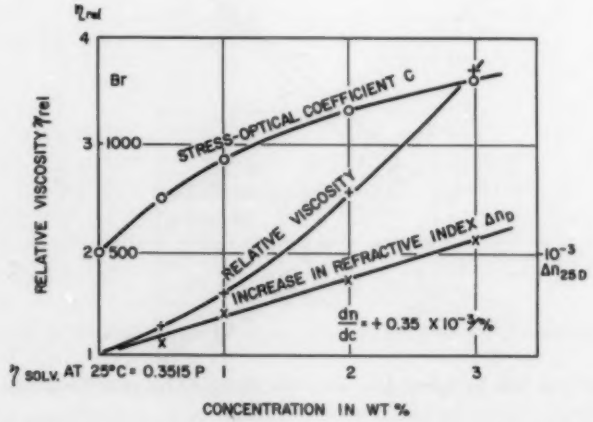

Fig. 4. Dependence of the stress-optical coefficient C, the relative viscosity $\eta_{rel.}$ and the increase of refractive index n of the solutions on the concentration.

brings all the values at lower shear stresses to one single line described by $C = 1600$ Br with very little scatter. However, at higher shear stresses, especially for the 3% concentration, the curve bends upward from the straight line. This evaluation of Figure 5 shows that

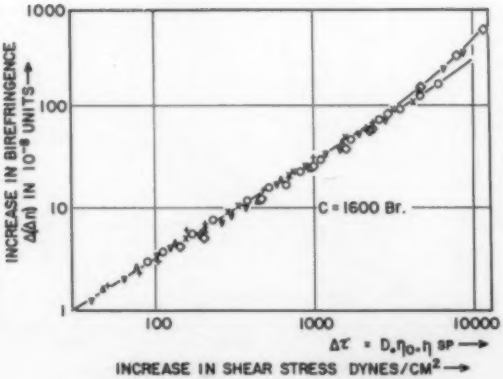

Fig. 5. Peterlin-Signer plot of all values.

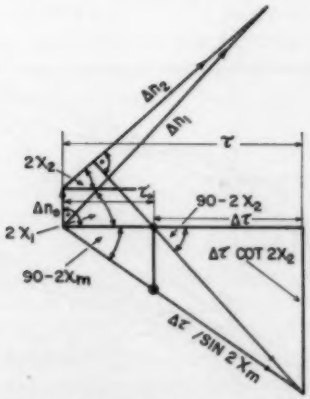

Fig. 6. Vector diagram of the stress-optical condition.

the Peterlin-Signer treatment is applicable for comparatively small shear stresses.

However, it doesn't seem right to arithmetically subtract the effects of the solution and solvent, because they are not occurring in the same direction. We therefore tried to apply the Sadron treatment by separating the birefringence into the component caused by the solvent and the component caused by the solute. The value for

the solvent was calculated as: $\Delta n_0 = 2DC_0\eta_0$ where $C_0 = 550$ Br, the value of the stress-optical coefficient for the solvent. In Figure 6 we plotted a vector equal to the measured Δn_1 at an angle $2\chi_1$ to the direction of flow and subtracted graphically:

$$\vec{\Delta n_2} = \vec{\Delta n_1} - \vec{\Delta n_0}$$

This gives Δn_2, the contribution of the solute. We then plotted the shearing stress $\tau_0 = \eta_0 D$ on the horizontal axis as well as $\tau = \eta D$, the shear stress caused by the solution, and directed a perpendicular to Δn_2 through the end point of τ_0 as shown in Figure 6 and continued until a perpendicular to τ_0 intersected this line. This end point gives us the stress contribution of the solute, with its angular position equal to χ_2.

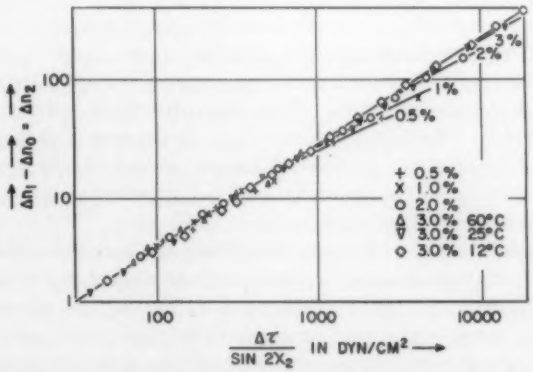

Fig. 7. Dependence of the degree of birefringence Δn_2 on $\Delta\tau/\sin 2\chi_2$.

However, the total shear stress is a composite of the solvent and of the contribution of the solute. It is obtained by connecting the end point of the intersection with the origin. The angle to the horizontal axis is $\pi/2 - 2\chi_m$. By the use of this diagram the experiments were evaluated as to Δn_2 and $\tau_{max} = \Delta\tau/\sin 2\chi_m$.

Both these evaluations are now shown in Figures 7 and 8. We see that a plot using χ_2 gives a definite divergence of the values at higher stress values where χ_2 significantly departs from 45°. However, the plot using χ_m gives a linear relationship for all six experimental

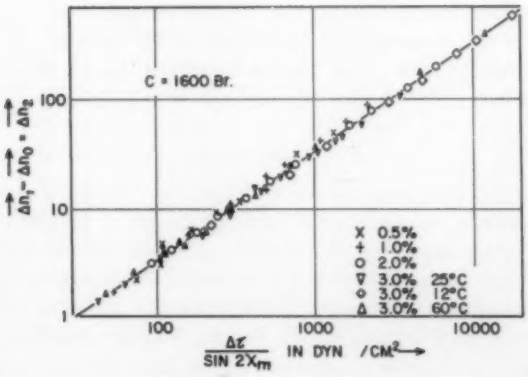

Fig. 8. Dependence of the degree of birefringence Δn_2 on $\Delta\tau/\sin 2\chi_m$.

curves in the whole range. Practically in the case investigated $\chi_1 \cong \chi_m$, so that Lodge's statement is found to be true within experimental error, that $\Delta\tau/\sin 2\chi_1$ is the quantity against which $\Delta\Delta n$ is to be plotted. This shows the method of treatment of a problem where the direction of the birefringence χ_0 is not identical with the direction of the principal stress axis χ_m. For concentrated solutions, as we have shown before, $\chi_m = \chi_0$.

In dilute solutions, as we have just shown, this is not the case. The diagram in Figure 6 shows obviously how the transition from a viscoelastic solution of high concentration to the solvent occurs. For more dilute solution the top triangle merges into a practically vertical line where the Peterlin-Signer relation holds because the directions of all three birefringences are (within precision) the same under 45° to the direction of flow. At the same time, the contribution of the solute to the total shear stress becomes so small that $\chi_m = 45°$ or $\pi/2 - 2\chi_m = 0$: the direction of the shear stress is identical to the direction of the flow. In concentrated solutions, the contributions of the solvent become negligible, $\chi_1 = \chi_2 = \chi_m$. Zvetkov and Frisman[9] in their numerous publications use a value $[n]/[\eta]$ to describe the condition.* This is the same as the Peterlin-Signer treatment

* Where $[\eta]$ is the intrinsic viscosity $[d\eta_{rel}/dc]_{c\to 0}$ and $[n] = [\Delta n/D_{\eta 0}c]_{c\to 0}$, the "dynamo-optical constant," with c in the same units $_{c\to 0}$ in both expressions.

with $[n]/[\eta] = 2C$. They perform the extrapolation to $c \to 0$ from measurements in dilute solutions, while $\chi_0 \geq 30°$, the differences between their treatment and the one proposed here are insignificant for practical cases. We feel that our treatment allows measurements at higher concentrations to be used for the same purpose, where the precision of measurements is much higher. The evaluation of Zvetkov and Frisman's values give the same stress-optical coefficient C as Lodge's method. The evaluation of the recoverable shear $s = 2 \cot 2\chi_1$ and the plotting of it against τ gave nonlinear relations, different for each concentration. However, evaluating $s_2 = 2 \cot 2\chi_2$ and plotting s against $\Delta\tau$ gave linear relationships for all concentrations. $G = \Delta\tau/s$ was proportional to C, as is expected by the expression $G = nkT$, valid for rubberlike elasticity. Inserting the values gave a molecular weight $M = 350{,}000$, which is probable, no other values of M being available for this polymer at the moment.

It seems, therefore, that the evaluation $s_2 = f(\Delta\tau)$ gives a physical significance to the measured extinction angles: the direction of the principal extension of the elastic strain tensor. Experimentally, it is distorted by the 45° orientation due to the solvent. This method of evaluating the extinction angles of dilute polymer solutions is distinctly different from the one of Cerf,[10] which considers $(\Delta\chi/\Delta D)_{D\to 0}$ as the pertinent constant, or Leray,[11] according to whom one plots $D/(45 - \chi_0)$ vs. D to obtain a linear relationship. Obtaining more numerous results on different systems will show which method is most appropriate; however, the proposed one has a definite physical significance for the parameters used. Incidentally by using the formula $s = 2 \cot 2\chi$ the slope of all curves in Leray's plot should be constant ($= 1/4$), which is indeed the case of some of Janeschitz-Kreigl's results. A correction for the birefringence of the solvent is not attempted in the other plots.

Conclusions

Using a new series of measurements of polyisobutylene in white oil where the contribution of the solvent both to the viscosity and birefringence is considerable, we have analyzed the conditions for the correction of both birefringence and shear stress for the effect of the solvent, taking into account the different directions of the contribution of solvent and solute in employing the Sadron method. The evaluations showed that it is then possible to correlate all available data to

a single stress-optical coefficient C in a wide range of variables. Of course, a more detailed test of these conditions is necessary before it can be ascertained if this is the only right way to treat experimental data. The method of Peterlin and Signer, as well as the one of Zvetkov and Frisman (which arithmetically subtract the birefringence and shear stress of the solvent), is shown to be valid at lower shear stresses. The whole purpose of this investigation was to reconcile the treatment peculiar to dilute solutions to the one of the rubber-like elasticity using the stress-optical coefficient.

References

1. Philippoff, W., *J. Appl. Phys.*, **27**, 984 (1956), *Trans. Soc. Rheol.*, **1**, 95 (1956).
2. Peterlin, A., for the latest summary see F. Eirich, *Rheology*, Vol. I, Chap. 15, Academic Press, New York, 1956.
3. Lodge, A. J., *Trans. Faraday Soc.*, **52**, 120 (1956).
4. Janeschitz-Kriegl, H., *Macromol. Symp. Wiesbaden* **1959**, in press.
5. Peterlin, A., and R. Signer, *Helv. Chim. Acta*, **36**, 1575 (1953).
6. Schmidli, A., Dissertation, Zurich, 1952.
7. Janeschitz-Kriegl, H., *Makromol. Chem.*, in press.
8. Sadron, C., *J. Phys. radium*, (7) **9**, 381 (1938).
9. Zvetkov, V. N., and E. Frisman, for example, *J. Polymer Sci.*, **23**, 151 (1957).
10. Cerf, R., Thesis, Strasbourg, 1951; *J. Polymer Sci.*, **23**, 103, 125 (1957).
11. Leray, J., *Compt. rend.*, **246**, 107 (1958).

Synopsis

In previous papers it could be shown that the stress optical coefficient C is reasonably independent of concentration at high concentrations of polymers. However, existing data on measurements in dilute solutions of both birefringence and viscosity at the same rate of shear were either not available or not exact enough. Measurements on a 3% solution of polyisobutylene in "white oil" have been reported. These measurements have now been extended to more dilute solutions. Since the "white oil" itself shows flow birefringence, it is very suitable for investigating the superposition of the properties (viscosity and flow birefringence) of the solute, polyisobutylene, on the properties of the solvent. The evaluation of the results showed that below a certain stress all concentrations give a constant stress optical coefficient, as long as the extinction angle χ does not depart too much from 45°. This is in agreement with the findings of Peterlin and Signer. However, when the angle χ assumes lower values than 45° a systematic departure from this behavior appears. If one follows Sadron's suggestion and adds tensorially the properties of the solvent and solute at constant shear stress, one obtains a constant value for C for all concentrations.

TRANSACTIONS OF THE SOCIETY OF RHEOLOGY IV, 169–177 (1960)

Stress-Optical Properties of Silicones

WLADIMIR PHILIPPOFF,* *The Franklin Institute, Philadelphia, Pennsylvania*

In previous articles[1] we have shown that the stress-optical behavior of rubberlike polymers and concentrated solutions are very similar. This has also been substantiated by Janischetz-Kriegl.[2] In this paper the evidence of polydimethylsiloxanes, commonly called silicones, is presented. These materials were especially suitable for the investigation of stress-optical properties as they are completely colorless, transparent, and easily soluble in, for instance, toluene. The difficulties encountered in other polymers of anomalous behavior at low shear stress has not been observed with silicones. This difficulty will be discussed in a future paper.

Materials Used

The silicones investigated were supplied by the General Electric Company in Schenectady to which thanks are extended. Four different samples were used. First, a homogeneous polymer, A, having a viscosity of 21,000 poises at 25°C., second, a high molecular weight material that could only be used in a 20% solution in toluene, B; and third a rubberlike material that could only be used in a 10% solution, C. Furthermore, a series that was crosslinked by atomic radiation of 20, 30, and 40 mr was supplied by Dr. A. M. Bueche in the shape of thin sheets. This material had been previously investigated by Dr. Bueche.[3]

Experiments

The program planned for the silicones included the investigation of the extinction angle χ_0 and the degree of birefringence Δn together with viscosity measurements in the same range of rates of shear and

* Present address: Esso Research & Engineering Co., Linden, N. J.

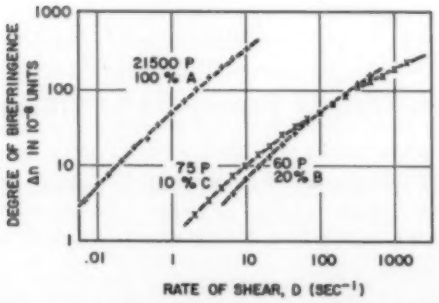

Fig. 1. Dependence of the degree of birefringence Δn on the rate of shear D for the solutions of silicones in toluene; viscosities listed.

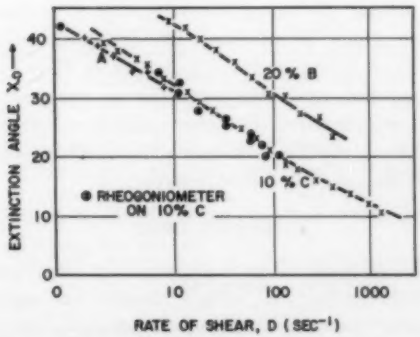

Fig. 2. Extinction angle X_0 as function of D for the silicone solutions.

measurements with the Weissenberg Rheogoniometer. This allows us to check the suggestion of Lodge[4] that the extinction angle χ_0 is identical with the direction of the principal tensile stress referred to the direction of flow χ_m. Similar measurements have been performed previously on polyisobutylene and cellulose derivative solutions.[1] The instruments used for this purpose have been described in the literature.[5] The silicone solutions were well suited for an investigation in a very large range of rates of shear, and the optical effects measured were quite considerable up to a one-wave length phase difference in our instrument. Measurements of the degree of birefringence and the rate of shear are shown in Figure 1. It is seen

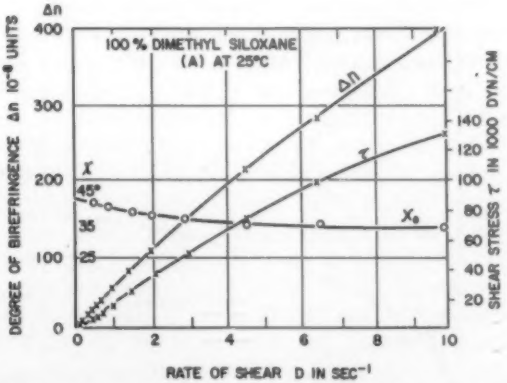

Fig. 3. Birefringence Δn, extinction angle X_0, and shear stress τ as function of the rate of shear D in sec.$^{-1}$ for the 100% silicone A.

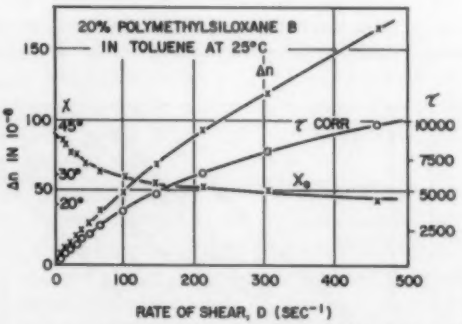

Fig. 4. The same properties as in Fig. 4: for the 20% solution of Silicone B in toluene.

that the measurements of rates of shear vary in a range of 1:10,000, and the observed degrees of birefringence vary in ranges of 1–100. The curves for B and C intersect, but this is only fortuitous as the concentrations were different for the two solutions. On Figure 2 the measurements of the extinction angle χ_0 are plotted as a function of the rate of shear D, and for the solution C the values for χ_m measured with the Weissenberg Rheogoniometer are included. From this series of experiments it was especially clearly seen that there is

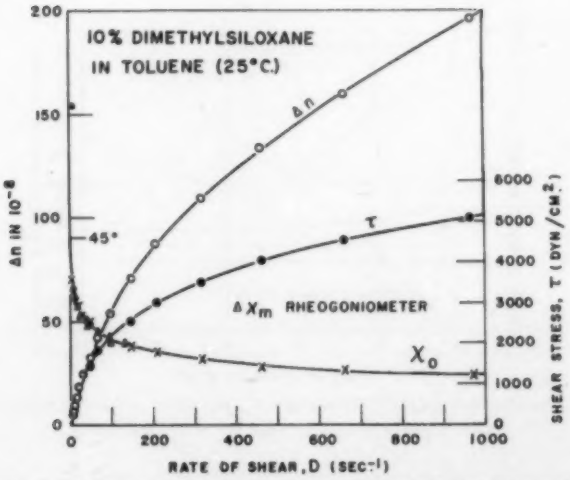

Fig. 5. The same properties as in Fig. 4: for the 10% solution of Silicone C in toluene. (Courtesy *Industrial and Engineering Chemistry.*)

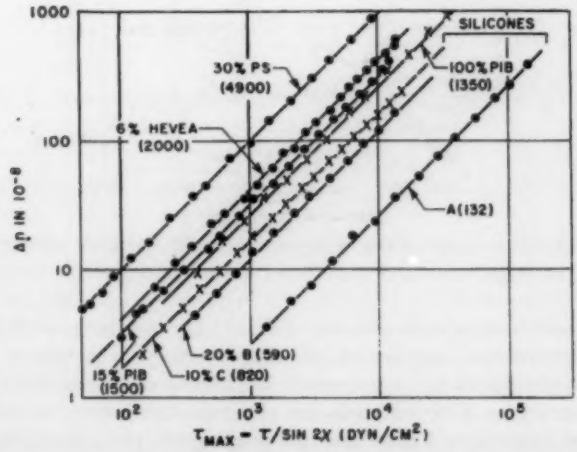

Fig. 6. Δn as function of the maximum shear stress τ_{max} for a number of polymer solutions (stress-optical coefficients C in Br listed in parentheses). (Courtesy *Industrial and Engineering Chemistry.*)

no essential difference in behavior of the solutions and the 100% polymer. To show this most clearly in Figures 3, 4, and 5 the measurements are plotted on a linear scale. It is seen that for the 100% polymer (Fig. 3) the angle χ_0 only decreases to about 35° and merges as it should into the 45° direction. With the C polymer, the behavior is typical of high polymer solutions, even the most dilute ones, with a sharp drop of χ_0 to about 15°. With increasing molecular weight, the nonlinear behavior of the Δn vs. D curve increases considerably—from the nearly linear behavior of polymer A to the sharply curved one of polymer C. Along with these measurements, flow curves i.e., D vs. τ, were measured both in the rotational and capillary viscometer in the same range of D. These results are also plotted on Figures 3, 4 and 5, From all these results, the evaluation of the degree of birefringence Δn versus maximum shear stress, τ_{max}, was performed and is plotted in Figure 6, which has previously been published.[6] It is seen that this plot is linear throughout the whole large range of variables. The highly nonlinear behavior of all the experimental values as a function of rate of shear D can be made linear by using the Δn vs. τ_{max} plot. This series of experiments is one of the best examples of the validity of this type of plotting for fairly concentrated polymer solutions. From Figure 6, the stress-optical coefficient C in Br [10^{-13} cgs] was determined and the values are shown in Table I.

The stress-optical measurements on the silicone rubbers were performed by using a strip of the material loaded with a known weight. The silicone rubbers used were fairly brittle as compared with Hevea rubber and did not extend very much during the experiments but were, on the other hand, completely transparent and very suitable for optical observations. Several load values were used. The results are shown in Table I. It must be emphasized at this time that, as is well known in optical-stress analysis, only one lateral dimension, e.g., the breadth of the sample, has to be known with precision under load. The reason is that the tensile stress and the optical path through the sample compensate in the direction of the light beam. This had led values in stress-optical analysis to be quoted as wavelengths per centimeter breadth. This fact is very helpful in performing such measurements because the exact measurement of the thickness under load is quite difficult. From Table I, it is seen that the dependence of the birefringence on stress was

TABLE I
G. E. Silicone Rubber—Radiation Crosslinked

Load, 10^6 dynes	Breadth, inches		Compensator degrees		C, in Br	
0.104	0.460	0.463	−6°05′	−5°20′	−206	−182
0.202	0.429	0.434	−12°00′	−12°00′	−194	−197
0.300	0.405	0.400	−18°40′	−19°00′	−194	−194
			n_D = 1.4011		Mean value	−194 Br
			Irradiation 30 mr			
0.104	0.469	0.469	−5°25′	−5°20′	−186	−184
0.202	0.442	0.447	−11°30′	−11°15′	−192	−191
			n_D = 1.4025		Mean Value	−188 Br
			Irradiation 40 mr			
0.104	0.493	0.495	4°20′	4°20′	−157	−158
0.153	0.476	0.478	8°54′	9°00′	−161	−163
0.202	0.491	0.485	6°40′	6°37′	−163	−161
			n_D = 1.4013		Mean Value	−161 Br
Polymer A: Mol. wt. 65000 n_D = 1.4029					C = −130 Br	
20% Polymer B					C = +590 Br	
10% Polymer C					C = +940 Br	

linear and the stress optical coefficient C could be determined with a fair degree of precision. The index of refraction n_D^{25} was measured for all samples.

Discussion

From the experimental results presented on the silicone solutions, it is quite obvious that there is no qualitative difference in behavior between the 100% polymer and the polymer solutions. Figures 3, 4, and 5 show the development of the phenomenon. Newtonian liquids, as far as they have been investigated, have a proportionality of both τ and Δn with D and a constant angle $\chi_0 = 45°$. The polymers have increasing departure from this behavior as is very clearly seen from these pictures and as is well known in the field. It is to be emphasized that these phenomena were measured at roughly the same amount of birefringence. However, the shear stresses are different by a factor of roughly 10 and the rates of shear are different by a factor of about 100. All these facts show that the quantitative

conditions are described by the stress-optical coefficient C and the shearing stress, and not so much by the applied rates of shear. In previous papers we have reported the measurement of the so-called recoverable shear, s. However, with these materials no such measurements could be made, as even the expected s values in the range of operation of the rotational viscometer were too small for experimental determination.

The experiments on polymer C have been reported in previous publications,[6] and are one of the best examples for the check of the χ_0 and χ_m of any system investigated until now. It confirms and extends the proof that at least in fairly concentrated solution, the equality of these two angles is present in a wide range of variables. The precision of the measurements of the angles is within 1° and probably less. There seems, therefore, to be little doubt on the validity of the theory that connects the degree of birefringence with the difference in principal stress via the stress-optical coefficient. The non-Newtonian behavior is not important for these conditions as distinct from the statements of Lodge, as it is fully compensated by using the maximum shear stress instead of the rate of shear. In many cases, the angle χ_0 deviates from 45° under conditions of a constant viscosity.

In a series of papers, Saunders[7] has experimentally determined the stress-optical coefficient of rubbers, gutta-percha, polyethylene, and polymethylene in the crosslinked rubbery state. (The last systems at 130 and 180°C.) He found for rubber (vulcanized natural rubber) that the stress-optical coefficient had only a very small dependence on the degree of crosslinking, and for gutta-percha at 85°C. practically no dependence at all. For polyethylene, however, there was a noticeable departure from this rule. The stress-optical coefficient decreased roughly twofold when crosslinking was increased by raising the radiation dose by a factor of 10. The same pertains to polymethylene, where the stress-optical coefficient fell from 1600 to 1260 Br with increasing crosslinking. We have evaluated the values for silicone rubbers in Table I which shows a comparatively small change of C from -194 Br at an irradiation of 20 mr to -160 Br at 40 mr. The other values are also shown in Table I. In previous publications[1,6] we showed that the stress-optical coefficient for natural rubber in the uncrosslinked state was (within error) equal to the one in solution. The 100% liquid polymer gave a slightly smaller value

of −130 Br. The measurements on solutions gave positive values of C, whereas the crosslinked polymer showed a negative birefringence distinct from the much higher and positive value of +2000 Br obtained by numerous investigators for natural rubber. The positive C for the silicone solutions is probably caused by the Wiener body effect. As is well known from theory, the stress-optical coefficient C is determined by:

$$C = \frac{2\pi}{45kT} \frac{(n^2 + 2)^2}{n} (\alpha_1 - \alpha_2)$$

where n is the index of refraction, T the absolute temperature, and $(\alpha_1 - \alpha_2)$ the anisotropy of the polarizability of the monomer link. For natural rubber apparently the main contribution is caused by the double bond in the isoprene unit. In the dimethylsiloxanes the negative sign of birefringence shows that the Si—CH_3— bonds give a larger contribution to the anisotropy than the —O—Si—O— bond in the chain. At the moment, we do not have enough data to quantitatively analyze these conditions, but it is to be hoped that in a short time, bond polarizabilities for the —O—Si—O— bond can also be determined with some precision.

Conclusions

The experimental results and their evaluation on silicones and silicone solutions have shown that their behavior is very similar to the polyisobutylene measured before. There seems to be no qualitative difference between the behavior of undissolved liquid polymers and concentrated polymer solutions, or for that matter, of dilute solutions also. Furthermore, the quantitative comparison of the stress-optical coefficient of the dissolved polymer and the crosslinked whole polymer are very similar, at least as similar as it is for other polymers. However, the stress-optical coefficient is negative (the same is true for polystyrene) in the rubbery state as compared to the positive value for natural rubber and polyethylene. The results substantiate the statement that the optical behavior is primarily dependent on the applied stress.

References

1. Philippoff, W., *Ind. Eng. Chem.*, **51**, 883 (1959).
2. Janischetz-Kriegl, H., *Z. Makromol. Chem.*, in press.

3. Buecha, A. M., *J. Polymer Sci.*, **19,** 275, 297 (1956).
4. Lodge, A. S., *Trans. Faraday Soc.*, **52,** 120 (1956).
5. Gaskins, F. H., and W. Philippoff, *Ind. Eng. Chem.*, **51,** 871 (1959).
6. Philippoff, W., *Acta Rheol.*, in press.
7. Saunders, D. W., *Trans. Faraday Soc.*, **52,** 1414 (1956); **53**, 860 (1957); *Rheology of Elastomers*, London, 1958, p. 30.

Synopsis

The stress-optical properties of silicone solutions have been reported in previous papers. However, the extensive description of the experiments including a check of the angle χ measured in flow birefringences with the one determined by the Weissenberg Rheogonimeter have not yet been given. This has now been done and is given in this paper. Furthermore, the stress-optical properties of silicone rubber, a transparent polymer crosslinked by atomic radiation, was investigated. The stress-optical coefficients C of the silicone solutions in toluene and of the crosslinked rubbers are very similar.

TRANSACTIONS OF THE SOCIETY OF RHEOLOGY IV, 179–189 (1960)

Rupture of Rubber

H. W. GREENSMITH, L. MULLINS, and A. G. THOMAS,
British Rubber Producers' Research Association, Welwyn Garden City, England

The physics of the fracture of solids began in earnest some forty or so years ago with the Griffiths energy balance theory. Since then developments in the metals field have come to a point where attempts are being made to explain practical strength on an atomic level. In the rubber field interest has largely centered on the process of tearing; that is, the propogation of a cut or crack already existing in the material.

A variety of methods have been proposed for measuring tear strength of rubbers and, as might be expected, they do not all rate a given set of materials in the same order, and it is difficult to arrive at a satisfactory basis for a fundamental investigation. A crucial question is what basic property determines when a tear test piece is on the point of tearing. It can plausibly be argued that at the instant of tearing the stress, or strain, at the tip of an incision reaches the limiting value found in a tensile measurement and evidence will be given which tends to support this. However, it is difficult to deduce consequences from this assumption which can be experimentally checked, such as what the applied tearing force will be for a test piece of a given shape, for two reasons: first, ignorance of the shape of the tip when tearing is about to occur, and second, the intractability of the problem in finite elasticity of calculating the strain distribution in the test piece. A different approach was therefore necessary.

In his work on the strength of glass, Griffith proposed that a crack in a sheet of glass would grow an amount Δc, creating an area ΔA of new surface, if the amount of elastic energy lost from the system

$(-\Delta W)$ was greater than the surface energy created $S\Delta A$ at the instant of rupture. This can be written

$$-(\Delta W/\Delta A) = S$$

This approach implies that the surface is formed with no dissipation of energy, an assumption which, from observation of a growing tear, is inapplicable in the case of rubber, as large scale irreversible relaxation of portions of the material can be seen. This will undoubtedly lead to the dissipation of energy as heat and invalidate the simple Griffiths approach. However, starting in this field some ten years ago, Rivlin and Thomas[1] argued that this irreversible loss of energy would take place in a region immediately around the tip and that the amount dissipated would depend upon the strain and the physical properties of the rubber there. As the rubber will be on the point of tearing it will be at its limiting strain, which is characteristic of the material, and thus it seemed likely that the irreversible losses would be dependent only on the physical properties of the material and not on the overall shape of the test piece. Thus for a sheet of thickness t it should be possible to set up the equation at the instant of tearing.

$$-(\partial W/\partial c)_t = tT$$

where W is the total strain strain energy in the test piece, c the cut length, and T the characteristic tearing energy of the material. The partial derivative indicates that the differentiation is carried out so that the applied forces do not move and so do no work.

This provides a tear criterion which can be verified, and in 1953 Rivlin and Thomas[1] described a detailed check on the applicability of the criterion to the tearing of natural rubber. This was achieved by using two types of test piece of novel design which permitted the direct calculation of $(\partial W/\partial c)_t$ from measured applied forces and

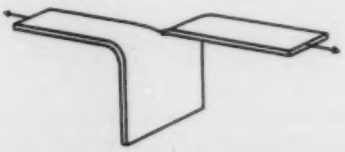

Fig. 1. "Simple extension" tear test piece.

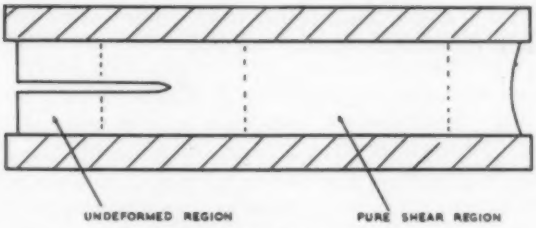

Fig. 2. "Pure shear" tear test piece.

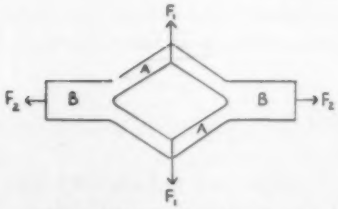

Fig. 3. "Split" tear test piece.

strains. These were the "simple extension" or "trousers" type in which the energy required to tear the specimen is measured by the force applied to it, and the "pure shear" type in which the energy involved in tearing is derived from the energy stored in the strained bulk of the specimen. The test pieces for these tests are shown in Figures 1 and 2, respectively.

Recently[2] yet a third novel design has been used to confirm the validity of the tearing energy criterion. This is the "split" tear test piece, shown in Figure 3.

The important feature of these test pieces is that $(\partial W/\partial c)_t$ can be determined without knowledge of the complex strains existing in the region around the tips of the growing tears. The relevant expressions for the determination of the tearing energy are:

(*a*) *Simple Extension Test*

$$T = -\frac{1}{t}\left(\frac{\partial W}{\partial c}\right)_t = \frac{2\lambda F}{t} - wE$$

where w and t are the total width and thickness of the test piece, E the strain energy per unit volume in the legs of the test piece, λ their

extension ratio and F the applied force. The values of w and t can normally be chosen so that $\lambda \simeq 1$ and

$$-\frac{1}{t}\left(\frac{\partial W}{\partial c}\right)_t \simeq \frac{2F}{t}$$

(*b*) *Pure Shear Test*

$$T = -\frac{1}{t}\left(\frac{\partial W}{\partial c}\right)_t = El_0$$

where l_0 is the unstrained length and E the strain energy per unit volume in that region of the test piece which is in a state of pure shear.

(*c*) *Split Tear Test*

$$T = -\frac{1}{t}\left(\frac{\partial W}{\partial c}\right)_t = \frac{1}{t}\left(F_1\lambda_1 \sin\theta + F_2(\lambda_1 \cos\theta - \lambda_2) - wt\,(E_1 - E_2)\right)$$

where $\tan\theta = F_1/F_2$, and where λ_1 and λ_2 are the extension ratios in the regions A and B, and E_1 and E_2 are the strain energies per unit volume in these regions. If λ_1 is not much greater than λ_2 this expression is approximately

$$T = \frac{1}{t}(1/2)(\lambda_1 + \lambda_2)(\sqrt{F_1^2 + F_2^2} - F_2)$$

The results obtained for these three test pieces of widely different shapes and characteristics showed that when expressed in terms of tearing energy they gave equivalent values and thus provided a good test for the validity and usefulness of this tearing energy approach. A value of tearing energy, formally equivalent to the surface energy in Griffiths theory, of the order of 10^6 ergs/cm.^{2} was obtained. This value is, of course, considerably in excess of the surface energy, and its high value indicates that surface energy is far outweighed by the irreversible dissipation of energy referred to earlier.

In recent studies of crack propagation in metals, use of the Griffith-type energy balance has also produced values considerably in excess of the surface energy, and here the large value of energy required to cause crack propagation has been attributed to work done in plastic deformation.

In view of the ignorance of what occurs at the tip of a tear at rupture, the behavior of the rubber in the vicinity of model tips has been studied. These were formed by giving definite radii to the tips by the use of a circular cutter. The resulting incision was then a parallel sided slit terminated by a semi-circle of diameter d. The value of $(\partial W/\partial c)_l$ can, of course, be defined for any specimen with an incision whether or not it is on the point of tearing, and its value can be directly deduced from measurements of strains around the tip.[3] Comparison of values obtained both from measurements of strains at the tip and from the overall applied forces gave similar values of $(\partial W/\partial c)_l$. Further, if the specimen is at the point of rupture then the theory predicts that the tearing energy is approximately given by

$$T = E_b d$$

where E_b is the work required to break per unit volume of the rubber in simple extension. This relation has been checked experimentally for test pieces in which the incision has a definite tip radius and adequate agreement between the calculated and observed values of the tearing energy was obtained.[2,4]

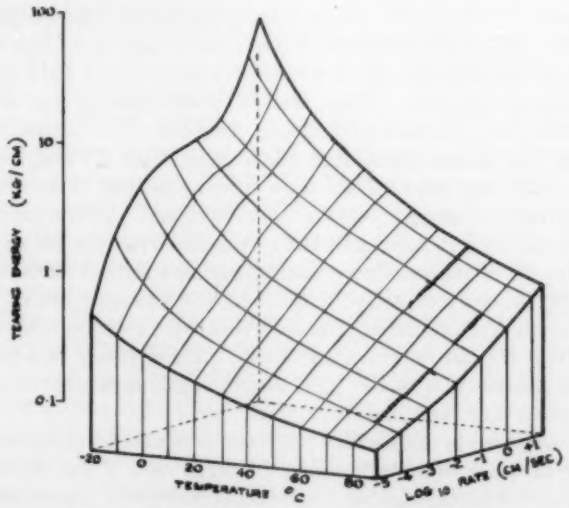

Fig. 4. Tearing energy surface for GR-S vulcanizate.

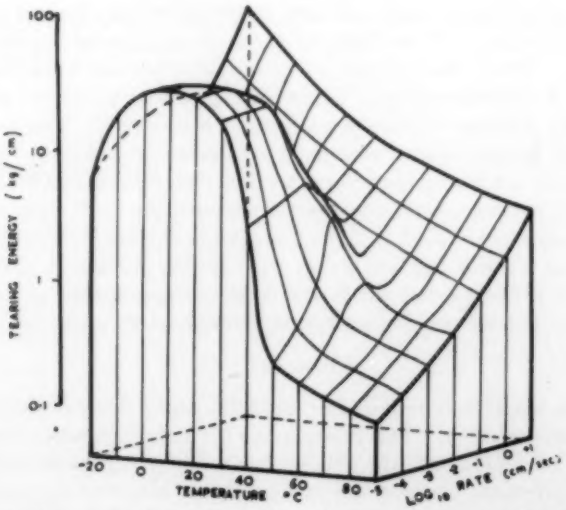

Fig. 5. Tearing energy surface for GR-S vulcanizate reinforced with FT Black.

It appears that there is a close connection between tensile and tear properties and that the effective diameter of the tip of the tear is properties and that the effective diameter of the tip of the rupture is an important concept. When tearing occurs from a cut, or nick, this relation may be used to calculate values of d from measurements of T and E_b. It was found that d is usually about 0.2 mm. for gum rubbers, and that this is of the same order as the size of the observed irregularities developed on the torn surfaces. This observation suggests that the roughness of the torn surface reflects the diameter of the tip of the tear, and that the roughnesses formed at the tip act as if they rounded it off and so reduced the stress concentration. With rubbers reinforced by strengthening fillers, such as carbon black, the value of d can be several millimeters. These much larger values of d are associated with the high tear strength shown by these materials when they tear "knottily."[4]

Of course the energy balance approach provides no information of the rate at which rupture proceeds. Nor, in view of the uncertainty of the mode of energy dissipation, could an analytical approach to the rate problem be envisaged. Hence an empirical study has been made

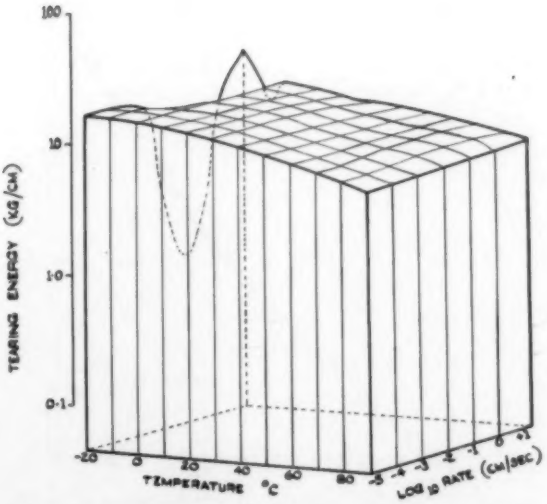

Fig. 6. Tearing energy surface for natural rubber vulcanizate.

of the dependence of tearing energy on rate and temperature; measurements were made using a simple extension tear test described earlier. This approach has proved fruitful in comparisons of the tear behavior of different rubbers.

The results can be displayed in the form of surfaces generated by variables tearing energy, rate, and temperature. Typical surfaces are shown in Figures 4, 5, and 6. Figure 4 shows values of the tearing energy for an unloaded GR-S vulcanizate. The main feature of this surface is a steady increase in tearing energy with both increase in rate or decrease in temperature; this is considered to reflect the viscous or viscoelastic dissipation of energy during the tear process. Figure 5 shows the effect of the addition of an FT carbon black to the GR-S rubber; this is a filler with limited reinforcing ability. Here a substantial increase in the tearing energy is shown over a range of rates and temperatures, but outside this range the carbon black produces a relatively small increase in strength. Figure 6 shows the behavior of an unloaded natural rubber vulcanizate. This crystallizes on stretching, and the crystallites so formed act in a comparable way to filler particles giving much increased strength.

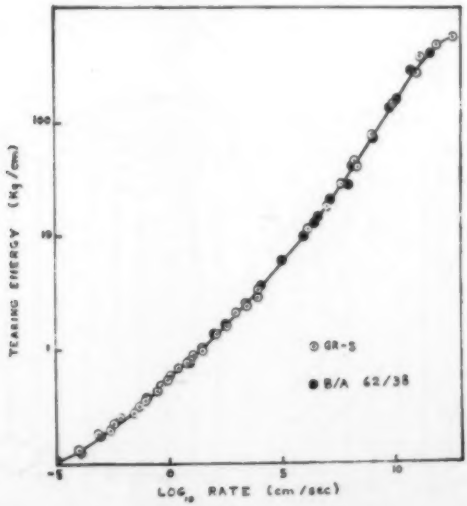

Fig. 7. Transformed tearing energy data for butadiene–styrene and butadiene–acrylonitrile copolymers.

At low temperatures little increase in strength due to crystallization is evident at the higher rates of tearing.

A considerable body of data has been built up on a wide variety of rubber compounds.[5–7] Some unification of the data has been achieved by the application of the concept of an effective diameter of the tip of a tear, and it is found that the observed variations with rate and temperature can be interpreted jointly in terms of (*1*) the work required to break the rubber in simple extension at the appropriate rate and temperature, and (*2*) the effective diameter of the tip, the latter being reflected by the roughness of the torn surface. Thus with the carbon black reinforced GR-S vulcanizate shown in Figure 5, an effective tip diameter of several millimeters characterizes the behavior under conditions of maximum reinforcement, but this is reduced to a few tenths of a millimeter at high rates of tearing where the carbon black has little reinforcing effect.

A further unification of the data confirms the importance of viscous or viscoelastic dissipative processes in determining the value of the tearing energy.[8] This involves the use of a method of reduced

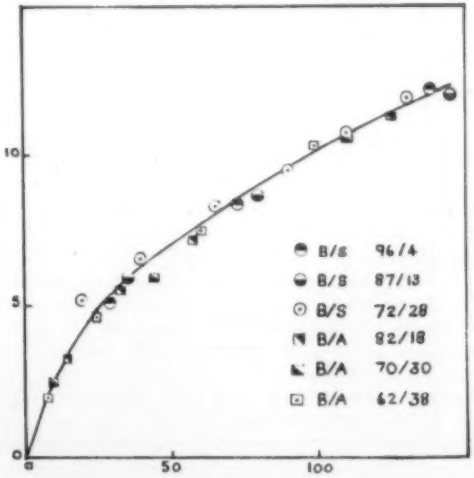

Fig. 8. Rate-temperature transform. Ordinate: $\text{Log}_{10}(a_\Theta)$. Abscissa: $(\Theta - \Theta_0)°C$.

variables which Ferry has shown can be used with considerable power in describing the dependence of viscous or viscoelastic behavior of materials on rate and temperature.[9] It has been found that the tearing energy of a wide range of rubbers, chosen to exemplify materials which are not reinforced by crystallization or by fillers, and in which, as a result, the progress of tearing is steady, can be completely described by two basic curves. One of these curves describes the dependence of a reduced value of the tearing energy on rate, and the other the interdependence of rate and temperature. Figures 7 and 8 show these master curves obtained on a range of butadiene–styrene and butadiene–acrylonitrile copolymers. Figure 7 gives the reduced value of the tearing energy obtained by multiplying the measured value by Θ_0/Θ, where Θ and Θ_0 are, respectively, the temperature of measurement and the second-order transition temperature of the polymer. The temperatures are expressed in degrees Kelvin. Figure 8 gives the logarithm of the increment a_Θ in rate which corresponds to an increment in temperature above the second-order transition temperature.

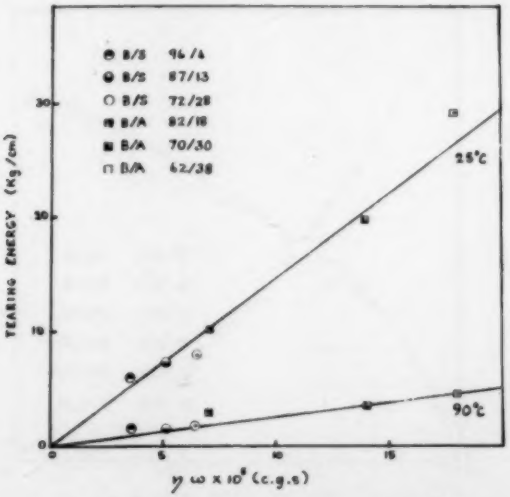

Fig. 9. Dependence of tearing energy on damping.

It appears that the tearing energy of these rubbers is controlled by their chemical composition only insofar as the latter affects their second-order transition temperatures. The success of this type of transform is considered to confirm the important role of viscous or viscoelastic processes in the steady tearing of rubber. This is also demonstrated in Figure 9, which shows values of the tearing energy determined on the range of copolymers at 25°C. at low, 0.0025 cm. sec.$^{-1}$, and high, 25 cm. sec.$^{-1}$, rates of tearing. These are plotted as a function of the imaginary part of the complex shear modulus, which was also determined at 25°C. and was derived from the damping of oscillations of a torsion pendulum with a period of approximately 2 seconds. The figure shows a simple proportionality between the values of the tearing energy and the damping.

References

1. Rivlin, R. S., and A. G. Thomas, *J. Polymer Sci.*, **10**, 291 (1953).
2. Thomas, A. G., *J. Appl. Polymer Sci.*, **3**, 168 (1960).
3. Thomas, A. G., *J. Polymer Sci.*, **18**, 177 (1955).
4. Greensmith, H. W., *J. Appl. Polymer Sci.*, **3**, 183 (1960).
5. Greensmith, H. W., and A. G. Thomas, *J. Polymer Sci.*, **18**, 189 (1955).

6. Greensmith, H. W., *J. Polymer Sci.*, **21**, 175 (1956).
7. Mullins, L., *Trans. Inst. Rubber Ind.*, **32**, 321 (1956).
8. Mullins, L., *Trans. Inst. Rubber Ind.*, **35**, 213 (1959).
9. Ferry, J. D., E. R. Fitzgerald, L. D. Grandine, and M. C. Williams, *Ind. Eng. Chem.*, **44**, 703 (1952).

Synopsis

The paper describes development of work started some ten years ago on the application of an energy criterion to describe the rupture of rubber. It is shown that, by the use of an energy balance theory analogous to that proposed by Griffith to explain the fracture of glass, it is possible to correlate the rupture behavior of rubber samples of widely differing shapes and sizes. This experimental study provides a stringent test of the validity of the energy criterion for the rupture of rubber and demonstrates the basic significance of the value of the rupture energy obtained. Values of this rupture energy of the order of 10^8 ergs cm.$^{-2}$, were obtained. This is considerably in excess of a surface energy and indicates that, in the rupture of rubber, the irreversible dissipation of energy in highly deformed regions around the rupture path dominates the rupture process. The important role of these dissipative processes is also demonstrated by a study of the dependence of rupture energy on rate, temperature, and the nature of the rubber polymer. It is found that using Ferry's method of reduced variables, previously applied to viscous and viscoelastic properties, the rupture energy of all the rubbers examined can similarly be described in a simple unifying way by two basic curves relating its dependence on rate, and the interdependence of rate and temperature.

TRANSACTIONS OF THE SOCIETY OF RHEOLOGY IV, 191-206 (1960)

Rheological Properties of Molecules in Fibers

SEIHUN CHANG, FRANCIS H. REE, TAIKYUE REE, and HENRY EYRING, *University of Utah, Department of Chemistry, Salt Lake City, Utah*

Stress-strain curves of synthetic and natural fibers usually exhibit hysteresis loops.[1-5] This is due to a breakdown of structure in the fibers. Thus, it seemed to us that a detailed study on the thixotropic loops would elucidate the rheological behavior of molecules in the fibers.

For this purpose, we obtained the thixotropic loops and the stress-relaxation curves for nylon 66 under various experimental conditions. The experimental results obtained are reported here and explained in molecular terms.

I. Apparatus and Experimental Procedure

An extensometer which makes use of a transducer was built in this laboratory and used in the present experiments. The capacity and precision of the extensometer could be changed by selecting from the transducers made by Statham Development Corporation. The ends of a fiber sample (monofil) were fixed to the upper and lower jaws of the extensometer by Duco cement. The sample was stretched by pulling the lower jaw at a constant rate using a gear system. The stress, f, exerted on the fiber at time, t, was recorded on chart paper using a Type 153 Electronik autographic recorder made by Brown Honeywell Co. After the sample was pulled to a given stress, the fiber was allowed to shorten at the same rate as in pulling the fiber, until the stress became zero. Since the elapsed time on the chart paper is proportional to the strain, the latter is readily calculated by a calibration.

The sample to be tested was held in an air bath whose temperature was kept constant within $\pm 0.05°C$. The humidity inside the bath was controlled by using a saturated salt solution.

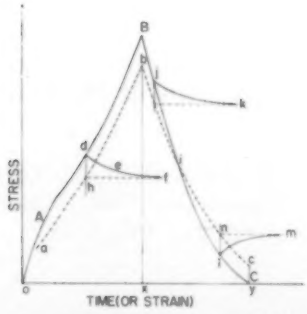

Fig. 1. Schematic representations of the stress-strain curve (ABC), spring line (abc), and stress-relaxation curves. AB (upcurve) and BC (downcurve) are obtained in elongation and contraction of the fiber, respectively.

In Figure 1, a stress versus time (strain) curve, ABC, is schematically shown. AB is the curve obtained during the elongation of the fiber, and is called the "upcurve." BC, the "downcurve," is obtained in the contraction process. The stress-strain curve, ABC, is represented as recorded on the chart. The elapsed times during the elongation, OX, and during the contraction, XY, are proportional to the positive and negative strains, respectively. In Figure 1, if the downcurve is reflected from the vertical line, bX, to the side of the upcurve, one obtains a hysteresis loop.

II. Stress-Strain Curve

Figure 2 represents the results obtained for nylon 66 at 30°C. and 28% R.H. (relative humidity) with a strain rate of 2.10×10^{-3} cm./sec. Here only the upcurves are shown to avoid complication arising from the intercrossing of the curves. In this paper, the stress is force per unit initial undeformed cross section, and strain is $\Delta l/l_0$, where Δl is the deformation from the length under zero load at the start of each experiment, and l_0 is the length under zero stress for a completely relaxed sample. The radius of the undeformed fiber is 1.03×10^{-3} cm. and the value of l_0 in each experiment is given in the caption of the corresponding figure. In Figure 2, the curve labeled $\Delta l = 0$ was obtained for the sample which, after repeatedly being pulled and contracted, showed a constant shape of the stress-strain curve. After the downcurve, following the upcurve ($\Delta l = 0$), was

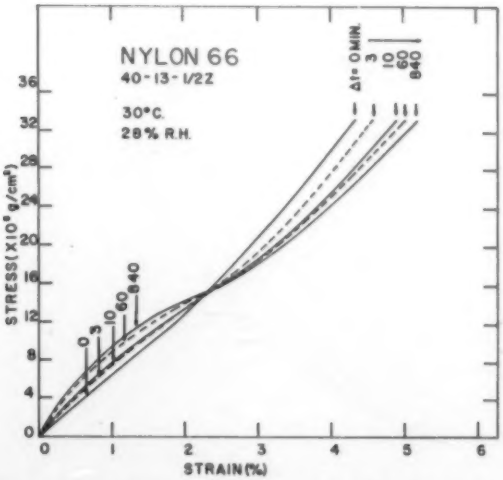

Fig. 2. The upcurves obtained at 30°C. and 28% R.H. for the monofil nylon 66 relaxed according to the program in the text. The initial length of the fiber, l_0 = 2.55 cm.

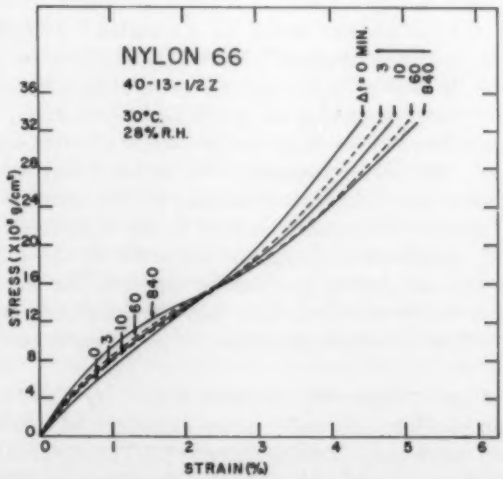

Fig. 3. The upcurves obtained at 30°C. and 28% R.H. for the monofil nylon 66 relaxed according to the program given in the text. l_0 = 2.55 cm.

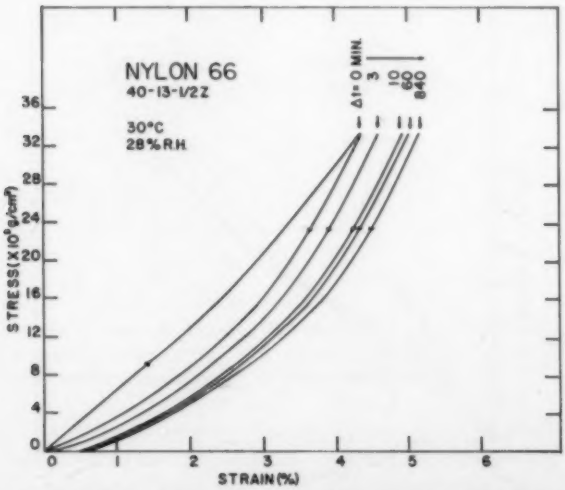

Fig. 4. The downcurves associated with the upcurves represented in Fig. 2. The upcurve associated with the downcurve corresponding to $\Delta t = 0$ is shown to exemplify the hysteresis loops formed during the cyclic deformations.

completed, the sample was rested for 3 minutes. At this time the upcurve ($\Delta t = 3$) was obtained followed immediately by the downcurve. The Δt labeled with each curve in Figure 2 indicates the resting time since completing the preceding downcurve. The order in which the curves were obtained is shown by a horizontal arrow in Figure 2, i.e., they were obtained in the order of increasing resting time. Figure 3 shows the curves obtained for the same sample under the same experimental conditions used in the experiments recorded in Figure 2 except for a change in the order of the experiments. Here, the first experiment was carried out with the sample which relaxed for a sufficiently long time, and the successive experiments were done with decreasing resting time, Δt, as shown by the horizontal arrow.

Figures 2 and 3 show the following facts: (*1*) The stress-strain curve is reproducible, i.e., under given experimental conditions, the stress-strain curve has a definite shape. (*2*) The upcurves converge approximately to a point, which is also the inflection point of each curve, except for the curve ($\Delta t = 0$) which has apparently no inflection

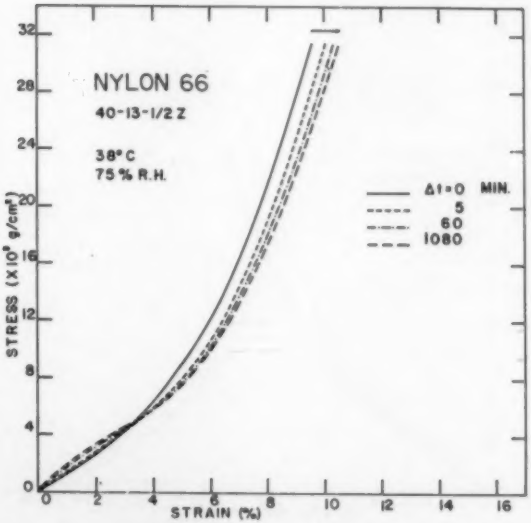

Fig. 5. The upcurves obtained at 38°C. and 75% R.H. for the monofil nylon 66 relaxed according to the program given in the text. l_0 = 3.35 cm.

point. (*3*) At low stresses, below the convergent point, the longer the resting time, the steeper the slope of the curve; immediately above the convergent point the reverse is true, whereas at higher stresses the stress-strain curves become parallel to each other.

In Figure 4, the downcurves associated with the upcurves in Figure 2 are shown, and the upcurve ($\Delta t = 0$) is only reproduced to show the hysteresis loop which was obtained during the cyclic deformation. One sees that the stress of the downcurves is monotonously decreasing with decreasing strain and that the curves are parallel to each other at high stresses. We shall not show the downcurves associated with the upcurves in Figure 3 and in the figures which will be given later, since they are very similar in form to those of Figure 4. We found similar experimental facts to those depicted in Figures 2, 3, and 4 for nylon 610, Dacron, and nylon 6. The results for these fibers will be published in a later communication.

We increased the pulling rate from 2.10×10^{-3} to 8.28×10^{-3} cm./sec., but no appreciable effect on the stress-strain curves was

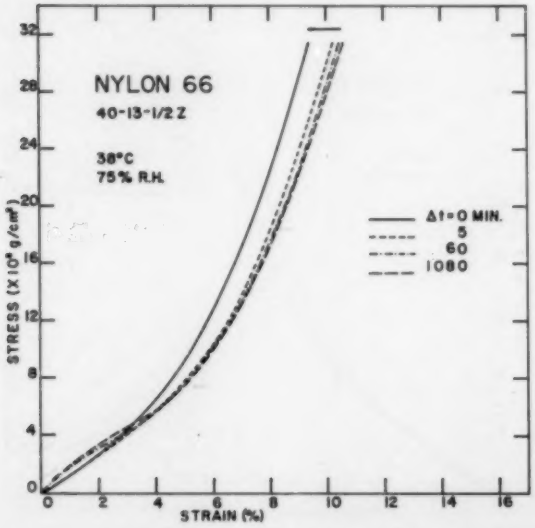

Fig. 6. The upcurves obtained at 38°C. and 75% R.H. for the monofil nylon 66 relaxed according to the program given in the text. $l_0 = 3.35$ cm.

observed in agreement with the facts reported by others.[6] Thus, only the results obtained with the pulling rate (2.10×10^{-3} cm./sec.) are reported here.

The curves in Figures 5 and 6 were obtained for nylon 66 at 38°C. and 75% R.H. in the increasing and decreasing order of Δt, respectively. The curves showed the same tendency as noted in the experiments in Figures 2 and 3. Here, however, the convergent point was depressed to a point of lower stress than in Figures 2 and 3.

Similar experiments were conducted at 49°C. and 75% R.H., and the results are represented in Figures 7 (increasing resting time, Δt) and 8 (decreasing Δt).

At 59°C. and 75% R.H. the curves showed neither convergent point (cf. Figures 9 and 10), nor inflection point.

In all experiments mentioned above, the fiber was first brought to zero stress on the previous downcurve, and then was further shortened for 20 seconds (the strain rate = 2.10×10^{-3} cm./sec.) before the fiber was rested. Since the resting time, Δt, included the 20 seconds.

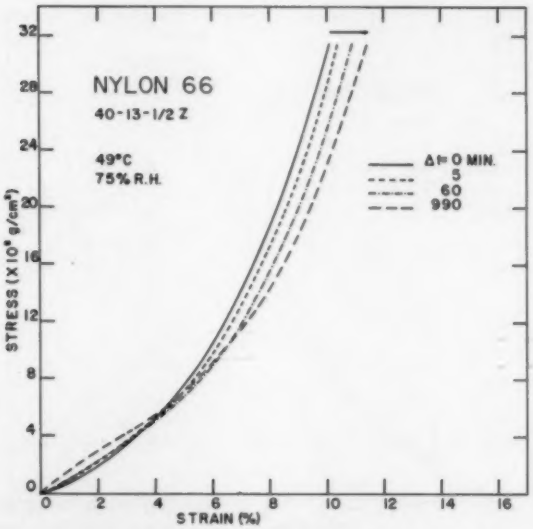

Fig. 7. The upcurves obtained at 49°C. and 75% R.H. for the monofil nylon 66 relaxed according to the program given in the text. $l_0 = 3.67$ cm.

only the sample for the experiment with $\Delta t = 0$ was not rested slack. Because of this procedure, the initial length of the sample in each measurement of a series of relaxation experiments was approximately equal to l_0, except the experiment with $\Delta t = 0$. This approximation was justified by experiments. For the case with $\Delta t = 0$, the initial length was extended from l_0 by 0.2% in the average.

III. Stress-Relaxation

1. Spring Line

In Figure 1, the curve *abc* is a "spring line," which is obtained from the stress-strain curve, ABC, by the following procedure:

(*a*). At a point *d* on the upcurve, the pulling is stopped and the fiber is kept at a constant length.

(*b*). The stress decreases with time as shown by the curve *def*, but reaches an equilibrium value of stress. A horizontal line showing the

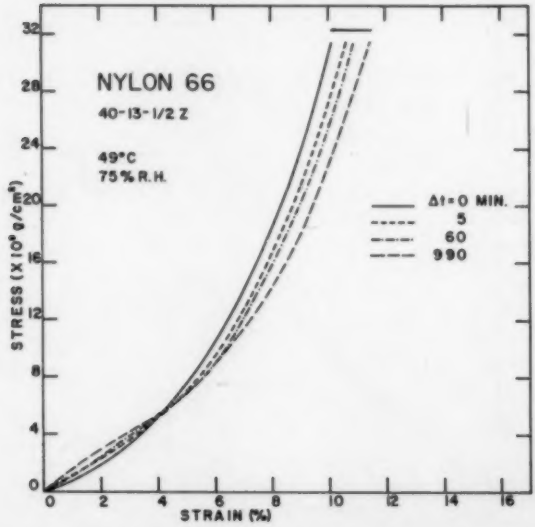

Fig. 8. The upcurves obtained at 49°C. and 75% R.H. for the monofil nylon 66 relaxed according to the program given in the text. $l_0 = 3.67$ cm.

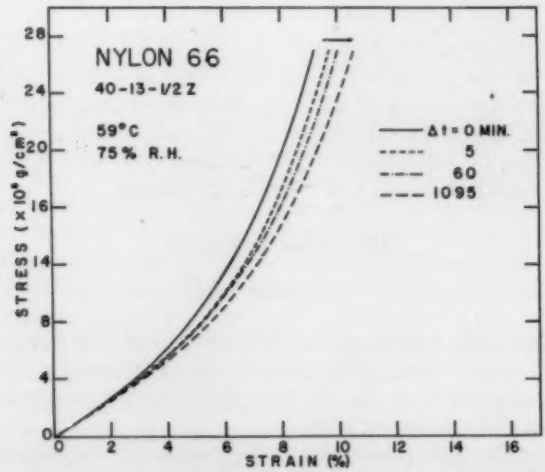

Fig. 9. The upcurves obtained at 59°C. and 75% R.H. for the monofil nylon 66 relaxed according to the program given in the text. $l_0 = 3.67$ cm.

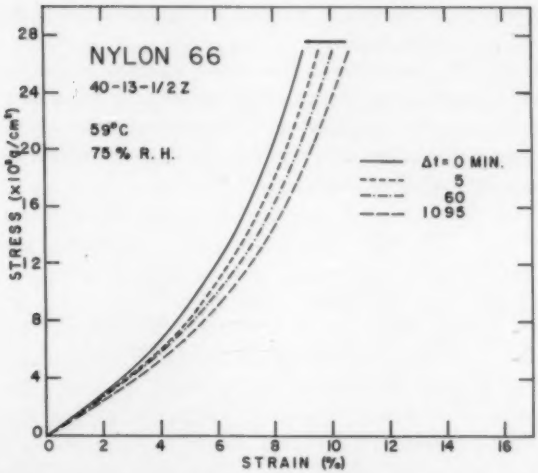

Fig. 10. The upcurves obtained at 59°C. and 75% R. H. for the monofil nylon 66 relaxed according to the program given in the text. $l_0 = 3.67$ cm.

equilibrium stress is drawn and the crossing point, h, with the vertical line at d is obtained.

(*c*). The relaxation experiments are carried out at other elongations, the crossing points being similarly obtained.

(*d*). By connecting the crossing points, the spring line *ab* results.

(*e*). Applying the above mentioned procedures for the downcurve *BC*, the spring line *bc* is obtained. One sees that the downcurve and the spring line cross at a point, *i*.

2. Reference Curve

We have not yet explained how to establish the stress-strain curve *ABC* for the spring line *abc*. The following is the detailed procedure for obtaining this curve:

(*a*). Repeat the cyclic deformation, with a given maximum elongation, Δl_m, several times, the fiber being rested for 3 minutes between two successive cycles. This procedure yields a reproducible stress-strain curve.

(*b*). After being rested for 3 minutes, the fiber is pulled to a given elongation, and the stress-relaxation is observed for 20 minutes.

within which time the stress reaches an equilibrium value (cf. the relaxation curve *def* in Figure 1).

(*c*). The fiber is contracted to zero stress, and is rested for 3 minutes. The stress-relaxation experiment is then repeated at other elongations, increasing the latter from zero to Δl_m. In each experiment, the stress-decay is observed for 20 minutes, and the fiber is relaxed for 3 minutes after being contracted to zero stress.

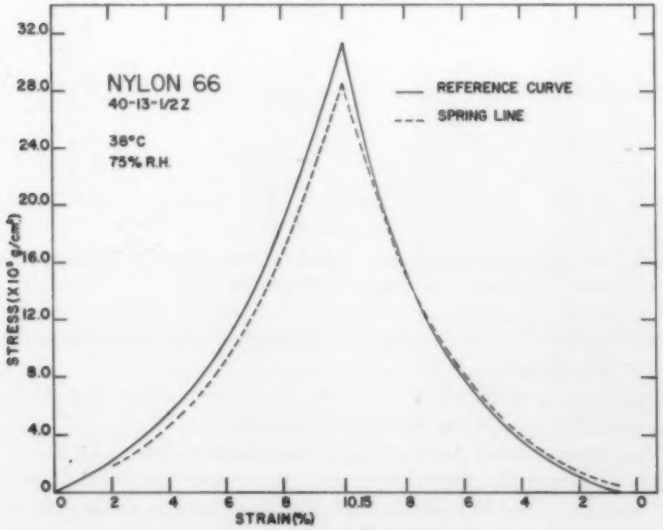

Fig. 11. The reference curve and the spring line obtained at 38°C. and 75% R.H. for the monofil nylon 66. $l_0 = 3.35$ cm.

(*d*). After the relaxation experiment at Δl_m is carried out, the fiber is rested at zero stress for 3 minutes. Then the fiber is pulled to Δl_m and then contracted to a given elongation, Δl. The relaxation experiment is then conducted at this elongation, Δl, for 20 minutes, as usual.

(*e*). Repeat the above relaxation experiment at other elongations, decreasing the latter from Δl_m to Δl_0, at which the stress becomes zero. Every time that the stress-relaxation experiment is carried

out, the fiber is previously relaxed at zero stress for 3 minutes, then is pulled to Δl_m and is contracted to Δl, where the stress-decay is observed for 20 minutes.

(*f*). After the relaxation experiment at Δl_0 is performed, the fiber is relaxed at zero stress for 3 minutes, as usual. Then, the fiber is pulled to Δl_m and contracted to zero stress. This stress-strain curve is taken as the "reference" curve, i.e., the curve *ABC*. The latter usually coincides with the stress-strain curve obtained prior to the first relaxation experiment (in procedure (*a*)).

Using the reference curve *ABC*, the spring line *abc* is procured using the method described in Section *1*. Figure 11 represents the results obtained for nylon 66 at 38°C. and 75% R.H. Here, the reference curve and the spring line are represented by a full curve and a dotted line, respectively. One sees that the spring line is nonlinear, i.e., non-Hookean,[2,7] and that the downcurve and the corresponding spring line cross at a point. Similar results were obtained for nylon 66 at 30°C., 28% R.H., at 49°C., 75% R.H., and at 59°C., 75% R.H. The results, however, are not reproduced here.

3. Relaxation Curve

The stress-relaxation curves, which were used for obtaining the spring lines for the up and down curves, are represented in Figures 12 and 13, respectively. Here the percentage elongation labeling each relaxation curve indicates the elongation of the fiber at which the stress-decay measurements were made. All relaxation curves in Figure 12 show that the stress decays with time. (This group of relaxation curves is represented by *def* in Fig. 1.) On the other hand, Figure 13 reveals that above 7.8% elongation, stress decays with time as usual, while below this percentage elongation, stress increases with time. The elongation of 7.8% corresponds to the crossing point *i* in Figure 1, and the decreasing and increasing relaxation curves are exemplified by the relaxation curves, *jk* and *lm*, respectively. Similar facts to those mentioned above were observed earlier by Stein, Halsey, and Eyring,[2,7] and were used to determine "the zero relaxation point," which corresponds to the crossing point *i*.

We performed many relaxation experiments for nylon under various conditions, and confirmed the above-mentioned experimental facts, but the results will not be presented here in any greater detail.

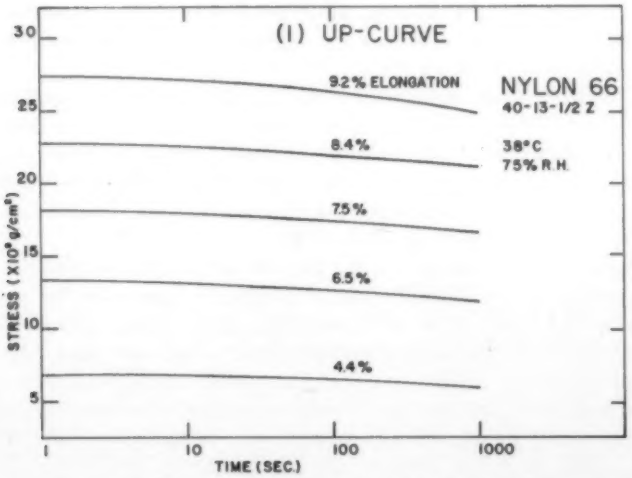

Fig. 12. Stress-relaxation curves obtained on the side of the upcurve represented in Fig. 11.

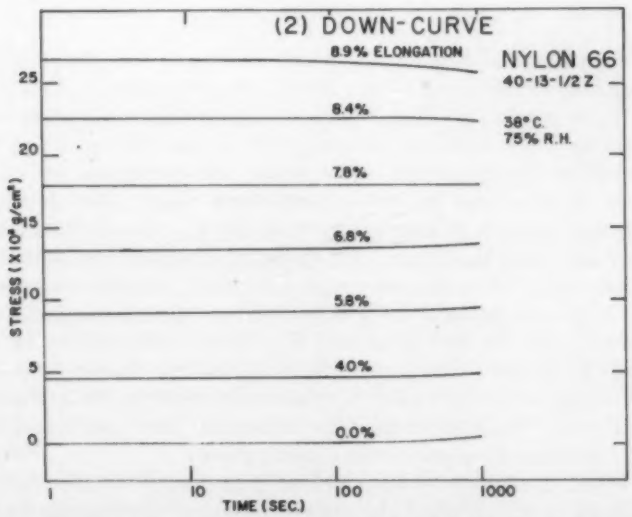

Fig. 13. Stress-relaxation curves obtained on the side of the downcurve represented in Fig. 11.

IV. Discussion

1. Thixotropy of Nylon

In an unstretched state, fiber molecules are in their relaxed tangled form. By applying stress, the entangled molecules disentangle. A thixotropy due to the transition, entanglement → disentanglement, has already been found in grease and related substances.[8] The hysteresis loops found in nylon 66 are due to the transition, entanglement → disentanglement, which occurs mainly below the convergent point. This conclusion is drawn from the following experimental evidences:

(*a*). Over the low range of stress, below the convergent point, the slope of the stress-strain curve (which corresponds to an apparent Young's modulus) becomes greater the longer the fiber is relaxed. This is explained as follows: when the fiber has rested for a long time, the fiber molecules restore the entangled state more completely than when more briefly relaxed. Thus, the more relaxed sample presents a larger Young's modulus, which is a function of the number of entanglements.

(*b*). The convergent point appears at a lower stress when the temperature and relative humidity are raised, and eventually it disappears at 59°C. and 75% R.H.

The entangled portion is thought of as a kind of dashpot, whose strength becomes weaker at high temperature and whose lubrication is improved by water. Thus, the above-mentioned facts are well explained.

2. Hydrogen-Bond Formation

When the fiber was pulled beyond the convergent point, the disentangled molecules begin to line up and hydrogen bonds will be formed between two adjacent molecules, as shown below:

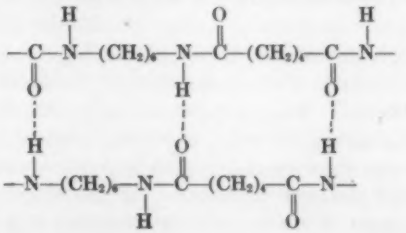

Thus, the Young modulus for this portion becomes larger than that below the convergent point, especially at high stresses. The reason that the up- and downcurves over the high stress and strain range are parallel to each other is due to the fact that the same molecular orientation is reached irrespective of the resting time.

At a given stress, above the convergent point, the shorter the resting time, the smaller the strain of the upcurve, while the reverse is the case below this point. The explanation for the phenomenon below the convergent point has already been given. In the following, we shall consider the reason for the situation above the convergent point.

We have already mentioned that the shorter the resting time between cycles the larger the degree of disentanglement. Thus, the molecules in the samples with small resting times readily line up, and consequently the hydrogen-bond formation occurs more easily than in fibers which have been relaxed sufficiently. As a result, the Young modulus for a briefly relaxed sample is relatively large. This explains why at high stresses, above the convergent point, the strain becomes smaller with decreasing resting time.

The hydrogen bond formed by lining up of the molecules hinders the recovery of the structure which was thixotropically broken down. Thus, a complete recovery, which is due to the transition, disentanglement → entanglement, occurs only when the sample is relaxed sufficiently.

3. Mechanism of the Stress Relaxation

Eyring and Halsey[1] proposed a model (Fig. 14) to explain the mechanical properties of high polymers. This model consists of a non-Newtonian Maxwell unit (a spring in series with a dashpot) in parallel with a spring. The Halsey-Eyring model needs some extension to explain the aforementioned thixotropic nature and the non-Hookean character of the fibers, but it still sufficies to elucidate qualitatively the stress-relaxation phenomena which we observed.

First, the significance of the spring line will be considered in terms of the original model. If we elongate a fiber, both the parallel and the Maxwell unit springs stretch. Since the strain is fixed at a given strain in relaxation experiments, the stress on the spring in the Maxwell unit decays through adjustment of the dashpot, eventually reaching zero stress. Even in this case, there remains on the parallel

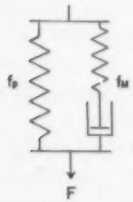

Fig. 14. The Eyring-Halsey model.

spring an amount of stress corresponding to the elongation of the spring. Thus, the spring line represents the stress acting on the spring in parallel with the Maxwell unit.

In the relaxations on the upcurve side, the Maxwell unit spring as well as the parallel one are both stretched; thus the stress always decays with time, as we found experimentally (Fig. 12). This is well explained using Figure 1 also. One sees that the spring line is located below the upcurve. Thus, the stress on the Maxwell unit spring is represented by the stress difference between the two curves at a given strain (e.g., *hd*), and this amount of stress-decay is brought about by the relaxation (cf. the relaxation curve, *def*).

In the "downcurve relaxation," the situation is quite different. When relaxed at fairly high stresses, the Maxwell unit spring is still in a highly elongated state; thus the relaxation accompanies stress decay as usual. But, when relaxed at fairly low stresses, the Maxwell unit spring is in a compressed state at the beginning. This is due to the following reasons: when the fiber is contracted from the maximum elongation to a given length, an immediate response occurs in the parallel and the Maxwell unit springs, but the response on the dashpot is slower, leaving the latter in an extended state only somewhat less than in the maximum elongation; as a result, the Maxwell unit spring is compressed. The compressed spring, whose stress is negative, relaxes through flow of the dashpot, decreasing the absolute value of the stress on it. Let F be the applied stress acting on the unit of the Eyring-Halsey model, and f_p and f_M be the stresses on the parallel and the Maxwell unit spring, respectively (cf. Fig. 14). Since $F = f_p + f_M = f_p - |f_M|$, the stress relaxation brings about a stress increase with time as observed (Fig. 13).

Figure 1 also provides a good explanation in the downcurve relaxations. Here, the downcurve and the spring line cross at the point *i*.

Above *i*, the spring line is below the downcurve; consequently the relaxation in this region follows the ordinary pattern, i.e., a stress decay. Below *i*, the spring line is situated above the downcurve; the negative stress on the Maxwell unit spring is represented by the stress difference between the two curves at a given strain (e.g., *nl*). This amount of negative stress disappears during the relaxation, thus stress increases in this case (cf. the relaxation curve *lm*).

We wish to express our appreciation to the National Science Foundation for support of this work. Acknowledgment is also made to the doners of the Petroleum Research Fund, administered by the American Chemical Society, for partial support of this research. One of the authors, S. Chang, thanks the Government of the Republic of Korea for the fellowship granted to him for the academic year of 1958, and F. H. Ree acknowledges the fellowship provided by the University of Utah Research Committee.

References

1. Eyring, H., and G. Halsey, *Textile Research J.*, **16,** 13, 335 (1946).
2. Stein, R., G. Halsey, and H. Eyring, *ibid.*, **16,** 53 (1946).
3. Katz, S., G. Halsey, and H. Eyring, *ibid.*, **16,** 378 (1946).
4. Reichardt, C. H., and H. Eyring, *ibid.*, **16,** 635 (1946).
5. Alexander, P., and R. F. Hudson, *Wool: Its Chemistry and Physics*, Reinhold, New York, 1954, p. 57.
6. *Tensile Stress-Strain Properties of Fibers*, Instron Engineering Corporation, Massachusetts, 1957, p. 24.
7. Halsey, G., and H. Eyring, *Textile Research J.*, **16,** 329 (1946).
8. Hahn, S., T. Ree, and H. Eyring, *Ind. Eng. Chem.*, **51,** 856 (1959); *Spokesman (J. Natl. Lubr. Grease Inst.)*, **23,** 129 (1959); *ibid.*, **21,** No. 3, 12 (1957).

Synopsis

Using an extensometer, the stress-strain curves and stress-relaxation curves were determined for nylon 66 at various temperatures (30–59°C.) and relative humidities (28–75%). The fiber sample (monofil) was relaxed for various durations of time between successive cyclic deformations (elongation and contraction). The stress-strain curves thus obtained crossed approximately at a point. It is concluded that below the convergent point, entangled molecules become disentangled (a thixotropic breakdown), and above the point hydrogen-bond formation occurs between lined-up disentangled molecules. Stress-relaxation experiments were conducted with fibers under different conditions, and it was found that there were two types of relaxations. In one type, the stress decreased with time, and in the other, it increased with time. The relaxation phenomena were qualitatively well explained by the Eyring-Halsey mechanical model consisting of a non-Newtonian Maxwell unit in parallel with a spring. The spring line, which represents the stress-strain relation for the parallel spring, was also non-Hookean.

TRANSACTIONS OF THE SOCIETY OF RHEOLOGY IV, 207–232 (1960)

The Significance of Rheology in the Making and Using of Paper

ALFRED H. NISSAN, H. G. HIGGINS* and A. LAGANI, JR.,
Department of Chemical Engineering, Rensselaer Polytechnic Institute, Troy, New York

INTRODUCTION

Paper is made from cellulose fibers. Wood or other plant material, such as straw, esparto grass, bagasse, or bamboo, is either mechanically or chemically treated to separate the fibers from each other. They are dispersed in water and subjected to mechanical "refining" or "beating" which shortens them but, more significantly, gives rise to fibrillation, i.e., the appearance of fine and ultra-fine fibrils. The fibers are further dispersed and the dilute suspension, of between 0.1 and 1.0% concentration, is drained on a moving screen of woven wire to form a sheet of some 20% solids. The tender sheet is further dewatered by pressing it between rotating rolls while it is supported on a woven woollen felt and finally dried on one or on a series of revolving steel cylinders through which steam is passed and supplies the necessary heat by condensation.

There are, of course, many other processes through which the wood, the pulp, and the fiber suspension pass before the wet web of paper is formed. Similarly, there are several treatments to which the paper web is subjected either during its dewatering and drying stages or after the dry paper is taken off the paper machine. Only the barest essentials are mentioned here. These essential steps are illustrated by Figure 1, which is reproduced by courtesy of the West Virginia Pulp and Paper Company. Working from the top left-hand corner diagonally to the bottom right-hand corner, wood is shown being pulped,

* Present address: Division of Forest Products, Commonwealth Scientific and Industrial Research Organization, South Melbourne, Australia.

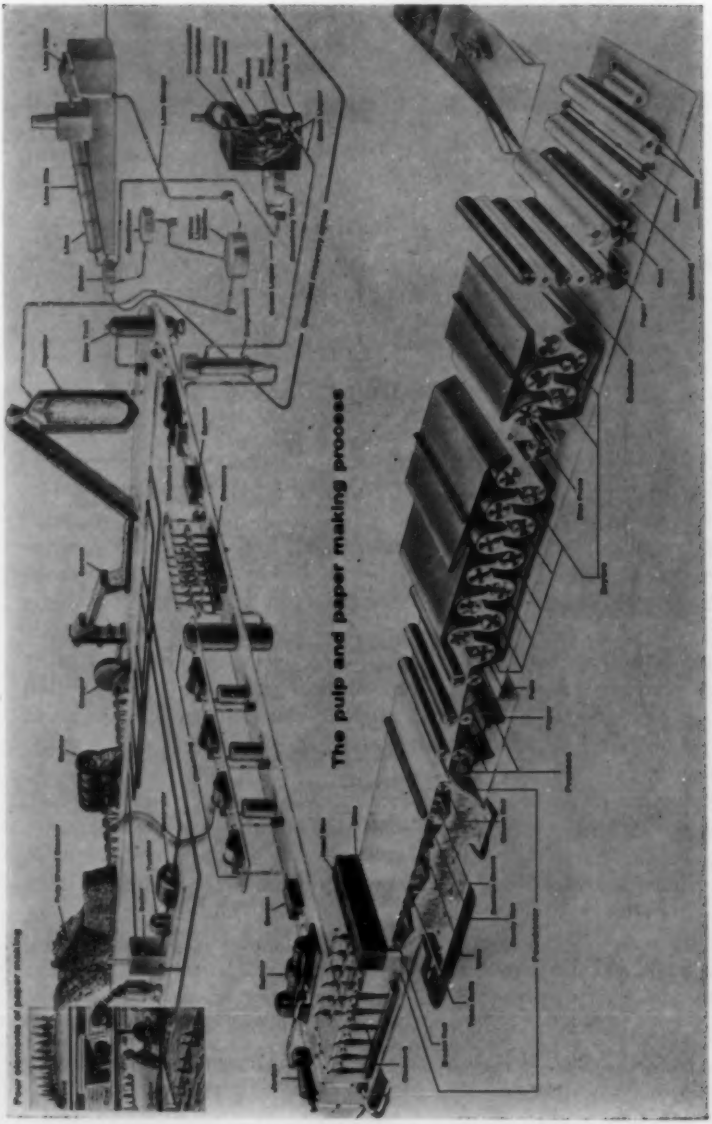

Fig. 1. The Pulp and Paper Making Process. (Courtesy West Virginia Pulp and Paper Company.)

refined and formed into a fiber suspension which in turn is drained over a bronze wire screen, pressed, dried, calendered, and finally slitted and wound into reels.

In order that the meaning of this discussion becomes clear it is necessary that, in addition to the rudimentary sketch of the processes involved, a picture of the form and nature of the fibers used

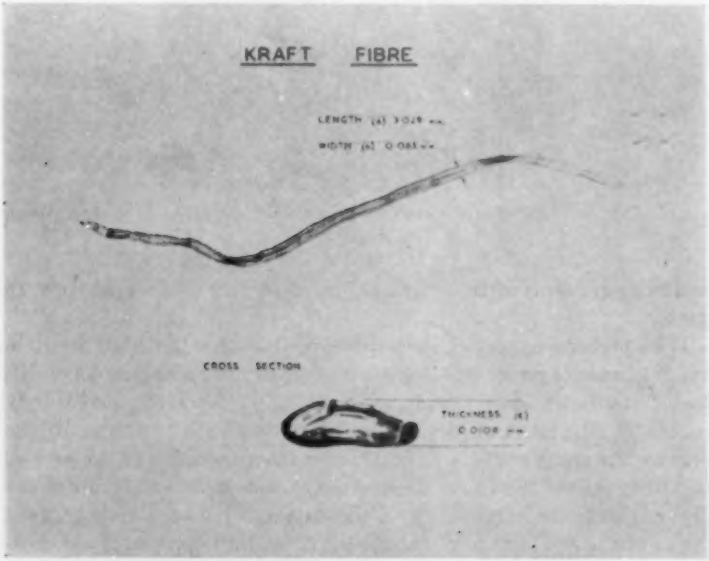

Fig. 2. Kraft pulp fiber in external view and cross section.[1]

be borne in mind. Figure 2 shows a typical wood fiber at low magnification.[1] Figure 3 illustrates, at a higher magnification, the fibrillation which results from beating the fiber and, furthermore, shows how these fibrils cross over and bind fibers to each other. This interfiber bonding is an essential step in paper making and in it lies the secret to the rheologically complex behavior of paper. During drying, the surface tension of the water pulls the fibrils and microfibrils together until they are within molecular distance of each other. As the last molecules of water evaporate from between such elementary units, hydrogen bonds are formed between the OH groups

Fig. 3. Paper-making fibers at high magnification (×9,000). (Courtesy Dr. J. Cronshaw.)

and oxygen atoms of the cellulose chains to give a coherent sheet of paper.

It is perhaps apparent that rheological studies are significant in many phases of paper making. The flow of fiber suspensions of different concentrations, the drainage of water from an increasingly concentrated mat, the yielding and recovery of a wet web in the presses, the transfer of the delicate sheet from the wires to the presses and from the presses to the dryers, the shrinkage and restraint of the drying sheet, the calendering of the dry web between rolls at very high normal and shearing stresses—each of these processes can provide the serious rheologist with ample opportunities for mathematical, physico-chemical and phenomenological studies which are both satisfying and useful. But this is not the end of the story. The *uses* of paper as a base for writing or printing, or as packaging material for light home-use or as heavy-duty industrial shipping containers, as insulating tapes and strings of high strength or as decorative light weight buntings, as a base for sand-paper or as soft tissue fit for milady's cheek—these and many other uses present a further series of rheological problems of great promise. Indeed, some of these problems are as yet undefined: one such is the "softness" of tissue; another is the mechanical property or properties which give paper its peculiar rattle; or the smoothness of paper during and after it re-

ceives the impression in printing as well as the complicated interaction between the rheologically complex ink and the equally complex surface and body of paper.

So that this discussion should have any depth at all, it is essential to be very selective. Accordingly, only the following subjects will be touched upon—and these very briefly: (*1*) Flow of fiber suspensions, (*2*) wet webs, and (*3*) dry paper.

FIBER SUSPENSIONS

The hydrodynamic behavior of single fibers in suspension was studied by one of the present authors[1] but much more elegantly by Mason and his colleagues at the Pulp and Paper Institute of Canada.[2] Probably the most interesting single fact which emerges from these

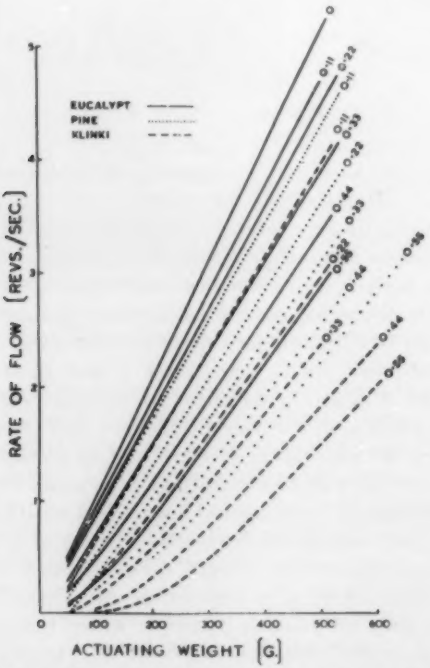

Fig. 4. Flow of fiber suspensions in rotational viscometer.

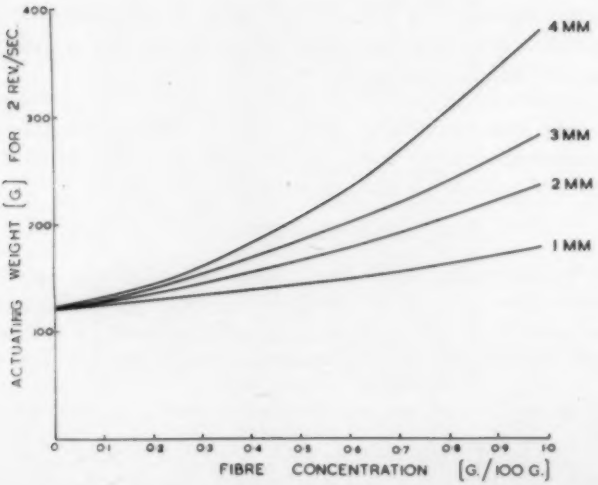

Fig. 5. Flow of suspensions of fibers of different lengths.

studies, which have been carried out in great detail by Mason et al., is the agreement between the observations carried out on single fibers with their complicated shapes and the predictions of classical hydrodynamic theory worked out for ideal cylinders. One of these theoretical predictions which has been confirmed by observations is that fibers in a shear field should rotate in certain orbits, although they should also tend to assume a preferred statistical orientation in the direction of flow. As a consequence of their rotation and their very large ratios of length to diameter, fibers begin to show hydrodynamic interaction at very low concentrations. In Figure 4 are shown the flow curves or more strictly, experimental consistency curves, measured in a modified Stormer rotational viscometer for wood cellulose fibers dispersed in concentrated sugar solution (Golden Syrup). The eucalypt, pine, and klinki fibers are all chemical kraft pulps and are in increasing order of fiber length. The numbers on each curve represent the concentration in grams oven-dry fibers/100 g. liquid. The deviation from Newtonian behavior, which manifests itself at low concentrations and which increases with fiber length, is apparent. The effects of fiber length are shown a little more clearly in Figure 5,

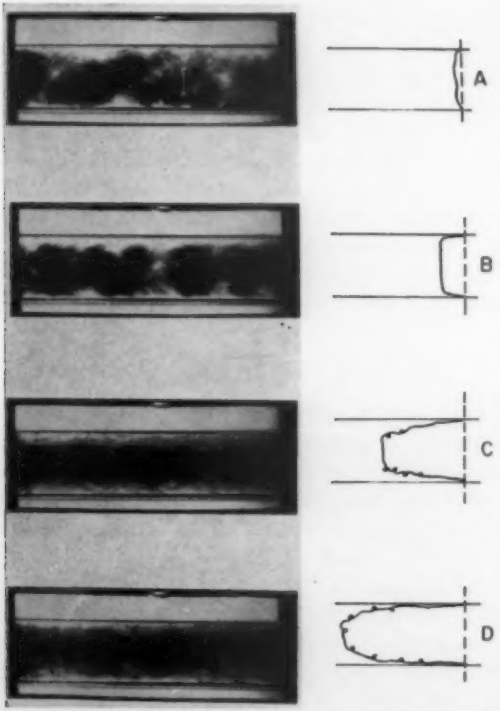

Fig. 6. Patterns of flow of fiber suspensions in tubes. (Courtesy British Paper and Board Making Association of Great Britain and Ireland.)

where the actuating weight necessary to produce an arbitrary rate of rotation of the inner cylinder of 2 revolutions per second is shown for different concentrations of fiber segments cut to various lengths from klinki pine fibers. The figures shown on the curves are the maximum length of fiber segment within each fraction. Details of this work are contained in a report, by one of us (H.G.H.) and Miss V. Goldsmith, which has not yet been published.

The hydrodynamic interference and physical entanglement of the fibers in all concentrations of practical usefulness have profound effects on the flow properties of fiber suspensions in paper making. The reader will find this subject succinctly discussed by Forgacs,

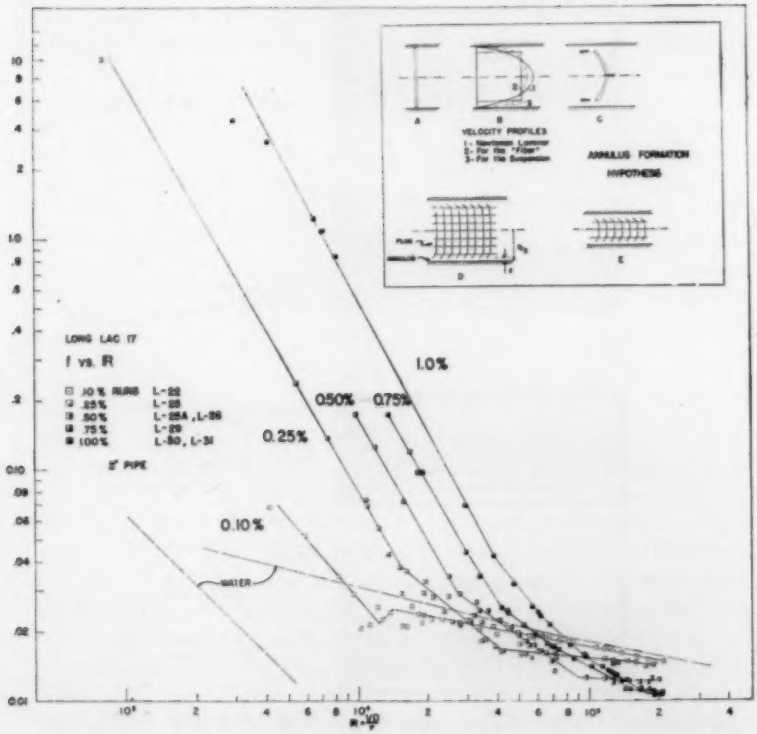

Fig. 7. Friction factor vs. Reynolds number for fiber suspensions. (Courtesy *Industrial and Engineering Chemistry.*)

Robertson, and Mason in a recent summary which they gave in England on the hydrodynamic behavior of paper-making fibers.[3] Figure 6, taken from this work, gives evidence of the formation of flocs which produce plug flow, as well as the clear layer of liquid near the wall. Daily and Bugliarello have confirmed these observations at the Massachusetts Institute of Technology and went further in both experimental observations at high Reynolds numbers as well as in the theory of turbulence suppression by these systems.[4] Figure 7 shows a typical set of results, plotted as a chart of the friction factor versus the Reynolds number (calculated on the basis of water vis-

cosity and density). The subject needs a great deal of further work in order to generalize these findings, but some clarification of long-known difficulties and paradoxes (note the lower values of f for higher concentrations of fibers at high Re) are already apparent from the point of view of the hypothesis of annulus formation. Space does not allow discussion of either the influence of the many factors involved or even the details of the theory which is emerging. The controlling factors are connected, essentially, with the tenacious entanglement of the fibers even at low concentration. Interfiber bonding manifests itself early in the making of paper and increases its influence as the wet web is formed and finally dried into a paper sheet.

THE WET WEB

The first occasion on which these interfiber bonds are subjected to a critical amount of stress in paper making is when the delicate sheet, consisting of about 1 part fiber to 4 parts water, is stripped off the woven wire on which it has been formed and is carried freely across a gap of up to a few feet to the first press of the machine, at a speed which may range from several hundred up to, say, 2,000 ft./min. The sheet is not only stretched by several per cent due to a direct pull but has also to overcome the adhesion which tends to hold it to the wire and the surface tension forces which arise due to the partition of the water film between itself and its support. The ability of the sheet to withstand these and other stresses due to centrifugal and Coriolis forces induced by the curved path it follows is of critical importance to the economics and efficiency of paper making on a modern high speed machine. Thus, rheological studies of this phase of paper formation are highly significant in practice.

A number of studies of the factors involved in this operation have been made. The most recent and comprehensive approaches have been published by Mardon and his co-workers,[5] by Howe et al.[6] in Canada, and by Gavelin in Sweden.[7] Figures 8 and 9 illustrate the geometry and the forces involved, respectively.[5] It is not possible to discuss here these engineering aspects of the problem but instead a brief summary of the rheological behavior of paper at this stage will be attempted.

In a paper which is destined to be of classical importance in this area, Lyne and Gallay[8] elucidated the development of strength in

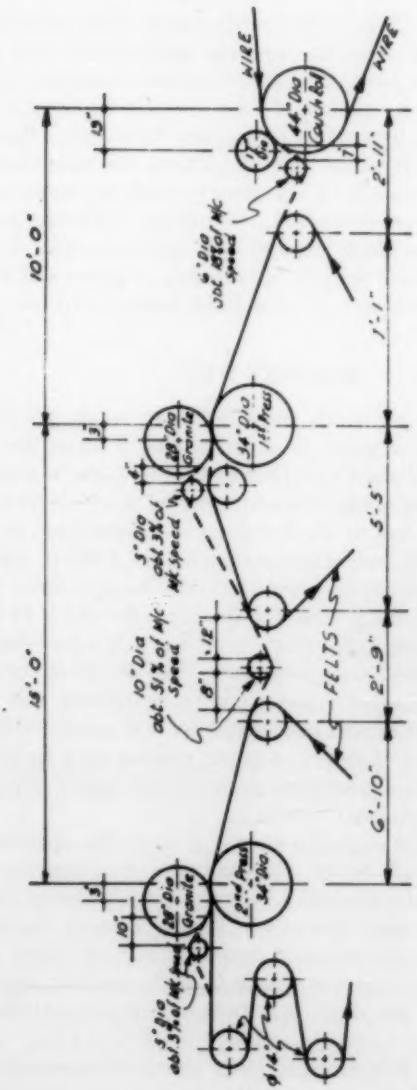

Fig. 8. Typical press part for a high-speed machine. (Courtesy *Pulp and Paper Magazine of Canada.*)

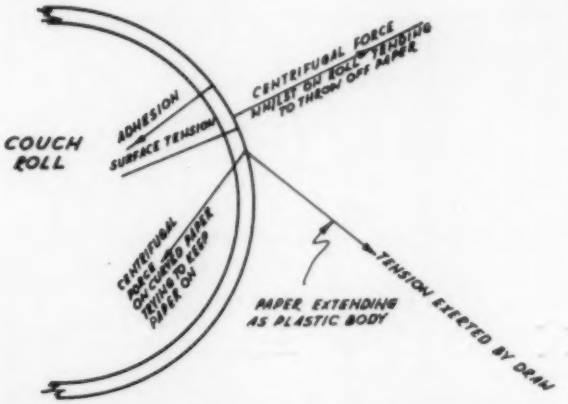
COUCH ROLL
ADHESION
SURFACE TENSION
CENTRIFUGAL FORCE
WHILST ON ROLL TENDING TO THROW OFF PAPER
CENTRIFUGAL FORCE ON CURVED PAPER TENDING TO KEEP PAPER ON
PAPER EXTENDING AS PLASTIC BODY
TENSION EXERTED BY DRAW

Fig. 9. Diagram of the forces involved in stripping the wet web of paper from a roll. (Courtesy *Pulp and Paper Magazine of Canada.*)

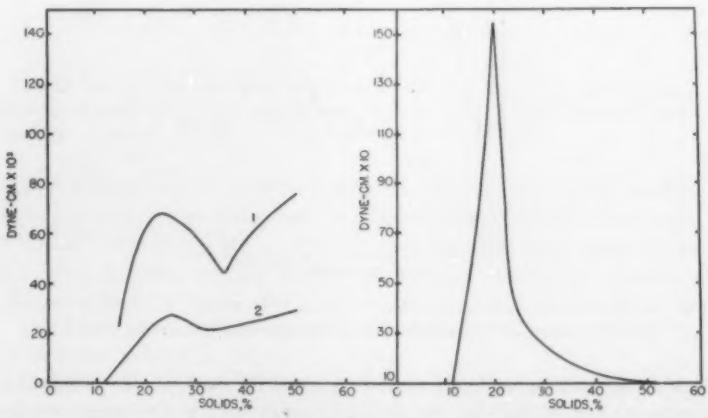

Fig. 10. Work capacity of pulp and glass fiber wet webs over a range of solid Contents. Left: Pulp. Right: Glass fiber. (Courtesy *Tappi.*)

wet webs as the solid content increases from about 8% until the sheet is dry. Coupling their work with that of Mason and co-workers[3] (who have devised an interesting method of measuring fiber network strength at solid contents down to 0.2% and who find a close correla-

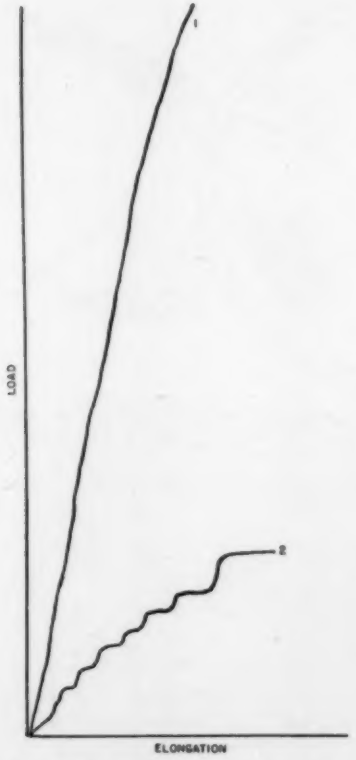

Fig. 11. Load-elongation relationship for glass fiber webs. 1: Surface tension, 72 dynes/cm. 2: Surface tension, 33 dynes/cm. (Courtesy *Tappi*.)

tion between strengths so measured at 0.8% and at 18–20% solid contents) and with other rheological studies on the dry paper, to be discussed below, we have a fairly complete picture of at least some aspects of these complex types of behavior.

Of the many findings of Lyne and Gallay, two deserve special attention. The first is that mechanical strength development proceeds along three distinct paths. Even at very low concentrations, the network resists deformation by virtue of "frictional" forces between the fibers and/or their fibrils. As water is removed and voids are created,

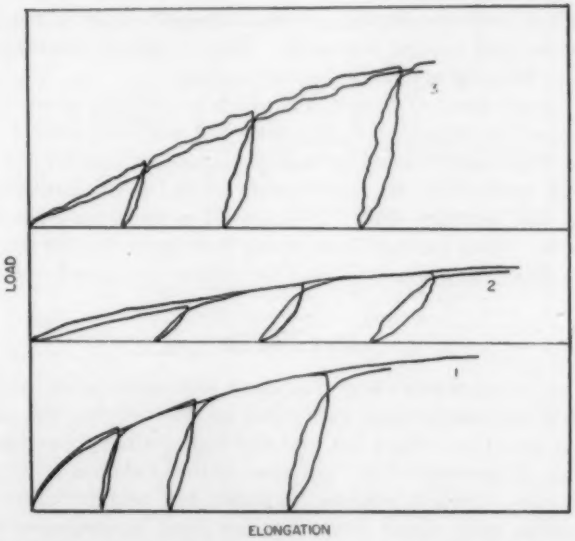

Fig. 12. Load-elongation relationships with and without recycling for wet webs showing memory effect, permanent set and creep recovery; autographically recorded. 1 and 2: Pulp. 3: Glass fiber. (Courtesy *Tappi*.)

surface tension forces come into play which tend to pull the flexible fibers together. The influence of surface tension reaches a maximum at 20–25% solids content. Beyond these points interfiber bondings of a more intimate and particular nature assert themselves between cellulose fibers.

The influence of surface tension is illustrated in Figures 10 and 11, taken from Lyne and Gallay.

It is seen that the work capacity shown in Figure 10 increases with solid content to a maximum for both pulp and glass fiber wet webs. Detailed studies, reported in the original paper, show that during this increase in work capacity, both types of materials develop their strength through the same mechanism. Thus, Figure 11 illustrates the fact that the surface tension of the suspending medium is of primary significance during this stage.

Above, say, 25% solids, glass fibers lose most of their ability to withstand stress as a coherent mass while cellulose fibers, after an

initial drop, begin to develop inherent strength to an increasing extent as the solid content increases. Thus, a different mechanism of interfiber bonding is coming into operation.

The second point of importance which we wish to stress in Lyne and Gallay's work is their finding that "the wet webs down to about 8% solids show all the usual rheological properties found for dry paper, including permanent set, recoverable creep, work hardening, resilience, and memory effect." Figure 12 is an illustration of this statement. Since we shall be studying these properties for dry paper in some detail, we propose to leave the subject of the wet web at this point.

DRY PAPER

The use of paper depends greatly on its rheological properties. Not only do direct relationships exist, such as that between the use of a board or paper as a rigid box and the high stiffness characteristics which are demanded for this purpose, or that between a soft tissue and the low Young's modulus required, but certain more subtle relationships exist which demand a far more sophisticated study. For example, when paper is used as a cement bag, it is found that the rigorous demands of transportation and storage are not necessarily satisfied by a high value of load to rupture. The total work to rupture, in which the extension to break naturally plays an important part, is more significant—provided certain other minimum requirements in breaking load, breaking stretch, and relaxation properties are met. Similarly, the interaction of moisture content and rheological parameters is of vital importance to certain processes in paper making, such as calendering and supercalendering, and to operations in its subsequent use, such as multi-color printing. It is not surprising that this subject has received attention by many workers in different countries. This work is well summarized by Rance,[9] who himself has spent a very great deal of time elucidating it.

The chief mechanical characteristics of paper may be summarized as follows:

(*1*) A load-extension plot yields a nonlinear curve as shown in Figure 13, where it is also seen that the properties of the sheet in the machine direction, i.e., in the direction in which the sheet is running when it is made, are different from those in the transverse or "cross" direction.

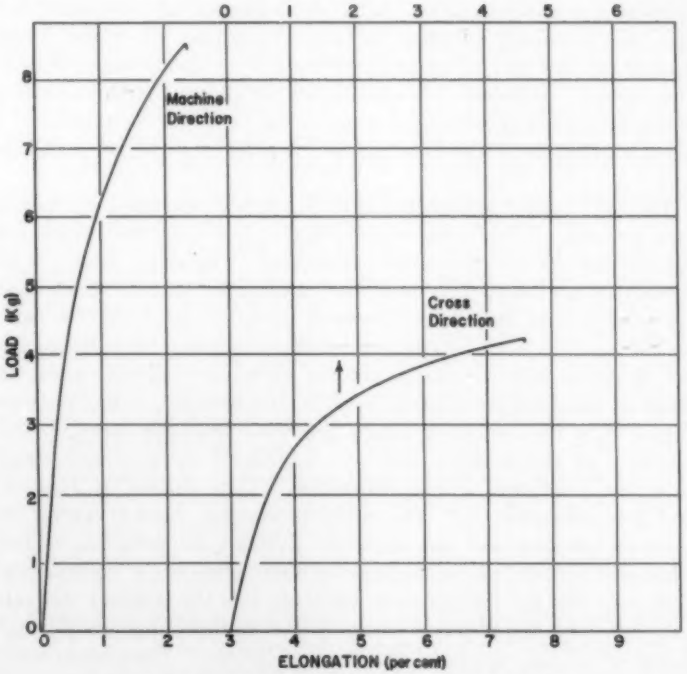

Fig. 13. Typical load-extension curves for paper.

(*2*) Paper shows time dependent rheological behavior—it creeps under constant load; it relaxes under constant stretch; the load-elongation curve is a function of the rate of loading; the maximum load to break and the maximum stretch similarly depend on the rate of loading.

(*3*) Paper is extremely sensitive to the humidity of the atmosphere.

In order to formulate the laws governing the behavior of paper, Steenberg and Ivarsson[10] adopted a mechanical model to represent it. A spring in parallel with a Maxwell element (a spring in series with a dashpot) was adopted. The general behavior of paper suggested that if the springs were Hookean, then the dashpot should have a non-Newtonian liquid. Since Halsey, White, and Eyring[11] had resolved a similar difficulty with cellulose fibers by assuming the

dashpot to contain an Eyring liquid–with a hyperbolic sine law–Ivarsson and Steenberg adopted the same equations for paper sheets. Elastic moduli and viscosity coefficients were then computed to fit the curves. Although it became apparent that a fourth element in series with this model was necessary, some very useful deductions, of great significance to the use of paper, resulted from the use of this device.

Rance[9,12] argued against the adoption of such models for paper on two grounds: (*1*) The irreversible flow is not "viscous" unless one ignores the specific technical meaning of "viscosity," and (*2*) the models are not linked with the known structure of paper. While these are moot points, the abandonment of models is inevitable for paper on the basis of work carried out by Steenberg and his colleagues in collaboration with one of the present authors.[13] In this work, instead of assuming an Eyring liquid in the dashpot, it was only assumed that the 3-element model possessed Hookean springs. The viscosity of the dashpot was then evaluated by graphical means from the rheological curves themselves. (The method is described in full in reference 13.) The resulting viscosity–load curve for the Maxwell element did *not* show an Eyring-type behavior. Thus, while such a model was still useful for many purposes, it became clear that not only the springs were arbitrary but the dashpot too—the only link with the physical nature of the material through Eyring's theory of liquids—was to be an arbitrary element. The system would degenerate to an empirical curve-fitting by an arbitrarily chosen set of equations.

This situation led Nissan[14] to reevaluate the problem and to produce a theory which is based on the one essential fact of paper making and use: at all concentrations of fibers in water exceeding 25% solids, the fiber network exhibits mechanical properties which are linked with the propensity of cellulose fibers to form hydrogen-bonds within and between fibers. By making some drastic simplifying assumptions, the problem became tractable, and a theory based on molecular and thermodynamic parameters which applies not only to paper but to all systems which owe their rheological characteristics primarily to the hydrogen-bond, such as ice, regenerated cellulose sheets and fibers, and nylon, became possible.

A uniform and homogeneous cellulose sheet is assumed to be strained in one direction. The strain energy is assumed to be stored

in stretching the OH——O links of the hydrogen bonds of the amorphous portion of the cellulose. The direction of the H——O link of the bond is assumed random; for small strains this is equivalent to saying that $^1/_3$ of the total number of bonds will be oriented in the direction of the applied strain and $^1/_3$ in each of the two directions at right angles thereto and to each other. Thus, each cubic centimeter of the sample is assumed to consist of n cubes each containing one hydrogen bond lying in the direction of the macroscopic tensile strain and each being subjected to a strain σ which is equal to the macroscopic strain of the sample. For a sample with random distribution of directions of bonds the total number of hydrogen bonds per cubic centimeter of the amorphous region will then be $3n$; the total number of hydrogen bonds per cubic centimeter of the sample will be $(3n + n_u)$, where n_u is the number of such bonds in the crystalline and other regions which are not available for taking part in the straining operation. If the side of each of the n cubes is $l = n^{-1/3}$ cm., it is postulated that the increment $\delta l = \sigma l$ is due to the sum of the stretch δr_1 in r_1 plus the stretch δr_2 in r_2, where r_1 is the length of the OH and r_2 is the length of H——O links of the OH——O bond. Finally, it is assumed that the Morse function

$$U = U_0[1 - \exp\{-a\sigma\}]^2 \tag{1}$$

will represent the energy U stored in the sample at strain value σ where U_0 and a are constants. A similar function is assumed to connect the energy stored in the hydrogen bond itself with the strain $\sigma_2 = \delta r_2/r_2$ of the H——O link, i.e.

$$U_b = U_{0b}[1 - \exp\{-a_2\sigma_2\}]^2 \tag{2}$$

where the suffix b denotes bond, i.e., $U_b = U/n$ and $U_{0b} = U_0/n$.

At any instant,

$$f = dU/d\sigma$$

$$= 2a^2U_0[\sigma - (^3/_2)a\sigma^2 + (^7/_6)a^2\sigma^3 \ldots] \tag{3}$$

$$= E\sigma - K\sigma^2u \tag{4}$$

where f = stress, E = Young's modulus, K = "second coefficient of elasticity," and u = a correction factor which is a function of σ since a does not differ greatly from 18 for most cellulose materials. Thus, since for the hydrogen bond $k_1dr_1 = k_2dr_2$, where k_1 and k_2

are the force constants for the OH and H----O links, respectively, and since $dl = dr_1 + dr_2 = dr_2\,[1 + (k_2/k_1)]$, it follows:

$$\sigma = dl/l = \sigma_2[1 + (k_2/k_1)]\, r_2/l = \sigma_2 r_0/l \tag{5}$$

$$a = a_2 l/r_2\,[l + (k_2/k_1)] = a_2 l/r_0 \tag{6}$$

$$E = 2a_2^2\,\Delta H/r_0 N l \tag{7}$$

$$K = 3a_2^3\,\Delta H/r_0^3 N \tag{8}$$

where ΔH is the heat of dissociation of N bonds and N is Avogadro's number. Putting known values for the different parameters, i.e., $a_2 = 2$, $\Delta H = 1.4 \times 10^{11}$ ergs/mole (= 4.5 kcal./mole), $r_1 = 1.0 \times 10^{-8}$ cm., $r_2 = 1.7 \times 10^{-8}$ cm. and $k_2/k_1 \sim 10{:}1$ (or $r_0 = 1.9 \times 10^{-8}$ cm.), $N = 6.02 \times 10^{23}$, then

$$f = 7.0 \times 10^3\,(1/l)\sigma - 1.1 \times 10^{12}\,(u)\sigma^2 \tag{9}$$

where u has the following values for cellulosic materials. The theory is developed for small strains; values of u for $\sigma > 0.01$ are of doubtful significance.

TABLE I

σ	0.00	0.01	0.02	0.03	0.04	0.05
u	1.000	0.873	0.767	0.679	0.605	0.540
σ	0.06	0.07	0.08	0.09	0.10	
u	0.489	0.447	0.409	0.383	0.352	

From a study of available information, it is concluded that the theory is probably valid because of the following valid predictions:

(*1*) According to eq. (7), E for ice should be 1.5×10^{11} dynes/sq.cm. if $\Delta H = 4.5$ kcal./N bonds as given by Pauling[15] or 1.1×10^{11} dynes/sq.cm. if $\Delta H = 3.4$ kcal/N bonds as given by Grunberg and Nissan.[16] The experimental values reported in the literature fall into a narrow band around 1.0×10^{11} dynes/sq.cm.

(*2*) The absolute value for K, the second coefficient of elasticity, for cellulose sheets is given by the theory as 1.1×10^{12}. Values calculated from published data[14] on paper give K as 1.0×10^{12}, for plasticized regenerated cellulose sheets as 2.0×10^{12}, and for regenerated cellulose fibers as 0.9×10^{12}, giving a grand mean of 1.3

$\times 10^{12}$. Nylon, another hydrogen bonded material, gives 1.7×10^{12}.

(*3*) By the use of further simplifying assumptions, it is shown that $(-d \ln E/dt)$, where t = temperature °C., should be between 2.1×10^{-3} and 6.3×10^{-3} for cellulose. Observations on paper yield average values of $(2.0 \text{ to } 2.6) \times 10^{-3}$ on dry rayons of various types yield $(4.43, 5.4, 3.0, 2.4, \text{ and } 1.8) \times 10^{-3}$, respectively.

(*4*) By taking into account previous observations on the interaction of water with dry cellulose, it is found that according to the theory, the effect of water adsorption by dry cellulose on E should be given by

$$\ln (E_w/E_0) = -w \tag{10}$$

where E_w and E_0 are the Young's moduli at water to solid ratios of w and 0, respectively. This relationship should hold until $^1/_3$ of the hydrogen bonds of the amorphous region are broken. Available data appear to support these predictions too.

(*5*) According to the theory $\Delta n/\Delta E^3$ should be equal to 2.92×10^{-12} approximately. Later work shows this to be not far off 3×10^{-12} in practice.[17]

All this evidence is indirect. However, recent work has provided evidence of a more direct nature that the theory is valid.

The most important aspect of the theory is that it relates the mechanical properties of paper to n, the number of hydrogen-bonds per cm^3 lying in the direction of strain and taking part in it. Thus $E^3 \propto n$. These quantities have been measured independently. A moderately beaten high α-cellulose content eucalypt pulp was acetylated[18] to various extents at two temperatures, 35 and 45°C. The percentage of the total OH groups so acetylated was determined and will be referred to as the degree of substitution. Paper sheets were made under standard conditions from these pulps and their stress-strain relationships for simple tension determined under standard conditions of temperature and relative humidity.

If E is in fact controlled by n, then a plot of $100(1 - E/E_0)$ vs. degree of substitution, where E_0 is the moduius for the unsubstituted pulp, should give a unique relationship. The lower curve of Figure 14 indicates that this is so.

However, the theory demands proportionality between E^3 and n, and the relationship between $100(1 - E^3/E_0^3)$ and degree of substitution is therefore of primary interest. Half the points on the upper

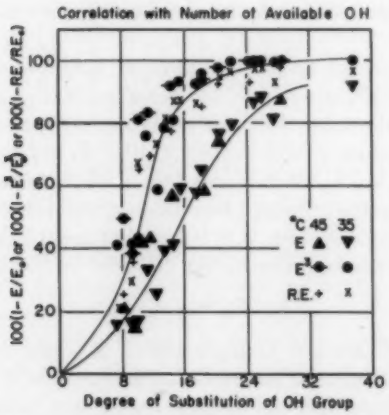

Fig. 14. Correlation with number of available OH.

curve of Figure 14 represent a plot of these quantities, and they show that a relationship does exist. However, confirmation of the theory lies in the following argument.

If each bond requires ($\Delta H/N$) ergs to break, then the rupture energy of the sample, *R.E.*, measured as the area under the stress strain curve should, *to a first approximation*, be proportional to n. Thus $100[1 - R.E./(R.E.)_0]$ should give an identical curve to that given by $100(1 - E^2/E_0^2)$. Figure 14 shows that this is so. It will be noticed, however, that the relationship is not linear. It is believed that this fact is due to (*1*) the opening up of the structure of the fibers by acetylation which makes the lower part of the curve lie below the straight line passing through the origin and the upper cluster of points; and (*2*) the OH bonds available for chemical reaction (36–40%) are greater in number than those available for paper making (approximately 16–18%) since OH groups on the surface of crystallites will react chemically but will not contribute significantly to the mechanical properties of the paper sheet. Again, stress concentrations in the region of bonding between fibers may render the behavior of hydrogen bonds so located of more significance during deformation than that of the bonds within the fiber.

It was stressed in the previous paragraph that these are first approximations only. This is because the energy per bond $\epsilon(= \Delta H/N)$

is not an absolute constant for all hydrogen bonds but has a statistical distribution around a mean $\bar{\epsilon}$. Thus, if all bonds possessed ϵ ergs per bond then $R.E.$ would equal $n\epsilon$. However, if the energy ϵ_i is given by a normal distribution so that $\epsilon_i = \bar{\epsilon}(1 + t_i\sigma/\bar{\epsilon})$, where σ = standard deviation and, if η is defined by

$$\eta = 100(R.E./n\bar{\epsilon})$$

then the efficiency of loading will be given by

$$\eta = 100[1 - t_{\max}(\sigma/\bar{\epsilon})] \tag{11}$$

Equation (11) states that if a centimeter cube containing $n^{1/3}$ bonds per side, i.e., containing n bonds in all, is strained, each chain will break when its weakest link, possessing energy $\bar{\epsilon}(1 - t_{\max}\sigma/\bar{\epsilon})$, breaks. Thus the probability of meeting such a link in $(n^{1/3})$ links is given by

$$(1/n^{1/3}) = (1/\sqrt{2\pi}) \exp\{-t_{\max}/2\} \tag{12}$$

and

$$\eta = 100R.E./n\bar{\epsilon} = 100\{1 - [\sqrt{2\ ln\ (n^{1/3}/\sqrt{2\pi})}](\sigma/\bar{\epsilon})\} \tag{13}$$

For a test piece which is S cm. long, the probability of finding a still weaker bond increases and

$$\eta = 100R.E./n\ \bar{\epsilon} = 100\{1 - [\sqrt{2 \ln\ (Sn^{1/3}/\sqrt{2\pi})}](\sigma/\bar{\epsilon})\} \tag{14}$$

If, finally, n for rupture is identical with n for controlling E, i.e., $n = E^3/3.43 \times 10^{11}$, then

$$\begin{aligned}\eta &= 100R.E./n\bar{\epsilon} \\ &= 1.1 \times 10^{26}(R.E./E^3) \\ &= 100\{1 - [\sqrt{2 \ln(SE/7 \times 10^3\sqrt{2\pi})}](\sigma/\bar{\epsilon})\}\end{aligned} \tag{15}$$

Thus the ratio of $R.E./E^3$ is not strictly a constant but decreases slowly with S and with E and depends on $(\sigma/\bar{\epsilon})$. Furthermore, micro- and macroheterogeneity in the structure introduce secondary effects arising from molecules, crystallites, and fibrils or fibers forming bridges across weak areas and strengthening them. These are as yet unknown functions, which probably can be best evaluated by putting them as

$$S_{\text{effective}} = S[1 - f_1(M/S)][1 - f_2(C/S)][1 - f_3(F/S)] \tag{16}$$

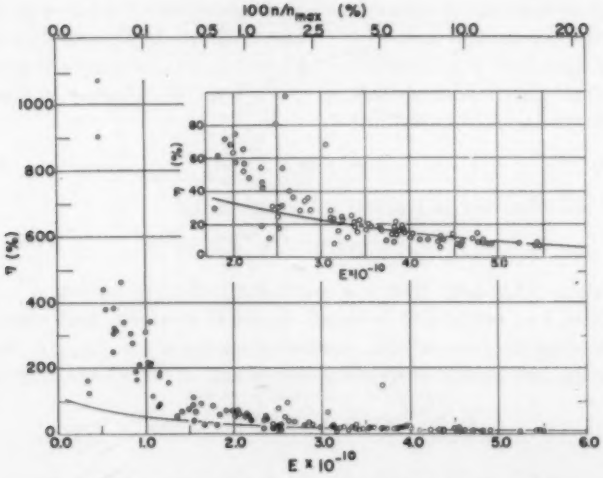

Fig. 15. The efficiency of loading vs. modulus of elasticity.

where f_1, f_2, and f_3 are 3 unknown functions of the molecular, crystallite, and fiber lengths M, C, and F, respectively.

In Figure 15 a large number of points taken from work by Higgins et al.[19] is reduced to an (η, E) plot. It is found that a value of $(\sigma/i) = 0.13$–0.15 gives the solid line both on the main figure and in the expanded-ordinate insert. The top of the figure is scaled in terms of the percentage of available OH groups actually taking part in the strain. It is found that this theory is adequate down to about 1–2% of total available bonds actually being formed; below this figure the principal hypothesis of the theory—that the mechanical properties are primarily a function of n, the number of hydrogen bonds per cm.^{3}—breaks down and van der Waals' and other influences begin to predominate.

If the theory is accepted in principle, how can it be used to further knowledge in this and allied fields? As was stated earlier, the principal contribution the theory makes is to relate rheological properties to n, the number of hydrogen bonds per cm.^{3} of sample which are taking part in deformation. These are inter- and intramolecular bonds. Therefore their behavior can be looked at from the standpoint of kinetics and thermodynamics. In other words, their rupture

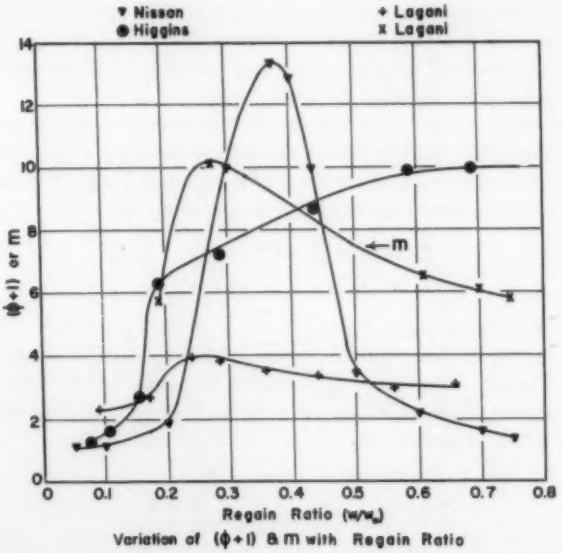

Fig. 16. Variation of the order of reaction with regain ratios.

and formation should be studied by the ordinary methods available in physical chemistry.

Such studies were described in the second part of reference 14. It was found that both the breakdown in E due to water absorption and that due to bond breaking under conditions of stress relaxation led to a high-order reaction in which cooperative phenomena between up to 12 OH----H bonds manifested themselves. Similar work by Lagani[20] has added further information to this question. In Figure 16, the results of work by Lagani are compared with previous work by Nissan and with an analysis of some of Higgins' results. The abscissa is the ratio of the regain W (g. water/g. solid) to the regain W_0 which would give each OH one molecule of water (i.e., 0.33). The ordinate is $\phi + 1$), i.e., the number of OH----H broken by one molecule of water as calculated from the drop in E with humidity and of m, the order of reaction in stress relaxation by bond breaking (Nissan[14]), and from creep studies. It is seen that up to a regain ratio of 0.15 (i.e., one third of the OH groups in the amorphous portion being

satisfied) the reaction corresponds to one OH group being broken at a time. When this value is exceeded, however, the reaction becomes autocatalytic with an increasing number of OH groups participating in bond breaking at the same time.

From these studies it would follow that when a stress-strain curve is determined for paper, bonds should be breaking while the test is being carried out. Therefore, if E is calculated from different points on the curve of, say, Figure 13, by means of eq. (17),

$$\begin{aligned} E &= (f + Ku\sigma^2)/\sigma \\ &= (f + 1.1 \times 10^{12} u\sigma^2)/\sigma \end{aligned} \tag{17}$$

E should decrease with time. Since $E = 7.0 \times 10^2 n^{1/3}$, then the change in E with time should be predictable from relaxation or creep tests. Thus, if from these latter tests the order of the reaction, m, is determined, then a plot of log n vs log θ (θ = time) should give a slope of $(-\beta)$ where

$$\beta = 1/(m - 1)$$

$$E_{\theta 2}/E_{\theta 1} = (n_{\theta 2}/n_{\theta 1})^{1/3} \tag{18}$$

and since

$$(n_{\theta 2}/n_{\theta 1}) = (\theta_1/\theta_2)^{\beta} \tag{19}$$

$$\begin{aligned} E_{\theta 2} &= E_{\theta 1}(\theta_1/\theta_2)^{\beta/3} \\ &= E_{\theta 1}(\theta_1/\theta_2)^{1/3(m-1)} \\ &= E_{\theta 1}(\theta_1/\theta_2)^{1/15} \end{aligned} \tag{20}$$

if $m = 6$. In Figure 17 the values of E vs. time are calculated by means of eq. (17) from stress-strain curves for paper in the machine direction. It is seen that at first E increases. This is unaccounted for by the theory and is believed to be due to the so-called "mechanical conditioning" which paper is known to show during rheological tests. This phenomenon may be due to breaking of bonds in which fibers or fibrils in a bent condition are involved. However, once the maximum value of E is reached, presumably when all "conditioning" is complete, it is seen that E falls according to the behavior predicted from the kinetics of bond breaking under creep and relaxation. The significant point of this example is that in time-dependent phenomena E itself increases or decreases rather than the parameters of an arbitrary "viscous" or "plastic" dashpot—i.e., a difference emerges

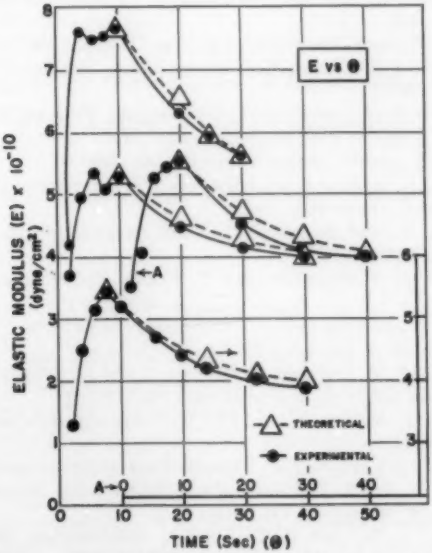

Fig. 17. The change of E with time during testing.

between a unified treatment by this method and a fragmentary treatment by means of mechanical models.

Conclusion

It is hoped that the above discussion has demonstrated that the rheology of paper offers rewarding work to those interested in applying mathematics, physics, physical chemistry, or engineering to the study of rheological problems. It is also our hope that a case has been made for an approach to rheological problems based on molecular and thermodynamic parameters which are related to the real structure of the material.

References

1. Nissan A. H., *Discussions Faraday Soc.* **No. 11,** 18 (1951).

2. Mason, S. G., *Tappi*, **37,** 494 (1954); S. G. Mason and R. St. J. Manley, *Proc. Roy. Soc.*, **A238,** 117 (1956).

3. Forgacs, O. L., A. A. Robertson, and S. G. Mason, *Fundamentals of Paper-*

making Fibers, British Paper and Board Making Association of Great Britain and Ireland, 1958, p. 447.

4. Daily, J. W., and G. Bugliarello, *Ind. Eng. Chem.*, **51**, 887 (1959).

5. Mardon, J., A. B. Truman, G. O'Blenes, and K. Meadley, *Pulp Paper Mag. Can.*, **59**, 135 (1958).

6. Howe, B. I., R. G. Lepine, and I. R. A. Gregory, *idem*, **60**, T-99 (1959).

7. Gavelin, G., *Svensk Papperstidn.*, **61**, 282 (1958).

8. Lyne, L. M., and W. Gallay, *Tappi*, **37**, 581 (1954).

9. Rance, H. F., in *Mechanical Properties of Wood and Paper*, R. Meredith, ed., North Holland, Amsterdam, 1953.

10. Steenberg, B., and B. Ivarsson, *Svensk Papperstidn.*, **50**, 127, 346. 419 (1947); *ibid.*, **51**, 383 (1948).

11. Halsey, G., H. J. White, Jr., and H. Eyring, *Textile Research J.*, **15**, 295 (1945).

12. Rance, H. F., in Some Recent Developments in Rheology, V. G. Harrison, ed., United Trade Press, London, 1950.

13. Andersson, O., B. Ivarsson, A. H. Nissan, and B. Steenberg, *Proc. Tech. Sect. Paper Makers' Assoc. G. Brit. & Ireland*, **30**, 43 (1949).

14. Nissan, A. H., *Nature*, **175**, 424 (1955); *Trans. Faraday Soc.*, **53**, 700, 709 (1957); **55**, 2048 (1959).

15. Pauling, L., *The Nature of the Chemical Bond*, Cornell Univ. Press, 1940.

16. Grunberg, L., and A. H. Nissan, *Trans. Faraday Soc.*, **45**, 125 (1949).

17. Nissan, A. H., *Tappi*, **41**, 131 (1958).

18. McKenzie, A. W., and H. G. Higgins, *Holzforschung*, **10**, 150 (1956); *Australian J. Appl. Sci.*, **6**, 208 (1955).

19. Higgins, H. G., A. W. McKenzie, and K. J. Harrington, *Tappi*, **41**, 193 (1958).

20. Lagani, A., Jr., M.S. Thesis, Rensselaer Polytechnic Institute, 1959.

Synopsis

A brief review of paper making indicates that rheology is an important factor at many points. The most significant are (*1*) rheology of fiber suspensions, (*2*) rheology of wet webs of fibers with 1:4 to 1:2 solid to water ratios, and (*3*) rheology of air-dry paper in use. The first two subjects are briefly reviewed. Attempts to represent paper behavior in terms of mechanical models of springs and dashpots are summarized and reasons for their rejection advanced. Instead, support is given to interpretations based on molecular and thermodynamic parameters as a basis for a theory of the rheological behavior of hydrogen-bonded solids. Predictions of the theory appear to be confirmed not only by paper but also by ice, cellulose sheets, nylon and other hydrogen-bonded materials. Attempts are made to explain by means of this theory the influence of water, chemical modification of the fibers, and other factors on the rheological constants of paper, and to account for its time-dependent behavior. The essential contribution of the theory is that it relates the variations in behavior to an important parameter, n, the number of hydrogen-bonds per unit volume of material. Thus, changes in rheological behavior reflect changes in n; these changes can be treated by methods of chemical kinetics.

TRANSACTIONS OF THE SOCIETY OF RHEOLOGY IV, 233–263 (1960)

Stress Analysis for Linear Viscoelastic Materials with Temperature Variation*

L. W. MORLAND and E. H. LEE, *Brown University, Providence, Rhode Island*

1. Introduction

The equilibrium problem of stress analysis in linear viscoelastic materials under homogeneous temperature conditions is now well developed, and a review is presented in Section 2. This paper is an attempt to extend this treatment to linear viscoelastic bodies under nonhomogeneous temperature fields, such as that resulting from the solution of the normal heat conduction problem in the absence of thermodynamic coupling. The analysis is particularized to a class of materials called "thermorheologically simple" which exhibit for constant change of temperature, a pure shift in the creep function, relaxation modulus, and other characteristic functions of the material, when plotted against the logarithm of time.

For materials of this type, and a given temperature field, a "reduced" or "pseudo" time can be defined for the system, in general a function of both time and space variables, for which the viscoelastic law is the same as for constant temperature in terms of real time. Unfortunately the equilibrium and compatibility conditions are changed in form, and the usual character of the elasticity equations is lost. Expressing the viscoelastic law in terms of the real time variable gives either differential operators with nonconstant coefficients, or integral operators whose kernels have functional arguments; in both cases there appears to be no general method of solution of the corresponding stress analysis equations.

In an attempt to assess the significance for stress analysis of this "shift" with change in temperature, more simplifications are made to

* Sponsored under a Department of Defense Contract, NOrd 18594, between the Bureau of Ordnance, Navy Department, and Brown University.

enable specific examples to be solved by standard methods. In particular the plane strain problem with cylindrical symmetry is treated. This requires the assumptions of incompressibility and consequently the absence of the usual thermal stresses arising from inhomogeneous thermal expansion, and steady state temperature conditions. The case is analyzed of the hollow cylinder under internal pressure, with no external support, and with reinforcement by an elastic shell, under a steady state temperature field due to a constant temperature difference across the cylinder. Exact solutions are obtained for the Kelvin model, for which the equations can be integrated directly, but for the Maxwell model and the general finite model an approximation scheme is introduced as regards the temperature field in order that the resulting Laplace transform solutions can be inverted. Asymptotic behavior at small and large times can be examined without inversion of the complete expressions, and lead directly to comparisons between the Kelvin and Maxwell material behavior.

Using a formula deduced from measurements on polyisobutylene which gives a variation in rate of creep by a factor 3 for the 30°K. change in temperature taken across the cylinder, tangential stress on the inner boundary is found to vary by a factor of more than 2 during a period of roughly twice the material's retardation time, in which the steady state solution is almost attained. The corresponding stress distribution for uniform temperature does not vary with time. It is seen then that moderate temperature changes can cause large differences in the stresses as calculated on uniform temperature theory, and should be considered in design problems where permissible stresses are limited.

2. Uniform Temperature Theory

As a preliminary to a discussion of stress analysis for nonhomogeneous temperature fields, it will be useful to outline the corresponding uniform temperature theory for linear viscoelastic materials. A review of this field has been given by Lee.[5] The scope of this paper is confined to quasi-static analysis with the hypothesis of infinitesimal deformation for linear viscoelastic materials which are both homogeneous and isotropic with respect to mechanical response.

The constitutive laws may be expressed in alternate forms. If the material can be represented by finite models, these become

$$P_1(D)s_{ij} = Q_1(D)e_{ij} \tag{2.1}$$

$$P_2(D)o_{ii} = Q_2(D)\epsilon_{ii} \tag{2.2}$$

where σ_{12}, ϵ_{12} are the stress and strain tensors, and s_{ij}, e_{ii}, the deviatoric components given by

$$\begin{aligned} s_{ij} &= \sigma_{ij} - 1/3\sigma_{kk}\delta_{ij} \\ e_{ij} &= \epsilon_{ij} - 1/3\epsilon_{kk}\delta_{ij} \end{aligned} \tag{2.3}$$

Thus eq. (2.1) governs shear response, and eq. (2.2) the hydrostatic behavior. The operators $P_m(D)$, $Q_m(D)$ $(m = 1, 2)$ have the general form

$$P_m(D) = \sum_{n=0}^{N_m} p_m^{(n)} D^n \tag{2.4}$$

where $D = (\partial/\partial t)$ is the partial derivative with respect to time for a fixed particle with space coordinates $(x_1, x_2, x_3) = x$, $D^n = \partial^n/\partial t^n$, and the $p_m^{(n)}$ are constants. The operators are thus finite polynomials in D. For an elastic medium, these operators are just constants, which can be represented by

$$P_1(D) = 1,\ Q_1(D) = 2G;\ P_2(D) = 1,\ Q_2(D) = 3K \tag{2.5}$$

where G and K are the shear and bulk moduli, respectively.

A more general representation is in terms of a relaxation modulus $G_m(t)$, or a creep function $J_m(t)$, which denote response to a unit applied strain and a unit applied stress, respectively, the $m = 1,2$ again refers to shear and hydrostatic parts. The law takes the form of a hereditary or Duhamel integral, formed by considering the stress or strain built up of increments applied at successive times t', thus

$$s_{ij}(x,t) = \int_0^t G_1(t - t') \frac{\partial e_{ij}(x,t')}{\partial t'} dt' \tag{2.6}$$

or

$$e_{ij}(x,t) = \int_0^t J_1(t - t') \frac{\partial s_{ij}(x,t')}{\partial t'} dt' \tag{2.7}$$

where stress and strain are taken as uniform zero until $t = 0$, and similarly for the hydrostatic relation. A linear differential viscoelastic law has an equivalent formulation by integral operators.

With reference to rectangular Cartesian coordinates x_i, neglecting the inertia term for quasi-static motion, the equilibrium equations become

$$\left.\frac{\partial \sigma_{ij}}{\partial x_j}\right|_t = 0 \tag{2.8}$$

where body forces are assumed zero. The field equations (2.1), (2.2), or (2.6), or (2.7), and (2.8), together with the compatibility conditions, must hold throughout the body, V. Boundary conditions may be in the form of prescribed surface tractions

$$\sigma_{ij} n_j = T_i \text{ on } B \tag{2.9}$$

where n_j is the unit outward normal to the boundary B, or prescribed displacement vector u_i on B, or some suitable combination. It can be assumed that the body is initially undisturbed, so that until $t = 0$, the stress, strain, and all their time derivatives are uniformly zero. Although the inertia term is neglected, changes with time occur through the viscoelastic laws, and it is therefore possible that essential difficulties may arise if surface regions over which particular boundary conditions are prescribed, or the body volume, vary with time, apart from the infinitesimal changes within the theory. Unlike the quasi-static elasticity problem which depends only on the instantaneous configuration and boundary values, for viscoelasticity the whole history of the process influences the distributions at a given time.

For the case of nonchanging volume and surface regions over which particular boundary conditions are prescribed, except for the infinitesimal displacements, the time dependence of the system of equations may be removed by application of the Laplace transform (for example, see Carslaw and Jaeger[1]). Thus, denoting transforms by a bar over the function, and the transform parameter by s, the system becomes

$$\begin{aligned} P_1(s)\bar{s}_{ij} &= Q_1(s)\bar{e}_{ij} \\ P_2(s)\bar{\sigma}_{ii} &= Q_2(s)\bar{\epsilon}_{ii} \end{aligned} \tag{2.10a}$$

or, as an example of the integral law,

$$\begin{aligned} \bar{s}_{ij} &= \bar{G}_1(s)s\bar{e}_{ij} \\ \bar{\sigma}_{ii} &= \bar{G}_2(s)s\bar{\epsilon}_{ii} \end{aligned} \tag{2.10b}$$

$$\left.\frac{\partial \bar{\sigma}_{ij}}{\partial x_j}\right|_s = 0 \tag{2.11}$$

and

$$\bar{\sigma}_{ij} n_j = \bar{T}_i(x, s) \text{ on } B \tag{2.12}$$

or alternatively prescribed displacements $\bar{u}_i(x, s)$ on B, or some combination, together with the compatibility conditions. This general procedure, given by Lee,[4] reduces the system to an associated elasticity problem which involves s as a parameter. Inversion of the solution to this elastic problem determines the viscoelastic solution.

3. The Influence of Temperature on Viscoelastic Behavior

In Section 2, the field equations for the stress analysis problem for a linear viscoelastic material were given. Of further interest is the same problem for a body subjected to a nonhomogeneous temperature field—the thermal viscoelastic problem. As in classical elasticity the stress-strain relations will contain terms due to thermal expansion but also important is the effect of temperature on the creep rate and viscoelastic behavior. In general, increase of temperature increases the rate of creep, that is, the rate of change of the creep function and relaxation modulus with time. Among the amorphous high polymers which satisfy approximately the linear viscoelastic laws at uniform temperature are a group which exhibit approximately a particular simple property with change of temperature. This is a translational shift—no change in shape—of the relaxation modulus plotted against the logarithm of time at different uniform temperature, which leads to an equivalence relation between temperature and ln t; its use to extend the time scale of experimental data was first proposed by Leaderman, reviewed in Chapter 1 of *Rheology*, Volume II, edited by Eirich.[2] Such a material has been classified as "thermorheologically simple" by Schwarzl and Staverman,[7] who show that all the characteristic functions of the material must obey the same property. To express this equivalence relation analytically, let $E_T(\ln t)$ be the relaxation modulus as a function of ln t at uniform temperature T, then

$$E_T(\ln t) = E_{T_0}[\ln t + f(T)] \tag{3.1}$$

where $f(T)$ is measured relative to some arbitrary temperature T_0. Since the rate of change is increased with increase of temperature,

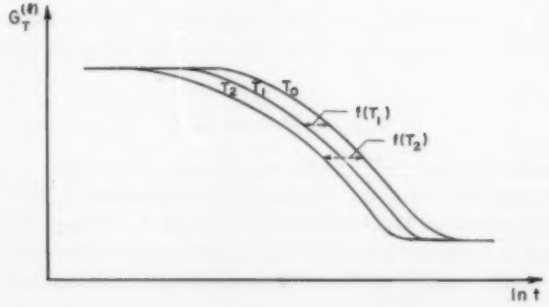

Fig. 1. Influence of change in temperature on the relaxation modulus (the thermorheologically simple material behavior).

the modulus curve will shift towards shorter times with increase of temperature, as illustrated in Figure 1, and $f(T)$ is a positive increasing function for $T > T_0$. If $G_T(t)$ denotes the relaxation modulus as a function of time at uniform temperature T, so that $G_T(t) = E_T(\ln t)$, and a shift factor $a(T)$ is defined by

$$a(T) = \exp\{f(T)\} \tag{3.2}$$

then

$$G_T(t) = G_{T_0}[t \cdot a(T)] \tag{3.3}$$

or, defining a "reduced time" ξ by

$$\xi = t \cdot a(T) \tag{3.4}$$

$$G_T(t) = G_{T_0}(\xi) \tag{3.5}$$

For an increase of temperature above T_0, ξ is greater than t, since by eq. (3.2), $a(T) > 1$. The relaxation modulus (and the other characteristic functions) at an arbitrary uniform temperature is thus expressed by the base temperature behavior related to a new time scale which depends on that temperature. Thus, expressing the stress and strain as functions of x and pseudo-time, the viscoelastic law becomes

$$\sigma(x,\xi) = \int_0^\xi G(\xi - \xi') \frac{\partial \epsilon(x, \xi')}{d\xi'} \partial\xi' \tag{3.6}$$

or, for differential operators,

$$P(d)\sigma = Q(d)\epsilon \tag{3.7}$$

where $d = \partial/\partial\xi$ is the partial derivative with respect to the pseudo-time for a fixed particle x, and $G(t)$ and the polynomials $P(D)$, $Q(D)$, are the corresponding viscoelastic functions at the chosen base temperature T_0. The differential law, (3.7), may be derived rigorously from the integral law (3.6) by taking Laplace transforms with respect to ξ giving, with p as parameter,

$$\bar{\sigma}(x,p) = p\bar{G}(p)\bar{\epsilon}(x,p) \tag{3.8}$$

but $p\bar{G}(p) = Q(p)/P(p)$—see eq. (2.10)—so that eq. (3.8) comprises the transform of eq. (3.7).

To account for the dependence of the equilibrium modulus on temperature, a slightly different reduction scheme was proposed by Ferry and by Tobolsky; namely, that $(1/\rho T)E_T(\ln t)$ was the function which exhibited simple shift, ρ being the slightly temperature dependent density. It is not settled which relation gives better agreement with experimental data. A full account of the reduction transformation is presented by Staverman and Schwarzl in Chapter 1 of *Die Physik Der Hochpolymeren*, edited by Stuart.[9]

The preceding paragraphs described the equivalence relation for the body held at different uniform temperatures, and this must now be extended to cover the case of a general temperature field $T(x, t)$. First consider the temperature dependent only on the space coordinates, $T(x)$, a steady state temperature field, then assuming that the shift law applies to each particle independently, the relation (3.5) holds for each particle with a pseudo-time which depends on its position. The stress-strain law again has the form of eq. (3.6) or eq. (3.7) where now $\xi = ta[T(x)]$, so it should be noted that $\sigma(x,\xi)$, and similarly for $\epsilon(x, \xi)$, means the mapping of the function $\sigma(x, t)$ from the (x,t) plane into the (x,ξ) plane, and not the same function with ξ replacing t.

The uniform temperature results show that at a given temperature T the time taken for a particular change in the relaxation modulus is equal to the time taken for the same change in the relaxation modulus at temperature T_0, divided by the factor $a(T)$, which is identical for all sections on the relaxation curve. That is, if the time taken for $G_{T_0}(t)$ to decrease from some value G_1 to some value G_2 is δt, then the

time taken for $G_T(t)$ to decrease from G_1 to G_2 is $\delta t/a(T)$. This implies that the molecular processes associated with the particular relaxation behavior (shear or dilatation) are accelerated by a constant factor $a(T)$ at a higher temperature. If now a temperature $T(x,t)$ is considered, each particle has a temperature varying with time, and the assumption is made that these molecular processes, and hence the rate of change of the relaxation modulus at each level, are accelerated by the same factor $a(T)$, where T is the current temperature, independent of temperature history. Letting $G^*(t)$ denote the relaxation modulus for a temperature field $T(x,t)$, accordingly dependent on the particle position, and deducing from the shift property that $G^*(t)$ decreases monotonically from the instantaneous modulus to the static modulus which are independent of temperature, then there is some mapping of the time coordinate, which depends also on the particle position, $\xi = \xi(x,t)$, such that

$$G^*(t) = G_{T_0}(\xi) \tag{3.9}$$

After a further increment of time δt, this gives $G^*(t + \delta t) = G_{T_0}(\xi + \delta\xi)$ where by the above assumption, the increment $\delta\xi$ satisfies

$$\delta\xi = a[T(x,t)]\delta t \tag{3.10}$$

and hence, since $G^*(0) = G_{T_0}(0)$, and therefore $\xi(x,0) = 0$,

$$\xi(x,t) = \int_0^t a[T(x,t')]dt' \tag{3.11}$$

Finally, consider the response under the same temperature field to a unit applied strain at some instant t_0, and let $G(t - t_0)$ denote the relaxation modulus, then there will be some $\zeta(x,t)$ such that $\zeta(x, t_0) = 0$ and

$$G(t - t_0) = G_{T_0}(\zeta) \tag{3.12}$$

where

$$\partial\zeta = a[T(x, t)]\delta t \tag{3.13}$$

so that

$$\begin{aligned}\zeta(x,t) &= \int_{t_0}^t a[T(x, t')]dt' \\ &= \xi(x,t) - \xi(x,t_0)\end{aligned} \tag{3.14}$$

That is, putting $\xi(x,t_0) = \xi_0$,

$$G(t - t_0) = G_{T_0}(\xi - \xi_0) \tag{3.15}$$

which defines the equivalence relation for the response starting at any instant, in terms of a fixed pseudo-time scale given by eq. (3.11). The corresponding viscoelastic law is again eq. (3.6) or eq. (3.7).

Now the stress analysis problem involves two independent viscoelastic laws, one governing shear behavior and the other hydrostatic behavior. In general the shift factor could be different for each of these, and consequently two reduced time scales would result. In the discussion presented below it is assumed that viscoelastic characteristics are limited to shear response, the dilatation being elastic, so that time effects arise only for shear response and only one reduced time scale occurs.

4. Field Equations for a Nonhomogeneous Temperature Field

In addition to prescribed mechanical boundary conditions on the body, the thermal stress analysis problem involves prescribed temperature or heat flux at each boundary. The resulting temperature field, $T(x, t)$, throughout the body, is assumed to satisfy the normal heat conduction equation in the absence of thermodynamic coupling,

$$\xi \nabla^2 T = \partial T/\partial t \tag{4.1}$$

where ξ is the constant thermal diffusivity, subject to the thermal boundary and initial conditions. Such an analysis is likely to be satisfactory in the present case, for the limitation to small strains prevents the dissipation of appreciable mechanical energy to constitute a distributed heat source within the body.

From the previous section, the stress-strain laws in the presence of a temperature field are

$$s_{ij}(x,\xi) = \int_0^\xi G(\xi - \xi') \frac{\partial e_{ij}(x,t')}{d\xi'} \partial\xi' \tag{4.2}$$

$$P(d)s_{ij}(x,\xi) = Q(d)e_{ij}(x,\xi) \tag{4.3}$$

and

$$\sigma_{ii}(x,\xi) = 3K\{\epsilon_{ii}(x,\xi) - 3\alpha[T(x,\xi) - T_0]\} \tag{4.4}$$

where $\xi(x,t)$ is given by eq (3.11), and

$$d^n = \left.\frac{\partial^n}{\partial \xi^n}\right|_x \tag{4.5}$$

$G(t)$, $P(D)$, $Q(D)$, are the viscoelastic shear functions for uniform temperature T_0, K is the constant bulk modulus for elastic dilatation, and α is the coefficient of linear thermal expansion, assumed constant in the above. For a temperature dependent coefficient of expansion, $\alpha(T)$, the expression $3\alpha(T - T_0)$ must be replaced by

$$\int_{T_0}^{T} 3\alpha(T')dT' \tag{4.6}$$

but this can be written as $3\alpha_0[T^*(T) - T_0]$, so that eq. (4.4) has the same form in terms of a pseudo-temperature field $T^*(x,\xi)$, α_0 being a constant.

The problem is now to solve the equilibrium equation

$$\left.\frac{\partial \sigma_{ij}}{\partial x_j}\right|_t = 0 \tag{4.7}$$

together with the laws (4.2) or (4.3) and (4.4), subject to the compatibility conditions and prescribed mechanical boundary conditions. It should be noted that the viscoelastic law (4.2) is expressed in (x,ξ) coordinates, while the equilibrium equation (4.7)—and the normal form of the expressions for strain components and the compatibility conditions—are expressed in (x,t) coordinates. Uniformity can be obtained by rewriting of (4.7) as

$$\left.\frac{\partial \sigma_{ij}}{\partial x_j}\right|_\xi + \left.\frac{\partial \sigma_{ij}}{\partial \xi}\right|_x \left(\frac{\partial \xi}{\partial x_j}\right)_t = 0 \tag{4.8}$$

where $(\partial\xi/\partial x_j)_t$ is a known function of (x,t), and hence of (x,ξ) because of eq. (3.11). But eq. (4.8) no longer has the form of the usual elasticity equilibrium equation. Alternatively, eqs. (4.2) and (4.3) can be expressed in terms of the (x,t) coordinates, using the relations (3.11) and

$$\left.\frac{\partial}{\partial \xi}\right|_{x_i} = \left.\frac{\partial}{\partial t}\right|_x \Big/ a[T(x,t)] \tag{4.9}$$

The differential viscoelastic law now has coefficients which are functions of both space and time coordinates, while in integral form the law becomes

$$s_{ij}(x,t) = \int_0^t G(\xi - \xi') \frac{\partial e_{ij}(x,t)}{dt'} \partial t' \tag{4.10}$$

where the argument $(\xi - \xi')$ is given by eq. (3.11), and is in general a complicated function of (x,t).

In the (x,ξ) plane, it is not possible to remove the ξ dependence by taking Laplace transforms because of the form of eq. (4.8), since $(\partial\xi/\partial x_j)_t$ is a function of ξ; and in the (x,t) plane, the time dependence cannot be removed by tranforms because of the viscoelastic law with nonconstant coefficients, or integral kernel with nonlinear time argument. It is the dependence of the temperature, and hence the shift factor, on time which causes this difficulty. The transform reduction to an associated thermoelastic problem for a linear viscoelastic material with temperature independent parameters has been described by Sternberg,[8] but here stresses due to thermal expansion only are obtained, in the absence of temperature effects on viscoelastic behavior. It is the importance of the latter effect we wish to investigate. Also, it is not meaningful to consider the space distribution of the corresponding elastic solution and to apply the differential viscoelastic law to this form, as suggested by Radok[6] for the isothermal case, since validity requires interchange of the space differential operators representing the equilibrium and compatibility conditions, and the time differential viscoelastic law, and now the latter has coefficients which are functions of the space variables. It is thus seen that there is no longer an associated thermoelastic problem to the thermal viscoelastic problem when temperature dependent material parameters are considered. Although in general there appears to be no comprehensive method of solving this system of equations, the thermal stress field during transient temperature conditions has recently been obtained in two particular cases, for a plate and for polar symmetry, by Muki and Sternberg (to be published).

The problem can be simplified by considering steady state temperature conditions, so that the temperature, and consequently the shift factor, are function of the space variables only. The initial conditions for the boundary value problem are now given by the thermal stress-strain field which develops during the transient temperature

period. Since the system of equations is linear, the stress field can be expressed as the sum of two parts, thus

$$\sigma_{ij}(x,t) = \hat{\sigma}_{ij}(x,t) + \sigma_{ij}^{*}(x,t) \tag{4.11}$$

where σ_{ij}^{*} is the thermal stress field which satisfies the same system for zero surface tractions, and $\hat{\sigma}_{ij}(x,t)$ is the mechanical stress field which satisfies the equations in the absence of the thermal expansion terms, for the given surface tractions. Thus, until the boundary loads are applied, at $t = 0$ say, $\hat{\sigma}_{ij}(x,t) = 0$. $\sigma_{ij}^{*}(x,t)$ is independent of the applied loads, and if it is assumed that during the time taken for the temperature field to become steady (strictly, only in an approximate sense), the thermal stress field $\sigma_{ij}^{*}(x,t)$ also reach steady state, at $t = 0$, then for $t \geq 0$

$$\sigma_{ij}(x,t) = \hat{\sigma}_{ij}(x,t) + \sigma_{ij}^{*}(x,0) \tag{4.12}$$

The thermal stress part, $\sigma_{ij}^{*}(x,0)$, is now the solution of the thermoelastic problem involving the steady state value of the viscoelastic shear modulus, and consequently independent of the shift factor. So for steady-state temperature analysis, the effects of the shift law are restricted to the mechanical part $\hat{\sigma}_{ij}(x,t)$. Since the coefficients in the viscoelastic differential operators are now time independent, and, alternatively, the integral kernel has argument linear in time, the time dependence can be removed by taking Laplace transforms, but the resulting system does not represent a classical elasticity problem since the coefficients in the transformed stress-strain laws are still functions of the space variables. The system of equations therefore requires independent solution which in general presents new difficulties.

By making the further assumption and simplification of incompressibility, the equations can in some cases be solved, and an example is given in the next section. This assumption should provide a satisfactory representation in cases where the shear strains dominate the deformation field. It must be noted that it implies the vanishing of the coefficient of thermal expansion, and hence an absence of strict thermal stresses. Sternberg[8] points out that solutions to thermal stress problems for incompressible media are physically meaningful, in an approximate sense, only if the hydrostatic component of the ensuing stress field is small compared to its derivatoric components. Hilton[3] treats the case of a hollow Kelvin cylinder under

steady state temperature conditions on the assumption of mechanical incompressibility but including the thermal expansion term, while neglecting the development of thermal stresses during the transient temperature period. The significance of this combination of assumptions is by no means clear, and it seems that the consistent neglect of all dilatation should be more satisfactory, and leads to a simpler analysis.

Having seen that the general problem does not yield to analysis by presently available methods, we shall limit our examination to the case of an incompressible material under steady state temperature conditions. The shift factor is now time independent, and thermal stresses which would be obtained in a compressible material during the transient temperature stage do not arise. This results in a mechanical stress problem dependent only on temperature through its effects on the viscoelastic response, and this latter dependence in the stress analysis, isolated from the occurrence of thermal stresses, is examined below.

5. Incompressible Cylinder under Steady State Temperature Conditions

Recall briefly that the stress analysis problem is now limited to an incompressible linear viscoelastic material which is thermorheologically simple in shear, for a steady state temperature field, and on the hypothesis of infinitesimal quasistatic displacement.

To illustrate a method of solution for various viscoelastic models, and to evaluate the effects of an inhomogeneous temperature field in a particular case, plane strain with cylindrical symmetry is studied. The case of a hollow infinite cylinder under internal pressure, uniform over the boundary, and under a steady state temperature field dependent only on the radial coordinate, is taken. Symmetry demands dependence of the stresses and strains on the radial space coordinate only, defined in dimensionless form by $x = r/a$, where $r = a$ is the inner boundary of the cylinder and $r = b$ the outer boundary. The field equations are expressed in terms of the radial stress σ_x, the tangential stress σ_θ, and longitudinal stress σ_z; a radial strain ϵ_r, and a tangential strain ϵ_θ; all other components being zero. The equilibrium equations reduce to

$$\left.\frac{\partial \sigma_x}{\partial x}\right|_t + \frac{\sigma_x - \sigma_\theta}{x} = 0 \tag{5.1}$$

The stress-strain law becomes

$$P(d)\{\sigma_z - \sigma_\theta\} = Q(d)\{\epsilon_z - \epsilon_\theta\} \tag{5.2}$$

or

$$\sigma_z - \sigma_\theta = \int_0^\xi G(\xi - \xi') \frac{\partial}{\partial \xi'} \{\epsilon_z - \epsilon_\theta\}_x d\xi' \tag{5.3}$$

where $d = \left.\frac{\partial}{\partial \xi}\right|_x$, and

$$\xi = \int_0^t a[T(x)]dt' = a[T(x)]t \tag{5.4}$$

For convenience, define the shift factor for a given temperature field by

$$a[T(x)] = \lambda(x) \tag{5.5}$$

so now

$$\xi = \lambda(x)t; \quad \left.\frac{\partial^n}{\partial \xi^n}\right|_x = \left(\frac{1}{\lambda(x)}\right)^n \left.\frac{\partial^n}{\partial t^n}\right|_x \tag{5.6}$$

Note that $G(\xi)$ in eq. (5.3) is twice the usual relaxation modulus because of the manner in which the shear strain is represented: $(\epsilon_z - \epsilon_\theta)$.

Incompressibility and zero longitudinal strain demands that

$$\epsilon_z + \epsilon_\theta = 0 \tag{5.7}$$

and this determines the component of the strain deviator in the z direction to be zero, so that

$$\sigma_z = {}^1/_2(\sigma_r + \sigma_\theta) \tag{5.8}$$

follows from the viscoelastic stress strain relation (4.10). The compatibility condition obtained by eliminating the radial displacement from the expressions for ϵ_r and ϵ_θ is:

$$\left.\frac{\partial \epsilon_\theta}{\partial x}\right|_t = \frac{\epsilon_r - \epsilon_\theta}{x} \tag{5.9}$$

Immediately, ϵ_r can be eliminated between eqs. (5.7) and (5.9), and the resulting equation integrated, giving:

$$\left.\frac{\partial \epsilon_\theta}{\partial x}\right|_t = -\frac{2\epsilon_\theta}{x}$$

$$\epsilon_\theta = \frac{f(t)}{x^2}, \quad \epsilon_x = -\frac{f(t)}{x^2} \tag{5.10}$$

where $f(t)$ is an arbitrary function of time to be determined by initial and boundary conditions, and depending on the particular viscoelastic law used.

The inner boundary condition, on $x = 1$, is given in terms of the prescribed inner pressure:

$$\sigma_x = -\Pi(t) \tag{5.11}$$

which is zero until $t = 0$. As discussed above, it is assumed that the steady state temperature has been attained before load application. For the outer boundary condition, on $x = b/a = x_2$, two cases will be considered. The first is the unsupported cylinder, when the boundary condition is

$$\sigma_x = 0 \tag{5.12}$$

The second, treated by Woodward and Radok[11] for uniform temperature, is the cylinder reinforced by a thin cylindrical elastic shell. The required conditions across the interface are continuity of radial stress and circumferential strain; the tangential stress and radial strain will generally be discontinuous. For if $u(r)$ is the radial displacement field, then it is clear that u must be continuous across the interface, and hence $\epsilon_\theta = u/r$, but not necessarily $\epsilon_r = \partial u/\partial r$. The configuration is shown in Figure 2. The elastic shell is an unsup-

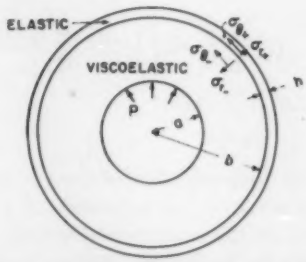

Fig. 2. Reinforced cylinder subjected to internal pressure.

ported cylinder under internal pressure $-\sigma_{x_1}$, the radial compressive stress on the outer boundary, x_2, of the viscoelastic cylinder, and so the stress field is the well known Lamé solution (for example, see Timoshenko and Goodier[10]). For the case we consider $h \ll b$, so that $(h/b)^2$ can be neglected. This gives, on $x = x_2$,

$$\epsilon_{\theta_2} = -\sigma_{x_2} \frac{1 + \nu_2}{E_2} \left\{1 + \frac{b}{h}(1 - \nu_2)\right\} \tag{5.13}$$

where E_2 and ν_2 are Young's modulus and Poisson's ratio, respectively, for the elastic material. Hence continuity of ϵ_θ across $x = x_2$, by eqs. (5.10) and (5.13), requires

$$\sigma_{x_1} = -\beta\epsilon_{\theta_2} = -(\beta/x_2^2)f(t) \tag{5.14}$$

where

$$\beta = E_2/(1 + \nu_2)\left\{1 + \frac{b}{h}(1 - \nu_2)\right\} \tag{5.15}$$

Since $b/h \gg 1$, and $\nu_2 \leqslant 1/2$, then $\beta \ll E_2$.

For a general material, the time dependence of the eqs. (5.1), (5.3), and (5.10) can be removed by taking Laplace transforms with respect to t. Denoting these by a bar over the corresponding function, with s as parameter, we get

$$\frac{\partial \bar{\sigma}_x}{\partial x} + \frac{\bar{\sigma}_x - \bar{\sigma}_\theta}{x} = 0 \tag{5.16}$$

$$\bar{\epsilon}_\theta = \frac{\bar{f}(s)}{x^2}, \quad \bar{\epsilon}_x = -\frac{\bar{f}(s)}{x^2} \tag{5.17}$$

$$\bar{\sigma}_x - \bar{\sigma}_\theta = \int_0^\infty e^{-st}\left[\int_0^\xi G(\xi - \xi')\frac{\partial}{\partial \xi'}\left\{-\frac{2f(t)}{x^2}\right\}_x d\xi'\right] dt$$

$$= -\frac{2s\bar{f}(s)\bar{G}[s/\lambda(x)]}{\lambda(x)x^2} \tag{5.18}$$

using eq. (5.6). Note that initial conditions in transform equations refer to $t = 0^-$ according to the approach of Carslaw and Jaeger (ref. 1, Chap. 11), and are therefore zero here since no loads are applied until $t = 0$, and there are no thermal stresses in accordance with the assumptions made. Equations (5.16) and (5.18) give

$$\frac{\partial \bar{\sigma}_x}{\partial x} = \frac{2s\bar{f}(s)\bar{G}[s/\lambda(x)]}{\lambda(x)x^3} \tag{5.19}$$

and integrating, and applying boundary condition (5.11) at $x = 1$

$$\bar{\sigma}_x[x, s] = -\bar{\Pi}(s) + 2s\bar{f}(s)\int_1^x \frac{\bar{G}[s/\lambda(x')]dx'}{\lambda(x')x'^3} \tag{5.20}$$

From eq. (5.18) the tangential stress is then given by

$$\bar{\sigma}_\theta(x, s) = \bar{\sigma}_x(x, s) + \frac{2s\bar{f}(s)\bar{G}[s/\lambda(x)]}{\lambda(x)x^2} \tag{5.21}$$

For convenience, define

$$I(x,s) = \int_1^x \frac{\bar{G}[s/\lambda(x')]dx'}{\lambda(x')x'^3} \tag{5.23}$$

For the unsupported cylinder, applying eq. (5.12) to eq. (5.20),

$$2s\bar{f}(s) = \bar{\Pi}(s)/I(x_2,s)$$

and hence

$$\bar{\sigma}_x(x,s) = -\bar{\Pi}(s)\left\{1 - \frac{I(x,s)}{I(x_2,s)}\right\} \tag{5.24}$$

and

$$\bar{\sigma}_\theta(x,s) = \bar{\Pi}(s)\left\{\frac{\bar{G}[s/\lambda(x)]}{\lambda(x)x^2 I(x,s)} + \frac{I(x,s)}{I(x_2,s)} - 1\right\} \tag{5.25}$$

For the reinforced cylinder, applying eq. (5.14) to eq. (5.20),

$$2s\bar{f}(s) = \bar{\Pi}(s)\Big/\left\{I(x_2,s) + \frac{\beta}{2sx_2^2}\right\} \tag{5.26}$$

and hence,

$$\bar{\sigma}_x(x,s) = -\bar{\Pi}(s)\left\{1 - \frac{I(x,s)}{I(x_2,s) + \beta/2sx_2^2}\right\} \tag{5.27}$$

and

$$\bar{\sigma}_\theta(x,s) = \bar{\Pi}(s)\left\{\frac{\bar{G}[s/\lambda(x)]/\lambda(x)x^2 + I(x,s)}{I(x_2,s) + \beta/2sx_2^2} - 1\right\} \tag{5.28}$$

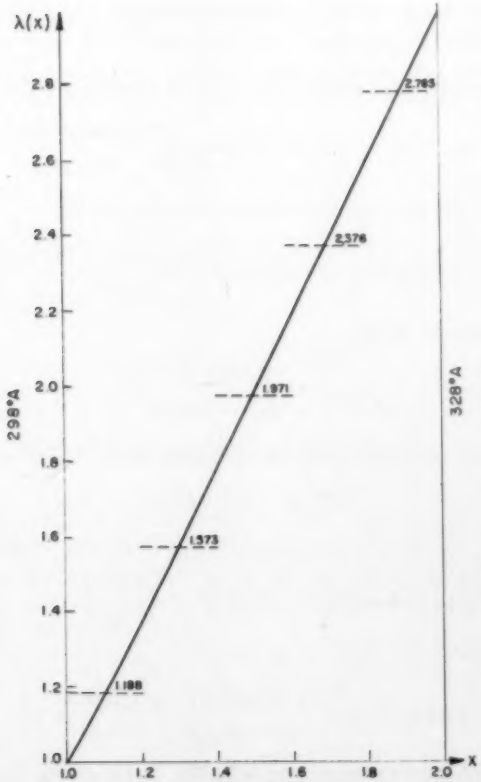

Fig. 3. Temperature shift factor across the cylinder as a function of the dimensionless radius.

It remains to invert the transforms obtained above for given viscoelastic materials and given temperature fields. For illustration we will choose a particular temperature field, and a particular value of x_2. First then, take $b = 2a$, so that

$$x_2 = 2 \tag{5.29}$$

The inner boundary, $x = 1$, is kept at the base temperature T_0, and the outer boundary $x = 2$, at a uniform temperature T_∞. The

steady state temperature distribution satisfying these conditions is

$$T(x) = T_0 + \frac{(T_1 - T_0) \ln x}{\ln x_2} \tag{5.30}$$

In particular, take $T_0 = 298°$K., and $T_1 = 328°$K., giving a difference of 30°K. across the cylinder; eq. (5.30) becomes

$$T(x) = 298 + 43.29 \ln x \tag{5.31}$$

For the shift function with respect to the base temperature 298°K., we adopt an expression for polyisobutylene given by Schwarzl and Staverman in Stuart,[9] namely

$$a(T) = \exp\left\{5.6 \times 10^5 \left(\frac{1}{298^2} - \frac{1}{T^2}\right)\right\} \tag{5.32}$$

Combining eqs. (5.31) and (5.32), the expresson for the shift factor, $\lambda(x)$, is found to be very complicated, but Figure 3 shows this relation to be in fact almost linear.

In the next section, the above problem of the determination of the stress distribution in a hollow cylinder under steady state temperature conditions with an increase in temperature of 30°K. from the inner to the outer boundary, subjected to an internal pressure, will be examined for various viscoelastic materials.

6. Methods of Solution for Various Viscoelastic Materials

The applied pressure on the inner surface will be taken as a step function at $t = 0$, so that

$$\Pi(t) = \Pi H(t); \qquad \bar{\Pi}(s) = \Pi/s \tag{6.1}$$

where Π is the constant pressure acting for $t > 0$, and $H(t)$ is the Heaviside function. Time dependence in the solutions must enter through the viscoelastic law since the pressure is maintained constant.

(a) *Kelvin Model*

This is the particular model for which only stress, and none of its derivatives, enters the viscoelastic law, and the equations can be integrated directly. The model is represented by the spring-dashpot configuration in Figure 4, and gives the shear stress-strain relation

$$\sigma_z - \sigma_\theta = G\left\{(\epsilon_z - \epsilon_\theta) + \tau \frac{\partial}{\partial \xi}(\epsilon_z - \epsilon_\theta)_z\right\} \tag{6.2}$$

where G, the spring constant, is the equilibrium modulus, τ the retardation time, and $\eta = \tau G$ the viscosity of the dashpot at temperature T_0. Note that G is twice the usual equilibrium shear modulus because of the form of the strain term in eq. (6.2). Using eqs. (5.6) and (5.10), eq. (6.2) becomes

$$\sigma_z - \sigma_\theta = -2G\left\{\frac{f(t)}{x^2} + \frac{\tau}{\lambda(x)}\frac{f'(t)}{x^2}\right\} \tag{6.3}$$

and combining with eq. (5.1),

$$\frac{\partial \sigma_z}{\partial x} = 2G\left\{\frac{f(t)}{x^3} + \frac{\tau f'(t)}{x^3\lambda(x)}\right\} \tag{6.4}$$

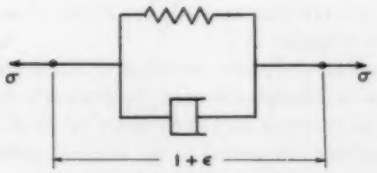

Fig. 4. The Kelvin model.

Integrating, and applying eq. (6.1) on $x = 1$,

$$\sigma_z(x,t) = -\Pi + 2G\int_1^x \left[\frac{f(t)}{x'^3} + \frac{\tau f'(t)}{x'^3\lambda(x')}\right] dx' \tag{6.5}$$

$f(t)$ must now be determined by the condition on $x = 2$, and the initial conditions at $t = 0_+$. Since the instantaneous strain for a Kelvin material subjected to any finite stress is zero, then $f(0) = 0$. For convenience, define

$$M(x) = \int_1^x \frac{dx'}{\lambda(x')x'^3} \tag{6.6}$$

Consider the unsupported cylinder, and apply eq. (5.12) to eq. (6.5), then

$$\Pi = 2G\{{}^3/_8 f(t) + \tau M(2) f'(t)\}$$

and integrating with the initial condition above,

$$f(t) = \frac{4\Pi}{3G}\left\{1 - e^{[-3/8M(2)](t/\tau)}\right\}, \qquad \geq 0 \tag{6.7}$$

Thus the tangential strain, ϵ_θ, is always positive and so an extension, and the radial strain, ϵ_x, is always a compression. Substituting eq. (6.7) into eq. (6.5),

$$\sigma_x(x,t) = -\Pi\left\{1 - \frac{4}{3}\left(1 - \frac{1}{x^2}\right) + \left[\frac{4}{3}\left(1 - \frac{1}{x^2}\right) - \frac{M(x)}{M(2)}\right] e^{-3/8M(2)](t/\tau)}\right\} \tag{6.8}$$

and by eq. (6.3),

$$\sigma_\theta(x,t) = \Pi\left\{\frac{4}{3}\left(1 + \frac{1}{x^2}\right) - 1 - \left[\frac{4}{3}\left(1 + \frac{1}{x^2}\right) - \frac{M(x)}{M(2)} - \frac{1}{x^2\lambda(x)M(2)}\right] e^{[-3/8M(2)](t/\tau)}\right\} \tag{6.9}$$

For comparison, the uniform temperature solution, given by $\lambda(x) \equiv 1$:

$$\begin{aligned} \sigma_x(x,t) &= -\Pi\left\{1 - \frac{4}{3}\left(1 - \frac{1}{x^2}\right)\right\} \\ \sigma_\theta(x,t) &= \Pi\left\{\frac{4}{3}\left(1 + \frac{1}{x^2}\right) - 1\right\} \end{aligned} \tag{6.10}$$

is just the time independent elastic solution for the same boundary conditions. Note from eqs. (6.8) and (6.9) that as $t \to \infty$, the stresses σ_x and σ_θ tend to the values given by eqs. (6.10); that is, the Kelvin model viscoelastic solution approaches the purely elastic solution as time increases. Further, in this, the hydrostatic component of stress is

$$1/3\sigma_{ii} = 1/2(\sigma_x + \sigma_\theta), = -1/3\Pi \tag{6.11}$$

which is uniform through the cylinder.

Now as $t \to 0_+$, by eqs. (6.8) and (6.9), the stresses approach the values

$$\sigma_r(x) = -\Pi \left\{1 - \frac{M(x)}{M(2)}\right\}$$
$$\sigma_\theta(x) = \Pi \left\{\frac{M(x)}{M(2)} + \frac{1}{x^2\lambda(x)M(2)} - 1\right\} \tag{6.12}$$

which represent the instantaneous response to the applied pressure. This is dependent on the space coordinate, and on the temperature field through $\lambda(x)$. An intuitive explanation of this behavior can be given with reference to the spring-dashpot model in Figure 4. The temperature-time shift concept implies that for the Kelvin model the spring constant, the equilibrium modulus, does not change with temperature, but that the viscosity decreases with increase in temperature to produce a shortening of the delay time. When the load is first

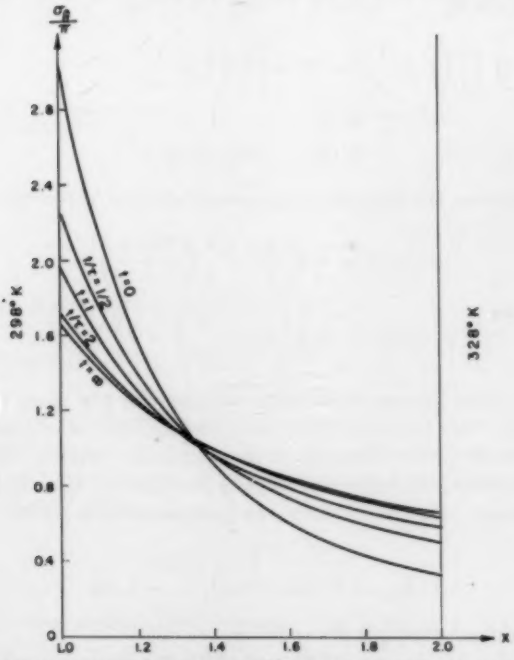

Fig. 5. Variation of circumferential stress distribution with time for heated cylinder of Kelvin material.

applied, the response is governed by the dashpot which starts to flow while the spring is virtually unstressed. This behavior is temperature dependent. After a long time under constant load, the spring in Figure 4 provides virtually the entire constraint, and because its modulus is independent of temperature, the solution yields the isothermal elastic stress distribution.

The stress field at several intermediate stages was calculated from the above formulas, and the corresponding tangential stress distributions, $\sigma_\theta(x)$, always tension, are plotted in Figure 5. There is a wide variation in values during the early stages, particularly on the inner boundary where the initial value is nearly twice the elastic limiting value, but after a period of twice the delay time of the material, the distribution is very close to the final one. The variation in the radial stress distribution, σ_x, is much smaller.

For the reinforced cylinder, applying eq. (5.14) to eq. (6.5),

$$\Pi = 2G\left\{\left(\frac{3}{8} + \frac{\beta}{8G}\right) f(t) + \tau M(2) f'(t)\right\} \tag{6.13}$$

which integrated, gives

$$f(t) = \frac{\Pi}{2G\gamma}\left\{1 - e^{-[\gamma/M(2)](t/\tau)}\right\} \tag{6.14}$$

where

$$\gamma = \frac{3}{8} + \frac{\beta}{8G} \tag{6.15}$$

From eqs. (6.5) and (6.3),

$$\begin{aligned}
\sigma_x(x,t) &= -\Pi\left\{1 - \frac{1}{2\gamma}\left(1 - \frac{1}{x^2}\right) + \left[\frac{1}{2\gamma}\left(1 - \frac{1}{x^2}\right)\right.\right. \\
&\qquad \left.\left. - \frac{M(x)}{M(2)}\right] e^{-[\gamma/M(2)](t/\tau)}\right\} \\
\sigma_\theta(x,t) &= \Pi\left\{\frac{1}{2\gamma}\left(1 + \frac{1}{x^2}\right) - 1 - \left[\frac{1}{2\gamma}\left(1 + \frac{1}{x^2}\right)\right.\right. \\
&\qquad \left.\left. - \frac{M(x)}{M(2)} - \frac{1}{x^2\lambda(x)M(2)}\right] e^{-[\gamma/M(2)](t/\tau)}\right\}
\end{aligned} \tag{6.16}$$

By eq. (6.15), $\gamma > {}^3/_8$, whence $1/2\gamma < {}^4/_3$, and so $f(t)$ and, consequently, the maximum strains for the supported cylinder are less

than those for the unsupported cylinder. Since $\gamma > {}^3/_8$, the exponential decay of both stress and strain components is faster for the supported cylinder.

Again, as $t \to \infty$, the stresses (6.16) approach the elastic solution (equivalent to $\tau = 0$), and on the boundaries,

$$\begin{aligned} \sigma_\theta(1, \infty) &= \Pi \left\{ \frac{1}{\gamma} - 1 \right\} \\ \sigma_\theta(2, \infty) &= \Pi \left\{ \frac{5}{8\gamma} - 1 \right\} \end{aligned} \tag{6.17}$$

Now the viscoelastic equilibrium modulus G will be roughly of order $10^{-6}E_2$, whereas even for $b/h = 100$, $\beta > 10^{-2}E_2$ when $\nu_2 \sim {}^1/_3$, so that $\beta/G > 10^3$ and $\gamma > 100$. Thus the maximum strains are much smaller for the supported cylinder, while the exponential decay factor is considerably greater than for the unsupported cylinder. Further, for the supported cylinder, the tangential stress σ_θ becomes compressive, since the boundary values given by eqs. (6.17) for large time are negative. But as $t \to 0_+$, σ_x and σ_θ approach the values given in eqs. (6.12) for the unsupported cylinder, independent of γ. That is, instantaneously the support has no influence, which is to be expected, since the instantaneous deformation of a Kelvin material is zero, and the elastic constraint is not brought into play. So now, the variation in σ_θ on $x = 1$ between the initial and final states is much greater than before, and actually changes from tension to compression. Quantitatively, this range in value is not likely to be of significance practically since it is associated with the artificial neglect of instantaneous elastic response associated with the Kelvin model.

The uniform temperature solution, given by putting $\lambda(x) \equiv 1$ in eqs. (6.16), is here time dependent:

$$\begin{aligned} \sigma_x(x, t) &= -\Pi \left\{ 1 - \frac{1}{2\gamma}\left(1 - \frac{1}{x^2}\right) \right. \\ &\qquad \left. - \left(\frac{4}{3} - \frac{1}{2\gamma}\right)\left(1 - \frac{1}{x^2}\right) e^{-[8\gamma/3](t/\tau)} \right\} \\ \sigma_\theta(x, t) &= \Pi \left\{ \frac{1}{2\gamma}\left(1 + \frac{1}{x^2}\right) - 1 \right. \\ &\qquad \left. + \left(\frac{4}{3} - \frac{1}{2\gamma}\right)\left(1 + \frac{1}{x^2}\right) e^{-[8\gamma/3](t/\tau)} \right\} \end{aligned} \tag{6.18}$$

(b) *Maxwell Model*

This is the alternative 2 element model, shown in Figure 6, with a spring and dashpot in series, which gives for the shear law in differential form,

$$\frac{\partial}{\partial \xi}(\sigma_z - \sigma_\theta) + \frac{\sigma_z - \sigma_\theta}{\tau} = G_0 \frac{\partial}{\partial \xi}(\epsilon_z - \epsilon_\theta)$$

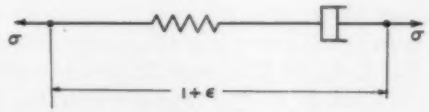

Fig. 6. The Maxwell model.

or a relaxation modulus

$$G(\xi) = G_0 e^{-\xi/\tau} \tag{6.19}$$

where G_0 is the instantaneous modulus and $\tau = \eta/G_0$ the relaxation time at temperature T_0. Hence

$$\bar{G}(s) = \frac{G_0}{s + 1/\tau}; \qquad \bar{G}[s/\lambda(x)] = \frac{G_0 \lambda(x)}{s + \lambda(x)/\tau} \tag{6.20}$$

Using the transform results obtained in Section 5, first consider the unsupported cylinder. By eqs. (5.24) and (5.25),

$$\bar{\sigma}_z(x,s) = -\frac{\Pi}{s}\left\{1 - \frac{I(x,s)}{I(2,s)}\right\} \tag{6.21}$$

$$\bar{\sigma}_\theta(x,s) = \frac{\Pi}{s}\left\{\frac{I(x,s)}{I(2,s)} - 1 + \frac{G_0}{x^2 I(2,s)[s + \lambda(x)/\tau]}\right\} \tag{6.22}$$

where

$$I(x,s) = \int_1^x \frac{G_0 dx'}{x'^3[s + \lambda(x')/\tau]} \tag{6.23}$$

To invert the above stress transforms, the integral $I(x,s)$ must first be expressed as a function of s. Using the exact expression for $\lambda(x)$, the integration does not appear to be representable in terms of elementary functions, but $\lambda(x)$ can be closely approximated by a quadratic form, when integration by partial fractions is possible. Unfortunately, the

resulting expressions for the stress transforms do not offer much hope of direct inversion. A simpler expression for the integral is obtained by taking $\lambda(x)$ as a linear function, which Figure 3 shows to be a good approximation in this particular case, but again the resulting transforms offer no ready inversion. Before proposing an approximation which does lead to direct inversion, we can examine the solutions for large and small times.

Large time behavior is governed by the transform singularities in s with the largest real part. Since $\lambda(x) > 0$, eq. (6.23) shows that $I(x,s)$ has no singularities for $\Re(s) > 0$, and $I(2,s)$ approaches zero like $1/s$ as $|s| \to \infty$. But in eqs. (6.21) and (6.22), the denominators contain $sI(2,s)$, which is nonzero as $|s| \to \infty$, and it is clear that ϑ_x and ϑ_θ have no singularity in $\Re(s) > 0$. For completeness, any different $\overline{\Pi}(s)$ which represents a bounded pressure will also behave like $1/s$ as $s \to \infty$, and so would not introduce a singularity there. Thus, $s = 0$ is the required singularity, and there,

$$\vartheta_x \sim -\frac{\Pi}{s}\left\{1 - \frac{I(x,0)}{I(2,0)}\right\}$$

$$\vartheta_\theta \sim \frac{\Pi}{s}\left\{\frac{I(x,0)}{I(2,0)} - 1 + \frac{G_0\tau}{x^2\lambda(x)I(2,0)}\right\}$$

and hence as $t \to \infty$

$$\begin{aligned}\sigma_x(x,t) &\to -\Pi\left\{1 - \frac{I(x,0)}{I(2,0)}\right\} \\ \sigma_\theta(x,t) &\to \Pi\left\{\frac{I(x,0)}{I(2,0)} - 1 + \frac{G_0\tau}{x^2\lambda(x)I(2,0)}\right\}\end{aligned} \tag{6.24}$$

Noting that $I(x,0) = G_0\tau M(x)$ by comparison with eq. (6.6), these values correspond to those in eqs. (6.12), which were the solutions for a Kelvin material at $t = 0_+$ (dependent on the temperature field).

Small time behavior is obtained from the power series expansion in $1/s$, as $s \to \infty$. It is found that

$$\begin{aligned}\frac{I(x,s)}{I(2,s)} &\sim \frac{4}{3}\left(1 - \frac{1}{x^2}\right) + 0\left(\frac{1}{s}\right) \\ I(2,s)[s + \lambda(x)/\tau] &\sim \frac{3G_0}{8} + 0\left(\frac{1}{s}\right)\end{aligned} \tag{6.25}$$

and therefore as $t \to 0_+$,

$$\sigma_x(x,t) \to -\Pi \left\{1 - \frac{4}{3}\left(1 - \frac{1}{x^2}\right)\right\}$$
$$\sigma_\theta(x,t) \to \Pi \left\{\frac{4}{3}\left(1 + \frac{1}{x^2}\right) - 1\right\} \tag{6.26}$$

This is the elastic solution, approached by the Kelvin material at large times; see eqs. (6.10).

The solutions for a Kelvin material and a Maxwell material are therefore reversed with respect to time, and the latter, initially, takes the elastic solution, and at large times approaches the initial Kelvin solution. Referring to the model in Figure 6, the initial response is governed by the spring which strains instantaneousy under load since the dashpot cannot here prevent its deformation, but at long times the increasing dashpot flow dominates the deformation since the spring extension is limited for finite stress. It must be realized that for long times for the Maxwell material, unrestricted viscous flow occurs so that the validity of the solution will break down when the strains cease to be small.

Examining eqs. (5.27) and (5.28), since $\beta > 0$, it is clear that the stress transforms for the supported cylinder have no singularity in $\Re(s) > 0$. So large time behavior is given by the residue at $s = 0$, and hence as $t \to \infty$,

$$\sigma_x(x,t) \to -\Pi$$
$$\sigma_\theta(x,t) \to -\Pi \tag{6.27}$$

and the corresponding hydrostatic stress component is

$$(1/3)\sigma_{ii} = (1/2)(\sigma_\theta + \sigma_x) = -\Pi \tag{6.28}$$

and the shear stresses are all zero. The viscoelastic cylinder therefore takes up a state of uniform hydrostatic compression, supported by the elastic shell, the shear stress relaxing completely to zero. This limiting behavior was also predicted by Woodward and Radok[11] in the isothermal case.

Expanding the transforms as a power series in $1/s$ leads to the following behavior as $t \to 0_+$:

$$\sigma_x(x,t) \to -\Pi\left\{1 - \frac{1}{2\gamma}\left(1 - \frac{1}{x^2}\right)\right\}$$
$$\sigma_\theta(x,t) \to \Pi\left\{\frac{1}{2\gamma}\left(1 + \frac{1}{x^2}\right) - 1\right\} \tag{6.29}$$

where the expression (6.15) is again used to define γ. Comparing eqs. (6.16), this is the distribution for the supported Kelvin cylinder as $t \to \infty$, which is identical with the elastic solution. Thus the instantaneous response of the supported Maxwell cylinder is the same as the elastic solution, determined by the spring response before the dashpot starts to flow. Because of the large time behavior though, the supported Maxwell cylinder does not show the reverse effect to that of the supported Kelvin cylinder.

The uniform temperature solution is obtained by putting $\lambda(x) \equiv 1$ in eqs. (5.27) and (5.28), when the transforms can be inverted to give

$$\sigma_x(x,t) = -\Pi\left\{1 - \frac{1}{2\gamma}\left(1 - \frac{1}{x^2}\right)e^{-(\beta/8G_0\gamma)(t/\tau)}\right\}$$
$$\sigma_\theta(x,t) = \Pi\left\{\frac{1}{2\gamma}\left(1 + \frac{1}{x^2}\right)e^{-(\beta/8G_0\gamma)(t/\tau)} - 1\right\} \tag{6.30}$$

These are time dependent, and since $\gamma > \beta/8G_0$, the decay factor is less than $1/\tau$ (or the delay time is a little greater than τ).

Having discussed the asymptotic behavior of the Maxwell solutions, we now suggest an approximation that allows inversion of the transforms for the whole range of temperature. $\lambda(x)$ is approximated by a series of step functions—the case for five equal divisions is shown in Figure 3—which means that the temperature distribution across the cylinder is assumed to be a series of stepped uniform values, each extending over a finite width. Thus, dividing the width, $1 \le x \le 2$ into N equal sections, $x_i \le x < x_{i+1}$, $(i = 1 \ldots N)$ with $x_1 = 1$, $x_{N+1} = 2$,

$$x_i \le x < x_{i+1}, \qquad \lambda(x) = \lambda_i \tag{6.31}$$

Now

$$\int_{x_i}^{x_{i+1}} \frac{G_0 dx'}{x'^2[s + \lambda(x')/\tau]} = \int_{x_i}^{x_{i+1}} \frac{G_0 dx'}{x'^2[s + \lambda_i/\tau]}$$
$$= \frac{G_0}{2}\left(\frac{1}{x_i^2} - \frac{1}{x_{i+1}^2}\right)\Big/\left(s + \frac{\lambda_i}{\tau}\right) \tag{6.32}$$

Defining for convenience,

$$\delta_i = \left(\frac{1}{x_i^2} - \frac{1}{x_{i+1}^2}\right) \tag{6.33}$$

we get further

$$I(x_{r+1},s) = \sum_{i=1}^{r} \frac{G_0\delta_i}{2(s + \lambda_i/\tau)} \tag{6.34}$$

with a similar extension to a value of x between two section limits.

Considering the unsupported cylinder, we are interested first, from eq. (5.21), in $I(x,s)/sI(2,s)$, $= R(x,s)$ say. With the above approximation,

$$R(x_{r+1},s) = \frac{\sum_{i=1}^{r} \frac{G_0\delta_i}{2(s + \lambda_i/\tau)}}{s\sum_{i=1}^{N} \frac{G_0\delta_i}{2(s + \lambda_i/\tau)}} \tag{6.35}$$

It is clear that $R(x_{r+1},s)$ has no singularity at $s = -\lambda_i/\tau$ (each i), as the same factor appears in both numerator and denominator. There is a pole at $s = 0$ for which the residue has already been evaluated to express the behavior as $t \to \infty$, and there are poles at each root of $I(2,s) = 0$, provided it is not identical with $-\lambda_i/\tau$ (any i). From eq. (6.34), bringing to a common denominator, these roots are those of an $(N - 1)$th order polynomial, and will in general be complex, and always have the real part less than zero. The required transform inversion is then simply a sum of residues at simple poles. In eq. (6.22), the additional expression is again regular at $s = -\lambda_i/\tau$, when $\lambda(x)$ has been replaced by the appropriate λ_i, and the poles are again at $s = 0$ and at the zeros of $I(2,s)$. The computation was performed for $N = 5$, as shown in Figure 3, when the roots of a quartic were required, but the results were unsatisfactory, and we conclude that a larger number of sections is necessary.

A similar procedure can be followed for the supported cylinder, where the transform stresses, given by appropriate substitution in eqs. (5.27) and (5.28), will have poles at the zeros of $sI(2,s) + \beta/8$, and at $s = 0$; again they are regular at $s = -\lambda_i/\tau$ (each i). The required zeros are now the roots of an Nth order polynomial. This approximation method gives direct inversion from the residues at simple

poles, but appears to require a large number of sections, and hence lengthy computation.

(c) *General Finite Model*

This model can be represented by a finite combination of Kelvin and Maxwell elements, and satisfies some higher order differential operator law. The relaxation modulus can be expressed in the form

$$G(t) = G_\infty + \sum_{m=1}^{M} G_m e^{-t/\tau_m} \tag{6.36}$$

where G_∞ is the equilibrium modulus, and the τ_m are a set of discrete relaxation times into which the continuous relaxation properties of a material are grouped, the G_m being the corresponding instantaneous moduli. Taking transforms,

$$\bar{G}[s/\lambda(x)] = \frac{G_\infty \lambda(x)}{s} + \sum_{m=1}^{M} \frac{G_m \lambda(x)}{s + \lambda(x)/\tau_m} \tag{6.37}$$

This leads to a more complicated set of transform equations than does the Maxwell model, but can be treated by the same approximation scheme. Now

$$I(x_{r+1},s) = \frac{G_\infty}{2s}\left(1 - \frac{1}{x_{r+1}^2}\right) + \sum_{m=1}^{M} G_m \sum_{i=1}^{r} \frac{\delta_i}{2(s + \lambda_i/\tau_m)} \tag{6.38}$$

and with increasing number of elements, M, the subsequent computation becomes rapidly more complicated, but all inversions can be expressed as sums of residues of simple poles.

References

1. Carslaw, H. S., and J. C. Jaeger, *Operational Methods in Applied Mathematics*, 2nd ed., Oxford Univ. Press, 1953.
2. Eirich, F. R., *Rheology II*. Academic Press, New York, 1958.
3. Hilton, H. H., *Proc. 2nd U. S. Natl. Congr. Appl. Mech.*, 547, 1954.
4. Lee, E. H., *Quart. Appl. Math.*, **13**, 183 (1955).
5. Lee, E. H., *Proceedings of the 1st Symposium on Naval Structural Mechanics*, Pergamon Press, 1960, p. 456.
6. Radok, J. R. M., *Quart. Appl. Math.*, **15**, 198 (1957).
7. Schwarzl, F., and A. J. Staverman, *J. Appl. Phys.*, **23**, 838 (1952).
8. Sternberg, E., *Proc. 3rd U. S. Natl. Congr. Appl. Mech.*, 673, 1958.
9. Stuart, H. A., *Die Physik der Hochpolymeren, IV*. Springer, Berlin, 1956.

10. Timoshenko, S., and J. N. Goodier, *Theory of Elasticity*, 2nd ed., McGraw-Hill, New York, 1953.

11. Woodward, W. B., and J. R. M. Radok, Brown University Report PA-TR/14, 1955.

Synopsis

The system of equations is presented which determine the stress and strain distributions for a linear viscoelastic material with varying temperature. Temperature influences on viscoelasticity are represented by a shift relation on the logarithmic time scale which equates temperature change to a translation on the logarithmic time scale for all viscoelastic functions. Methods of treating the general equations are discussed, but solution by standard methods is shown to be possible only for restricted situations. Stresses in a cylinder of incompressible material under a steady axisymmetrical temperature distribution are evaluated when a constant internal pressure is suddenly applied and maintained. Because of the assumption of incompressibility, thermal stresses due to inhomogeneous expansion do not appear, but the temperature effect on viscoelastic response produces a marked effect on the stress field as compared with the isothermal case. Particular features of the stress distributions for Kelvin and Maxwell materials are contrasted. An approximate method of solution applicable to the Maxwell body and more general viscoelastic materials is described.

TRANSACTIONS OF THE SOCIETY OF RHEOLOGY IV, 265–278 (1960)

The Rheology of Asphalt.* II. Flow Characteristics of Asphalt

FREDERICK H. GASKINS,† JOHN G. BRODNYAN,‡
WLADIMIR PHILIPPOFF,§ and EDMUND THELEN,
The Franklin Institute Laboratories for Research and Development, Philadelphia, Pennsylvania

I. Introduction

The National Asphalt Research Center (NARC), established in 1951 under the sponsorship of many industrial asphalt producers and consumers, was charged with elucidating the rheological properties and surface energy relations of asphalt. Heretofore, these behaviors in asphalt, especially their viscoelastic nature, had not been explicitly defined as was shown by Thelen.[1] To accomplish this, ten asphalts were selected which represented a wide variety of the continental industrial stocks available. These materials were phenomenologically categorized as Sol, Medium, and Gel, based on characteristic physical properties due to source or processing conditions undergone. The asphalts were described by Brodnyan in the first paper of this series.[2] Further analyses of them have been carried out by Gzemski of the Atlantic Refining Co.,[3] Orr of the Gulf Refinery Technology Laboratory,[4] and Scott and Cunningham of the Union Oil Co.[5]

The surface energy relations have been described.[6]

The rheological investigation was designed to: (*a*) Determine the mechanical properties under conditions of dynamic oscillatory shear and under steady-state laminar flow; (*b*) investigate the correlati-

* Five-year program conducted from 1951 to 1956 by the National Asphalt Research Center at The Franklin Institute.

† Present address: Aeroprojects Inc., West Chester, Pennsylvania.

‡ Present address: Rohm & Haas Co., Philadelphia, Pennsylvania.

§ Present address: Esso Research & Engineering Co., Linden, New Jersey.

bility of these two different conditions of stress-imposition; (*c*) discover any generalities in rheological behavior existing among the various types of asphalts: and, (*d*) show how to predict the performance to be expected under service conditions from rheological behaviors.

The prediction of performances was discussed in the first paper of this series.[2] The dynamic mechanical properties are the subject of the third paper.[7]

II. Experimental Methods

Two rheological instruments were used in the investigation of the flow characteristics of asphalts, both of which can measure both viscous and elastic responses of viscoelastic bodies.

1. Rotational Viscometer

This is a concentric coni-cylindrical viscometer, which has been described.[8] It is designed to yield the same distribution of velocity gradients throughout the entire annulus between the cylinders and was utilized to study the behavior of the asphalts at low rates of shear (10^{-6} to 10^{3} sec.$^{-1}$). The reference cited discusses corrections that need to be applied (e.g., to determine the maximum shear stress): the equations for evaluating rheological data have been derived.[9]

It has been shown[10,11] that the recoverable shear, s, can be determined experimentally from either the "fore-effects", i.e., the retarded elastic deformation, or the "after-effects" i.e., the retarded elastic recovery which occurs after the shear stress is removed. In the study of deformation, the equilibrium state ($\partial\gamma/\partial t$ = constant) of the strain-time behavior can be extrapolated to zero time. The resultant γ-intercept in the γ vs. t plot is the recoverable shear strain. In recovery studies, the maximum strain recovery after removal of external stress is the recoverable shear strain.

2. Capillary Viscometer

This instrument, as previously discussed,[12] has been designed to permit the exertion of a constant pressure gradient as a driving force across the capillary tubes. Volumetric flow rates are obtainable corresponding to rates of shear in the range 10^{-3} to 10^{6} sec.$^{-1}$ under shear stresses of 10^{0} to 10^{6} dyne/cm.^{2} Rheological parameters are calculated from the equilibrium conditions.

The rheological data obtained with these instruments are shown to be superposable. Therefore the choice of instrumentation is dictated by the experimental conditions desired, e.g., range of rates of shear.

III. Experimental Results

The ten representative asphalts were investigated in one or both of the viscometers in a temperature range of 0 to +300°C. Typical results obtained are as follows.

1. Rotational Viscometric Studies

A high consistency asphalt, designated as Gel B, was measured. Deformation-recovery behavior was determined as shown in Figure 1. During the time (1 hr.) and temperature (75°C.) under which the experiment was conducted, an equilibrium strain-time function was not obtained. Therefore, an empirical graphical analysis was performed, which in essence consists of evaluating the expression

$$\gamma(\tau) = \int [\tau/\eta(\tau)d\tau] + \tau/G(\tau) \tag{3.1}$$

which states simply that the total strain exerted on a body by the shear stress is a resultant of the additive effect of the strain taken up

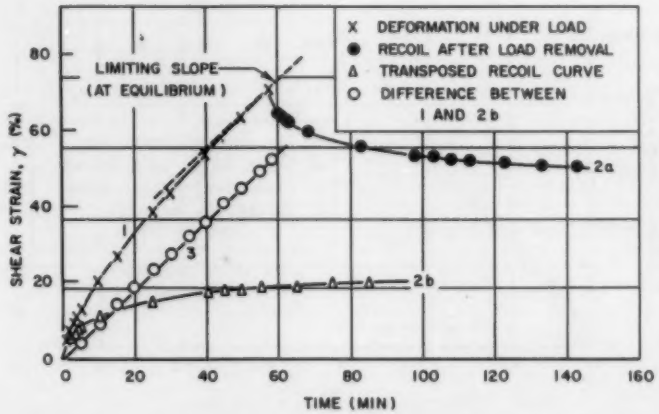

Fig. 1. Deformation and recovery measurements with the rotational viscometer: Gel B asphalt.

TABLE I
Rheological Parameters for Typical NARC Asphalts

Designation	Gel B	Med C
Temperature, °C.	75	75
Shear stress, τ, dyne/cm.^{2}	1450	3620
Rate of shear, D, sec.$^{-1}$	1.52×10^{-4}	2.72×10^{-3}
Apparent viscosity, η, poise	9.54×10^6	1.33×10^6
Recoverable shear, s, dimensionless	0.20	0.25
Shear modulus, G, dyne/cm.^{2}	7250	14,500

differentially with respect to time due to the energy dissipated in viscous flow and the strain taken up due to the energy stored elastically.

In graphical analysis, the strain-time behavior, curve *1* in Figure 1, is plotted for the time-interval of measurement, t_0 to t_1, At t_1, the shear force is removed, resulting in the recoil curve, curve *2a*. The recovery curve is inverted and translated to time t_0, curve *2b*. Graphical subtraction of (*2a*) from (*1*) results in curve *3*. This graphical procedure is analogous to the stated analytical expression, and, hence, subject to the same limits of empiricism. Nevertheless, a close approximation to the actual rheological parameters is generally obtained,; therefore, the requirement of long time intervals of

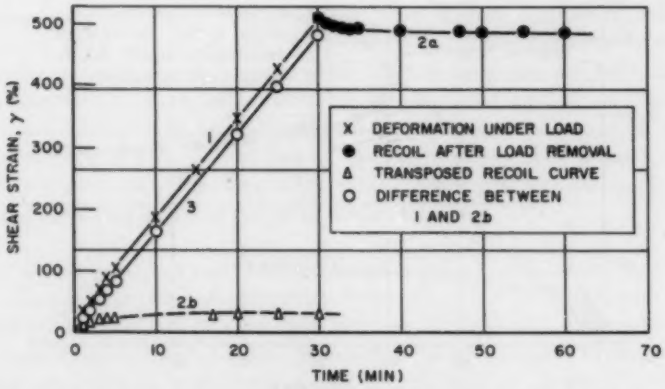

Fig. 2. Deformation and recovery measurements with the rotational viscometer: Med C asphalt.

measurement for high consistency materials, such as Gel B asphalt under these conditions, can often be circumvented. In the example shown, the deformation-time curve is approaching an equilibrium state that would presumably be identical in slope to that derived analytically.

The rheological parameters calculated from the data are given in Table I.

The deformation-recovery characteristics for a lower consistency asphalt, designated as Med C, were also investigated. An equi-

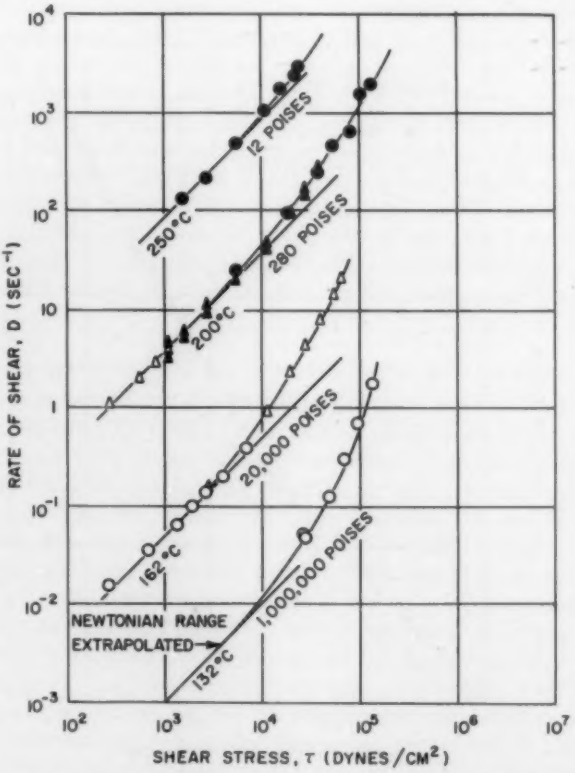

Fig. 3. Temperature dependence of flow curves: Med D asphalt.

librium strain-time relationship was obtained at 75°C., as demonstrated in Figure 2. This asphalt had a lower apparent viscosity and higher shear modulus than Gel B at the same temperature. The variation among other asphalts was much greater in many cases.

2. Capillary Viscometer Studies

A high consistency asphalt, designated as Med D, was investigated. Flow curves were measured at various temperatures between 130 and 250°C., as shown in Figure 3. The viscosity-temperature relationships were studied for these experiments. The Newtonian viscosities

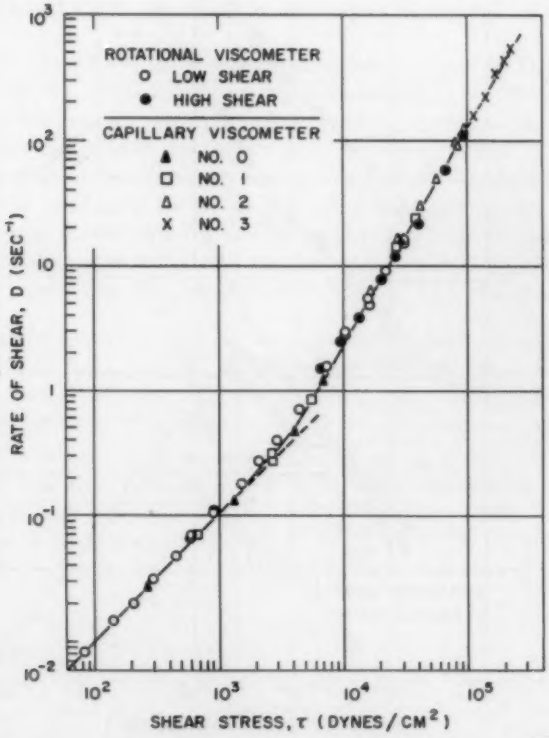

Fig. 4. Flow curve: Med C asphalt.

measured, or in one case extrapolated, were 1,000,000 to 12 poise, which were observed in seven logarithmic decades of time. It is seen in these results, which are confirmed by other data, that for asphalts the transition from Newtonian to non-Newtonian flow occurs at approximately 3000 dyne/cm.^{2}. This is independent of temperature and type of asphalt.

3. Comparison of Viscometric Results

Flow curves were determined for several of the asphalts in both viscometers to test the degree of correlation between capillary tube flow and concentric cylinder shearing. A typical result obtained for a high-consistency asphalt, designated as Med C, is shown in Figure 4. The data were taken at 100°C., utilizing the rotational viscometer (two gap clearances at rates of shear of 10^{-2} to 10^{2} sec.$^{-1}$ and the capillary viscometer (four tube sizes) at rates of shear of 10^{-2} to 10^{3} sec.$^{-1}$. This provided overlapping points in four logarithmic decades of rate of shear. The data points are indistinguishable as to the instrumentation used. The correlation of viscometric data has been firmly established (for example, see Reference 13); the present data serve to confirm these results and to extend the generality of applicability of the concept beyond "normal" molten polymers and polymer solutions.

4. Comparison of Dynamic and Steady-State Results

Several investigators[14,15] have compared rheological data obtained in dynamic oscillatory shear with that in steady-state laminar flow. Their results have shown that the variation in apparent viscosity with rate of shear is substantially different from the variation with frequency. Van der Poel,[16] and more recently Cox and Merz[17,18] proposed that the complex viscosity or complex modulus yields essentially the same curve for variance with rate of shear and with frequency. Checks have been made at the FIL which indicate that a better concordance of data does result. However, there is no basis in present rheological theory to account for the stated results, nor, apparently, do the proposals offer complete explanation. However, it has been generally found that the viscosity curves for high molecular weight materials coincide in the Newtonian region and in the non-Newtonian region to the point that $\eta_{app} = (1/2)\eta_0$. This has been found under the NARC program to hold true for asphalts.

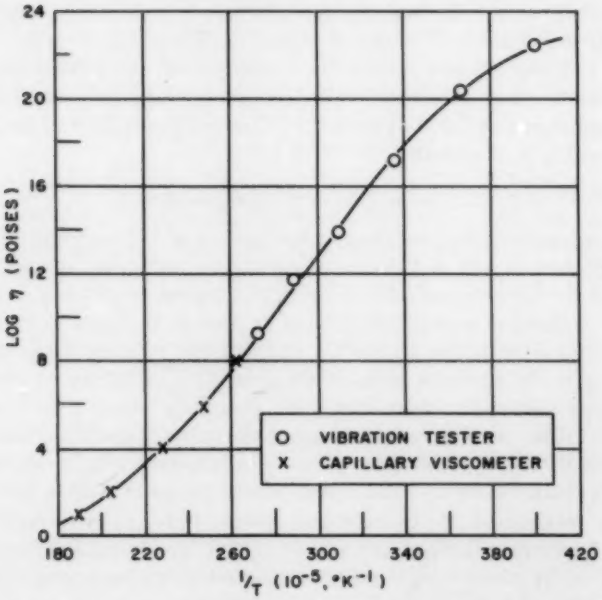

Fig. 5. Temperature dependence of initial viscosity: Med D asphalt.

Data that were obtained in the Newtonian region using the Dynamic Tester and Capillary Viscometer are shown in Figure 5.

In the temperature range used, −23 to +250°C., the initial viscosities are between 10^1 and 10^{23} poise. The data points do not overlap, but it seems apparent that they form a smooth, continuous curve.

IV. Discussion and Conclusions

1. The Nature of Asphalt

Asphalt has been shown to possess viscoelastic behavior in which both Newtonian and pseudoplastic non-Newtonian flow characteristics are evidenced as shown by the following examples.

(*a*) *Viscoelastic Nature.* The experiments, typified by the curves in Figures 1 and 2, clearly show the occurrence of elastic deformation followed by steady-state flow. The elastic recovery is also quite

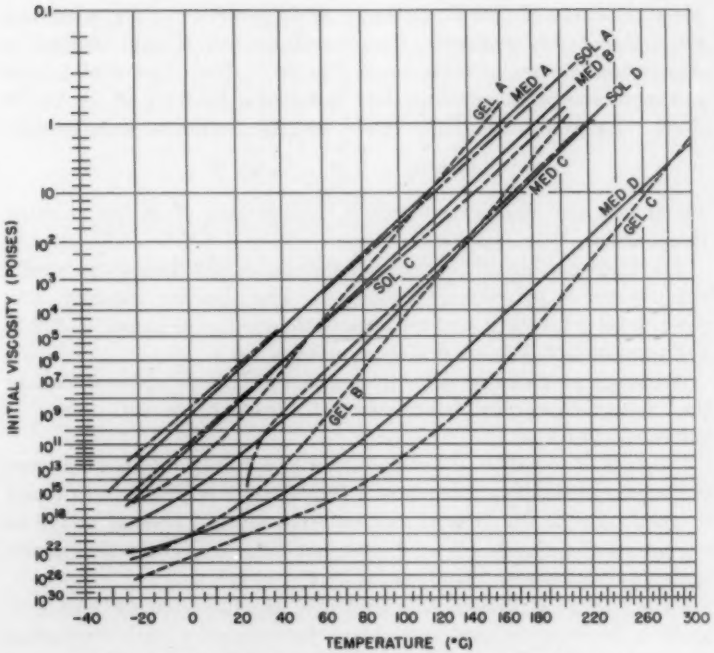

Fig. 6. Initial viscosity of NARC asphalts: REFUTAS chart.

evident. Quantitative correlation was generally obtained between the elastic deformation and the elastic recovery, indicating no structural change under constant force.

Simple viscous or Newtonian flow was measured for most of the asphalts at high temperatures. At the temperatures where viscoelastic behavior occurred, initial regions of Newtonian viscosity before the onset of non-Newtonian flow was found for many of the asphalts; the initial viscosity of some of the asphalts was too high to measure. For example, the initial viscosity of Gel C at 25°C. extrapolated by the "Reduced Variables" technique[19] from data at higher temperatures and frequencies is found to be approximately 10^{23} poise.

(*b*) *Viscosity-Temperature Relationships.* The continuity of viscosity-temperature curves has been shown for asphalt. In a tem-

perature range of 320°C. (from −20 to +300°C.) over which asphalt shows the solidus-liquidus transition, no abrupt changes in slope were detected as is shown in Figure 6. This type of plot, used widely in the petroleum industry, is called a REFUTAS or ASTM chart. Its coordinates are based on the empirical relationship:

$$\log \log (\mu + 0.8) = m \log T$$

where μ is the kinematic viscosity, centistokes; T is the absolute temperature, °K.; and m is the slope.

The chart has been extended to higher viscosities than are generally encountered in petroleum technology. The absolute viscosity, η in poise, has been substituted for μ using the relation η (poise) = 100 × μ (centistoke) × ρ (g/cm.^{3}) and assuming $\rho = 1$.

Although empirically developed, the REFUTAS chart linearizes the viscosity-temperature curves over a wide range and, hence, is extremely useful.

Changes of viscosity of twenty-seven logarithmic decades occurred in the stated temperature range. The changes in phase from liquid to solid, specifically, the transition from simple viscous liquid to viscoelastic fluid to elastic solid, were not reflected as inflection points in the viscosity-temperature curves.

Flow curves at various temperatures, as illustrated by Figure 3, show a decrease in non-Newtonian characteristics with increasing temperature. Such behavior is typical of high polymer solutions and molten polymers.

An interesting observation is that, in a temperature range of 120° (130 to 250°C.) with the viscosity of Med D varying from 1 million down to 10 poise, non-Newtonian flow occurred in all cases at approximately the same shear stress, 3000 dyne/cm.^{2}. This emphasizes the importance of shear stress as the controlling parameter in viscoelastic flow. Philippoff has discussed this fact, particularly as related to flow birefringence experiments.[20] Other researchers have emphasized the rate of shear or strain tensor as the primary frame of reference (for example, see refs. 21 and 22).

The constancy of the critical shear stress leads to theoretical implications concerning the force-levels sustainable by structural units in laminar flow.

Analysis of the change in initial viscosity with temperature was performed to determine the apparent activation energy for viscous

flow of asphalts. The data were evaluated from plots of log η *vs.* $1/T$(°K.). The results, as shown in Table II, show values for ΔE of 41 to 127 kcal./mole, with a mean value of about 65 kcal./mole. These are to be associated with the value generally assumed for chemical reaction of 30 kcal./mole.

TABLE II
Apparent Activation Energies for the NARC Asphalts at 25°C.

Asphalt	Activation energy, E, Kcal./mole
Sol A	41
Sol C	57
Sol D	127
Med A	49
Med B	55
Med C	59
Med D	67
Gel A	65
Gel B	78
Gel C	50
Gel C at 95°C.	83

The rule that high viscosity leads to a high activation energy seems substantiated for asphalts as for many plastics, for which typical data were presented in reference 8.

(*c*) *Viscosity vs. Softening Point.* A standard ASTM test for determining the softening-point (SP) of materials is by the "ring and ball technique" (R & B). Logic indicated that equal rates of fall of the ball may occur at a constant viscosity. This point was investigated. It was found that at SP the viscosity is 50,000 poise; in comparison, Saal found 12,000 poise.[23] Despite the discrepancy, the constancy of viscosity at the softening point was confirmed. The flow curves for various asphalts were analyzed to determine what shear stresses and rates of shear exist at this point for various asphalts. The results, as shown in Table III for five asphalts, are an apparent viscosity of 50,000 poise, initial viscosities at SP between 80,000 and 300,000 poise, shear stresses averaging 15,000 dyne/cm.^{2} and rates of shear averaging 0.3 sec.$^{-1}$.

TABLE III
Shearing Stress and Rate of Shear at the Softening Point for Several NARC Asphalts

Asphalt	Softening point, SP °C.	Apparent viscosity at SP poise	Initial viscosity at SP poise	Shear stress at SP dyne/cm.^{2}	Rate of shear at sec.$^{-1}$
Med. C	88	50,000	83,000	10,000	0.20
Med. D	150	50,000	135,000	20,000	0.40
Gel A	53	50,000	100,000	~10,000	0.20
Gel B	90	50,000	280,000	16,000	0.32
Gel C	159	50,000	140,000	20,000	0.40
			Mean Values:	*15,000*	*0.30*

This indicates that, although the mechanism of deformation of asphalt in the R & B test is quite complicated, the rheological parameters existent are reasonably constant.

2. Correlation of Viscoelastomeric Experiments

One of the major goals of this experimental program has been to establish the reality of rheological parameters. The experiments conducted and the data obtained have been directed toward this aim. Results have been presented which are typical of the more extensive experiments that emphasize the correlation of fundamental rheological properties independent of the rheological instrumentation employed.

(*a*) A typical curve was presented in Figure 4 which shows that capillary viscometer and rotational viscometer rheological data correlate. Therefore, no serious question should exist regarding differences in concentric cylindrical shearing as opposed to capillary-tube flow in general.

(*b*) Attempts have been made to correlate theoretically dynamic vibrational data with steady-state data on the basis of the η vs. D and η vs. ω functions. Experimental results, however, do not confirm this except to the extent that the initial viscosities measured are identical throughout the entire temperature spectrum. Correlations have been deduced for the complex shear modulus, i.e., complex viscosity, as a function of D and ω. The complex modulus takes both viscosity and elasticity of viscoelastic materials into account. How-

ever, the apparent viscosity is found experimentally to decrease more rapidly with increasing frequency than with rate of shear. Consequently, the exact nature of the correlation seems to require clarification on a sound theoretical basis.

V. Summary

The investigation of asphalt by steady-state rheological experiments has established that asphalts are viscoelastic bodies which exhibit Newtonian and non-Newtonian flow behavior. In essential characteristics they respond to shear forces in a manner similar to high polymer solutions and molten plastics.

The experiments have supported the independence of rheological parameters from specific viscometric techniques.

This investigation together with the dynamic tests[7] allow the rheological characteristics of asphalt to be categorized and provide essential information for deriving a "Rheological Equation of State" that may be valid for pseudoplastic materials in general as well as asphalt.

The authors express their appreciation to the member-companies who sponsored and supported the National Asphalt Research Center. In addition, acknowledgment is due to the many members of the Franklin Institute Laboratories for Research and Development who contributed to the program.

References

1. Thelen, E., *Proc. Assn. of Asphalt Paving Technologists*, **18,** 154 (1949).
2. Brodnyan, J. G., *Highway Research Board, Bull.*, **No. 192** (1958).
3. Gzemski, F. C., "Sternberg-Rostler Analysis of NARC Asphalts," presented at Annual Meeting, NARC, Philadelphia, Pa., 1954.
4. Orr, A. S. "Further Conventional Tests on NARC Asphalts," presented at Annual Meeting, NARC, Philadelphia, Pa., 1954.
5. Scott, F. S. and Cunningham, O. D. "Electron Microscope Study of Asphalts," presented at Annual Meeting, NARC, Philadelphia, Pa., 1954.
6. Thelen, E., *Highway Research Board, Bull.*, **No. 192** (1958).
7. Brodnyan, J. G., F. H. Gaskins, W. Philippoff, and E. Thelen, *Trans. Soc. Rheol.*, **4,** 279 (1960).
8. Philippoff, W., and F. H. Gaskins, *J. Polymer Sci.*, **21,** 205, (1956).
9. Gaskins, F. H., and W. Philippoff, *J. Appl. Polymer Sci.*, **2,** 143 (1959).
10. Philippoff, W., and F. H. Gaskins, *Trans. Soc. Rheol.*, **2,** 263 (1958).
11. Leaderman, H., *J. Polymer Sci.*, **13,** 371 (1954).
12. Philippoff, W., *ASLE Trans.*, **1,** 1 (1958).
13. Brodnyan, J. G., F. H. Gaskins, W. Philippoff, and E. G. Lendrat. *Trans. Soc. Rheol.*, **2,** 285 (1958).

14. DeWitt, T. W., H. Markowitz, F. J. Padden, Jr., and L. J. Zapas, *J. Colloid Sci.*, **10,** 174 (1955).
15. Philippoff, W., *J. Appl. Phys.*, **25,** 1102 (1954).
16. Van der Poel, C., S.P.E. *Journal*, **11,** 7 (1955).
17. Cox, W. P., and E. H. Merz, *J. Polymer Sci.*, **28,** 619 (1958).
18. Cox, W. P., and E. H. Merz. *ASTM Special Tech. Public. of Intern. Symposium on Plastics Testing and Standarization*, in print.
19. Ferry, J. D., E. R. Fitzgerald, L. D. Grandine, and M. L. Williams, *Ind. Eng. Chem*, **44,** 703 (1952).
20. Philippoff, W., *Rheol. Acta*, **1,** (1958); *Ind. Eng. Chem.*, **51,** 7 (1959).
21. Peterlin, A., and M. Čopič, *J. Appl. Phys.*, **27,** 5 (1956).
22. Pao, Y.-H., *J. Chem. Phys.*, **25,** 1294 (1956).
23. Saal and Koens, in *Proc. Intern. Congr. Rheol., 2nd Congr.*, Oxdord, 1953.

Synopsis

The rheological properties of ten representative asphalts were investigated under conditions of steady-state shear and laminar flow. Two instruments were utilized: a coni-cylindrical (rotational) viscometer and a high-pressure capillary tube viscometer. The results of the investigation show that asphalts are viscoelastic bodies which exhibit both Newtonian and non-Newtonian flow behavior with no evidence of yield value, structural breakdown or work-hardening. Thus asphalts, deliberately selected to represent extremes in structures and properties, are similar to concentrated polymer solutions and molten polymers in their response to stress. The extreme variations noted in the rheological behaviors of asphalts can generally be accounted for by the parameters—time, temperature, and stress.

TRANSACTIONS OF THE SOCIETY OF RHEOLOGY IV, 279–296 (1960)

The Rheology of Asphalt. III. Dynamic Mechanical Properties of Asphalt

JOHN G. BRODNYAN,* FREDRICK H. GASKINS,† WLADIMIR PHILIPPOFF,‡ and EDMUND THELEN,
Franklin Institute, Laboratories for Research and Development, Philadelphia, Pennsylvania

Introduction

This paper is the third in a series describing the rheological behavior of ten asphalts, representing three major categories. The characterization of these asphalts by the conventional ASTM tests has been presented in the first paper in the series.[1] The second paper in the series[2] treats the steady state behavior of the asphalts; there it has been shown that these representative asphalts are viscoelastic bodies exhibiting non-Newtonian behavior and elastic recoil. This paper will describe the investigation of the viscoelastic behavior of the asphalts under sinusoidal loading over a wide range of frequency and temperature.

Van der Poel[3] has also investigated bitumens under dynamic loading, measuring a stiffness which is related to the complex modulus. However, he could not separate the complex modulus into its components as was possible with the equipment described below. Van de Poel also has a gap in the transition region from elastic to viscous behavior where he has no data, but in the work reported here it was possible to cover this part of the time scale, giving more information.

At the time this work was begun the validity of the time-temperature superposition techniques was not established, and it was necessary to check experimentally Ferry's method of "reduced variables."[4]

* Present address: Rohm & Haas Co., Philadelphia, Pa.
† Present address: Aeroprojects, Inc., West Chester, Pa.
‡ Present address: Esso Research & Engineering Co., Linden, N. J.

Therefore work is reported here on the comparison between moduli predicted from low frequency work and actual measurements at higher frequencies.

Experimental Methods

A number of instruments were used in the investigations described here. However, the FIL dynamic tester was employed in gathering most of the data. This instrument, which measures by means of a sandwich-type shear attachment the storage shear modulus, G', and the loss shear modulus, G'', from 10^{-6} to 10^{1} cycles/sec. and from $-20°$ to 300°C., has been described in the literature in some detail.[5-7] A compression attachment[8] and an attachment for measuring the Young's moduli[5] (E' and E'') in bending have also been described. The bending data could be correlated reasonably well with the shear data if one assumed $E' = 3G'$, i.e., that Poisson's ratio equals one-half.

The torsion crystal has been described in the literature in some detail.[9] The experimental data reported here was obtained only at the resonant frequency of the crystal, approximately 20 kcycles/sec., but over a wide range of temperature.

A rebound (impact) tester was also constructed to provide a simple inexpensive test machine, and since it has not been described a detailed outline of its principles and operation will be given here.

The impact tester uses a hammer arm based on a mathematical pendulum whose center of percussion forms the striking surface which would hit the sample. The instrument consists of a large, shock mounted, steel base plate, a pendulum hammer arm mounted on the base plate, a mount for a piezoelectric crystal and the sample, an electromagnet to hold the hammer arm for the drop, and positioning pins to hold the sample in place. The piezoelectric crystal is cemented in place in the instrument by an epoxy resin. A photograph of the instrument is given in Figure 1. Experimentally a time calibration trace is given on an oscilloscope screen by a Hewlett-Packard Model 200B Audio-Oscillator, and the instant of release of the head as well as the times of striking the piezoelectric crystal are recorded as blips on the screen. A picture is taken of these traces by a Polaroid Oscillograph Camera. From the measurements of the duration of the first impact and the time between successive impacts the necessary raw data is obtained.

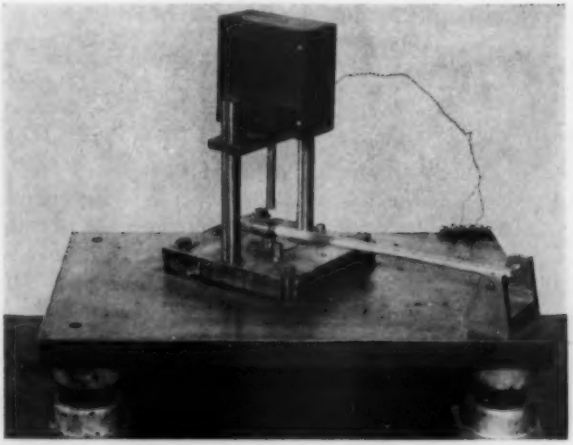

Fig. 1. The Impact Tester.

The Young's modulus, E', of the sample may be found from the following relationship:

$$E' = 4\pi^2 LM/At^2 \tag{1}$$

where L is the sample height, A is the sample area, M is the equivalent mass of the pendulum at the center of percussion, and t is the period of the motion, i.e., the duration of the impact.

All of the above quantities are measured experimentally. The ratio of rebound height, h, to the distance of fall of the hammer h_0, gives the loss angle:

$$h/h_0 \simeq 1 - \pi \tan \delta \tag{2}$$

The drop height is a fixed quantity and the rebound height can be calculated from the time between impacts. The frequency is calculated from the period. The Young's moduli are converted to shear moduli for comparison purposes. This instrument is limited in that: (*1*) no temperature control has been built, (*2*) the stiffness of the epoxy resin mounting puts an upper bound on stiffness which can be measured, and (*3*) only small loss angles can be measured accurately. However, this instrument was found to be useful in making comparisons and in obtaining data rapidly.

The Elastic Moduli as a Function of Frequency

A typical set of data gathered by the FIL dynamic tester is shown in Figure 2. It presents storage moduli, loss moduli, and dynamic viscosity (η') as a function of frequency at six temperatures for the Sol C asphalt. These curves were then superposed by Ferry's method of "reduced variables"[4] to give a reduced curve covering fourteen decades of reduced frequency with 25°C. as reference temperature (Fig. 3). The overlap of points is such as to lead one to believe that the superposition principle holds. However, a more severe test of the validity of this type of construction is the comparison of the values so determined with the ones directly measured at another temperature

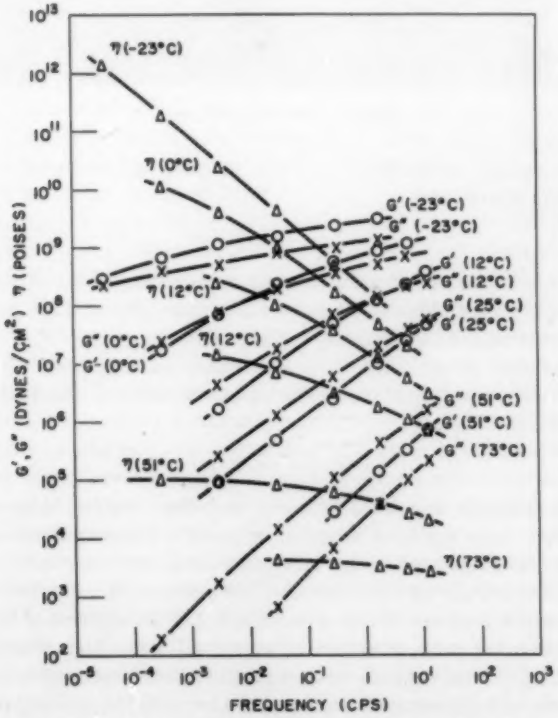

Fig. 2. Mechanism of reduction: Sol C isotherms.

and quite different frequencies. Such a test is described in the next section.

All the dynamic data for the ten asphalts have been treated in the way outlined above for Sol C. These results give reduced curves over a range of frequency for each asphalt and they are all shown in Figure 4. The data points are not given since this would lead to great confusion.

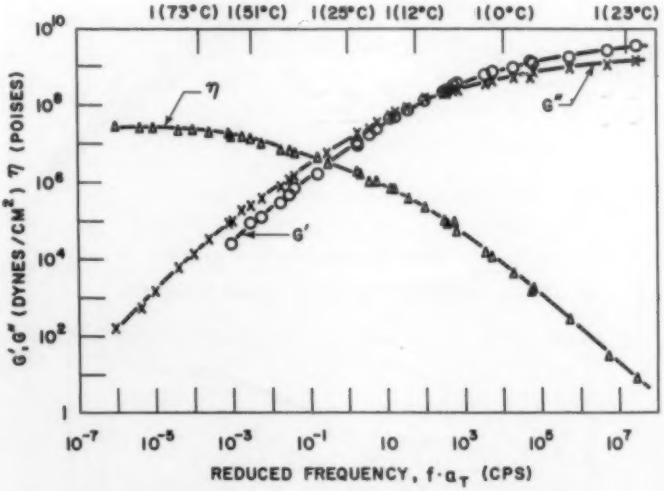

Fig. 3. Mechanism of reduction: Sol C reduced curves.

In trying to compare the curves of the separate families, Sols, Mediums, and Gels, we found that the reduced curves for the members of each family could be shifted to one single curve. The shifting procedure required the arbitrary choice of one asphalt curve as a base, Sol C for the Sol family, and the translation of the other curves in two directions until the data points superimposed. The results obtained for the Sol family are seen in Figure 5. The coincidence of the Sol D data was not good at higher frequencies and low temperatures, giving G'' values lower than the other Sol family members. This is the reason for the second G'' curve shown in Figure 5. Similar results were obtained for the Medium and Gel families. However, the Gel

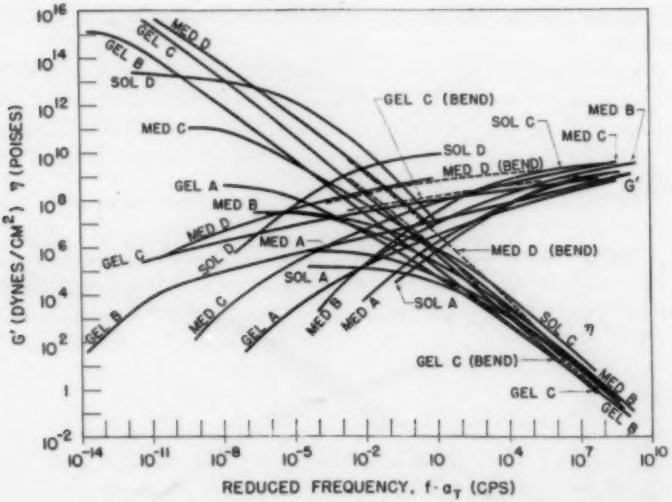

Fig. 4. Reduced curves of representative asphalts.

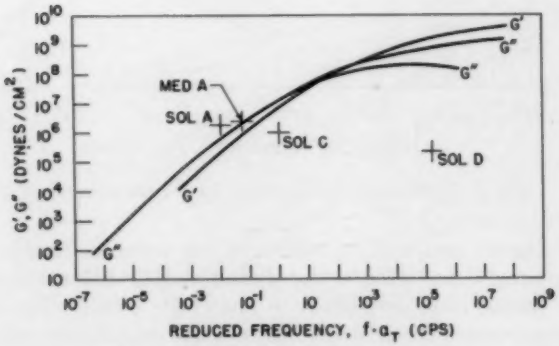

Fig. 5. Sol family reduced master curves.

family curves had a much slower change of G' and G'' with frequency as can be seen for the individual family members in Figure 5. The Medium family curves were intermediate between the Sol and Gel. From this shifting procedure it could be seen that the members of the three families behaved very much alike, with only the time scale dis-

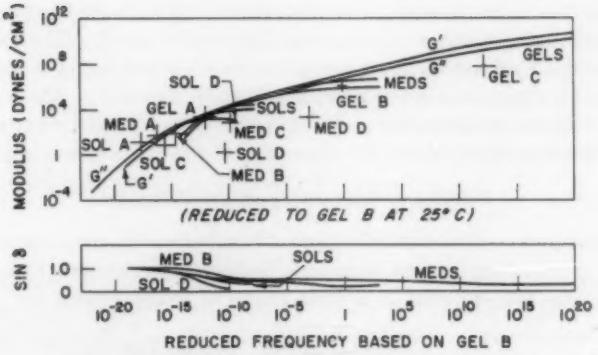

Fig. 6. Master curves for the representative curves.

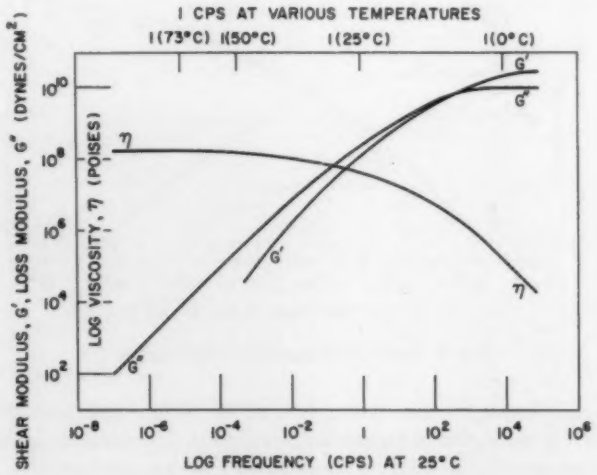

Fig. 7. Coal tar reduced curves.

placed while the three families were distinct, giving different rates of change of moduli with frequency. The similarity of the family members moreover made it possible to extrapolate the reduced curves, albeit with reduced accuracy, of each asphalt further than experimental data on the individual permitted.

The behavior of a coal tar sample and a filled asphalt (the filler was rubber) under dynamic loading was also investigated. The reduced curves for coal tar No. 150 are given in Figure 6 and the reduced curves for the rubberized asphalt are given in Figure 7. The coal tar curves appear to be similar to those for hard Sol asphalts, whereas the rubberized asphalt curves are typical of those for Medium asphalts.

Validity of the Superposition Principle

A test such as described in the preceding section has been carried out using a vibrating quartz crystal. Medium C, a representative asphalt, was investigated in a wide range of temperatures and these

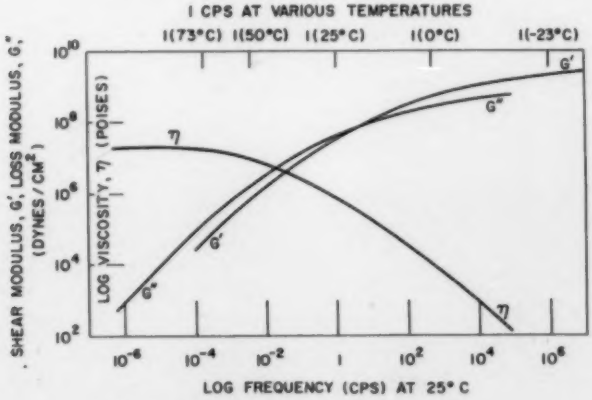

Fig. 8. Rubberized asphalt reduced curves.

ultrasonic measurements were reduced to 25°C. and another frequency by using the temperature coefficient (a_T values) determine from the use of the FIL vibration tester at low frequencies. The values measured with the torsion crystal are plotted in Figure 8 together with the reduced curves of Medium C. We see a general coincidence of values measured by the two methods. At higher temperatures or lower frequencies there is a discrepancy in G' amounting to a factor of 1.5, the values at ultrasonic frequencies being higher than the ones on the reduced curve. In G'' the discrepancy is more complicated; the ultrasonic values are larger or smaller depending on the

temperatures by a maximum factor of 2. The discrepancies are not bad considering the different modes of operation and the enormous difference in amplitudes used. The amplitudes used in the ultrasonic testing are at least 10^6 times smaller than the ones used in the FIL vibration tester. The difference may have been caused by a small amplitude dependence of G', especially since sin δ when measured by both methods was identical within error limits.

Impact Tester Data

The impact tester gives deformations of the material of the same order of magnitude as the vibration tester at frequencies higher than those obtained using the FIL vibration tester. Therefore we could check for coincidence between the values predicted from the reduced curves and those obtained experimentally with the impact tester. Table I shows this comparison and the results in most cases are quite good.

TABLE I
Experimental Check of the Superposition Principle

Material	Frequency, cycles/sec.	Impact tester		Reduced curves	
		G', dynes/cm.^{2}	Sin δ	G', dynes/cm.^{2}	Sin δ
Med D	316	6.1×10^8	0.245	10.7×10^8	0.248
	292	9.1×10^8	0.225	10.5×10^8	0.255
	407	8.6×10^8	—	11.0×10^8	—
Med C	249	2.2×10^8	0.471	1.95×10^8	—
	191	1.63×10^8	0.365	1.66×10^8	0.259
	187	1.79×10^8	0.316	1.66×10^8	0.259
Gel B	62	2.5×10^7	—	2.2×10^7	—
Med B	76	3.9×10^7	—	3.0×10^7	—
Gel C (34°C.)	114	9.9×10^7	0.318	11.5×10^7	—
Sol D (37°C.)	435	1.21×10^9	0.235	6.5×10^9	0.139
Gel C (0°C.)	219	3.8×10^8	0.287	4.1×10^8	0.238
Med C (−8°C.)	338	1.0×10^9	—	2.2×10^9	—
Med C (−2°C.)	317	$.89 \times 10^9$	—	1.40×10^9	—
Med C (−1°C.)	505	2.1×10^9	—	1.70×10^9	—

The only large discrepancies are for materials with very large stiffnesses and for measurements at low temperature where the lack of

TABLE II
Values of Log A_T for the NARC Asphalts

	−23°C.	0°C.	12°C.	25°C.	38°C.	50°C.	73°C.	95°C.
Sol A	7.08	3.58	—	0.0	—	−1.59	−2.69	—
Sol C	7.23	4.04	1.74	0.0	—	−2.50 (51°C.)	−3.86	—
Sol D	—	—	—	0.0	—	−5.61	−8.00 (71°C.)	—
Med A	7.74	4.10	—	0.0	—	−1.89	−3.17	—
Med B	8.41	4.00	—	0.0	—	−2.45 (51°C.)	−3.87	—
Med C	7.80	3.47	—	0.0	—	−3.16	−5.06	−6.82
Med D	5.04	3.13	—	0.0	—	−3.35	−5.61	−8.04
Gel A	7.61	3.93	—	0.0	—	−3.49	−5.27	—
Gel B	8.32	4.74	—	0.0	−1.87	−3.92	−7.84	−10.07
Gel C	6.92	3.04	—	0.0	—	−2.64	−4.92	−7.56

proper temperature control would make the data less reliable than that taken at room temperature. Therefore, the impact tester gives reasonably accurate results rapidly for materials which have storage moduli from 10^7 to 10^9 dynes/cm.^{2} at the frequency of test.

The Dynamic Compressibility of Asphalt

The relationship $E' = 3G'$, etc. which we used is valid only if the Poisson ratio, ν, is 0.5, i.e., if the bulk modulus (K) is much higher than the shear modulus. Measurements of the static (under steady load) compressibility of asphalts have been reported[10] and they gave values of the order of 2.5×10^{10} dynes/cm.^{2} for $(K).G'$ for very high frequencies or low temperatures may become equal to approximately 10^{10} dynes/cm.^{2} If these were the values to be used a maximum error of approximately 13% would be introduced in the calculation of G' as $E'/3$. On the other hand there has been no information as to the possible changes of the compressibility using loading with harmonic vibration of the pressure. We used the compression attachment of the FIL vibration tester[8] to investigate this point and found for Gel B that the bulk modulus was approximately 2.5×10^{11} dynes/cm.^{2} and independent of temperature and frequency. There-

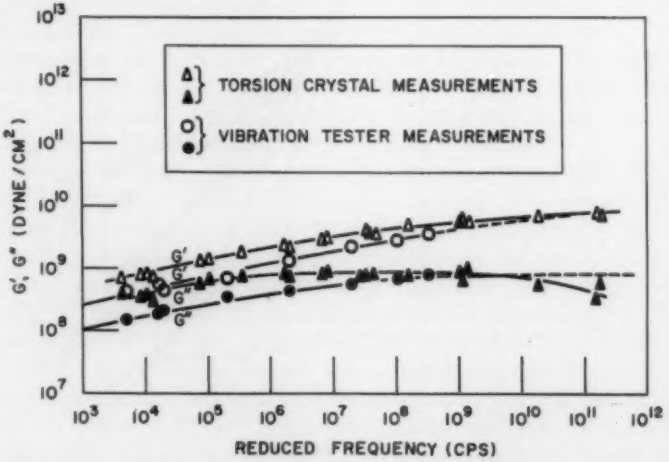

Fig. 9. Comparison of ultrasonic measurements with the reduced curves.

fore for the conditions in which we were interested our assumption was reasonable.

The Temperature Dependence of Asphalts

Having shown that the method of "reduced variables"[4] is applicable to asphalts, it becomes possible to describe their properties by three general curves. The first two, the dependence of G' and η' on the reduced frequency, are given in Figure 4. The third one, the temperature dependence of the shift factor a_T, which is essentially the

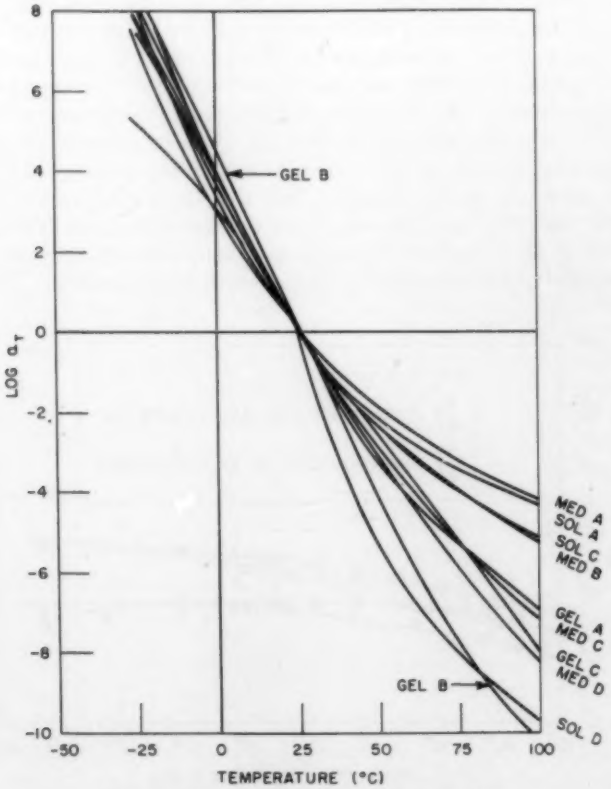

Fig. 10. Temperature dependence of a_T values.

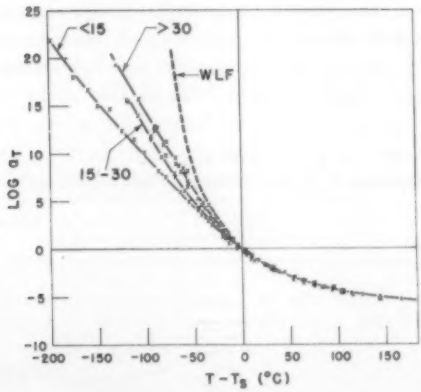

Fig. 11. Williams-Landel-Ferry plot of a_T values.

temperature dependence of the Newtonian viscosity, will be given in this section.

The temperature reduction factor a_T had been obtained for each asphalt during the shifting process required to obtain the "reduced curves." The experimental values are given in Table II. These values are then plotted as a function of temperature on Figure 9. No points are given because it would cause confusion in this figure. These then are the second general curves and we may say that the dynamic behavior of our representative asphalts are completely known over very wide ranges of time and temperature.

Recently, Williams, Landel and Ferry[11] have found that upon choosing suitably a separate reference temperature, T_s, for each system, and expressing a_T as a function of $T - T_s$, this function turns out to be identical for a wide variety of polymers and their solutions. This has also been found true for all the asphalts investigated here. In Figure 10 we see that all the asphalts form one curve from $T - T_s$ equal to -25°C. to $T - T_s$ equal to 150°C, but below $T - T_s$ equal to -25°C. one has three distinct curves which can be differentiated by using penetration values.[1] The data from $T - T_s$ equal to -25°C. to $T - T_s$ equal to 150°C. agrees with the WLF function. Ferry and his associates have also found that the T_s temperatures determined are approximately the glass temperature plus 50°C. As we have no

measurements of the glass temperatures of the asphalts, we cannot correlate T_g and T_s but it is interesting to note that the reference temperatures, T_s, found are very similar in value to the ring and ball softening points.[1] This is shown in Table III.

TABLE III
Correlation of T_s with Ring and Ball Softening Point

Material	T_s, °C.	Softening point, °C.
Gel A	65.5	52.8
Gel B	106	89.5
Gel C	174	168.2
Med A	44	44.5
Med B	56	56.6
Med C	84	88.4
Med D	137	148.2
Sol A	34	38.9
Sol C	56	58.4
Sol D	86	84.5

Distribution of Relaxation Times

In order to discuss the mechanical properties of asphalts unimpeded by the necessity of having two curves, G' and G'', one can reduce them to a single curve by the calculation of the distribution of relaxation times. The method developed by Williams and Ferry[12] was used and the results are shown in Figure 11. These curves of the distribution of relaxation times are also more amenable to theoretical interpretations.

In some cases the time scale was extrapolated to the cutoff region at long times by using the family curves. The accuracy of this extrapolation was enhanced by imposing the condition that the extrapolated dynamic viscosity at long times equal the Newtonian viscosity determined by the use of rotational or capillary viscometers. The most notable case of this extrapolation was for the Gel C asphalt.

The theory of Rouse[13] describing the viscoelastic properties of dilute solutions of linear coiling polymers has been extended by Ferry, et al.[14] to undiluted linear polymers. These predict the mechanical properties from the physical chemical composition of the

polymer However, one can reverse the process and estimate the mass of the flow particles acting in dynamic tests from the known mechanical properties.

Rouse's theory predicts a series of discrete relaxation times associated with the changes of configuration of the polymer molecules. By suitable mathematic manipulation, using the second approximation of the mechanical relaxation distribution of Ferry,[12] one obtains:

$$\Phi = 0.90 \left(\frac{3\eta\rho RT}{16M} \right)^{1/2} \tau^{-1/2} \tag{3}$$

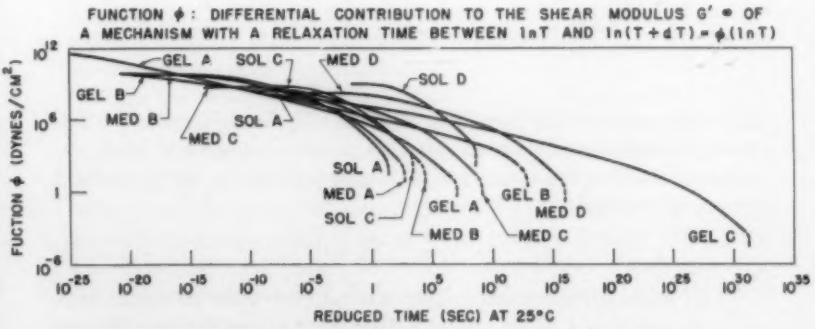

Fig. 12. Distribution of relaxation times of representative asphalts.

This equation predicts a dependence of Φ on $\tau^{-1/2}$. In Figure 11 we see that this dependence is found only in a rather short range toward long times. This range is that in which the large units, whole molecules, are moving. By rearranging eq. (3) one obtains:

$$M = 0.152\eta\rho RT/\tau\Phi^2 \tag{4}$$

Therefore, if one determines Φ and τ at the point on the log Φ vs. log τ plot where the theoretical slope of $-1/2$ is obtained and uses the Newtonian viscosity determined by steady-state instruments,[2] one can solve for the molecular weight by using the above equation. This molecular weight would be a highly weighted one. This was done for the ten representative asphalts and the results are given in Table IV. These molecular weights are the only estimates that are available of the size of the asphalt flow units. However, Scott and Cunningham[15] have obtained electron microscope pictures of asphalts

TABLE IV
Molecular Weights of Representative Asphalts

Materials	Molecular weight
Gel A	1.6×10^7
Gel B	5.6×10^7
Gel C	3.3×10^8
Med A	5.8×10^4
Med B	1.8×10^5
Med C	2.8×10^5
Med D	4.3×10^6
Sol A	9.9×10^4
Sol C	1.5×10^5
Sol D	2.2×10^5

that are similar to Medium B or Medium C. They found a fine network of small particles about 200 A. in diameter which are tightly associated. Using the functional relationship between size and weight for a coil[16] one has:

$$M = m \cdot {}^3/_4 (L/b)^2 \tag{5}$$

If we assume the monomer unit is a $—CH_2—$ unit we would have $m = 14$ and $b = 1.54$ A. Substituting these values into eq. (5), one obtains a molecular weight of 1.8×10^5. This is in reasonable agreement with the values of 1.8×10^5 for Medium B and 2.8×10^5 for Medium C which were obtained from rheological data.

Discussion

The reduced curves of the individual asphalts shown in Figure 4 exhibit the behavior of viscoelastic liquids in agreement with the findings of the second paper[2] in this series. No plateau region was found when the storage modulus is of the order of 10^7 dynes/cm., and this indicates that there can be but few crosslinks or entanglements present. At low temperatures and high frequencies all the asphalts have similar properties, the moduli approach a value of 10^{10} dynes/cm. which seems to be common to the whole class of "hard" plastics. The main differences between asphalts occur in the low frequency range or for that matter at high temperatures. In that region the Sol asphalts quickly turn to Newtonian liquids and have appreciable creep. On

the other hand, the Gel asphalts retain their dimensional stability due to the high viscosity up to much higher temperatures.

The agreement between data obtained at high frequencies and the values predicted by superposition of low frequency, low temperature measurements supports the validity of Ferry's time-temperature superposition technique and supplements the experimental proof already found in the literature.[17] The acceptance of the validity of Ferry's method of "reduced variables" then makes it possible to describe the rheological properties of the asphalts by three general curves: the dependence of G' and η' on the reduced frequency and the temperature dependence of the reduction factor, a_T. This reduction factor is found to obey the empirical Williams-Landel-Ferry equation over a wide range of temperature.

From the reduced curves it was possible to compute the distribution of relaxation times for the asphalts. Making use of Rouse's theory it was then possible to estimate the molecular weights from the curves giving the distribution of relaxation times. These molecular weights were found to be quite large. They may be in error since we are extrapolating a theory derived for completely flexible linear polymer molecules to a system as complex as asphalt. However, these are our only estimates of size and must suffice until other measurements are made.

Conclusions

There are several conclusions that can be drawn from the investigations reported here.

(*1*) The moduli versus frequency curves show that asphalts are viscoelastic liquids similar to polymer solutions. The lack of a plateau region indicates that there are no crosslinks or entanglements present.

(*2*) The principle of time-temperature superposition is valid for asphalts.

(*3*) The temperature dependence of asphalts is similar to that of linear polymers and obeys the empirical WLF equation over a wide range of temperature.

(*4*) Asphalts apparently contain rather large flow units.

The authors wish to express sincere gratitude to the sponsoring companies who supported the National Asphalt Research Center.

Also gratefully thanked are Mr. R. Hollinger, who gathered the impact tester data, and Dr. K. Sittel, who obtained the data with the torsion crystal.

References

1. Brodnyan, J. G., *Highway Research Board, Bull.* No. **192,** 1 (1958).
2. Gaskins, F. H., J. G. Brodnyan, W. Philippoff and E. Thelen, to be published.
3. Van der Poel, C., *Proc. 2nd Intern. Rheol. Congr., Oxford* (1953); *J. Appl. Chem. (London),* **4,** 221 (1954).
4. Ferry, J. D., E. R. Fitzgerald, L. D. Grandine, and M. L. Williams, *Ind. Eng. Chem.,* **44,** 703 (1952).
5. Philippoff, W., *J. Appl. Phys.,* **25,** 1102 (1954).
6. Philippoff, W., *J. Appl. Phys.,* **24,** 685 (1953).
7. Gaskins, F. H., and W. Philippoff, *Ind. Eng. Chem.,* **51,** 871 (1959).
8. Philippoff, W., and J. G. Brodnyan, *J. Appl. Phys.,* **26,** 846 (1955).
9. Rouse, P. E., and K. Sittel, *J. Appl. Phys.,* **24,** 690 (1953).
10. *The Properties of Asphaltic Bitumen,* J. Pfeiffer, ed., Elsevier, New York, 1950, pp. 92–93.
11. Williams, M. L., R. F. Landel, and J. D. Ferry, *J. Am. Chem. Soc.,* **77,** 3701 (1955).
12. Williams, M. L., and J. D. Ferry, *J. Polymer Sci.,* **11,** 169 (1953).
13. Rouse, P. E., Jr., *J. Chem. Phys.,* **21,** 1272 (1953).
14. Ferry, J. D., R. F. Landel, and M. L. Williams, *J. Appl. Phys.,* **26,** 359 (1955).
15. Scott, F. S., and O. D. Cunningham, Union Oil Co. of California, private communication.
16. Treloar, L. R. G., *The Physics of Rubber Elasticity,* 2nd ed., Oxford Press, 1958.
17. Philippoff, W., K. Sittel, J. D. Ferry and D. J. Plazek, *SPE Journal,* **11,** No. 7, 7 (1955).

Synopsis

The dynamic mechanical properties of ten asphalts, representing three major categories, have been determined using a variety of instruments. The validity of the time-temperature superposition principle was established by the agreement between data obtained at high frequencies and values predicted by superposition of low frequency, low temperature, measurements. This made it possible to describe the properties of asphalts by three general curves: the dependence of G' and η' on the reduced frequency and the temperature dependence of a_T. These curves have been determined experimentally. The curves of the moduli versus reduced frequency cover approximately twenty-three decades of reduced frequency at 25° C. The temperature dependence was seen to be that given by the Williams-Landel-Ferry equation over a wide range of temperature. The characteristic temperature, T_s, was found to be nearly equal to the Ring and Ball softening points of the asphalts. Other bitumens, such as coal tar and a filled asphalt, have the same general characteristics. A rearrangement of Rouse's theoretical equations as modified by Ferry made it possible to estimate the molecular weights of the flow units and these were seen to be quite large.

TRANSACTIONS OF THE SOCIETY OF RHEOLOGY IV, 297–313 (1960)

Thermodynamics of Stretching of Nylon Fibers*

MALCOLM L. WILLIAMS, *Research Center, The Chemstrand Corporation, Decatur, Alabama*

Introduction

One of the approaches used to relate the mechanical properties of polymeric materials to their structure involves the application of thermodynamics to an extension process. For rubber, the force of extension is found to be primarily related to a decrease in entropy of the sample. One mechanism which satisfies these thermodynamic results is the change of a polymeric coil from a random to a more extended, consequently more ordered, conformation. The application of statistical mechanics to this mechanism leads to the theory of rubberlike elasticity, which has been quite successful for amorphous polymers in relating mechanical properties in extension to structure, i.e., chain conformation.

This investigation has applied the thermodynamic approach to a semi-crystalline polymer—nylon. The objective was to determine whether the extension properties of nylon could be explained in terms of rubberlike elasticity. In structural terms, can the crystalline areas be postulated as being rather large crosslinking points with the amorphous regions behaving in a manner analogous to that of vulcanized rubber? In thermodynamic terms, is the force of extension primarily related to an entropy change on stretching? Before considering these questions, the general thermodynamics of stretching will be reviewed with particular emphasis on the comparisons and contrasts when amorphous and semi-crystalline polymers are the materials to be studied. Details of the derivation and its application to rubber can be found in Flory's book.[1]

* Contribution No. 61 from the Research Center of The Chemstrand Corporation.

Theory

Application of the first and second laws of thermodynamics to the equilibrium stretching of an elastic body results in

$$dE = TdS - PdV + fdL \tag{1}$$

where f is the equilibrium external force required to maintain the reversible extension dL, and L is the length of the sample. The other symbols have their usual meaning.

Equation (1) can be substituted in the differential form of the expression for either the free energy F or the work function A. The results are

$$f = \frac{(\partial H)}{(\partial L)_{T,P}} - T\frac{(\partial S)}{(\partial L)_{T,P}} = \frac{(\partial H)}{(\partial L)_{T,P}} + T\frac{(\partial f)}{(\partial T)_{P,L}} \tag{2}$$

and

$$f = \frac{(\partial E)}{(\partial L)_{T,V}} - T\frac{(\partial S)}{(\partial L)_{T,V}} = \frac{(\partial E)}{(\partial L)_{T,V}} + T\frac{(\partial f)}{(\partial T)_{V,L}} \tag{3}$$

Any mechanism devised to explain the extension process must predict enthalpy (or energy) and entropy changes in accordance with these equations, but thermodynamics cannot predict possible mechanisms; it can serve only as a check for consistency of a *proposed* mechanism. It cannot ascertain what the mechanism is, nor if the *correct* mechanism has been chosen.

Experimentally, measurements are performed under constant pressure conditions and the application of eq. (2) to most of the data for natural rubber results in the enthalpy term being small, with the slope $(\partial f/\partial T)_{P,L}$ positive. Thus the force is primarily due to an entropy effect. However, for extensions less than 10%, it was found that the slope $(\partial f/\partial T)_{P,L}$ is negative, thus requiring an appreciable value for the enthalpy term. The explanation suggested[2] for this thermoelastic inversion was that there is a slight volume expansion on stretching due to the lowering of the *internal* pressure by the *external* tensile force. If true, the inversion would disappear if eq. (3) (constant volume conditions) were used instead of eq. (2) (constant pressure conditions).

Since the maintenance of constant volume involves experimental difficulties, the following approximation was proposed and experimentally verified[2] for natural rubber.

$$\frac{(\partial f)}{(\partial T)_{V,L}} \approx \frac{(\partial f)}{(\partial T)_{P,\lambda}}$$

Here λ is the ratio of extended length L to initial length L_0. Use of this approximation to obtain $(\partial f/\partial T)_{V,L}$ did indeed result in the elimination of the thermoelastic inversion.

In accordance with this observation, "rubberlike" behavior is defined *in thermodynamic terms* as a positive value of $(\partial f/\partial T)_{V,L}$ while "ideal rubberlike" is defined as $(\partial E/\partial L)_{V,T}$ equal to zero or the equivalent statement f equal to $T(\partial f/\partial T)_{V,L}$.

Some seventy years after the first application of these thermodynamic equations to data on rubber, a mechanism was proposed to account for them. The essential step was the concept of a polymer as a long flexible chain. The most probable conformation of such a chain is a random coil. Therefore, the equilibrium force of extension is required to maintain the chains in an extended, less probable conformation—an entropy effect. The application of statistical mechanics has produced the theory of rubberlike elasticity where rubberlike *in terms of mechanism* refers to the extension of this random coil.

Thus, the use of the word rubberlike is ambiguous. Any given material may be similar to rubber thermodynamically but yet have a different mechanism. Correspondingly, the energy and entropy effects associated with the uncoiling of chains may be masked by thermodynamic effects related to polymer-solvent interactions or change of phase.

In this investigation of extension properties, attention is focused first on the thermodynamic similarities between nylon and rubber. Secondly, it will be pointed out what would be involved if a similar mechanism were applicable.

Application to Crystalline Polymers

Consider three general types of mechanical deformation of a solid body.

Reversible Extension of an Elastic Body (Fig. 1a). The application of the stress alters the size and/or shape of the body; however, removal of the stress restores the original dimensions, indicating that the body is elastic. The course of the deformation is the same on both loading and unloading, so each stress S_i is unambiguously associated with a single extension ΔL_i or strain $\Delta L_i/L_0$, where L_0 is the original

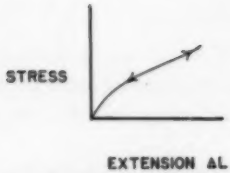

Fig. 1a. Reversible extension of an elastic body.

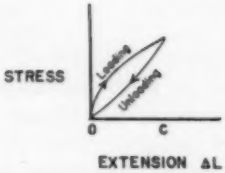

Fig. 1b. Irreversible extension of an elastic body.

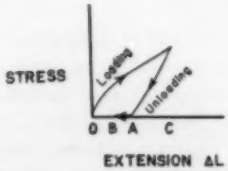

Fig. 1c. Irreversible extension of a non-elastic body.

length. Thus, the deformation of this elastic body proceeds by a reversible path. It is *only* for this type of extension that eqs. (2) and (3) above are valid, for they are derived on the basis of equilibrium thermodynamics.

Irreversible Extension of an Elastic Body (Fig. 1b). The difference between the loading and unloading cycles indicates that there is a loss of energy during the deformation process. The magnitude of the hysteresis depends upon the rate of the extension process. The recovery is complete, indicating an elastic body.

For a given extension, there are now two stresses, or for a given stress, there are two extensions. Should the strain be defined as $\Delta L_i/L_0$ and some choice made of the stress? Alternatively, is the loading stress associated with a tensile strain $\Delta L_i/L_0$ while the unloading stress is associated with a compressive strain $(C - \Delta L_i)/(L_0 + C)$?

Irreversible Extension of a Non-Elastic Body (Fig. 1c). Most of the extension remains as a quasi-permanent orientation ($\overline{OA}$) when the stress is removed; the distance $\overline{AC}$ or ΔL_r being the immediately recoverable extension. The term "quasi-permanent" is used since the amount of orientation of an extended sample under zero stress depends on the mechanical and thermal history prior to the time of measurement of the orientation. That is, the sample of length L_0

$+ A$ may shrink under zero stress to a length $L_0 + B$ after some period of time or it may be quenched to some lower temperature maintaining its length.

Considering the time dependence of polymer mechanical properties, it is conceivable that $\overline{OB}$ does not represent a permanent set but rather a limit imposed by the length of time the shrinkage is observed. Therefore, it is a moot question whether such an oriented body is in a true thermodynamic equilibrium state, a metastable state, or a state where the disorientation process is occurring at some rate, albeit infinitesimally slow.

According to the literature, the extension of rubber is thermodynamically irreversible; it is considered elastic for there is a very small amount of permanent set when the stress is removed. In order to avoid the rate or time dependence, a particular kind of mechanical conditioning step has been used in stress-temperature experiments on rubber. This procedure is extension at the highest temperature to be used, followed by a period of stress relaxation for several hours.

The extension of nylon, on the other hand, not only is thermodynamically irreversible but also most of the extension remains as a permanent orientation.

The contrast is that rubber, under zero stress, is isotropic with the polymer chains in a random coil conformation and the equilibrium tension f is then related to the stretching of these random coils. However, with nylon, a sample under no load may range from the completely isotropic to a highly oriented state. It would be expected that the orientation resulting from the application of a force will depend on the previous orientation of the nylon sample. The effectiveness of a force in producing orientation may depend on the per cent crystallinity. Also, interactions between crystallinity and orientation may be important. In thermodynamic terms, specifying T, P, and L_0 for a rubber sample means an unoriented sample at T and P under zero tension. However, for nylon, these three variables are not enough to define the state of the sample. At the present time, it is not known what additional variables are required to specify the state.

Since an undrawn nylon sample does not return to its original dimensions when the stress is removed, it is clear that the extension process is not reversible. However, after a mechanical conditioning step similar to that used for rubber, it is found experimentally that the force as a function of temperature for a given individual fiber is

thermodynamically reversible, since there is no hysteresis. Therefore, valid thermodynamic data can be obtained for crystalline fibers and indeed have been reported for nylon[3] and various cellulosics.[4] In the opinion of the present author, there have been several omissions in the interpretation of such data. (*1*) The possibility of a thermoelastic inversion due to a volume dilation on stretching has not been considered. (*2*) While measurements are made at constant length, it is usually necessary to convert this length into an elongation or strain which must be an equilibrium value corresponding to the equilibrium force; this strain is not necessarily the total strain imparted to the sample. (*3*) As recently discussed,[5] the effects of the heat exchange medium on the sample may be of some importance. (*4*) It must be remembered that rubberlike in thermodynamic terms does not imply the same extension mechanism found in rubber.

Experimental

The samples used were *undrawn* nylon monofilaments, approximately 100 μ in diameter. They contained no additives or visible spherulites. The equipment is sketched in Figure 2. A motor drives the screw, *A*, at a constant velocity of 0.354 cm./min. The arms, *B*, are constructed of Invar to minimize thermal expansion. The fiber, *C*, is attached to the screw by means of a clamp, *D*. A similar type of clamp connects the fiber to a Statham strain gage, *F*. The lower part of the assembly (below *L*) is placed in a beaker containing silicone oil

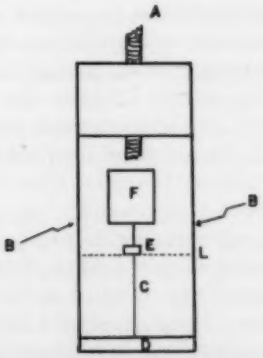

Fig. 2. Experimental arrangement for stress-temperature measurements.

(Dow Corning 550). A nichrome wire heater in the bottom of the beaker is the heat source. Agitation is provided by a magnetic stirrer. Cooling is accomplished by placing Dry Ice on the outside of the beaker.

The experimental procedure for the stress-temperature experiments was to thermally relax a sample by heating at 160°C. under zero load for 30 minutes. After quenching to room temperature, the initial diameter (d_i) was measured microscopically. The filament was placed in the apparatus, reheated to 160°C. and extended an amount, ΔL, between 2 and 50% of the original length L_0. The decay of stress with time was followed for approximately 4 hours, keeping the filament at constant length. The temperature was then lowered to 10°C. and raised to 160°C. with the force measured at 10°C. intervals. At any temperature, the forces recorded during heating and cooling were averaged provided there was no hysteresis between the two cycles. At 160°C., the length of the fiber was decreased at the same rate as the original extension; the force decreased at the same time. When the force reached zero, corresponding to a contraction ΔL_r, the filament was quenched to room temperature and the final diameter (d) measured. A separate filament was used for each stress-temperature experiment.

In an additional experiment, the coefficient of linear expansion was measured on various undrawn nylons. The technique used was to mount the fiber and, at any temperature, extend it until just taut, as indicated by a slight deflection of the strain gage. The length was then measured with a cathetometer. The volume coefficient of thermal expansion is computed to be 4.88×10^{-4} in the range 80 to 160°C., in excellent agreement with the value of 4.85×10^{-4} reported in the literature.[6]

A comparison of the tenacity and elongation of drawn fibers heated for 30 minutes at 160°C. in both silicone oil and dry nitrogen indicates no effect of silicone oil.

Calculations

From the measured diameters at room temperature and the coefficient of linear expansion, the diameters in the unstretched state at 160°C. can be computed. If constant volume stretching is assumed, the diameters in the stretched state can be calculated from the known extension. These diameters are used in converting the force measured

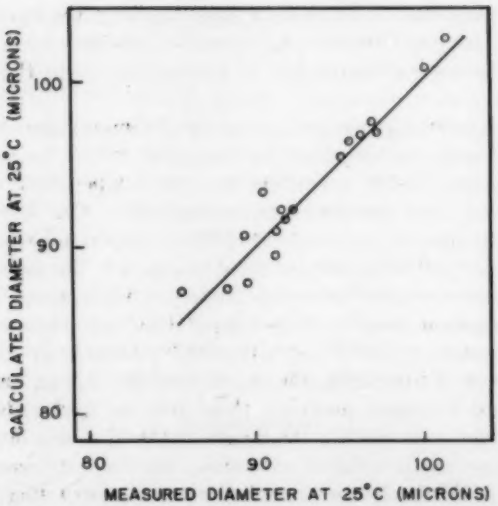

Fig. 3. Calculated diameters versus measured diameters at completion of stress-temperature experiments. Line is drawn with unit slope.

in grams to a stress in dynes/cm.^{2}. Assuming the retraction to be also at constant volume gives the diameters at 160°C. under zero force at the completion of the stress-temperature experiments. Finally, under the assumption that the coefficient of linear expansion of undrawn nylon is applicable, the diameters at room temperature are computed and are compared with the measured values in Figure 3. The agreement indicates that all these assumptions are reasonably correct. It is especially noted that although the importance of volume changes in interpreting the thermodynamics has been stressed, the absolute value of these volume changes is not enough to affect calculations of diameter under load.

The initial length L_0, the extension ΔL, and the initial contraction ΔL_r for the filaments are measured at 160°C. The total $(\Delta L/L_0)$, quasi-permanent $((\Delta L - \Delta L_r)/L_0)$, and recoverable $(\Delta L_r/(L_0 + \Delta L - \Delta L_r))$ extensions in per cent have been calculated. These latter two are labeled quasi-permanent and recoverable with some reserve. When the fibers are quenched to room temperature, there is no further change in length; however, if left at 160°C. there is continued

shrinkage under zero load. The amount of this shrinkage as a function of time has not been quantitatively determined. Furthermore, the experiment was conducted at a given constant rate of extension and nothing is known about the effect of rate. Based on these extensions, various quantities which refer to a non-equilibrium state of the material can be defined.

Total extension ratio:

$$\lambda_t = 1 + \frac{\Delta L}{L_0} = \frac{L_0 + \Delta L}{L_0} \tag{4}$$

Quasi-permanent extension ratio:

$$\lambda_e = 1 + \frac{\Delta L - \Delta L_r}{L_0} = \frac{L_0 + \Delta L - \Delta L_r}{L_0} \tag{5}$$

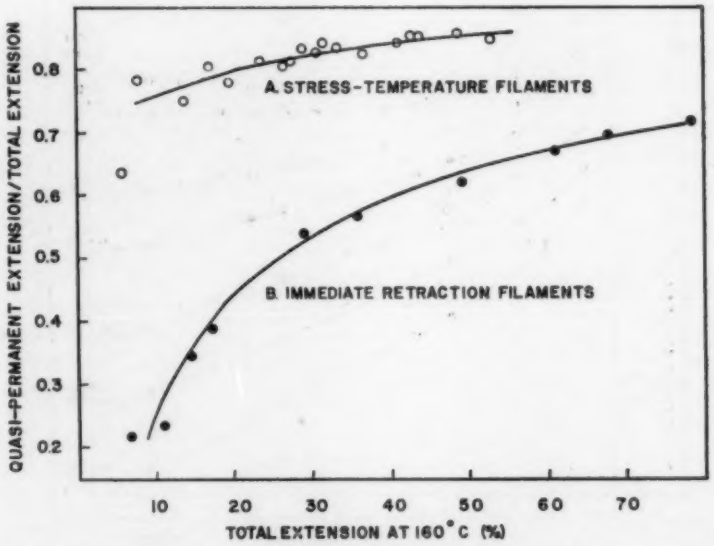

Fig. 4. Percentage of extension which is quasi-permanent as a function of total extension. (A) Filaments at completion of stress-temperature experiments. (B) Filaments retracted immediately following original extension.

Immediately recoverable extension ratio:

$$\lambda_a = 1 + \frac{\Delta L_r}{L_0 + \Delta L - \Delta L_r} = \frac{L_0 + \Delta L}{L_0 + \Delta L - \Delta L_r} \tag{6}$$

It is seen that $\lambda_t = \lambda_c \lambda_a$, and that only λ_t and λ_c are based on the same length L_0. These definitions can be illustrated by referring to a usual textile test where a nylon of draw ratio 5.00 is extended 4%. The quasi-permanent extension ratio would be 5.00; the immediately recoverable extension ratio would be 1.04; the total extension ratio would be 5.20.

The non-elastic nature of nylon is illustrated in Figure 4, Curve A, where the ratio of quasi-permanent to total elongation is plotted against total elongation. Curve B illustrates the same ratio for filaments retracted immediately after extension. Even in the absence

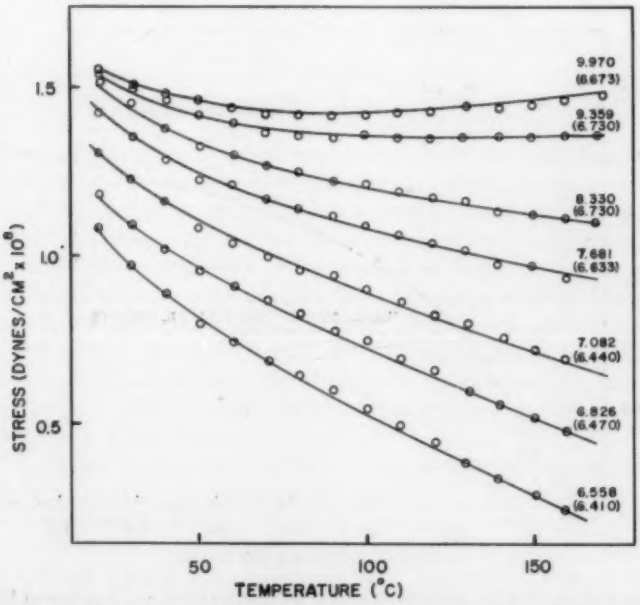

Fig. 5. Stress as a function of temperature for fibers held at constant extended length. Original lengths in parentheses.

of stress relaxation at constant length, a substantial amount of the total extension is not immediately recoverable.

The stress-temperature results are plotted in Figure 5 for several of the fibers of various extended lengths. In discussing mechanical

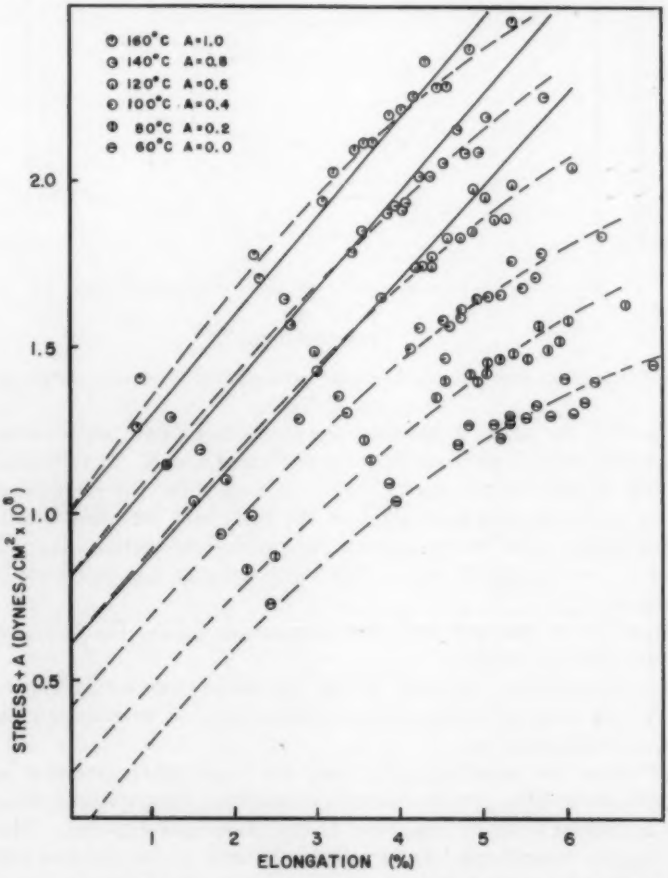

Fig. 6. Stress-strain curves calculated from data of Fig. 5. Dashed lines are smooth curves drawn through the points. Solid lines drawn according to eq. (8). Curves displaced along ordinate by amount A for clarity.

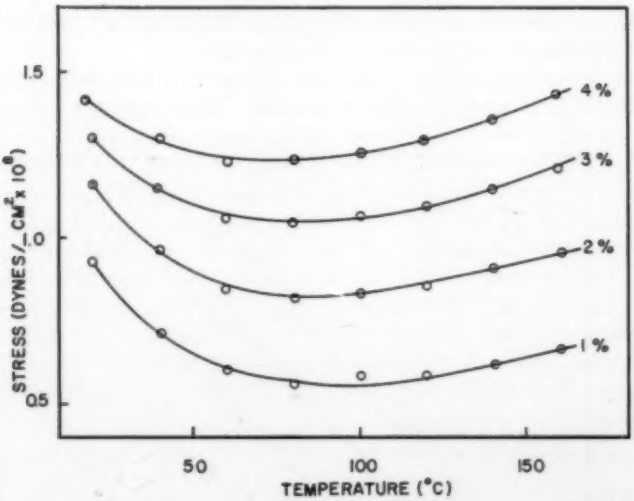

Fig. 7. Stress as a function of temperature for fibers held at constant elongation.

properties, the relevant variables are stress and strain, while in the thermodynamic derivation, they are force and length. If the initial sample dimensions are normalized to a unit cube, the mechanical stress and strain are equivalent to the force and extended length, respectively. The thermodynamic quantities calculated here will refer to 1 cc. at 160°C. rather than the customary 1 g. or 1 mole of material.

In order to interpret the stress-temperature data, the following assumptions are made:

(*1*) The stresses measured during the stress-temperature experiments are close to the equilibrium values required to maintain the recoverable extension.

(*2*) From the experimentally measured recoverable extension at 160°C., extensions can be calculated at lower temperatures using the coefficient of linear expansion of the unoriented material. This assumption is considered to be valid in the light of the diameter calculations given previously.

Assumption (*1*) is only approximately true. Since the fiber will continue to shrink under zero load, the measured stress must contain

TABLE I
Internal Energy and Entropy Components of the Stress for the Extension of Nylon

Temp., °C.	f, dynes/cm.^{2} × 10^8	$\frac{T(\partial f)}{(\partial T)_{P,\lambda}} = -\frac{(\partial S)}{(\partial L)_{V,T}}$, dynes/cm.^{2} × 10^8	$\frac{(\partial E)}{(\partial L)_{V,T}}$, dynes/cm.^{2} × 10^8
		Strain = 2%	
150	0.63	1.02	−0.39
140	0.61	0.83	−0.22
130	0.59	0.64	−0.05
120	0.58	0.47	+0.11
110	0.57	0.31	0.26
100	0.56	0.11	0.45
		Strain = 3%	
150	0.92	1.18	−0.26
140	0.90	1.03	−0.13
130	0.87	0.85	+0.02
120	0.85	0.67	0.18
110	0.84	0.54	0.30
100	0.83	0.34	0.49
		Strain = 4%	
150	1.17	1.10	+0.07
140	1.15	1.03	0.12
130	1.12	0.97	0.15
120	1.10	0.86	0.24
110	1.08	0.73	0.35
100	1.06	0.60	0.46
		Strain = 5%	
150	1.39	1.35	+0.04
140	1.35	1.28	0.07
130	1.32	1.17	0.15
120	1.29	1.06	0.23
110	1.27	0.88	0.39
100	1.24	0.67	0.57

a component to maintain this additional length. If the recoverable strain is used, the measured stress is too high. If the total measured stress is used, the recoverable strain is too low. Clearly this state of the material is not one of equilibrium. Nevertheless, the thermodynamics of stretching will be applied to the measured values of the stress and immediately recoverable strain.

Figure 5 represents the stress as a function of temperature for various values of extended length. At constant temperature the ordinates of the curves give the stress as a function of extended length. This extended length can be converted into a strain by taking into account, at each temperature, the effect of thermal expansion on the known unextended length. The resulting stress-strain curves are shown in Figure 6 where the dashed lines represent smooth curves drawn through the experimental points.

At constant strain, the ordinates of the curves of Figure 6 give the stress at constant elongation as a function of temperature, shown in Figure 7. This procedure of converting from stress at constant extended length (Fig. 5) to stress at constant elongation (Fig. 7) is identical with that used for rubber.

The slopes of the curves of Figure 7 have been measured for temperatures greater than 100°C. The approximation that $(\partial f/\partial T)_{V,L}$ equals $(\partial f/\partial T)_{P,\lambda}$ is considered to be valid. It is seen that, for temperatures greater than 80°C., the slope of $(\partial f/\partial T)_{P,\lambda}$ is positive for all elongations in contrast to the data of Figure 5. Therefore, rubber-like behavior is indicated and the minimum of the curves of Figure 7 around 80°C. represents a glass to rubber transition. In harmony with this result, from the maximum of the loss tangent-temperature curves, measured in a dynamic experiment, Woodward et al.[7] report a transition temperature of 77°C. The entropy component of the stress $T(\partial f/\partial T)_{P,\lambda}$ has been computed and compared to the total stress in Table I. The internal energy component of the total force is smaller than the entropy component; however, the data are not precise enough to decide if the rubber-like behavior is ideal.

Discussion

The structure of nylon is normally approximated as a mixture of crystalline and amorphous regions. In terms of this structure, these mechanical results are suggestive of the following mechanism. The amorphous areas are crosslinked by the crystallites. The application of an external stress orients both structural types. As the crystallites rearrange to be in equilibrium with the new extended length, the stress decreases. The extended amorphous regions do not equilibrate but return to their original conformation on release of the stress. Since the fiber continues to shrink under zero load, the crystallites

also may disorient to some extent, possibly at a much slower rate than the amorphous areas. The extension of these amorphous regions and their subsequent recovery is at least thermodynamically similar to the behavior of a vulcanized rubber, and this behavior is independent of the orientation of the crystallites. In order to make a quantitative comparison, a highly crosslinked rubber should be considered since the degree of crystallinity of nylon is probably high enough to prevent the amorphous chain conformations from being Gaussian.

If the statistical treatment of rubber-like elasticity is applicable, the stress-strain curves of Figure 6 are described by:

$$S = KT\left(\lambda_a^2 - \frac{1}{\lambda_a}\right) \tag{7}$$

which, for $\lambda_a \approx 1$ reduces to

$$S = 3KT(\lambda_a - 1) \tag{8}$$

Here, S is the stress based on *actual* cross section, K is a constant, T is the absolute temperature, and the extension ratio λ_a is equal to $1 + \epsilon_a$, where ϵ_a is the strain. The straight lines of Figure 6 have been drawn using a value of K of 2.36×10^6 dynes/cm.^{2} degree, and reasonably good agreement is obtained.

Young's modulus E is equal to $3KT$ and is computed to be 3.06×10^9 dynes/cm.^{2} at 160°C., some hundredfold higher than for a typical rubber.[8]

Since $E = \rho RT/M_c$, the molecular weight between crosslinks M_c can be calculated to be 11.

From low angle x-ray results, Hess[9] obtains a repeat distance along the chain of 74 to 88 A., depending on pre-treatment. If this distance approximately represents the crystallite length, it would correspond to a molecular weight of 970 to 1150. Since the fiber is approximately 50% crystalline, one would expect the molecular weight of the amorphous chains between crystallites to be of the same order of magnitude.

If the crystallites were considered similar to reinforcing fillers for the network, the modulus of the system would be increased by a factor depending primarily on the volume concentration of filler. Since Bueche has shown[10] that 15% filler can increase the modulus by a factor of 12, it is conceivable that the modulus of the filled, i.e., semicrystalline network, might be two orders of magnitude higher than that of the unfilled, i.e., amorphous only, network.

When these results are discussed in terms of crystalline and amorphous regions, several additional inherent assumptions should be noted. The immediately recoverable strain has been computed from the changes in length of the entire fiber, but this strain has been associated only with the amorphous areas. Since these amorphous areas are roughly one-half of the fiber, the deformation is not affine, in contrast with rubber. Furthermore, it has also been assumed that there is no change of phase on stretching or, if present, it is unimportant.

The effects of several potentially important variables have not been studied. Among these are the presence of spherulites, the thermal pretreatment, and the rate of the extension.

Any quantitative description of the extension mechanism will depend upon a statistical mechanical treatment of the semi-crystalline state. Such treatment may well depend on the proper choice of a model analogous to the random coil used for rubber.

Beyond these questions of mechanisms and the proper structural units to use, the thermodynamic analysis depends on three main assumptions: (*1*) The immediately recoverable part of the extension is sufficiently reversible that equilibrium thermodynamics can be applied. (*2*) The stresses measured are values associated only with these recoverable strains. (*3*) The thermodynamic effect of volume changes due to stretching can be eliminated in a manner similar to that used for rubber.

This work is presented only as a first approximation to the extensional behavior of nylon. Primarily it points out some of the problems in applying the thermodynamic approach to the extension of a semi-crystalline polymer. Solving of these problems may aid in the use of mechanical properties for casting light on the structure of semi-crystalline polymers.

The author wishes to thank Dr. Thomas W. DeWitt for his constant encouragement during the course of the work, and Dr. Alberto Ciferri for many helpful discussions on critically reviewing the manuscript. The author is indebted to Mr. B. G. Johnson and Mr. E. P. Staley for securing the experimental results. Appreciation is expressed to The Chemstrand Corporation for permission to publish the results.

References

1. Flory, P. J., *Principles of Polymer Chemistry*, Cornell Univ. Press, Ithaca, New York, 1953, pp. 432–494.

2. Gee, G., *Trans. Faraday Soc.*, **42,** 585 (1946); G. Gee, J. Stern, and L. R. G. Treloar, *ibid.*, **46,** 1101 (1950); F. G. Hewitt and R. L. Anthony, *J. Appl. Phys.*, **29,** 1411 (1958).

3. Bryant, G. M., *Textile Research J.*, **23,** 788 (1953).

4. Roseveare, W. E., and L. Poore, *J. Polymer Sci.*, **14,** 341 (1954), *Textile Research J.*, **25,** 709 (1955); G. M. Bryant and H. Wakeham, *Textile Research J.*, **25,** 224 (1955).

5. Passaglia, E., and H. P. Koppehele, *J. Appl. Polymer Sci.*, **1,** 28 (1959).

6. Boyer, R. F., and R. S. Spencer, *J. Appl. Phys.*, **15,** 398 (1944).

7. Woodward, A. E., J. A. Sauer, C. W. Deeley, and D. E. Kline, *J. Colloid Sci.*, **12,** 363 (1957).

8. Baldwin, F. P., J. E. Ivory, and R. L. Anthony, *J. Appl. Phys.*, **26,** 750 (1955).

9. Hess, K., and H. Kiessig, *Kolloid-Z.*, **130,** 10 (1953).

10. Bueche, A. M., *J. Polymer Sci.*, **25,** 139 (1957).

Synopsis

The thermodynamics of the reversible stretching of an elastic body is reviewed, and its application to the theory of rubberlike elasticity and to semicrystalline polymers is discussed. Experimental data are given for the stress-temperature behavior of undrawn nylon filaments extended from 2 to 50% at 160°C. It is found that a large proportion of the total elongation remains as a quasi-permanent orientation. That part of the total extension which is immediately recoverable on removal of stress at the end of the stress-temperature experiment is used to define the strain to be used in the thermodynamic analysis. This definition is rather arbitrary since time effects are not considered. The thermodynamic effects of volume changes during the deformation are eliminated in a manner similar to that used for rubber by converting from stress at constant length to stress at constant elongation. The result is that the stress is primarily accounted for by an entropy term above 80°C., indicating that nylon is rubberlike, at least in thermodynamic terms. The resulting stress-strain curves can be approximated by a form of the equation predicted by the theory of rubberlike elasticity. However, the calculated modulus (3×10^9 dynes/cm.^{2}) leads to a molecular weight between crosslinks much too low. If the crystallites were acting as fillers to the amorphous rubbery chains, the magnitude of this discrepancy would be lessened.

TRANSACTIONS OF THE SOCIETY OF RHEOLOGY IV, 315–334 (1960)

Flow Properties of Lithium Stearate-Oil Dispersions

WALTER H. BAUER, DUANE O. SHUSTER,* and STEPHEN E. WIBERLEY, *Walker Laboratory, Rensselaer Polytechnic Institute, Troy, New York*

INTRODUCTION

In a grease such as that formed by dispersions of lithium stearate in lubricating oils, it has been proposed that the soap[1–3] exists as randomly-oriented, entangled fibers or fiber aggregates,[4–6] at least partially crystalline. Within the fibers, ionic and van der Waals' forces contribute to the strength. At points of entanglement or contact between the fibers, van der Waals' and polar attractive forces give a three-dimensional network character to the system of soap fibers, in which the very dilute saturated solution of soap in oil constitutes a second continuous phase. The grease thus formed is a viscoelastic material with very complex responses, reversible and irreversible at constant temperature, to shear stresses. Deformation properties are affected by the rate of strain in shear, by the acceleration of the rate of shear, and by the magnitude and time of flow at a particular rate of shear to which the system has been previously subjected.[7] For a lithium-base grease, Hutton and Matthews[7] reported an acoustic elastic modulus of 1.6×10^6 dyne cm.$^{-2}$, measured in compression by means of a parallel plate plastometer. Criddle and Dreher,[8] for a grease of 14% lithium stearate in a base oil of 2.3 poise viscosity at 25°C., found elastic behavior with larger values of stress required to produce a given strain when measured in compression than when measured in shear. Tests were made on samples of grease contained between two concentric cylinders in shear, and on un-

* Present address: Socony Mobil Oil Co., Inc., Technical Service Laboratory, 412 Greenpoint Ave., Brooklyn 22, New York.

supported cylinders of grease in compression. From dynamic tests made on a vibrating system of a lithium-calcium grease between two concentric cylinders, Forster and Kolfenbach[3] obtained a rigidity modulus of 3.8×10^3 dyne cm.$^{-2}$. Elastic deformations under constant strain rate at low strains were followed by a region of creep,[7,8] in which stress no longer varied linearly with strain. The value of the stress at which the relation of stress to strain varied from linearity, the "yield point" or "yield stress," was 2.8×10^3 dyne cm.$^{-2}$ for the grease tested by Criddle and Dreher and 5.5×10^3 dyne cm.$^{-2}$ for the grease tested by Hutton and Matthews, at 25°C. Yield stresses were found and measured directly by Singleterry and Stone,[9] by means of a blade-penetrometer, for a lithium stearate grease in di(2-ethylhexyl)-sebacate, in the order of 5×10^3 dyne cm.$^{-2}$. It was found[7-9] that the yield stresses exhibited by greases of a given formulation depended on the previous shear history, in manufacture or in working tests. As shown by Criddle and Dreher, and by Hutton and Matthews, the region of linear stress-strain variation was followed by a region of creep, in which neither the rate of shear strain nor the strain varied linearly with the stress. The region of creep flow ended at an "ultimate yield stress" whose value was dependent on the rate of strain, and which was followed by a region of rapid shear rate thinning.

Thus, within a specified time scale of experiment, greases show definite yield values, at constant temperature, corresponding to specified strain rates and type of deforming stress. Yield is followed by flow (creep at low rate of shear). During this flow the grease is not in a steady state, and after sufficient time of flow and magnitude of shear rate, an ultimate yield stress is reached above which a regime of viscous flow with shear rate thinning or thickening appears. In many industrial applications of greases, such as the flow in low pressure delivery systems, intermittent pumping, slumping in delivery under the gravitational head, or penetration into bearings, a knowledge of yield behavior under defined conditions would be very important.

Capillary viscometers have been widely used in flow tests on greases, and attempts have been made to define yield phenomena in greases by extrapolation based on capillary flow measurements,[9-14] with the assumption of a Bingham type of yield point and a Bingham viscosity. Such extrapolations, even when made with the Buckingham equa-

tion,[15] give values of yield stresses sensitive to the range of shear rate data used, as pointed out by Criddle and Dreher.[8] The existence of entrance effects[16,17] in capillary studies, and the change of original structure on passage through a capillary tube[18–20] make it unlikely that yield stresses with defined parameters of strain rate, deformation type, and shear history can be obtained in capillary viscometry of greases.

Dynamic methods[3] and methods based on rotary movement, as in the case of the cone-plate viscometer,[17,21] offer more promise in providing known initial conditions and controlled time of application and magnitude of rate of shear strain. It appeared valuable to compare closely the effects of flow in the capillary and cone-plate viscometers for model greases of simple composition and known work history, and this investigation was made with that objective.

MATERIALS

Lithium stearate was prepared from a solution of stearic acid in ethyl alcohol by neutralization with a carbonate-free, 50% aqueous alcohol solution of lithium hydroxide. The precipitated lithium stearate was digested, filtered, washed with alcohol and with ethyl ether, and dried at 100°C. Reagent grade stearic acid and purified, crystal lithium hydroxide monohydrate were used. An acid-treated naphthenic oil, oil D described by Cox[22] was used. The viscosity at 25°C. was 4.2 poises.

Soap-oil dispersions were prepared in a kettle designed for grease making,[23] with a system of counter-rotating blades bearing a net-work of wall scrapers, and with provisions for heating and measurement of temperature. Soap and oil were mixed, stirring was commenced, and the mixture was heated from 25 to 210°C. in 40 minutes. Heating was then stopped, and the samples were cooled to 25°C. in 4 hours. System I was not stirred; systems II and III were stirred throughout the cooling period. The compositions of systems I, II, and III were 4, 4, and 8% soap by weight, respectively. For the preparation of dispersions with additives, samples of system III were reheated to 210°C., the additive was rapidly mixed with the dispersion, and the resulting mixture was cooled without stirring in a covered container to 25°C. in 6 hours. A control without additive was similarly prepared from a sample of system III. The dispersions were approximately 1% by weight in additive.

The finished dispersions were not subsequently agitated, and samples were transferred to viscometers with the minimum possible disturbance.

CAPILLARY VISCOMETER

A capillary viscometer with a floating drive piston in a viscometer reservoir tube, 1.5 inches in diameter and 10 inches long, was used.[24] Interchangeable borosilicate glass capillary tubes were mounted flush with the surface of the base plate of the viscometer. The volume rate of flow of the grease through the capillary tube was calculated from the rate of descent of the piston and the dimensions of the reservoir. By means of a transducer, rate of movement of a graduated follower rod attached to the piston was recorded as voltage versus time by an automatic recorder. The driving pressure was supplied from a source of compressed nitrogen at pressures measured by a calibrated Bourdon gauge. Uniformity of bore of the capillaries was checked by measurement of the length of a weighed mercury drop moved along the tube. The diameters were calculated from the weights of mercury filling measured lengths of the tubes, and by means of the measurement of the viscosity of Newtonian oils. The whole viscometer was immersed in a chest with controlled temperature.

CONE-PLATE VISCOMETER

In the viscometer[25,26] used in this work a cone of low angle is immersed in a sample of test material on a flat plate, temperature controlled, with sensing thermocouples imbedded in insulating material in contact with the sample. The cone may be set in rotary motion by a drive shaft, manually controlled, or at accelerations governed automatically.[27] The drive shaft is connected to the cone shaft through a horizontal coiled spring, and extension of the spring when the drive shaft rotates through a greater angle than the cone shaft provides a driving torque to the cone. Voltages from shear stress and rate of shear strain transducers were brought to an x-y recorder and plotted directly.

Four types of operation were used in this investigation:

(*1*) For measurement of stress decay or creep, a shearing stress was applied to the cone immersed in a sample as the result of a rapid,

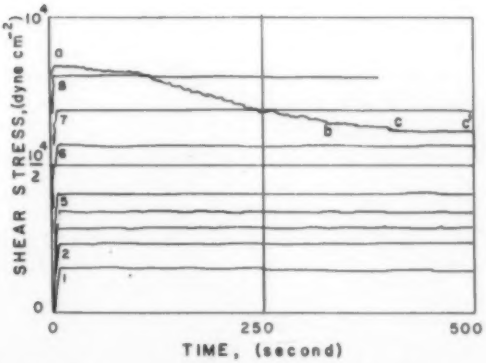

Fig. 1. Stress decay curves for lithium stearate-oil dispersion, system III. Stresses 1, 2, . . ., 8, and *a* successively applied to same sample.

limited rotation of the drive shaft. As long as the cone remained in a fixed position, a fixed stress was thus applied, as shown in Figure 1, curves 1–8. When creep occurred during the period of test, the angle of separation of the drive shaft and the cone shaft was diminished, and the stress decayed during the period of time (*a*-*b*, Fig. 1) until a lower constant value of stress was reached, after which no further change of stress occurred during the time of the experiment (*c*-*d* Fig. 1). During the application of each stress (1–8 Fig. 1), it is assumed that elastic deformation took place. If it is assumed that the acoustic elastic modulus was of the order reported by Hutton and Matthews (2×10^6 dyne cm.$^{-2}$), it was calculated that the motion of the cone during elastic deformations below the onset of creep was less than the limit of observation for the instrument used.

(*2*) For measurement of the initial yield value, ultimate yield stress, and comparative extent of shear rate thinning in a given time, the rate of rotation of the drive shaft was increased at a constant rate for a specified time, after which the rate of rotation was linearly decreased and brought to zero. The time at which movement of the cone commenced was noted. The results of five such cycles of flow applied successivly to the same sample are shown in Figure 2, for the same cycle time in each case. The shear stress at the time flow was observed to commence is shown at y_1 in the curve for cycle 1, and at y_2, y_3, y_4, and y_5 in the curves for successive cycles. Since the rate of

acceleration was the same in each cycle, the initial portions of the curves from 0 to the points marked y are identical because for these portions no motion of the cone has occurred, except that corresponding to the negligible elastic deformation of the sample. During the period from y_1 to x in cycle 1, creep flow of the sample occurred, and when the shear strain had reached the value corresponding to the point x, ultimate yield occurred and a regime of flow commenced in

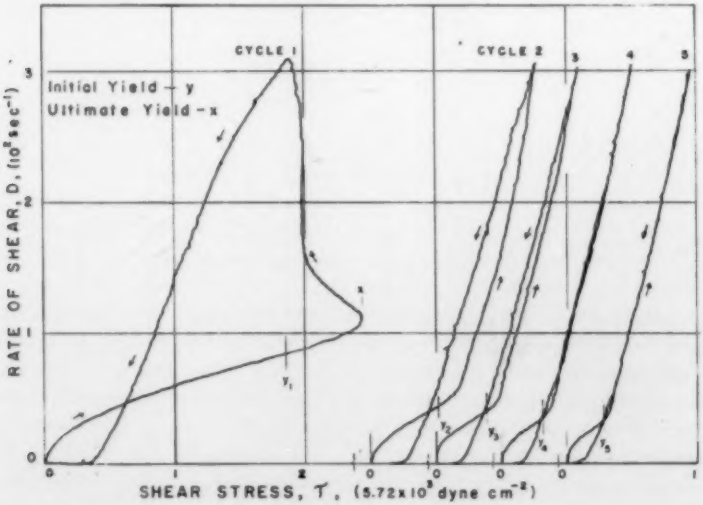

Fig. 2. Initial flow properties of lithium stearate-oil dispersion, system III. Time of cycles, 30 sec. Cycles 1, 2, . . . , 5 carried out successively on single sample.

which the speed of rotation of the cone closely approximated the speed of rotation of the drive shaft. Although the vertical coordinate in Figure 2 is labeled "rate of shear," it should be noted that, from the construction of the Ferranti instrument, the speed of rotation of the drive shaft is directly measured, not the speed of rotation of the cone, and the two are equal only when a steady state has been reached. Since the difference in total angle of rotation of the drive shaft and the cone shaft is directly proportional to the stress at all times, and since the total angle of rotation of the drive shaft at any time, t, is

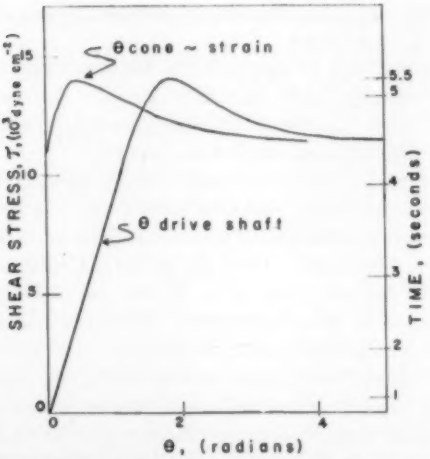

Fig. 3. Initial flow properties, system III. θ is angle of rotation. $(\theta_{drive}-\theta_{cone})$ is proportional to stress measured at same times.

proportional to t^2 at the constant acceleration used, it is possible to determine the relation of the angle of rotation of the drive shaft to the angle of rotation of the cone shaft. In Figure 3 are shown the angles of rotation of the drive shaft and of the cone shaft during the first portion of cycle 1 shown in Figure 2. Points x and y in Figure 3 correspond, in time, to points x and y in Figure 2. At the yield stress corresponding to y, the angle θ of rotation of the cone is zero and the strain is very small. When the strain has reached the value corresponding to the angle θ of rotation of the cone shown by the point x, the stress is at a maximum, the ultimate yield stress. From Figure 3 it is apparent that ultimate yield values obtained with the cone and plate viscometer are not measured at constant rates of strain. However, they are measured at a determinable relation of strain with time. The initial yield stress value was not found to be dependent upon the rate of application of stress, within the time scale of the experiments. It is possible that creep would occur below the yield stress if sufficient time were allowed. The greater the time allowed for creep, the lower the shear stress at which ultimate yield took place. For this reason, ultimate yield stresses measured were larger for the more rapid rates of acceleration of the cone, while the initial yield values were inde-

pendent of the rate of increase of the applied stress, within the scale of rates used in these tests.

(*3*) In a third type of operation of the viscometer, the speed of the cone was rapidly raised until the rate of shear reached a desired value, after which the stress at constant shear rate was recorded versus time, until a steady state was reached.

(*4*) In time cycles, the drive shaft was accelerated from zero speed to a predetermined rate of rotation, after which the speed of rotation of the drive shaft was decreased to zero at a rate of deceleration equal to the rate of acceleration. Until the initial and ultimate yield values were exceeded, the rate of shear in the sample was not measured by the rotation rate of the drive shaft. After the regime of flow was reached, and for the remainder of the cycle, the speed of the cone closely approximated the speed of the shaft. It should be noted, however, that in all programmed accelerations in instruments with a spring-connected torque element between the drive shaft and the viscous element shaft the speed of rotation of the shaft and cone are exactly the same only at constant stress.

RESULTS AND DISCUSSION

Determination of Flow Variables for Systems I and II from Capillary Viscometry

Entrance Effects

For both systems I and II, plots of the driving pressure, P, versus capillary length, L, for constant flow rate, Q, and radius, R, gave straight lines with a common intercept, L' at $P = 0$, for various values of Q. The magnitude of these effects was well beyond experimental error, and is illustrated in Table I.

TABLE I
Entrance Effect in Capillary Flow of Lithium Soap-Oil Dispersions[a]

Capillary diameter, cm.	L' (intercepted at $P = 0$), cm.
0.0740	1.3
0.1020	1.4
0.1286	1.6

[a] Range of capillary length, 4.20–25.6 cm.

Determination of Real Wall Rate of Shear

As shown in Figure 4 for system I, curves A and B, plots of the flow variable, $D = 4Q/\pi R^3$, versus shearing stress, $\tau = PR/2L$, were widely separated for the two values of radius to length ratio of the capillaries shown. Values of D obtained with capillaries of different size, but with the same radius to length ratio, fell on the same curve. Corrected values of the shear stress were obtained from plots of τ vs. R/L for selected values of D throughout the range of D, by determination of the intercept, τ_0, at $R/L = 0$, according to the method proposed by Bauer and Weber.[28] The values ot τ_0 thus obtained were plotted versus the corresponding values of the rate of shear, D, illustrated by curves C in Figures 4 and 5 for systems I and II, respectively. It was found that for both systems a plot of the slope $[d\tau/d(R/L)]_Q$ vs. $(\tau_0)_Q$ for various values of Q was linear and extrapolated through the origin. It is interesting to note that the constant B in the relation thus found, $[d\tau/d(R/L)]_Q = B(\tau_0)_Q$, was 40

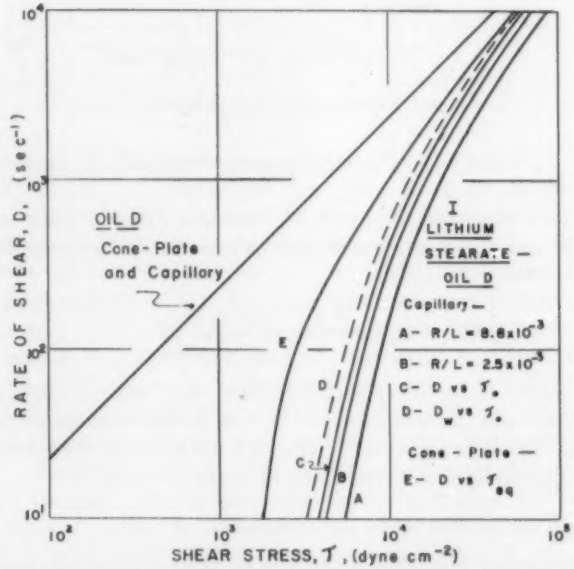

Fig. 4. Flow curves, lithium stearate-oil dispersion, system I.

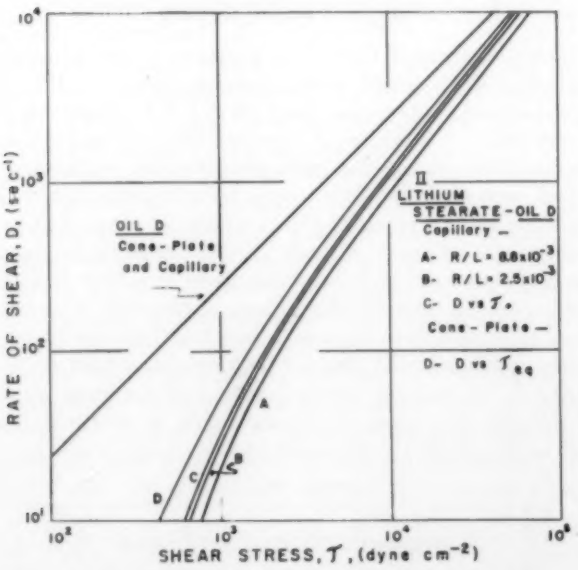

Fig. 5. Flow curves, lithium stearate-oil dispersion, system II.

for both systems I and II, dispersions of which had the same concentration of soap in oil.

From the flow curves, D vs. τ_0, values of $d(\log D)/d(\log \tau_0)$ were obtained at selected values of D and the real wall rate of shear, D_w, was calculated from the relation

$$D_w = \frac{D}{4}\left(3 + \frac{d(\log D)}{d(\log \tau_0)}\right)$$

A plot of D_w vs. τ_0 for system I is shown in Figure 4, curve D. A similar plot was made for system II, but in this case the divergence between the curve representing D_w vs. τ_0 and that of D vs. τ_0 was too small to be conveniently shown in the diagram (Fig. 5).

Correction for Temperature Effects

When the flow properties of the base oil D were measured, nominally at 25°C., in the cone and plate viscometer and in the capillary vis-

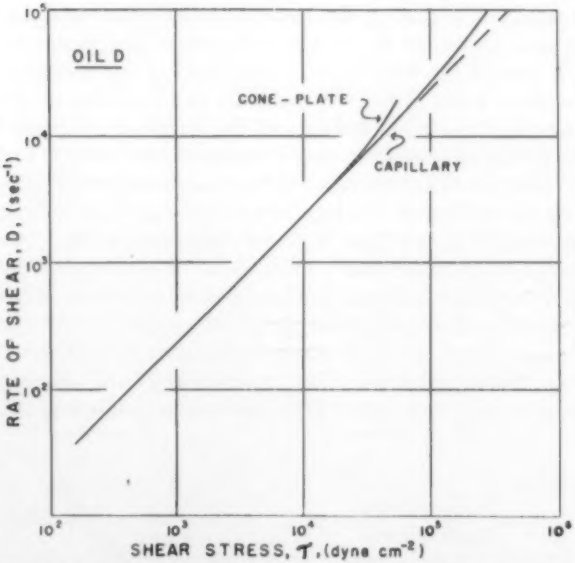

Fig. 6. Comparison of effect of flow heating on flow curves, oil *D* in capillary and in cone-plate viscometers.

cometer, the results over comparable ranges of D and τ are shown in Fig. 6. When the plots of log D vs. log τ are linear, it may be assumed that neither shear rate thinning nor change of temperature occurred. During even very short shearing times, the relation of log D to log τ for the base oil deviated from linearity at shear rates above approximately 8×10^3 sec.$^{-1}$ when the cone-plate viscometer was used. When the capillary instrument was used, the flow curve remained linear until a shear rate of 18×10^3 sec.$^{-1}$ was reached. In the shear rate range of 8×10^3 to 18×10^3 sec.$^{-1}$ in which the capillary measurements indicated Newtonian behavior, the oil sheared in the cone-plate instrument rose in temperature significantly above 25°C. Since the viscosity of the grease approached that of the base oil in the shear rate region concerned, a correction was made for temperature rise of the greases in the shear rate range 8×10^3 to 10×10^3 when the cone-plate viscometer was used. It was assumed that the divergence of τ from linearity with D in this range was no

greater than that shown by the base oil. At high rates of shear, the temperature coefficient of viscosity of greases has been shown to approach that of the base oil.[21] Corrections of the cone-plate data in the region of temperature rise could not be based on a temperature coefficient of viscosity for greases and the temperature registered by the sensing thermocouples in the viscometer base plate. From the known characteristics of the base oil, the temperature rise above 25°C. shown by the measured viscosity in the heating range of shear rate was from 1–2°C. larger than the rise of approximately 1°C. shown by the sensing thermocouple. From these observations it must be concluded that when temperature increases during shear of a sample are indicated by the Ferranti viscometer plate sensing system, portions of the sheared medium have reached substantially higher temperatures than those indicated. The chief value of the thermopile in base plate systems is to show when the rate of production of heat in

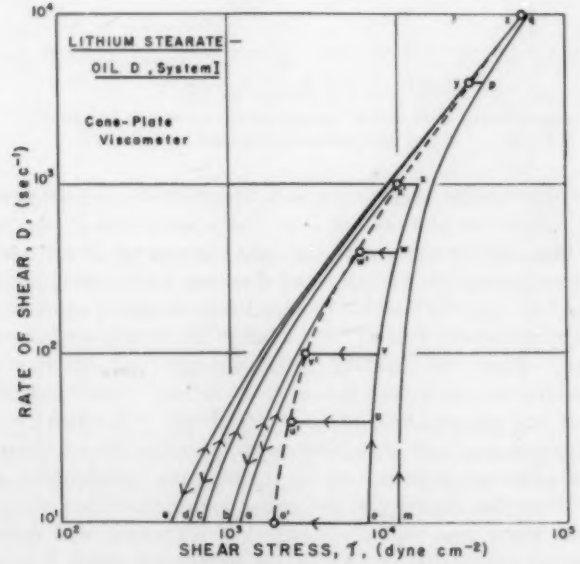

Fig. 7. Effect of maximum rate of shear and time of shear on flow curves. $\overline{mp,y}$ $\overline{mqz}$, $\overline{ouu'o'}$, $\overline{ov}$ . . ., $\overline{ow}$ . . ., $\overline{ox}$ . . ., from measurements on fresh samples in each case.

shearing has exceeded the rate of conduction to the base plate reservoir.

Stress Decay in Shear Strain

During cycles of shear rate acceleration and deceleration while greases were tested in the cone-plate viscometer, changes of structure with time of shearing occurred in the greases. When limiting values of shear stress had not been reached, D vs. τ flow curves were not equilibrium curves, and were sensitive to time of cycle, as shown by curves $\overline{ox}$ and $\overline{mq}$ in Figure 7. When a sample of grease was rapidly subjected to a particular fixed rate of shear, it was found that the stress developed decayed, reaching a limiting value in time at which any further changes were outside the scale of test.

Typical results are shown in Figure 7 for the system I grease. When the shear rate was raised to that corresponding to points o, u, v, w, and x for successive fresh samples of grease (at the same acceleration of shear rate in each case), the points o', u', v', w', and x' were reached. After such a limiting stress was reached at a particular rate of shear, the D vs. τ curve obtained in cycles of shear showed no hys-

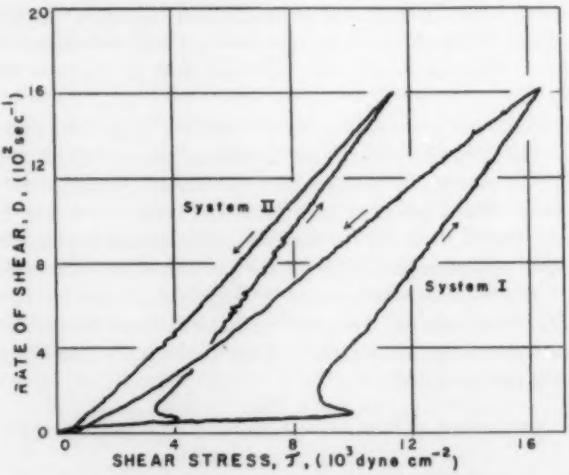

Fig. 8 Comparison of initial flow curves for lithium stearate-oil dispersions. System I cooled without stirring; system II cooled with stirring. Cycle time, 180 sec.

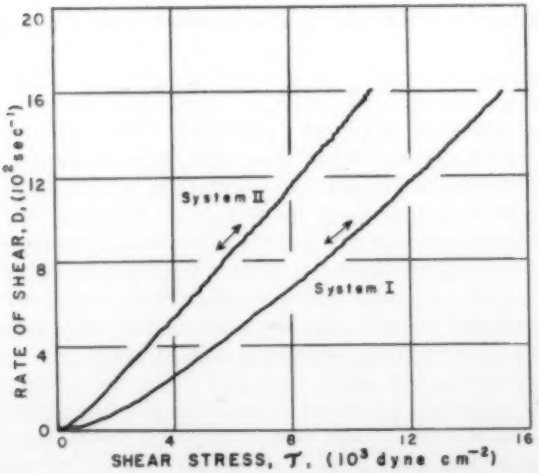

Fig. 9. Comparison of flow curves for system I and system II after 1000 sec. at 1600 sec.$^{-1}$ shear rate. Time of cycle, 180 sec.

teresis, and could be repeated reversibly on the same sample if the rate of shear at which the limiting stress had been established was not exceeded. The curves $\overline{av'}$, $\overline{bw'}$, $\overline{cx'}$, $\overline{dy'}$, and $\overline{dz'}$ were of this type (Fig. 7).

The behavior of systems I and II in cycles of shear rate increase and decrease are shown in Figure 8 for the initial cycle of shear on samples undisturbed except for loading the viscometer, showing the typical initial yield values exhibited and the initial cycle hysteresis. In Figure 9 are shown flow curves for the same samples obtained after the greases had been sheared for 1000 sec. at a shear rate of 16×10^2 sec.$^{-1}$. The yield values were greatly diminished, and the flow cycles could now be repeatedly traversed without further change within the limits of the testing times used, as long as the shear rate of 16×10^2 sec.$^{-1}$ was not exceeded.

Comparison of Flow Curves Obtained in Cone-Plate and Capillary Viscometry

When the shear history of a material affects its flow properties, two of the characteristics of laminar flow in capillary tubes become very

important when comparisons are to be made with flow of the material in cone-plate viscometers. In capillary flow in tubes of the same R/L, each point of the D vs. τ flow curve is obtained for samples which have in no part exceeded the real rate of shear at the wall, and for which the energy on entrance work must be supplied to all the material traversing the tube, a volume much larger than that involved in cone-plate viscometry. Because of the first of these characteristics, capillary data, obtained at successive points of maximum rate of shear in the sample, should be compared to flow curves obtained with the cone-plate viscometer in which the particular rates of shear, D, for which the corresponding limiting stresses, τ_0, have been measured, have not been exceeded. Such curves are given by the locus of the points o', u', v', w', x', y, and z, in Figure 7, and examples are curve E in Figure 4, and curve D in Figure 5. For both systems I and II, the flow curves D vs. τ obtained in cone-plate viscometry do not coincide with D_{real} vs. τ_0 curves obtained for corresponding samples in capillary viscometry. A likely reason for this is that in the short residence time during which a sample is exposed to D_{real} in the capillary, the grease has not had time enough to reach the limiting value of stress corresponding to D_{real}. The (R/L) correction described in obtaining τ_0 compensates only for the stresses involved in entrance effects. It thus appears that only when a grease is already shear stable with respect to yield value and time of shearing can the results from cone-plate viscometry and capillary viscometry coincide. This requirement was not met by our model greases, and by none of the eight currently marketed greases as supplied by the manufacturers. The excellent correlation obtained by Sisko, Brunstrum, and Leet[29] for a highly worked grease shows that the requirement may be met by special products. For the more shear-sensitive greases generally supplied to users, it should be valuable to obtain flow curves both for capillary flow, approximating many handling and dispensing conditions, and for cone-plate steady-state flow, approximating bearing conditions. The cone-plate or other rotary arrangement appears best for measurement of the initial value of yield stress and initial flow resistance before major destruction of transient structure.

Effect of Dispersion Preparation Method

Systems I and II were prepared and tested under such conditions that the chief differences in structure should lie in the length of the

lithium stearate fibers and the extent of aggregation of the fibers. The system II grease, prepared by crystallization on cooling with stirring, showed lower initial yield stresses and less change in viscosity on shear than did the system I grease, in which the lithium stearate fiber had been allowed to form undisturbed, as shown in Figure 8. These results are in agreement with the expectation that the fibers in system II were originally shorter than those of system I, and that the chief effects of shear were destruction of the three-dimensional fiber network and breaking of fibers in shear strain.

Two other characteristics of the two systems are notable. First, even after severe shear strain at 16×10^2 sec.$^{-1}$ for 1000 sec., the limiting flow curve of system I showed much higher stresses at common rates of shear than were shown by the flow curve of similarly sheared system II, as shown in Figure 9. It is concluded that, although the system I grease underwent the greatest proportionate change in flow properties, the fibers in this system prepared from the same weight of lithium stearate must have been more resistant to shear breakup than the fibers in system II. It may be that crystallization in the fiber was more complete in the case of fibers formed without agitation in cooling, while those formed with stirring may have contained more short range imperfections.

A second, unexpected characteristic of the two types of greases is not readily explained. For both system I and system II, the ratio of $d\tau/[d(R/L)]_Q$ to $(\tau_0)_Q$ in capillary studies was constant and equal, having a value of 40. If the slope of τ at constant Q vs. R/L is constant and proportional to the intercept, τ_0, at $R/L = 0$ for various values of Q, it is apparent that the τ vs. R/L curves constitute a set of straight lines with a common intercept with the R/L axis. The length of this intercept has been interpreted by Philippoff and Gaskins[30] to be a measure of the recoverable shear, s, giving rise to a normal stress of τ_s at a shear stress of τ for certain systems. In this case, however, the entrance effects are irreversible at constant temperature, and the intercept should perhaps be regarded simply as a measure of the energy irreversibly expended in rupture of fiber contacts and orientation of fibers[6] on entrance of the grease into the capillary. In any case, the energy stored for the same flow volume is the same for both system I and system II greases, for which the initial "ultimate yield stresses," shown in Figure 8, are very different, 10×10^3 and 4×10^5 dynes cm.$^{-2}$, respectively. The entrance effects are thus propor-

tional to the concentration of the lithium stearate in these dispersions, rather than the mode of organization.

Effect of Additives

In addition to a base oil and principal thickening agent, greases commonly contain small amounts of additives. The studies of such lithium stearate greases, modifications of system III, were made with the cone-plate viscometer because of the possibility of measurement of initial yield stresses in the unworked condition and after a specified work treatment at a uniform shear rate The additives used are listed in Table II, together with the yield stress results.

TABLE II
Flow Properties of Lithium Stearate-Oil-Additive Systems

Additive	Yield stress, τ, 10^3 dyne cm.$^{-2}$	
	$\tau_{initial}$	$\tau_{equilibrium}$[a]
None (control)	8	0.3
Diphenylamine	8	0.3
2,6-Di-*tert*-butyl-*p*-cresol	7	0.3
2-Ethyl hexanoic acid	7	<0.1
Caproic acid	4	<0.1
m-Cresol	4	<0.1
Stearic acid	3	<0.1
Cyclohexanol	3	<0.1
Glycerol	3	0.35
Caprylic acid	2	<0.1

[a] $\tau_{equilibrium}$ measured after 1000 sec. at $D = 4.0 \times 10^3$ sec.$^{-1}$.

The values of initial yield stress were measured for samples loaded into the viscometer shearing region with a minimum of disturbance. The yield stresses marked $\tau_{equilibrium}$ were measured after 1000 sec. at a shear rate of 4×10^3 sec.$^{-1}$ and a period of rest. No change was noted in the flow characteristics of these greases for a period of rest of 48 hours, and the changes in initial structure occurring in shear, were thus not restored in the period of these tests. The chief effect of the additive was to change the initial yield stress. The viscosities at 4×10^3 sec.$^{-1}$ rate of shear after 1000 sec. were equal to that of the control within the limits of accuracy of the measurement.

The effect of the additives is believed to result from adsorption on the soap fibers or penetration in the polar regions, with consequent weakening of the fibers. Either of these actions would be expected to weaken the interparticle attraction. All the compounds chosen have a polar group capable of hydrogen bonding at the lithium carboxyl oxygen regions of the lithium stearate crystallites.

CONCLUSIONS

When the dispersion has structural complexities which are changed with shear strain according to the magnitude of the strain and the rate of strain, and according to the time the rate of strain is maintained, capillary and cone-plate rheological measurements each give unique information. The choice of the instrument depends on the rheological properties of interest. For the lithium stearate-hydrocarbon oil dispersions investigated, capillary measurements showed that a considerable fraction of the energy required to initiate flow is irreversibly stored at constant temperature in amounts independent of the conditions of fiber formation used. When it was desired to isolate properties such as initial yield stress and limits of stress decay at fixed shear rates for correlation with method of fiber formation, the information was readily obtained with the cone-plate viscometer. Assuming, from the results of electron diffraction studies on other lithium stearate greases, that the primary effects of flow are orientation and rupture of soap fibers, it may be concluded that inherently stronger fibers are produced when crystallization takes place without stirring. From the cone-plate measurements, it was possible to show that the addition of materials capable of hydrogen bonding with the soap fibers could greatly reduce the initial yield stress without substantial effect on the viscosity at high rates of shear.

For the grease prepared without stirring, separation was large between the flow curve at shear rate versus limiting shear stress obtained with the cone and plate viscometer and the curve of real wall rate of shear versus the corrected shear stress obtained from capillary measurements. Stresses required to maintain the same shear rate were always lower in the cone-plate studies than in the capillary experiments. The cone-plate shearing conditions have a much more drastic working action on the uniformly sheared sample in the repeated path

between the cone and the plate than is applied by the passage through the capillary. When the initial fiber lengths are already comparatively short, as in the system II grease prepared by fiber formation with stirring, less reduction in viscosity because of fiber rupture is possible. Thus the extent of change of flow properties on shearing and the difference between the flow curves from cone-plate and from capillary measurements are less for the system II grease than for the system I grease. It is concluded that the use of the cone-plate type of viscometer with appropriate automation of control and recording greatly extends the amount of information useful to grease manufacturers and users over that obtainable from capillary measurements. Neither type of apparatus is adapted to measurement of elastic moduli and relaxation times for structural changes, which appear to be most readily obtained by other methods.[3] At present, information concerning the viscous behavior of greases is much more complete than knowledge of the elastic characteristics of the clearly viscoelastic grease dispersions.

This investigation was supported in part by grants from the Esso Education Foundation to the Chemistry Department and from the Socony Mobil Oil Company, Inc. to the friction and lubrication program, Research Division, Rensselaer Polytechnic Institute.

References

1. Vinogradov, G. V., and G. Klimov, *J. Tech. Phys. U.S.S.R.*, **18,** 355 (1948).
2. Forster, E. O., and J. J. Kolfenbach, *NLGI Spokesman*, **20,** No. 3, 16 (1956).
3. Forster, E. O., and J. J. Kolfenbach, *NLGI Spokesman*, **23,** 215 (1959).
4. Vold, M. J., G. S. Hattiangdi, and R. D. Vold, *Ind. Eng. Chem.*, **41,** 2539 (1949).
5. Vold, M. J., *J. Phys. Chem.*, **60,** 439 (1956).
6. Brown, J. A., C. N. Hudson, and L. D. Loring, *NLGI Spokesman*, **15,** No. 11, 8 (1952).
7. Hutton, J. F., and J. B. Matthews, *Proc. Second Intern. Congr. Rheol., Oxford*, **1953,** 408 (1954).
8. Criddle, D. W., and J. T. Dreher, *NLGI Spokesman*, **23,** 97 (1959).
9. Singleterry, C. R., and E. E. Stone, *J. Colloid Sci.*, **6,** 171 (1952).
10. McLennan, L. W., and G. H. Smith, *ASTM Bull.*, **152,** 71 (1948).
11. Green, J., *Am. Soc. Testing Materials, Proc.*, **20,** 451 (1920).
12. Moses, G. B., and I. E. Puddington, *Can. J. Research*, **27B,** 616 (1949).
13. McMillen, E. L., *Chem. Eng. Progr.*, **44,** 537 (1948).
14. Averson, M. H., *Ind. Eng. Chem.*, **24,** 71 (1932); *ibid.*, **26,** 628 (1934).
15. Buckingham, E., *Am. Soc. Testing Materials, Proc.*, **21,** 1154 (1921).
16. Zimmer, J. C., and J. B. Patberg, *Inst. Spokesman*, **9,** No. 5, 1 (1945)

17. Bauer, W. H., A. P. Finkelstein, D. O. Shuster, and S. E. Wiberley, *NLGI Spokesman*, **23,** 15 (1959).

18. Wilson, J. W., and G. H. Smith, *Ind. Eng. Chem.*, **41,** 770 (1949).

19. Miller, W. R., T. J. Walsh, and R. R. Slaymaker, *Lubrication Eng.*, **14,** 216 (1958).

20. Moore, R. J., and A. M. Cravath, *Ind. Eng. Chem.* **43,** 2892 (1951).

21. Bauer, W. H., A. P. Finkelstein, and S. E. Wiberley, "Flow Properties of Lithium Stearate-Oil Model Greases as Functions of Soap Concentration and Temperature," presented before the 14th Annual Meeting of A.S.L.E., Buffalo, N. Y., April 22, 1959.

22. Cox, D. B., *J. Phys. Chem.*, **62,** 1254 (1958).

23. Armstrong, E. L., *NLGI Spokesman*, **17,** No. 7, 8 (1953).

24. Weber, N., and W. H. Bauer, *J. Phys. Chem.*, **60,** 270 (1956).

25. McKennell, R., *Proc. Second Intern. Congr. Rheol., Oxford*, **1953,** 350 (1954).

26. McKennell, R., *Anal. Chem.*, **28,** 1710 (1956).

27. Bauer, W. H., A. P. Finkelstein, C. A. Larom, and S. E. Wiberley, *Rev. Sci. Instr.*, **30,** 167 (1959).

28. Bauer, W. H., N. Weber, and S. E. Wiberley, *J. Phys. Chem.*, **62,** 1245 (1958).

29. Sisko, A. W., L. C. Brunstrum, and R. H. Leet, *NLGI Spokesman*, **23,** 57 (1959).

30. Philippoff, W., and F. H. Gaskins, *Trans. Soc. Rheol.*, **2,** 263 (1958).

TRANSACTIONS OF THE SOCIETY OF RHEOLOGY IV, 335–346 (1960)

Rheological Measurements with the Brabender Plastograph

C. C. McCABE, *E. I. du Pont de Nemours & Company, Inc., Elastomer Chemicals Department, Wilmington, Delaware*

The search for new or improved instruments to characterize high polymers, especially elastomers, is an ever-continuing one. The importance of such instruments cannot be overemphasized, and their need is clearly evident by examination of any one of the numerous fabrication processes for elastomers. From the very time the elastomeric molecule is manufactured to the time that its cure, is completed, structural changes are occurring, and consequently its rheological properties are affected. The complete history of the polymer is therefore of primary importance and must be held within established limits if the end product is to be within manufacturing specifications.

One of the areas in which flow characterization has achieved marked success is that of relating shear stress and shear strain. This is not surprising, since a test of this nature attempts to measure flow properties which simulate actual processing mechanics. It makes little difference what type of instrument is employed, whether it be a rotating cylinder, a plate and cone viscometer, a vibrating reed, or other instruments—each subjects the sample to shear forces under some restricted conditions. Most of these instruments operate over a range of conditions, but all too often, in an effort to expedite results, only a single value of the shear stress-shear rate relation is determined. With most elastomers, steady state shear stress conditions may not even be attainable during processing operations, and any single value of flow characteristics must assume some arbitrary criterion as to when the flow properties are changing slowly enough to be considered constant. The inadequacy of single value determinations is also emphasized by the shear stress-shear rate curves for various polymers

Figure 1.

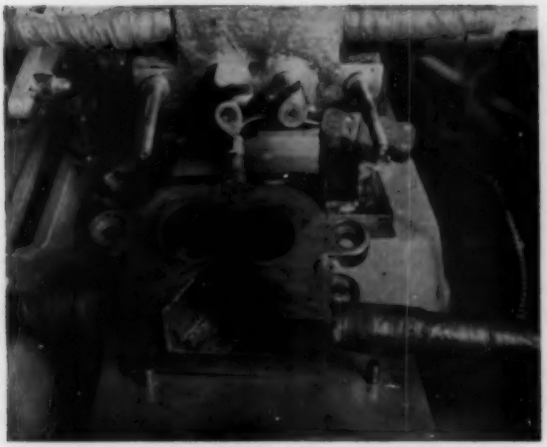

Figure 2.

which cross one another, and any single point measurement may therefore be misleading.

It is only necessary to examine processing equipment in a cursory sense to realize that the range of operating conditions is large. Consequently, if results of rheological tests are to be most meaningful, measurements over a wide range of shear rates are necessary.

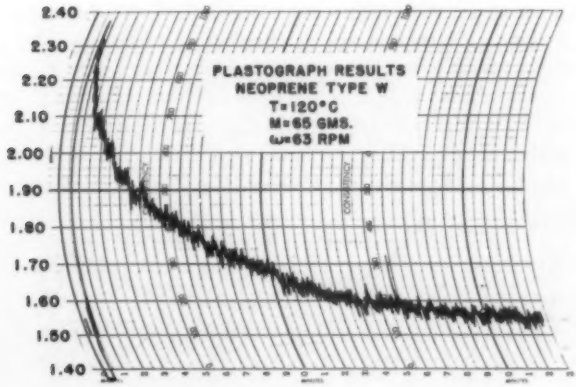

Figure 3.

It is anticipated that the Brabender Plastograph will provide a new testing instrument for rheological properties of high polymers in general, and be particularly useful for elastomers. Basically, this is another instrument which subjects a polymer sample to shear forces and measures the torque as a function of shear rate and temperature. The instrument is illustrated in the Figures 1 and 2, with the Figure 1 illustrating the overall view of the plastograph. It consists of a jacketed mixing chamber which is shown in greater detail in Figure 2. In back of the chamber is the motor with motor housing which is mounted on flexible bearings. By means of a series of levers, the reaction of the motor housing to the load required to turn the rotors in the mixing chamber actuates both the scale and recorder. In the rear is the oil bath which circulates oil continuously through the chamber jacket. Figure 2 illustrates the chamber and cam-type rotors which operate in opposite directions and are specifically designed for plastics and elastomers. The speed ratio of the two rotors is 3:2 over a range of speeds which is variable from 20–150 r.p.m. for the fast rotor. The chamber has a volume of approximately 50 cc. and is held at constant temperature by oil circulation through the chamber jacket. The polymer temperature is measured by a thermocouple situated in the chamber wall between the two rotors. Results of measurements on the plastograph are expressed in meter-kilogram units of torque.

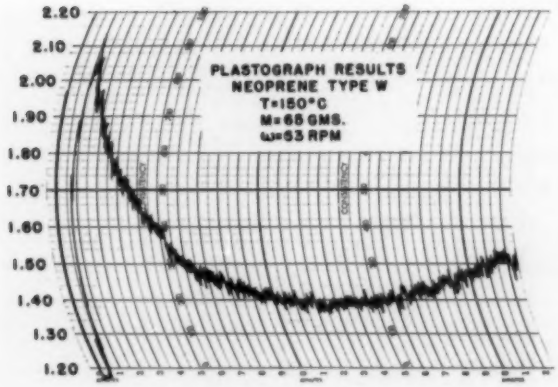

Figure 4.

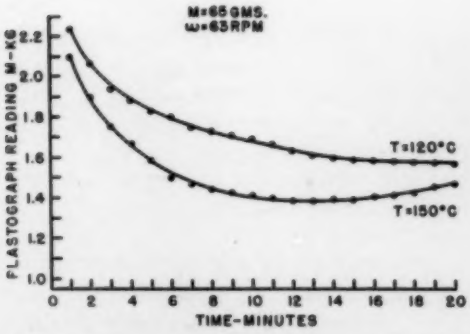

Fig. 5. Plastograph results for Neoprene, Type W.

Operation is very simple and entails little more than loading the chamber with a sample which can be in the form of powder, small chips, or continuous ribbons. After loading, which for most elastomers requires less than 45 sec., no further operations, other than adjusting scale weights, are required.

A typical chart recording for Neoprene, Type W (a synthetic polychloroprene elastomer), is shown in Figure 3. The initial rise in torque demonstrates the loading of the chamber with the sample, followed by the breakdown period, after which the plastograph read-

ing tapers to nearly a constant value. The effect of operating the plastograph with the same type elastomer at a higher jacket temperature is shown in Figure 4. The initial torque level is somewhat lower, and after the minimum has been reached the effect is similar to that obtained by increasing the shear rate. In either case, the tail end of the curve rises as a result of elastomer crosslinking which is initiated by heat and oxygen. This phenomena is commonly called scorching or premature curing in the elastomer industry. Reproducibility of these plastograph curves for elastomers is within $\pm 2\%$.

The results of Figures 3 and 4 are replotted and shown in Figure 5 for comparison. It is primarily these types of characteristic curves for Neoprene that are to be discussed. Some results for natural rubber, SBR, and butyl elastomers are included in a later section of this article.

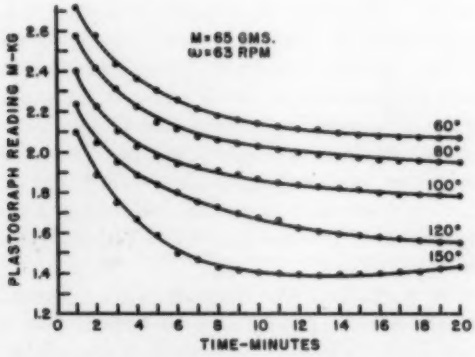

Fig. 6. Plastograph results for Neoprene, Type W.

In order to evaluate the plastograph results and to characterize the sample by a limited number of parameters, it would be desirable to represent the complete plastograph curve by a mathematical expression. However, there is no simple mathematical expression which completely describes this curve. Therefore, for practical purposes, it is easy to measure the following parameters: (*1*) Rate of breakdown (slope of plastograph curve), (*2*) minimum value, if one occurs, (*3*) value at specific time and temperature, and (*4*) scorching tendency as measured by the slope of the plastograph curve after passing a minimum.

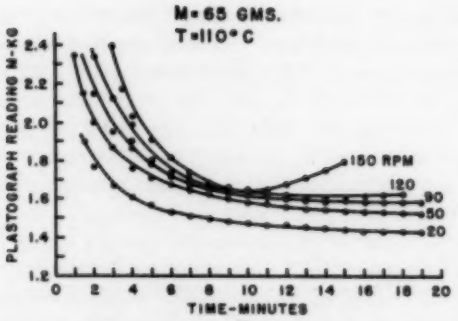

Fig. 7. Plastograph results for Neoprene, Type W.

Each of these is influenced by several phenomena which may be occurring simultaneously, namely; chain scission, shear thinning, temperature effect, density change, and crosslinking. However, it is the summation of these effects which is measured and likewise encountered in the manufacturing process, and therefore it is not essential to isolate the individual parameters at this time. The four characteristic parameters listed above provide a satisfactory description of flow properties for elastomers in general. However, the selection of specific parameters will, in some degree, depend upon the nature of the elastomer being tested.

As previously mentioned, the chamber has a volume of approximately 50 cc. and all data presented in this report were obtained by using constant volume samples. However, it should be noted that the plastograph results are directly dependent upon the volume of the sample in the chamber.

The effect of temperature on flow properties as measured by the plastograph is shown in Figure 6. Samples of Neoprene were run at various temperatures as indicated, where the designated temperatures are those of the circulating oil. The stock temperature increases above that of the jacket due to the high shearing forces and internal friction in the elastomer. As previously mentioned, this temperature is measured by a thermocouple situated in the chamber wall between the rotors.

The second variable of the plastograph is shear rate, and curves obtained at various shear rates are shown in Figure 7. This family of

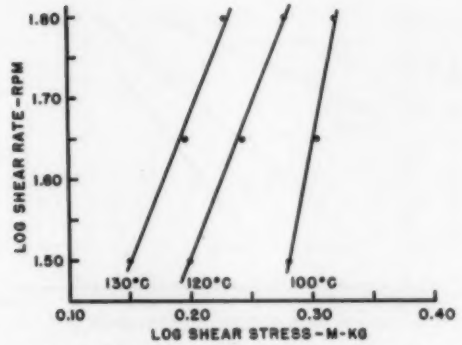

Fig. 8. Flow curves for Neoprene, Type W.

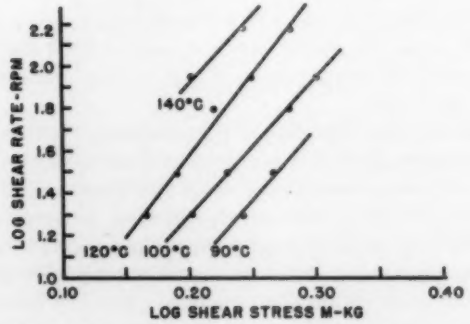

Fig. 9. Flow curves for natural rubber (pale crepe).

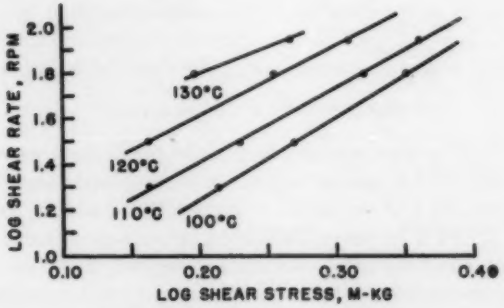

Fig. 10. Flow curves for SBR 1502.

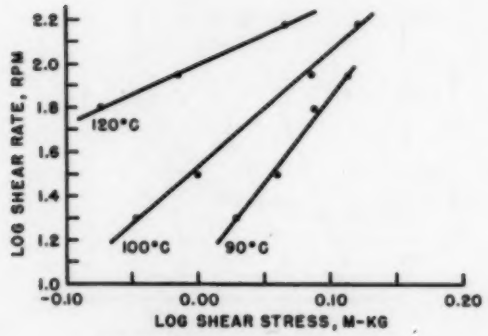

Fig. 11. Flow curves for butyl 150.

curves is quite similar to that which results from varying the temperature. From these two sets of curves it can be noted that an increase in temperature produces a shifting of curves in the same direction as a decrease in shear rate.

In order to interpret the data of Figures 6 and 7 with respect to the molecular theories of flow, it is convenient to replot the data on the usual log *shear-stress* versus log *shear-rate* graph as illustrated in Figure 8. In this figure and subsequent ones, values of shear stress and shear rate are taken directly from the plastograph in m.-kg. and r.p.m. units, respectively, since constants of proportionality for conversion to the more commonly employed units are functions of the geometry and are not accurately defined for this instrument. Such values of shear-stress and shear-rate are in reality averages over the various points in the chamber. These data can than be represented by straight lines for each of the different temperatures of the elastomer and give positive agreement with the Ostwald de Waele equation:

$$\text{shear rate} = C\ (\text{shear stress})^n$$

in which C and n are characteristics of the particular elastomer represented. Results for natural rubber, SBR, and butyl are expressed in the same manner and are shown in Figures 9, 10, and 11, respectively. Values of C and n for these elastomers are shown in Table I. From these results, and the curves of previous figures, it can be noted that the constants for natural rubber are insensitive to temperature variations, in contrast to those for butyl which change quite markedly.

TABLE I
Shear Rate = C (Shear Stress)^n

	100°C.		120°C.	
	C	n	C	n
Neoprene, Type W	1.21	7.5	0.95	3.7
Natural rubber	1.00	6.6	1.00	7.4
SBR 1502	0.71	3.6	0.46	3.0
Butyl 150	0.50	5.3	0.18	2.7

Many theoretical expressions have been set forth relating viscosity (η) and absolute temperature (T), with one of the most common ones, although somewhat simplified, being:

$$\eta = (\text{constant}) \exp \{E/RT\}$$

where E is defined by

$$E = Rd \ln \eta/d(1/T)$$

and is the activation energy for the primary process of flow; namely, that energy for the jump of a small molecule or a segment of elastomer molecule from one equilibrium position to the next. It has been noted that this relationship, in many cases applies only over a narrow temperature range. This is necessarily a limiting condition for most elastomers because of molecular instability.

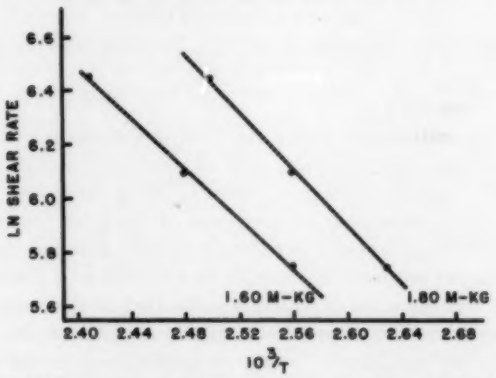

Fig. 12. Temperature coefficient of flow rate for Neoprene Type W.

In the case of elastomers which exhibit shear sensitive flow, the viscosity depends upon the value of the shear stress. It is convenient to compare the above formula with data by considering the temperature dependence of the rate of flow at a constant value of shear stress. In Figure 12 the log shear rate is plotted against the reciprocal of absolute temperature for two values of shear stress. These points lie on straight lines which are nearly parallel and from the slopes value of E are determined. These values are 9.9 and 10.5 cal./mole. These values compare favorably with reported values by Treloar[1] for natural rubber (8.1 to 10.2 kcal./mole). Consequently, general agreement exists with the Eyring concept[2] that the unit involved in flow processes is a relatively short segment of the molecular chain.

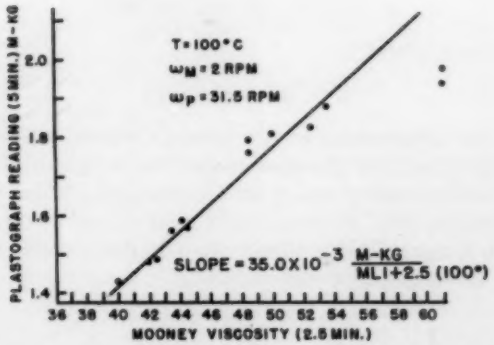
PLASTOGRAPH READING (5 MIN.) M-KG
2.0
1.8
1.6
1.4
T = 100°C
ωM = 2 RPM
ωp = 31.5 RPM
SLOPE = 35.0 X 10⁻³ M-KG / ML1+2.5 (100°)
36 38 40 42 44 46 48 50 52 54 56 58 60
MOONEY VISCOSITY (2.5 MIN.)

Fig. 13. Comparison of Plastograph and Mooney viscometer for Neoprene, Types W and G.

In addition to characterizing the flow properties previously mentioned, it is important that any new or improved instrument be correlated with those instruments currently being employed, whenever feasible. In the elastomer industry one of the most frequently used and universally accepted instruments is the Mooney viscometer.[3] This instrument subjects the sample to a continuous shearing deformation by turning a rotor which is imbedded in the sample. Both constant speed and constant temperature are maintained. The resulting Mooney viscosity is a number proportional to the torque required to turn the rotor. This viscometer is a low shear rate instru-

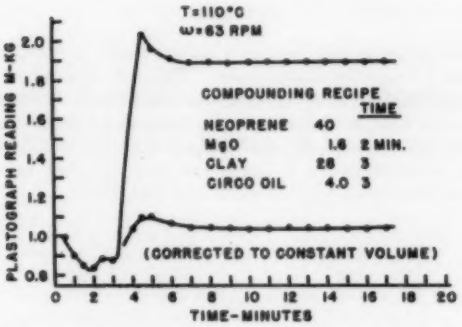

Fig. 14. Plastograph results for compounding Neoprene, Type W.

ment, and consequently the correlation with the plastograph was made at a relatively low shear rate (31.5 r.p.m.) and the plastograph reading taken at 5.0 min. These data points are shown in Figure 13 with a line of slope $35.0 \times 10^{-3} \pm 1.5$ for Neoprene, Types W and CN, which when extended will pass through the origin within experimental error. Since different elastomers have different shear rate versus shear stress characteristics, a conversion constant must be obtained for each type elastomer or a correction factor determined to take into account the different shapes of the characteristic curves.

The normal procedure for fabricating elastomers is to incorporate fillers, such as clay and carbon black, and other compounding ingredients by very thorough mechanical mixing with the raw elastomer. The rheological properties are drastically affected by both amount and kind of compounding ingredients used in the operation. With the plastograph it is easy to follow the changes in flow properties as they occur throughout the addition period and mixing. A typical example is shown in Figure 14 with the recipe and addition times indicated thereon. Two curves are shown following the major addition of clay and oil, with the lower being corrected to constant volume in contrast to the actual observations (top curve).

References

1. Treloar, L. R. G., *Rubber Chem. and Technol.*, **23,** 347 (1950).
2. Eyring, H., et al., *Theory of Rate Processes*, McGraw-Hill, New York, 1941.
3. Mooney, M., *Physics*, **7,** 413 (1936).

Synopsis

The Brabender Plastograph provides a simple, rapid, precise characterization test for rheological properties of elastomers. These are determined at shear rates which nearly approximate those of industrial applications. The dependence of flow characteristics upon both shear rate and temperature is illustrated and gives good agreement with the Ostwald de Waele relation. Values for the activation energy of flow were computed for neoprene from the flow rate temperature coefficient at constant stress and averaged 10.2 kcal./mole.

TRANSACTIONS OF THE SOCIETY OF RHEOLOGY IV, 347-362 (1960)

The Dynamic Compressibility of a Rubber-Sulfur Vulcanizate and Its Relation to Free Volume

J. E. McKINNEY, H. V. BELCHER, and R. S. MARVIN,
National Bureau of Standards, Washington, D. C.

1. Introduction

The purpose of this work was to investigate the effect of pressure, temperature, and time-scale on the compressibility of a typical rubber-like polymer in the vicinity of the glass transition temperature. It was thought that such investigations should yield information about the nature of the free volume which has been used in the derivation of temperature-frequency reductions, notably the Williams-Landel-Ferry expression.[1]

The transition between the glassy and rubbery states of a polymeric material is frequently explained in terms of a free volume which in essence represents the space available for the motion of chain elements. Such motions must take place freely in order to permit a chain to assume the many configurations of equal energy which account for the high compressibility typical of the rubbery state. If the chains are prevented from moving freely between these several configurations, the material shows the much smaller compliance characteristic of a glass or a rigid plastic. The assumption of Williams, Landel, and Ferry, following in general the concepts of Doolittle,[2] was that there exists a critical value of the (fractional) free volume which is just large enough to permit the required chain motions, and which therefore determines the glass transition temperature as defined by the volume-temperature curve. This critical free volume, and the change of free volume with temperature, appears to be nearly constant for a wide variety of glass-forming liquids.

Free volume should probably not be taken literally as corresponding to any physical volume, or volume fraction,[3] but it has been a use-

ful concept. Its simplest definition would involve the difference between the actual volume, above the glass transition, and the volume extrapolated from the volume-temperature curve in the glassy region. While the value thus obtained does not match those predicted by the "universal" WLF equation, the temperature coefficient in this equation is very close to the difference in the temperature coefficients in the rubbery and glassy regions for many polymers. By analogy, one would expect the pressure coefficient of the free volume to be related to the difference in compressibilities above and below the glass transition. The measurements reported here gave us an opportunity to check whether such a relation would yield shifting factors giving superposition of measurements made at different temperatures, pressures, and time-scales, that is, reduced frequencies of the WLF type which include the effect of both temperature and pressure.

When the mechanical properties, either shear or dilatational, of a viscoelastic material are measured by a dynamic technique, that is, one in which a sinusoidal force is applied, the response will show a dispersion region over a certain frequency range. At frequencies below this range the response will correspond to that observed during static measurements and thus, if the measurements are made above the glass transition, will correspond to motions of the whole polymer chain. At frequencies above this dispersion region the response will represent motions of only short segments of the chains, and will appear quite similar to the response found from static experiments below the glass transition. It is quite probable, as found by Litovitz and Lyon[4] for glycerol, that the slope of compressibility versus temperature would differ above and below the glass transition temperature even if the frequency were so high that all measurements represented were above the dispersion region. The measurements reported here did not extend to low enough temperatures to establish the slopes below the glass transition temperature.

As the response goes through this dispersion region, the loss compliance† will exhibit a maximum and the storage compliance an inflection. If measured at constant frequency and pressure against temperature, this maximum is often referred to as a psuedo-glass transition. It will be clearer for the purposes of this discussion, however, to

† Compliance here is equivalent to compressibility in the usual acoustic usage. This follows the recommendations of the Committee on Nomenclature of the Society of Rheology.[5]

restrict the term glass transition to the value indicated by volume-temperature measurements, with a sufficiently long time allowed between measurements so that an equilibrium state is maintained insofar as this can be done.

2. Experimental Method

The dynamic compressibility measurements were made with an apparatus described previously.[6,7] It consists of a cylindrical cavity whose dimensions (1.6 cm. in length and 1.6 cm. in diameter) are small compared to a wavelength of sound in the transmitting medium at all frequencies used. Two identical PZT† ceramic transducers, which when subjected to an electric field undergo a change in volume, are mounted in the cavity on compliant copper springs. It is assembled with the sample and a pressure transmitting fluid [di(2-ethyl hexyl)-sebacate] filling the cavity, and a driving voltage applied to one transducer. The voltage appearing across the second transducer will depend on the sum of the acoustic compliances of the materials in the cavity. The dynamic pressure generated is of the order of 10^{-4} bar (1 bar = 10^6 dyne/cm.^{2} $\cong$ 1 atm.); static pressure of any desired magnitude can be superposed by means of a hand pump used to force the oil (transmitting fluid) into the cavity. We have limited the static pressures to 1000 bars, at which level the various seals in the apparatus hold satisfactorily for several months.

To assure removal of the last traces of air and obtain reproducible values, the following procedure was used on all runs. The oil was evacuated with a mechanical pump for about 20 min., the sample inserted in the cavity, the cavity closed, and the pressure and electrical leads connected. Oil was pumped into the cavity, forcing the air out, through the "pressure lead" and "bleeding lead" shown in Figure 1. After no further air bubbles were apparent in the oil emerging from the bleeding lead, the valve was closed and the pressure built up to 100 bars. The cavity was then immersed in a constant temperature bath, controlled to ± 0.02°C., from which the electrical leads emerge through brass tubes extending above the liquid surface, and sufficient time allowed for attainment of temperature equilibrium. After this the pressure was adjusted to the desired value and the measurements commenced.

† A solid solution of lead titanate and zirconium titanate supplied by Clevite Research Laboratory, Cleveland, Ohio.

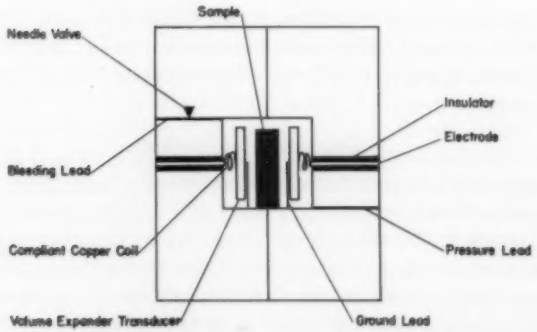

Fig. 1. Schematic drawing of cavity.

The measuring circuit is an a.c. potentiometer described in reference 6. The relation between the input voltage E_1, output voltage E_2, and sample volume V_s is:

$$E_1/E_2 = C^* + A(B_s^* - B_l)V_s \tag{1}$$

where C^* and A are apparatus constants, B_s^* is the complex compressibility of the sample, and B_l the compressibility of the transmitting fluid. Both A and B_l are real, as confirmed by the constancy of the imaginary parts of the voltage ratio when copper, iron, or potassium iodide were used as samples for calibrating the apparatus. C^* is a complex quantity depending on the oil, the crystals, and the acoustic compliances of the apparatus seals, but independent of the sample. It therefore vanishes when the slope of E_1/E_2 vs. V_s is taken at constant temperature, pressure, and frequency.

B_l was determined from static compressibility mesurements carried out in a glass dilatometer with mercury as the confining fluid. This was placed in a pressure cell with windows to permit observation of the dilatometer, and the cell in turn immersed in a thermostat. Isothermal compressibilities from -25 to $+100$°C. and from 1 to 1000 bars were obtained with this apparatus. These were converted to the desired adiabatic compressibilities using the thermal expansion coefficient obtained from the above measurements and values of the specific heat at 1 atm. from -43 to $+92$°C. measured by Mrs. Jeanette H. Piccirelli of the NBS Low Temperature Calorimetry Laboratory. Since this calculated difference between the adiabatic

and isothermal compressibilities amounted to only about 15%, our neglect of any change in specific heat with pressure could introduce only a small error.

Earlier calibration measurements using copper, iron, and potassium iodide, using compressibilities from Bridgeman,[8] permitted check calculations of B_t. These agreed with the values calculated above as closely as could be expected in view of the small differences between the compressibilities of these calibrating materials.

The value of A, though real, depends slightly on temperature and pressure, and C^* depends on frequency, temperature, and pressure. Therefore, three measurements were required at each value of frequency, temperature, and pressure: one with no sample, one with a copper sample, and one with the rubber sample whose compressibility was sought. From the three complex voltage ratios obtained, plus B_t at the temperature and pressure of measurement and the known value of B_s for copper, the real and imaginary parts of the compliance of the rubber were calculated.

The use of only two points to determine each slope (coefficient of V_s) has been found previously to yield values of the storage compliance which, while not quite as precise as those obtained from the three to five sample volumes used in previous work, are reproducible to within 2%. The values of the loss compliance obtained are not this precise. The loss peaks are defined fairly well, but the values away from these peaks show considerable scatter. It is always difficult to measure precise values of the loss compliance when it becomes very small compared to the storage compliance. It was particularly difficult to define this function at temperatures below the peak, since our measurements could not be extended to temperatures much below the glass transition.

3. Rubber Samples

The samples were prepared by Mr. George Bullman of the NBS Rubber Section. 41 g. of sulfur were milled into 300 g. of highly purified pale crepe natural rubber. The mixture was vulcanized for 20 hr. at 150°C. in the form of sheets, $6 \times 6 \times {}^1/_8$ in. Analysis of the vulcanized samples showed 12.1% combined and 0.01% free sulfur.

One-half inch diameter disks were stamped out of the vulcanized sheets, weighed at 25°C., and their volume $V_s(T,P)$ calculated from

an equation of state given by Scott.[9] This equation gave values at 1 atm. which differed by only 0.2% from those measured on the same material used here by Martin and Mandelkern.[10]

Significant swelling of the samples was observed if they were left in the oil for periods as long as 1 week, and the measured compressibility changed by as much as 5%. To avoid this swelling, a new sample was used for each day's determinations. Duplicate measurements at the beginning and end of the day agreed. All samples were cut from the same sheet. A few duplicate determinations made on separate samples indicated that the compliance varied by no more than 2% throughout the sheet.

4. Results

Figure 2 shows the storage compliance at 1 atm. as a function of temperature, measured at several frequencies in the range of 50 to 1000 cycles/sec. No dependence on temperature or pressure history was observed; in this work all runs were carried out along an isobar, starting with the lowest temperature of the run. It will be observed that the effect of changing the frequency is to shift the dispersion region along the temperature axis in a fashion which suggests that a reduced

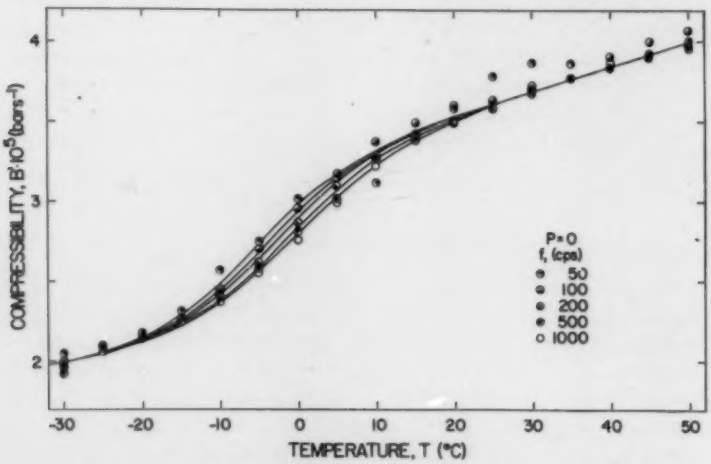

Fig. 2. Storage compliance at 1 atm.

frequency treatment should be applicable. The formulation of such a treatment will be given in the next section.

A characteristic type of electronic noise proportional to reciprocal frequency increases the scatter of the measurements at low frequency. For this set of measurements, where the values of the loss compliance were nearly zero over a large part of the temperature range covered,

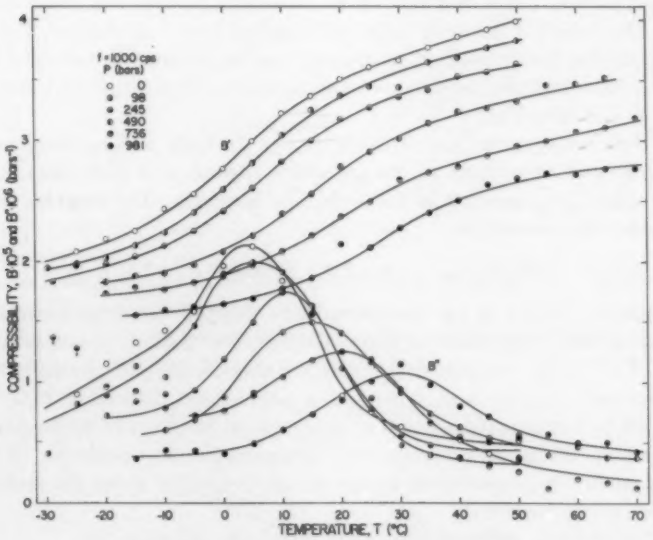

Fig. 3. Storage and loss compliances at 1000 cycles/sec.

this scatter prevented us from defining the loss curve at any single frequency, although on a reduced plot a reasonable curve is defined by all the 1 atm. measurements.

Figure 3 shows measurements at 1000 cycles/sec. as a function of temperature for several pressures. Here the loss compliances are clearly defined, at least in the region of the maxima. Some of the scatter at the lowest temperatures is apparently associated with a stiffening of the transmitting medium. Here again it appears that the curves have similar enough shapes to permit superposition.

5. Reduced Variables

It is well established, both from a consideration of the molecular mechanisms which are used to account for the dependence of rubber-like behavior on frequency and by explicit experimental verification for several systems, that a change of temperature shifts the frequency dispersion region of both the bulk and shear moduli in the same fashion. It is, therefore, logical to use the William-Landel-Ferry[1] formulation, which has proved so successful in reducing shear data, as the basis for deriving reduced variables here. Moreover, Figure 3 indicates that the effect of pressure can be included in an expanded reduction formula, as shown earlier by the work of Singh and Nolle[11] on polyisobutylene.

Both temperature and pressure change the high- and low-frequency compressibilities (beyond the dispersion region), and this effect must be taken into account in the reduction formula. The complex compliance can be written:

$$B^*(T,P,\omega) = B_\infty(T,P) + \Delta B(T,P)\, \mathfrak{B}^*(\omega_r) \tag{2}$$

where B_∞ (T,P) is the compressibility beyond the high-frequency end of the dispersion region, $\Delta B(T,P) = B_0(T,P) - B_\infty(T,P)$, $B_0(T,P)$ is the compressibility beyond the low-frequency end of the dispersion region, and $\mathfrak{B}^*(\omega_r)$ is a normalized dispersion function equal to 1 at $\omega_r = 0$ and to 0 at $\omega_r = \infty$. ω_r is a reduced frequency, a function of the actual frequency, temperature, and pressure, which we assume is proportional to the actual frequency times the steady-state shear viscosity.

To derive a reduced frequency expression we take:

$$\omega_r = \omega\eta(T,P)/\eta_0(T_0,0)$$

where η is the shear viscosity at the temperature and pressure of measurement and η_0 that at the temperature to which reduction is desired and 1 atm. pressure. Gage pressures are used, so that $P = 0$ corresponds to 1 atm. The viscosity is supposed to depend on a free volume,

$$\varphi(T,P) = \varphi_s(T_s,0) + \alpha(T - T_s) - \beta P$$

according to:

$$\eta = Ce^{1/\varphi}$$

T_g refers to the ordinary glass transition temperature at 1 atm., and φ_g the free volume at $T = T_g$ and $P = 0$.

From these definitions we can obtain the expression for the compressibility reduced to $T = T_0$ and $P = 0$ in terms of the actual temperature, pressure, and frequency, T, P, and ω.

$$B^*(\omega_r) = B_\infty(T_0,0) + \frac{\Delta B(T_0,0)}{\Delta B(T,P)} [B^*(T,P,\omega) - B_\infty(T,P)] \quad (3)$$

where

$$\log_{10} \omega_r = \log_{10} \omega - \frac{\dfrac{1}{2.303\varphi_g \left[1 + \dfrac{\alpha}{\varphi_g}(T_0 - T_g)\right]} \left(T - \dfrac{\beta}{\alpha} P - T_0\right)}{\dfrac{\varphi_g}{\alpha}\left[1 + \dfrac{\alpha}{\varphi_g}(T_0 - T_g)\right] + \left(T - \dfrac{\beta}{\alpha} P - T_0\right)} \quad (4)$$

This reduces to the usual form of the WLF equation if T_0 is taken as T_g and P set equal to zero.

An equivalent representation in terms of a reduced temperature can be derived, reduced to $\omega = \omega_0$ and $P = 0$:

$$B^*(T_r) = B_\infty(T_r,0) + \frac{\Delta B(T_r,0)}{\Delta B(T,P)} [B^*(T,P,\omega) - B_\infty(T,P)] \quad (5)$$

where

$$T_r = T - \frac{\beta}{\alpha} P + \frac{\dfrac{\alpha}{\varphi_g}\left(\dfrac{\varphi_g}{\alpha} + T - \dfrac{\beta}{\alpha} P - T_g\right)^2 \log \dfrac{\omega_0}{\omega}}{\dfrac{1}{2.303\varphi_g} - \dfrac{\alpha}{\varphi_g}\left(\dfrac{\varphi_g}{\alpha} + T - \dfrac{\beta}{\alpha} P - T_g\right) \log \dfrac{\omega_0}{\omega}} \quad (6)$$

The "universal" constants, $1/(2.303\ \varphi_g) = 17.44$ and $\varphi_g/\alpha = 51.6$ (from ref. 12) yielded a satisfactory reduced plot of both B' and B'' at one atmosphere.

6. Evaluation of dT/dP for Constant Jump Rate

Before the temperature-pressure equivalence factor, β/α, (or the value of dT/dP for a constant jump rate), can be determined, $\Delta B(T,P)$ must be known. $B_0(T,P)$ is well defined in these data, but

B_∞ can only be approximated because the measurements could not be carried out much below the glass transition.

An expression for $B_0(T,P)$ was derived as follows. The compressibilities were plotted against $T' = T - 0.024P$, a plot selected to line up the peaks of the loss curves. Asymptotic lines for the high-temperature portions of the storage compliances at each pressure were then drawn in, and the intercepts of these lines at $T' = 0$ and 50 fitted to expressions linear in P. This gave the following expression for B_0:

$$B_0(T,P) \times 10^5 = 3.21 + 1.58 \times 10^{-2}\, T - 1.22 \times 10^{-3} P - 5.80 \times 10^{-6} PT + 1.42 \times 10^{-7} P^2 \quad (7)$$

B_0 is in bars^{-1}, T in °C., and P in bars. The P^2 term arises in converting from T' to T; that in PT represents the fact that the slopes of the limiting lines depend on P.

Relative values of ΔB could be obtained from the loss curves if we could define equivalent values of ω_r on each curve. Equivalent reduced frequencies, however, will be displaced slightly from the peaks of the loss curves when plotted against temperature, and our frequency range is insufficient to go through the peaks with an actual frequency plot. Thus an approximate value of B_∞ and its temperature coefficient is required, to be used only in establishing temperatures corresponding to equal values of ω_r at each pressure.

The 490 bar curve for B' seems to define the best value of B_∞, and moreover 490 bars is the median pressure employed. Therefore a trial function for B_∞ $(T,490)$ was fitted to this curve, and from it and eq. (7) we obtained:

$$\Delta B(T,490) \times 10^5 = 0.65 + 5.6 \times 10^{-3} T$$

From eq. (2) we derive the following condition for the peak in the B'' vs. temperature curves:

$$\frac{\partial \ln B''}{\partial T} = \frac{\partial \ln \Delta B(T,P)}{\partial T} + \frac{\partial \ln \mathfrak{B}''(\omega_r)}{\partial T} = 0$$

Therefore, equal values of $\omega_r(T,P)$ at constant actual frequency are found at temperatures for which:

$$\frac{1}{B''}\frac{\partial B''}{\partial T} = \frac{1}{\Delta B}\frac{\partial \Delta B}{\partial T}$$

The expression for $\Delta B(T,490)$ above was used for obtaining values of $(1/\Delta B)(\partial\Delta B/\partial T)$ at all pressures, and the values shown in Table I calculated. It can be seen that the shift from the peaks of the B'' vs. T curves are so small that the error involved in using $\Delta B(T,490)$ for all pressures is negligible.

TABLE I

	$\frac{\partial B''}{\partial T} = 0$		$\frac{1}{B''}\frac{\partial B''}{\partial T} = \frac{1}{\Delta B}\frac{\partial \Delta B}{\partial T}$			
				$(B'' = \Delta B (T, P)$		
P	T	$B'' \times 10^5$	T	$\mathfrak{B}''_{max}) \times 10^5$	$\Delta B(T,P) \times 10^{5a}$	$B_\infty \times 10^{5b}$
0	4	2.13	2.8	2.12	1.02	2.23
98.1	6	2.02	4.0	2.00	0.96	2.19
245.3	11	1.75	10.0	1.74	0.83	2.23
490.5	15	1.49	13.6	1.48	0.71	2.11
735.8	20	1.25	18.4	1.24	0.59	2.00
981.0	29	1.08	27.6	1.07	0.51	1.91

[a] Using $\Delta B(13.6,490) \cong \Delta B(15,490) = 0.71 \times 10^{-5}$.
[b] Using tabulated $\Delta B(T,P)$ and B_0 from eq. (7).

The last two columns of Table I were obtained by assuming the trial value of $\Delta B(13.6,490)$ found above. The values of B_∞ in the last column were then plotted at the appropriate temperature and pressure on the graph of B' vs. T, and straight lines passing through each point and agreeing with the measurements at the lowest temperatures drawn. It was found that a reasonable fit (and lines defined as well as the measurements in this region justified) could be obtained using temperature coefficients independent of pressure. Intercepts of these lines at $+30$ and $-30°$ were read off, linear functions of pressure fit to each set of intercepts, and the final expression for B_∞ obtained as:

$$B_\infty \times 10^5 = 2.25 + 0.85 \times 10^{-2}T - 0.57 \times 10^{-3}P \quad (8)$$

From eqs. (7) and (8), the following expression for ΔB was obtained:

$$\Delta B \times 10^5 = 0.96 + 0.73 \times 10^{-2}T - 0.65 \times 10^{-3}P - 5.79 \times 10^{-6}PT + 1.41 \times 10^{-7}P^2 \quad (9)$$

The slope of a plot of the values of the temperatures corresponding to maxima in $\mathcal{B}''(\omega_r)$ against the corresponding pressures gave $\beta/\alpha = 0.024°C./bar$.

7. Reduced Variable Presentation; Discussion

Figure 4 shows all measurements presented on a reduced frequency plot, calculated from eqs. (3) and (4), the "universal" WLF constants for φ_g and α, and the expressions for B_∞, ΔB, and β/α derived in the previous section. The reduction here is to 0°C. and 1 atm. ($P = 0$).

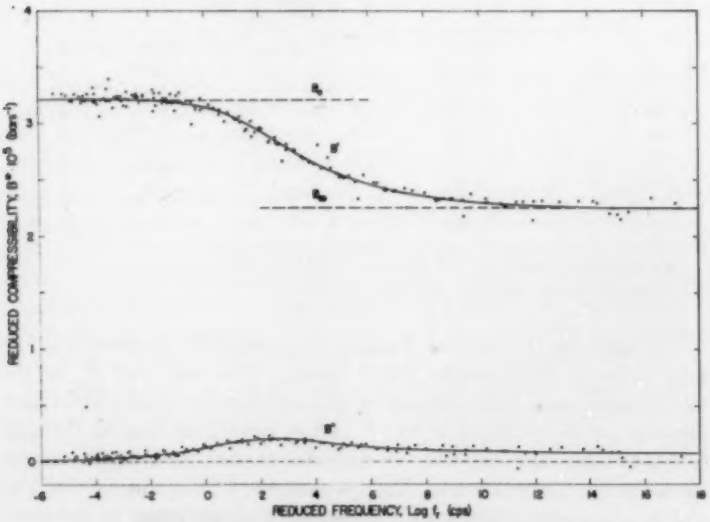

Fig. 4. Storage and loss compliances versus reduced frequency.

Most of the storage compliance values are within 2% of the reduced curve, and the derivation of the points from the reduced curve seems to be random. Thus our reduction represents the data correctly so far as our precision permits us to judge. The loss curve is of significance only in the vicinity of the maximum, the large deviations at high reduced frequency coming from measurements at low temperatures where the difficulties due to stiffening of the transmitting fluid were encountered.

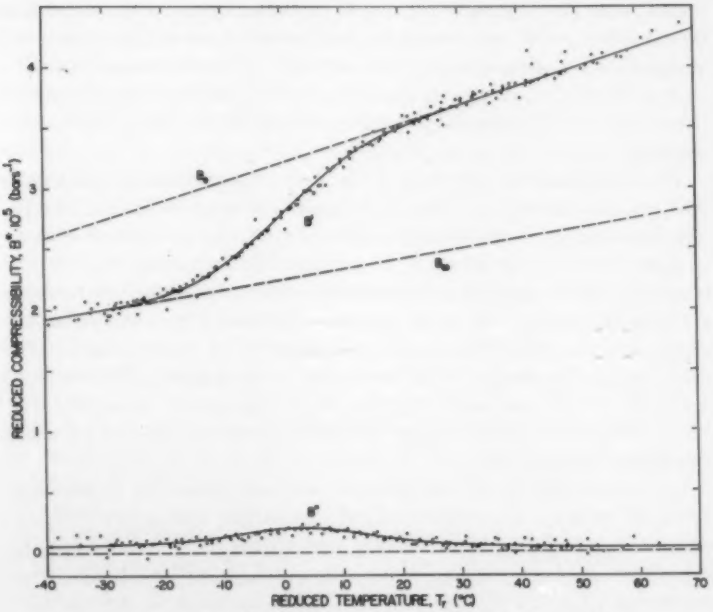

Fig. 5. Storage and loss compliances versus reduced temperature.

Figure 5 shows the data presented on a reduced temperature plot, taking $f_0 = 1000$ cycles/sec. ($f = \omega/2\pi$) in eqs. (5) and (6). These two plots are, of course, entirely equivalent; the reduced temperature plot involves a smaller shifting of the observed data, but the reduced frequency presentation leads to simpler interpretation in some respects.

The scatter of the points on the reduced plots is somewhat greater than that of the original data. This is not surprising in view of the approximations made in arriving at the constants used for the reduced variables, although there is not any systematic deviation of points at any particular temperature or pressure on the reduced frequency plot, or at any particular frequency or pressure on the reduced temperature plot. No great significance should be attached to the loss compliance at low temperatures (or high reduced frequencies), but it is interesting to note that the values appear to remain finite

rather than to approach zero, and indeed suggest a constant loss term. This same phenomenon has been observed by Litovitz[13] in some of his measurements on liquids; no explanation consistent with a linear theory appears possible unless the apparent scatter of the storage compliance indicates the presence of additional dispersion regions.

The temperature coefficient of the free volume used in our derivation was that shown by Ferry and Landel[12] and by Williams, Landel, and Ferry[1] to give satisfactory reduced variables for a wide variety of glass-forming substances. It corresponds in general to the difference between the thermal coefficients of expansion of the rubbery and glassy states. The measurements of Martin and Mandelkern[10] show that the difference in these coefficients is approximately the same for the compound used here also; they report a difference of 4.4×10^{-4} to be compared with the WLF "universal" value of 4.8×10^{-4}. We could hardly choose between values this close in reducing the data presented here.

It is more difficult to compare our derived values for β, the coefficient of pressure in the free volume expression, with other work because of the lack of compressibility measurements covering both the glassy and rubbery regions. Our value of 1.15×10^{-5} bar^{-1}, from our value of 0.024°C./bar and the WLF constant of 4.8×10^{-4} (°C.)$^{-1}$, should, from the viewpoint adopted here, be equal to the difference in compressibilities in the rubbery and glassy states. Our ΔB values should approximate this difference, if converted from adiabatic to isothermal values. Since we have found only an average value for β, we should compare this with our $\Delta B(15{,}490)$ which is 0.74×10^{-5}. Using an expression given by McPherson and Bekkedahl,[14] we find C_p for rubber-12% sulfur equal to 2.206 joules/(g. °C.). This is an average value for the temperature range of +25 to +175°C. at a pressure of 1 atm., but appears to be the only one available. Using this and the appropriate volumes and temperature coefficients for the rubbery and glassy states from Martin and Mandelkern,[10] we find the correction terms $(TV\alpha^2/C_p)$ for converting B_0 and B_∞ to isothermal values are (at 15°C.) 5.22×10^{-6} and 4.94×10^{-7} bar^{-1}. The difference between these two, added to our ΔB-(15,490), gives 1.21×10^{-5} bar^{-1}. This appears reasonably close to the value of 1.15×10^{-5} found from our shifting factors, considering the approximate values used in the conversion.

The only direct measurements of the isothermal compressibilities of this material in our pressure range appear to be those of Scott,[9] and his measurements did not extend below the glass temperature, so there is nothing with which we can compare our value of B_∞ or of ΔB. He gives 3.75×10^{-5} bar^{-1} for the compressibility at 25°C. and 1 atm., to be compared with our value (converted to an isothermal compressibility as above) of 4.14×10^{-5}.

It is interesting to note that Singh and Nolle[11] find a value of dT/dP for polyisobutylene of 0.025°C./bar, which is so close to our value of 0.024 as to suggest that this may be a characteristic constant applicable to many different materials, much like the universal temperature coefficient. Since we have this constant for only two polymers, it is decidedly premature to do more than speculate on this point, but the possibility is intriguing.

References

1. Williams, M. L., R. F. Landel, and J. D. Ferry, *J. Am. Chem. Soc.*, **77,** 3701 (1955).
2. Doolittle, A. K., *J. Appl. Phys.*, **23,** 236 (1952).
3. Hildebrand, J. H., *J. Chem. Phys.*, **31,** 1423 (1959).
4. Litovitz, T. A., and T. Lyon, *J. Acoust. Soc. Am.*, **30,** 856 (1958).
5. Leaderman, H., *Trans. Soc. Rheol.*, **1,** 213 (1957).
6. McKinney, J. E., S. Edelman, and R. S. Marvin, *J. Appl. Phys.*, **27,** 425 (1956).
7. McKinney, J. E., and C. S. Bowyer, *J. Acoust. Soc. Am.*, **32,** 56 (1960).
8. Bridgman, P. W., *The Physics of High Pressure*, Bell, London, 1952.
9. Scott, A. H., *J. Research NBS*, **14,** 99 (1935).
10. Martin, G. M., and L. Mandelkern, *J. Research NBS*, **62,** 141 (1959).
11. Singh, H., and A. W. Nolle, *J. Appl. Phys.*, **30,** 337 (1959).
12. Ferry, J. D., and R. F. Landel, *Kolloid-Z.*, **148,** 1 (1956).
13. Litovitz, T. A., and T. Lyon, *J. Acoust. Soc. Am.*, **26,** 577 (1954).
14. McPherson, A. T., and N. Bekkedahl, *J. Research NBS*, **14,** 601 (1935).

Synopsis

The dynamic bulk compliance of natural rubber-12% sulfur was measured for varying static pressure (0 to 1000 bar), temperature (−30 to +70°C.), and frequency (50 to 1000 cycles/sec). The data can be represented by reduced frequency or temperature plots, assuming viscosity is proportional to exp $\{1/\varphi\}$. φ is a fractional free volume which can be taken as a linear function of temperature and pressure, $\varphi = \varphi_g + \alpha(T - T_g) - \beta P$. The "universal" WLF constants, $\varphi_g = 0.025$ and $\alpha = 4.8 \times 10^{-4}$ (°C.)$^{-1}$, reduce the temperature-frequency data satisfactorily. A value for β of 1.15×10^{-5} bar^{-1} was found from the shift

of the peaks of the imaginary compressibility vs. temperature at various pressures; this corresponds to a value of dT/dp at constant free volume of 0.024 bar/°C. which is nearly the same as the value of 0.025 found by Singh and Nolle for polyisobutylene. β agrees reasonably well with the difference in compressibilities between the rubbery and glassy states.

TRANSACTIONS OF THE SOCIETY OF RHEOLOGY IV, 363–368 (1960)

Abstracts of Additional Papers Presented at the Society of Rheology Meeting, November 4–6, 1959

Rheology in Search of Structures. Part II

ANDRIES VOET and WM. N. WHITTEN, JR.
J. M. Huber Corporation, Borger, Texas

An investigation was made of the structures in dispersions of carbon blacks in white mineral oil. A selection of twelve blacks was made, representative of the commercially available types.

In addition to the conventional rheological approach, measurements were made of the electrical conductivities and dielectric constants in quiescent dispersions as well as in dispersions deflocculated by shear or by chemical means.

A detailed picture of the structural involvement could be derived from conductivity data, such as the minimum in the conductivity-shear rate relation, the induction period, and the rate of rebuilding of destroyed structures as well as the magnitudes of minimum and maximum conductivities. These conclusions are supported by dielectric data and can be explained from the standpoint of potential energy curves representing particle interaction.

Rheological data, however, do not allow straightforward conclusions about the structure. Yield values, derived either from a rheological diagram, obtained with the aid of a high-shear rotational viscometer, or by means of a parallel plate viscometer fail to show a correlation with actual structures. Oil adsorption data, when obtained under carefully controlled conditions, show a limited correlation with structure. A somewhat better correlation was found to exist for the specific plastic viscosity.

[To be published in *Am. Ink Maker*]

Fluid Mixing in Agitated Vessels

A. B. METZNER
University of Delaware, Newark, Delaware

Fluid motion in an agitated tank has been studied by following the motion of tracer particles in both Newtonian and non-Newtonian fluid systems. Measured velocity distributions were differentiated to obtain local shear rates and local rates of power dissipation.

The above analysis indicated that the contents of an agitated vessel may be considered as consisting of two portions: a small region near the impeller which is nearly "perfectly-mixed," and a surrounding region in which the rates of turbulent mixing are nearly zero. The equation describing mixing rates which was based on this model has been experimentally verified in Newtonian fluids. While no experimental verification has as yet been obtained in non-Newtonian systems, the tracer-particle work indicates that in this case the model would be obeyed even more closely than in Newtonian fluids.

[To be published in *A.I.Ch.E. Journal*]

Heat Transfer to Non-Newtonian Fluids under Laminar Flow Conditions

A. B. METZNER and D. F. GLUCK*
University of Delaware, Newark, Delaware

Rates of heat transfer to non-Newtonian fluid systems passing through smooth round tubes under laminar flow conditions have been studied, both experimentally and theoretically, for the case in which viscous heat generation may be neglected. The data of three independent investigators have been correlated with an average deviation of 16%. The final equation contains the conventional Grashof number type of correction to account (empirically) for natural convection effects and the Sieder-Tate correction for radial variation of

* Present address: National Aeronautics and Space Administration, Cleveland, Ohio.

fluid consistency. Interestingly, up to 37% of the total heat was transferred by natural convection even in systems which were highly non-Newtonian, hence viscous, in nature.

[To be published in *Chem. Eng. Sci.*]

A Re-Interpretation of the Rouse-Bueche Theory of Viscoelastic Behavior

R. S. MARVIN
National Bureau of Standards, Washington, D. C.

The Rouse and Bueche theories of the viscoelastic response of a rubberlike polymer were derived considering the response of a single polymer molecule to force, displacement, or velocity fields resulting from macroscopic forces or deformations applied to a bulk sample. From this point of view, Ferry and Bueche have derived expressions for the response of a bulk sample containing a distribution of molecular weights finding the equilibrium compliance proportional to $M_z M_{z+1}/M_w$.

An alternative point of view for the derivation is presented here, in which the form of the function can be shown to be equivalent to the empirical Voigt or Maxwell representations. From this point of view the expressions of the theories (or the equivalent model) correspond to the response of the bulk sample rather than that of a single chain.

The constants are calculated from the equilibrium kinetic theory, the resistance per unit length of the particular polymer, the critical molecular weight where the dependence of viscosity on molecular weight undergoes an abrupt change in form, and the molecular weight of the sample. They are calculated entirely from measurements of molecular weights and steady-flow viscosities, and represent very well the response over the whole time scale of interest. Also the effect of entanglements is introduced in a more direct fashion than in previous work.

Results for steady-state dynamic response are presented and the problem of the calculation of transient response (creep and stress relaxation) discussed.

The Behavior of Particles in Laminar Shear

S. G. MASON
Physical Chemistry Division, Pulp and Paper Research Institute of Canada, Montreal and *Department of Chemistry, McGill University, Montreal, Canada*

Particles suspended in a liquid subjected to a velocity gradient undergo rotational and translational movements and, when they are deformable, changes in shape. The general behavior of solid spheres, fluid drops, rigid and flexible rods and fibers are described with the aid of cine photomicrographs.

The relevance of these phenomena to theories of viscosity of dilute suspensions are discussed.

The Influence of Viscometer Design on Non-Newtonian Measurements

R. McKENNELL
Ferranti Ltd., Moston, Manchester, England

Uncertainty arising from viscometric data obtained from non-Newtonian fluids is minimized by observing two principal conditions: the shear rate should be uniform throughout the measured sample; and a consistent experimental procedure, including the amount and duration of shear, should be adopted. The effect of shear rate variation within the sample fluid is discussed for some viscometers in common industrial use. An outline is given of the methods available for eliminating variations in shear rate, and hence the tedium of applying corrections to flow curves for different types of non-Newtonian behavior. A viscometer is described which combines uniform shearing conditions with a flexible automatic flow curve recorder giving a wide range of rheological test programs. The recorder enables the duration of shear to be minimized in the higher ranges so that shear-induced heating in the thin layer of fluid is greatly reduced. Comparative data are presented for several rotation viscometers to show this effect.

Dynamics of Frictional Compressible Fluids—Application to Plastico-Dynamics

C. TORRE
Research and Development Laboratory, M. W. Kellogg Co., Jersey City, New Jersey

The dynamics of frictional compressible fluids is formulated mathematically by eleven equations. There are three equations of motion of a continuum: the continuity equation, the "specifying" equation, and six stress-rate of strain relations. The eleven unknowns are: six stresses, three velocities, pressure, and density.

The system contains eleven quasi-linear partial differential equations. To obtain the real characteristics (hyperbolic case) which are different from zero, we have to complete Stokes' stress-rate of strain relations by stress and pressure derivatives with respect to time and space (methods of rheology).

Assuming a density which is a given scalar function of space and time or a constant density, we relate our system of equations to the plastico-dynamics of a solid body. The governing differential equations are of the Hamilton-Jacobi type, while the characteristic directions are expressed in Hamilton's or canonic differential equations. Results describing the motion of a plastic mass have been obtained.

A Thermodynamic Approach to Rheology

HARRY H. HULL
Research and Development Department, R. R. Donnelley & Sons Co., Chicago, Illinois

The mechanical work done in deforming a body is either completely or partially dissipated into heat. That portion which is not dissipated into heat is a potential energy. This potential energy is the elastic energy of deformation. It is also the Gibbs free energy if the deformation is done at constant pressure. This could be called the rheological free energy.

Since this rheological free energy is a function of rate of shear and amount of deformation in shear, these two variables are variables of

state with certain limitations as to the proper equilibrium conditions and as such are thermodynamically similar to pressure, temperature and volume. This permits the statement of various modifications of Gibbs phase rule and writing of partial differential equations of the usual thermodynamic type but including rate of shear and amount of deformation in shear.

A perfect viscous fluid is defined as one which has no elastic component of deformation no matter what the rate of shear or the amount of deformation. This fluid obeys the conventional phase rule $F' = C - P' + 2$ and the conventional partial differential thermodynamic equations under either static or deforming conditions.

A perfect viscoelastic fluid is defined as one in which the free energy increases with the rate of shear but for which there exists a condition at each rate of shear such that the free energy does not vary with the amount of deformation in shear. The phase rule for this fluid is $F' = C - P' + 3$. Partial differential equations involving P, V, T and the rate of shear are developed for this fluid. It is shown that the rheological free energy must result in a Weissenberg effect and equations are developed for the normal forces which are indicated by the Weissenberg Rheogoniometer and the Garner Nissan and Wood Viscometer.

Any change in molecular orientation caused by deformation indicates a change in entropy and this implies a change in free energy.

The elastic solid and the general case of the viscoelastic body are discussed in a way similar to the perfect viscoelastic fluid.